

INTRUSION INFLUENCE ON CHILD OCCUPANT BEHAVIOUR IN THE CASE OF A SIDE IMPACT MADYMO SIMULATION

Marius-Dorin Surcel

Michel Gou

École Polytechnique de Montreal

Canada

Paper Number 05-0050

ABSTRACT

The effectiveness of child restraint systems has been very well proven in the case of frontal collision but the performance of the protective devices in side-impact situation were not, as yet, clearly demonstrated.

This research was aimed at the development of a numerical method to simulate the behavior of a child passenger restrained in a protective device in the case of a vehicle side impact, considering vehicle body deformation. The model was mainly based on a multi-body method. However the side wings of the child restraint system and the vehicle body have been modeled by the finite-element technique, to allow for a better representation of the contacts between the child dummy, the restraining device and the structure of the vehicle and to make possible the simulation of the vehicle body deformation, based on available side impact test data. The model had been validated for side impact and we have used it to study the influence of the intrusion against the child dummy behavior in the case of side impact.

The intrusion influence is most important for the head injury criteria, being proportional with the impact speed. The study of various installation configurations showed that the usage of ISOFIX lower anchorages offers the best protection for the head, followed by the lower flexible anchorages and vehicle belt installation. The intrusion influence is most important when the child restraint system is installed using the vehicle safety belts, the results being much higher than for the case where the intrusion is not considered. Chest deceleration is less influenced by the intrusion and the three considered installation configuration give similar results.

Although the results of the project successfully responded to the initial objectives, the model is offering a lot of possibilities of improvement, development and exploitation.

INTRODUCTION

Children are the most innocent victims of road accidents and therefore their protection is a major issue for all involved in automotive safety.

The effectiveness of the specialized child restraint systems was well proved in the case of frontal collision, where regulations, standards and test procedures are available. As a result of educational campaigns, most child restraint systems are now installed on the rear seat of the vehicle so that vehicle body deformation influence for the child occupant injuries was considerably reduced in the case of frontal impact. Table 1 illustrates the trend of the gradually increasing rear seat placement of the child restraint system (Stern, 1998).

Table 1.
Child Seat Distribution by Row
(from Stern, 1998)

Year	88 – 90	91 – 93	94 - 96	Total
Front	40 %	41 %	34 %	38 %
Rear	59 %	59 %	66 %	62 %

However, the performances of these protective devices in side-impact situation were not, as yet, clearly demonstrated. The applicable regulations are only stipulating that the child passenger should be not ejected from the car in the case of a side impact and crash data shows that they are side impact situations when the child restraint system is unable to offer sufficient protection, resulting in serious injuries or even the death of the child occupant. The FARS data shows that in U.S.A., 1,317 children between the ages of zero to twelve have been killed in motor vehicle crashes in 1999 and 31.89 percent of them were involved in side impact crashes. Of these, children seated on the side nearest to the impact represent 55 percent of the fatalities (NHTSA, 2002). Canadian statistics side impact accident data confirms that this is the most dangerous position in the vehicle. Moreover, the vehicle body intrusion is very important especially when the child restraint system is positioned on the outboard nearside to the impact place (Howard, Rothman, Moses McKeag, Pazmino – Canizares et al., 2003).

Thus this project was aimed at the development of a numerical method to evaluate the influence of the intrusion on the behavior of a child passenger restrained in a protective device placed on the nearside to the impact place, in the case of a vehicle

lateral collision, considering different installation possibilities and impact speeds.

METHODOLOGY

General Approach

Child restraint system, vehicle body vehicle, child dummy, belts and anchorages models have been built using finite element and multi-body techniques. The MADYMO software was chosen to build the model because it reduces the computational time and the related cost, allows the use of already validated dummy models from the MADYMO library and makes possible the comparison with other simulations created with the same software. The side wings of the child restraint system and the vehicle body have been modeled by the finite-element technique, to allow for a better representation of the contacts between the child dummy and the restraining device and the structure of the vehicle and to make possible the simulation of the vehicle body deformation, based on available side impact test data. The reverse engineering method (Monclus-Gonzales, Eskandarian, Takatori et al., 2001; Zaouk, Marzougui and Kan, 1998) was used to obtain the necessary constructive data, because the manufacturer information is generally proprietary. The model was then evaluated for side impact against available similar test data.

Finally model exploitation was conducted to assess side impact simulation with and without considering the intrusion and for different installation configurations and impact speeds.

Because the majority of tests and studies have been done using three years old dummies and moreover, the available test results to evaluate the model being obtained for the Hybrid III three years old child dummy, this model was chosen for the comparative study.

Models

The Hybrid III 3-years-old child dummy numerical model is available in MADYMO Data Base (TNO Automotive, 2003) and has been validated by TNO for frontal loading. The model consists of 28 ellipsoids while certain head regions are built using the finite elements method. The contact between head and thorax is defined by default but additional contacts have been defined: between both femurs; between each femur and the abdomen, the thorax, the neck and the head; between both tibias; between each tibia and the neck and the head; between both arms; between each arm and the neck and the head. The child dummies were positioned in the child restraint

system by applying the gravitational force on the dummy, which allowed for an equilibrium state. In agreement with the chosen child dummy model, the required child seat is the convertible restraint system designed for use by infants and toddlers. The Cosco Touriva child seat was chosen, for which test results and a specimen were available for analysis. The central region of the child seat was built using multi-body technique and the child seat side wings have been reconstructed using finite elements, to allow for a better representation of the contacts between the child dummy and the restraining device and between the side wings of the child restraint system and the vehicle interior.

The child restraint system was placed on the outboard nearside to the impact place and the following installation configurations were considered: vehicle safety belts, lower anchorage belt system and ISOFIX system. A supplementary top tether was also used (figure 1).

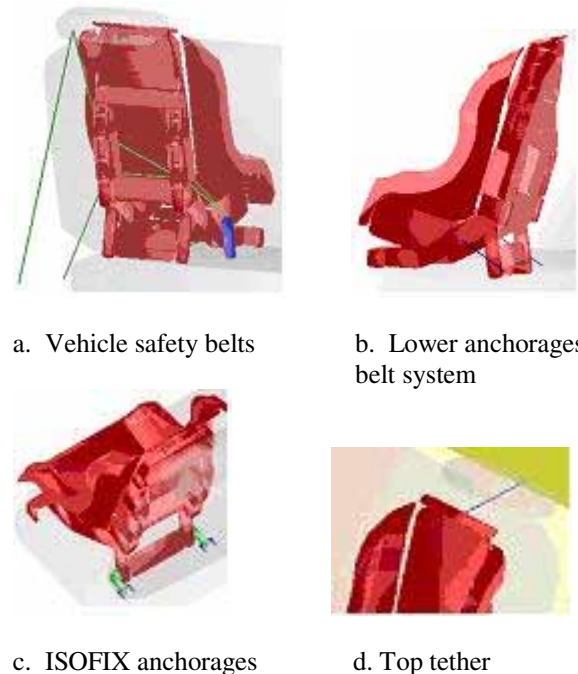


Figure 1. Child restraint system installation.

The child restraint system harness, lower anchorage belt system straps and vehicle safety belt characteristics have been measured or adapted from the available literature data (TNO Automotive, 2003). The straps were represented using MADYMO belt segments. The child restraint system attachments (release button and the harness retainer clip), vehicle safety belt anchorages and ISOFIX anchorages were built by ellipsoids.

The available test results (vehicle side impact test and child restraint system test) were obtained from a Pontiac Grand Am 1999, so this vehicle model was chosen for the simulation. Vehicle body dimensional characteristics and constitutive material properties were measured or experimentally determined on a similar vehicle and its components. The rear bench and the front seats were represented using ellipsoids and were linked to the reference space using point restraints (a combination of three mutually perpendicular parallel springs and dampers), to allow their displacement for the case of the side impact. Vehicle side frame, rear doors, rear panel, rear shelf, rear glasses and rear doors glasses were built by finite element, to allow for a better representation of the contacts between the vehicle interior and child dummy and child restraint system side wings and to make possible the simulation of the vehicle body deformation, based on available test data (figure 2).

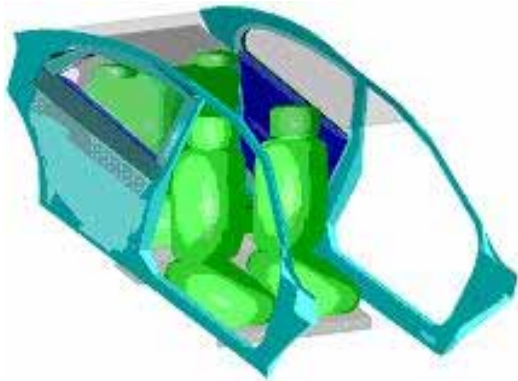


Figure 2. Vehicle model.

Simulation

To simulate the side impact, a lateral acceleration field (figure 3) and the gravity field were applied to the child dummy and to the child restraint system. The lateral acceleration field complies with SNCAP (Side impact – New Car Assessment Program) specifications and had been used during the tests performed by NHTSA in 2001 (Sullivan, Willke and Brunner, 2001). The lateral acceleration field corresponds to an impact speed of 33,8 km/h (21 mph), with a peak acceleration of 26 g (255 m/s^2). The simulation results are compared with the results of the above-mentioned tests, performed with a Hybrid III 3-years-old child dummy seated on a Cosco Touriva child seat installed on a Pontiac Grand Am 1999, using the vehicle safety belts.

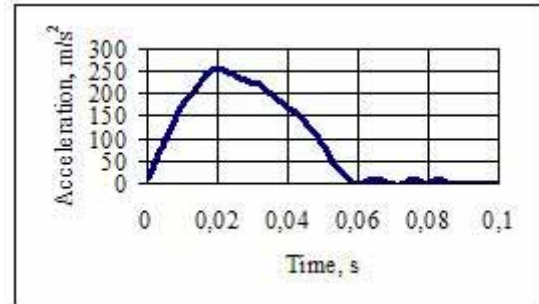


Figure 3. Side impact pulse (adapted from Sullivan, Willke et Brunner, 2001).

Model Exploitation

The model exploitation was conducted to compare the behavior of the child dummy model in the case of the side impact both with and without considering the intrusion, based on the available test data (the intrusion profiles measured as a result of the NCAP side impact tests at a 90° angle and 62.1 km/h actual test speed, NHTSA, 1999).

Because full finite element models are large in terms of CPU time consumption, the vehicle deformation was simulated using the MADYMO's prescribed structural motion feature.

The project considered three impact situations:

- 90° side impact at 33.8 km/h without intrusion.
- 90° side impact at 33.8 km/h with the intrusion profiles recalculated based on 62.1 km/h available intrusion profiles (using the simplified energetic balance between deformation energy and kinetic energy).
- 90° side impact at 62.1 km/h with the acceleration pulse recalculated based on 33.8 km/h available pulse (using the equations of motion and considering the same impact duration).

The following installation configurations were taken into account:

- Vehicle safety belt installation, with and without top tether.
- Lower anchorages belt system.
- ISOFIX system.

EVALUATION RESULTS

The simulation results were compared with the results of the above-mentioned tests, performed by NHTSA in 2001 and with the Injury Assessment Reference Values (IARV), stipulated by FMVSS 208 and FMVSS 213. These injury parameters are for frontal impact and may not accurately reflect the risk of injury in side impact and the corresponding Injury

Assessment Reference Values should be used for reference purposes only. Figures 4 and 5 illustrate the comparisons of the variation of head acceleration and thorax acceleration. Test variations were calculated based on the available test signals (NHTSA Vehicle Crash Test Database).

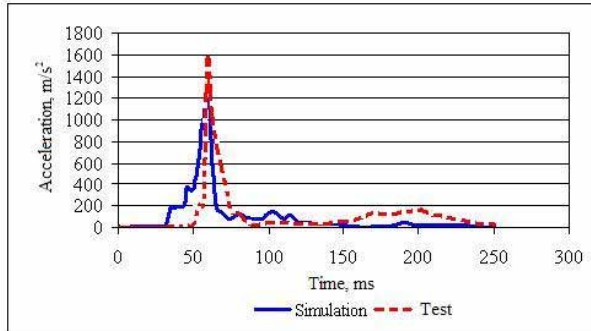


Figure 4. Comparison of head acceleration variation.

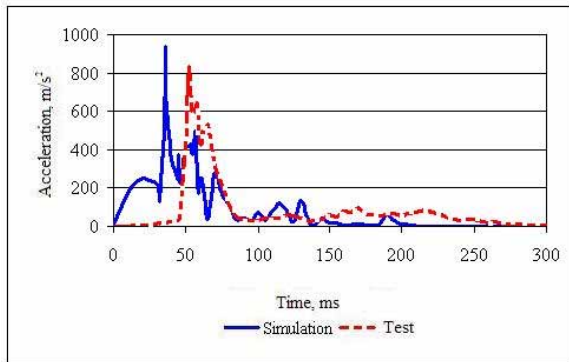


Figure 5. Comparison of thorax acceleration variation.

The comparison of head acceleration curves shows good reproduction of the experimental data. However, the comparison of the thorax acceleration curves shows a time lag between the two peaks and a less progressive variation at the beginning, for the simulation curve. These discrepancies are the results of using standard MADYMO belt model for both harness straps and vehicle safety belts straps because MADYMO standard belt model has fixed attachments points and cannot reproduce the effects of slip on the dummy model. As a result, some differences between the tested belt and harness and the belt and harness model behaviour are possible. The effect is not important for the head acceleration since the peak is related here to the contact between the dummy head and the door panel and the two curves coincide at this point. For the thorax

acceleration, the peak is given by the brutal stop of chest movement caused by the restraint forces in the harness and in the belts and thus detail of belt and harness model is very important for this value. Table 2 presents the maximal values of some injury parameters. The maximal head acceleration was calculated based on the available test signals (NHTSA Vehicle Crash Test Database). The simulation results were generally very close to the experimental data.

Table 2. Evaluation results

Injury parameter	Simulation	Test	IARV
HIC 15	1001	1085	570
HIC unlimited	1001	1085	1000
Thorax deflection, mm	6,14	3,56	34
Thorax acceleration, 3 ms, m/s ²	639	646	540 589
Head acceleration, m/s ²	1193	1582	-

INTRUSION INFLUENCE ASSESSMENT

Safety belts installation without top tether

Figure 6 illustrates the model during the simulation of the side impact at 62.1 km/h with intrusion when the child restraint system is installed using vehicle safety belts.

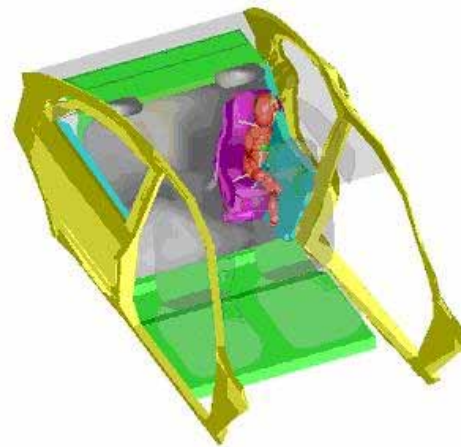


Figure 6. Side impact simulation at 62.1 km/h with intrusion.

The compared parameters were:

- Head injury criteria: HIC15 and HIC unlimited,

- Maximal head acceleration and head acceleration variation, a_H ,
- Maximal thorax acceleration with a duration of at least 3 ms, a_T , thorax acceleration variation and chest deflection, d_T ,
- Neck axial forces, F_Z (compression and tension) and flexion and extension moments about the occipital condyles, M_Y ,
- Biomechanical neck injury predictors (tension-extension NIJ TE, tension-flexion NIJ TF, compression-extension NIJ CE and compression-flexion NIJ CF).

Table 3 and figures 7 and 8 illustrate the comparisons when the child restraint system is installed using vehicle safety belts but without top tether.

Table 3.
Injury parameters comparison, safety belt installation, no top tether

Parameter	No intrusion	With intrusion		IARV
	33.8 km/h	33.8 km/h	62.1 km/h	
HIC 15	1001	2271	7450	500
HIC	1001	2271	7450	1000
Nij TE	1.615	1.885	1.439	1
Nij TF	0.242	0.294	0.760	1
Nij CE	0.625	0.300	1.168	1
Nij CF	0.706	0.422	0.338	1
F_z , N	1251	1721	1591	2340
$-F_z$, N	1276	558	514	2120
M_y , Nm	13.8	13.7	28.9	-
$-M_y$, Nm	29.0	29.3	29.4	-
d_T , mm	6.14	11.81	19.04	34
a_T , m/s^2	639	678	969	540 / 589
a_H , m/s^2	1193	1925	3577	-

The intrusion influence is very important for the head injury parameters, the results being much higher than seen in the case when the intrusion is not considered (up to 600 % for HIC15 and HIC unlimited and near to 200 % for head maximal acceleration) and they are proportional to the impact speed. The IARV's are largely exceeded when the intrusion is considered. The peak is reached sooner when the intrusion is considered, being related to the moment when child dummy's head hits the door panel (figure 7). Thorax deceleration is also influenced by intrusion but here the differences are smaller, up to 60 % when the impact at 62.1 km/h is simulated. The results are greater than the IARV. The peak is reached almost at the same time when the intrusion is considered, compared to the collision without intrusion, because it is more related to the restraint forces in belts and

harness than to the impact between the child dummy and the vehicle body (figure 8). Thorax deflexion is also proportional to the impact speed but the IARV is not exceeded. Neck injury parameters are not clearly influenced by intrusion but the IARV for neck predictors is exceeded in tension-extension in all the cases while the neck forces are under the limits.

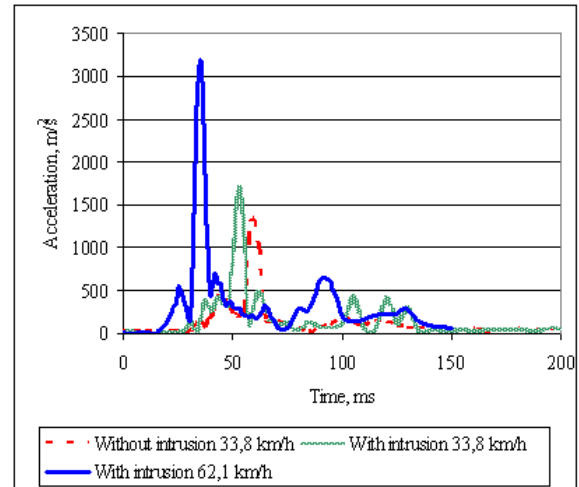


Figure 7. Safety belt installation, no top tether: head acceleration variation.

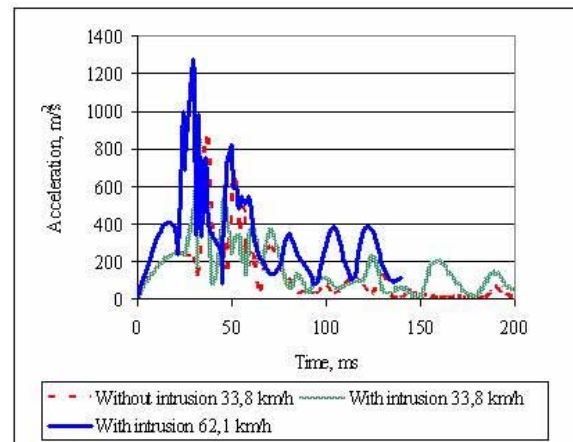


Figure 8. Safety belt installation, no top tether: thorax acceleration variation.

Safety belts installation with top tether

The vehicle safety belt installation with top tether is analyzed in table 4 and figures 9 and 10.

The same trends noticed before can be observed in this case too for the head injury criteria, being much higher than in the case when the intrusion is not considered (up to 700 % for HIC15 and HIC

unlimited and more than 200 % for head maximal acceleration) and they are proportional to the impact speed. The IARV's are exceeded in all the cases for HIC15 and for HIC unlimited when the intrusion is considered.

Table 4.
Injury parameters comparison, safety belt installation, with top tether

Parameter	No intrusion	With intrusion		IARV
	33.8 km/h	33.8 km/h	62.1 km/h	
HIC 15	848	1454	6584	500
HIC	848	1454	6584	1000
Nij TE	0.704	1.330	2.740	1
Nij TF	0.431	0.413	0.667	1
Nij CE	0.390	0.681	2.618	1
Nij CF	0.205	0.203	0.217	1
F_z , N	863	1005	1834	2340
$-F_z$, N	380	971	420	2120
M_y , Nm	6.9	15.1	19.7	-
$-M_y$, Nm	13.0	23.8	68.9	-
d_T , mm	9.03	13.45	21.53	34
a_T , m/s^2	605	586	1007	540 / 589
a_H , m/s^2	1337	1704	3220	-

The maximum for the head acceleration is again reached sooner when the intrusion is considered, being again related to the moment when child dummy's head hits the door panel (figure 9).

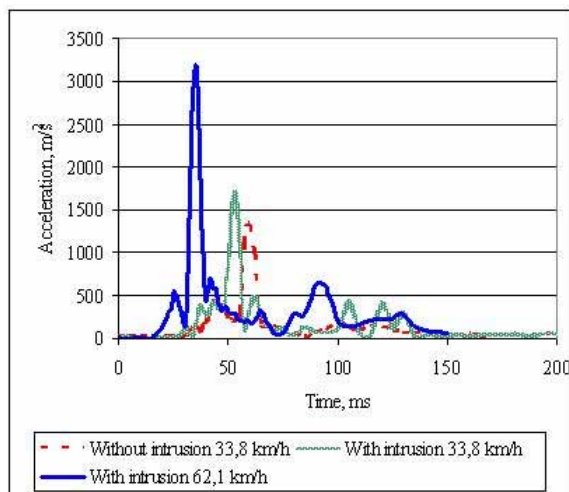


Figure 9. Safety belt installation, with top tether: head acceleration variation.

Thorax acceleration variations show a larger time lag between peaks in this case, probably induced by top

tether's supplementary restraint forces and moment of rotation (figure 10).

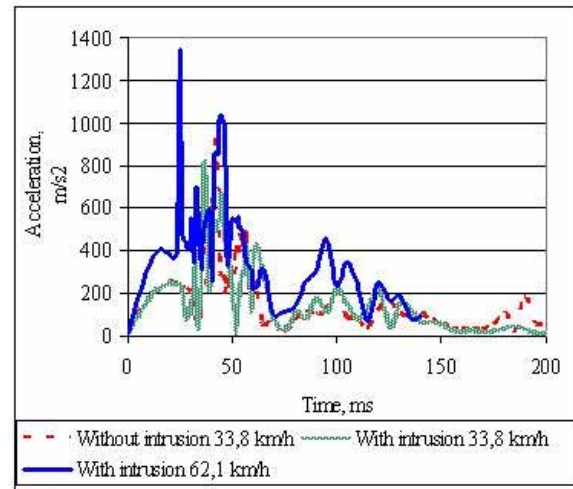


Figure 10. Safety belt installation, with top tether: thorax acceleration variation.

Practically the intrusion has no influence on the thorax deceleration at lower impact speed but an increase of about 40 % can be observed when the impact speed is higher. Thorax deflexion is also proportional to the impact speed but the IARV is not exceeded.

Intrusion generally gives now an increase of all neck injury parameters, probably caused by the top tether which induces supplementary restraint forces that make possible a larger head rebound. The IARV is exceeded especially for the extension neck predictors in the case of 62.1 km/h side impact.

In conclusion, when the child restraint is installed using vehicle safety belts, the intrusion causes lethal head injuries to the child occupant and serious injuries for the chest and the neck.

Lower anchorage belt system and rigid ISOFIX installations

The comparative results of the simulations at 33.8 km/h side impact speed, without and with intrusion, when the child restraint system is installed using lower belts and rigid ISOFIX system, are presented in table 5 and 6 and figures 11 to 14.

The intrusion influence is very important for the head injury criteria, especially for lower belt anchorages. The IARV's are exceeded for lower belt anchorages with 200% increase for the HIC unlimited and a 500 % increase for the HIC15. When ISOFIX anchorages are used, only the HIC15 is higher than the allowed limit. Head maximal acceleration is almost double for lower belts anchorages when intrusion is simulated

but the influence is not important in the case of ISOFIX anchorages.

Table 5.

Injury parameters comparison, lower anchorage belt system installation, 33.8 km/h impact speed

Parameter	No intrusion	With intrusion	IARV
HIC 15	899	3042	500
HIC	899	3042	1000
Nij TE	1.320	1.657	1
Nij TF	0.475	0.223	1
Nij CE	0.569	0.489	1
Nij CF	0.037	0.196	1
F_z , N	1138	1670	2340
$-F_z$, N	262	619	2120
M_y , Nm	11.3	9.7	-
$-M_y$, Nm	23.7	24.0	-
d_T , mm	10.00	11.38	34
a_T , m/s^2	578	696	540 / 589
a_H , m/s^2	1266	2239	-

Table 6.

Injury parameters comparison, rigid ISOFIX installation, 33.8 km/h impact speed

Parameter	No intrusion	With intrusion	IARV
HIC 15	379	859	500
HIC	379	915	1000
Nij TE	1747	1.849	1
Nij TF	0.370	0.552	1
Nij CE	0.197	0.738	1
Nij CF	0.199	0.400	1
F_z , N	1059	1783	2340
$-F_z$, N	106	835	2120
M_y , Nm	13.7	9.9	-
$-M_y$, Nm	37.6	35.7	-
d_T , mm	12.75	14.96	34
a_T , m/s^2	848	728	540 / 589
a_H , m/s^2	919	1149	-

The head acceleration variations show a small time lag for the case of lower belts installation (figure 11). The main peaks coincide for ISOFIX installation but the intrusion gives a second pronounced peak that corresponds to the second impact between dummy head and the door panel. The first peak is related to the primary contact between dummy head and door panel surface. The second impact is caused by the rigidity of the ISOFIX anchorages that forces the child dummy to remain in the vicinity of the deformed door panel and to bend forward, entering

into contact again with the deformed door panel front surface (figure 12).

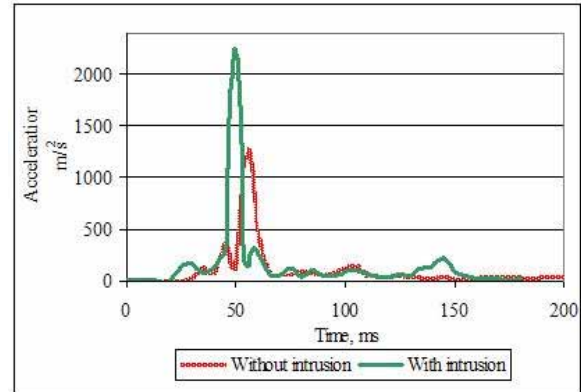


Figure 11. Lower anchorage belt system installation: head acceleration variation.

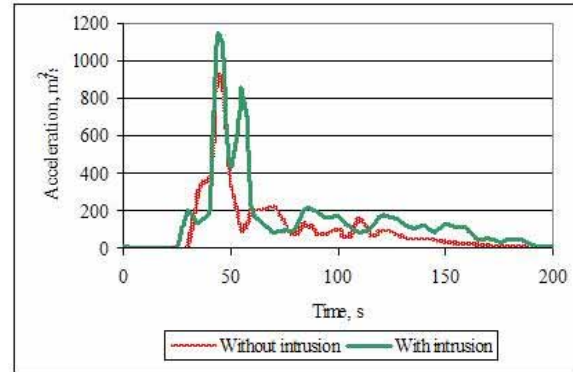


Figure 12. Rigid ISOFIX installation: head acceleration variation.

Thorax acceleration variation curves show some time lag, especially for the case of lower belts installation, and some fluctuations occur too (figure 13 and 14).

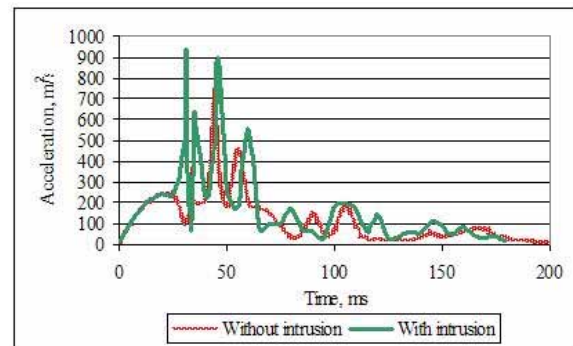


Figure 13. Lower anchorage belt system installation: thorax acceleration variation.

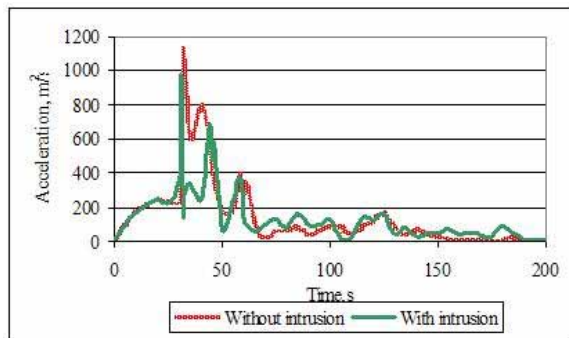


Figure 14. Rigid ISOFIX installation: thorax acceleration variation.

Thorax deceleration is less influenced by the intrusion but the IARV's are almost always exceeded. The increase in thorax deflection when the intrusion is considered is minor and the IARV is not exceeded.

Intrusion causes increase of neck forces, which are very important in the case of ISOFIX anchorages installation but the results are still within the allowed limits. Neck moments are not clearly influenced by the intrusion. Neck biomechanical injury predictors are larger for the ISOFIX installation when intrusion is considered but the trend is not clear for lower belts anchorages installations and the IARV is exceeded only in tension-extension.

In conclusion, when the child restraint is installed using lower belts anchorages or ISOFIX anchorages, the intrusion causes large increase of the head injury criteria, more pronounced for lower belts installation. Thorax and neck injury parameters are less influenced by intrusion.

CONCLUSIONS

This project was aimed at the development of a numerical method to evaluate the intrusion influence in the case of the simulation of vehicle side impact. Child restraint system and vehicle body model have been built using multi-body technique combined with the finite element method, to allow for a better representation of the contacts between the child dummy, the restraining device and the structure of the vehicle and to make possible the simulation of the vehicle body deformation, based on available side impact test data. The model was evaluated against similar test results and simulations results were generally in agreement with the experimental data. When the child restraint system is installed using vehicle safety belts, the intrusion influence is very important for the head injury parameters, the results being much higher than in the case when the

intrusion is not considered. The peak is reached sooner when the intrusion is considered, being related to the moment when the child dummy's head hits the door panel. Thorax deceleration is also influenced by intrusion but here the differences are smaller, especially when the top tether is used. The time lag for thorax acceleration is less pronounced than for head acceleration, because it is more related to the restraint forces in the belts and harness than to the impact between the child dummy and the vehicle body. However, when the top tether is used, the time lag between peaks is larger, probably because of the top tether's supplementary restraint forces and supplementary induced moment of rotation. Thorax deflexion is also proportional to the impact speed. Neck injury parameters are increased when the top tether is used and the intrusion is considered, probably due to the supplementary restraint forces that make possible a larger head rebound. In the case of lower belts and ISOFIX installation, intrusion increases the head injury criteria, more pronounced for lower belts installation. Head maximal acceleration is almost double for lower belts anchorages when intrusion is considered but the influence is not important for the case of ISOFIX anchorages. The head acceleration variations show a small time lag in the case of lower belts installation. The main peaks coincide for ISOFIX installation but the intrusion causes a second pronounced peak that corresponds to the second impact between dummy head and the door panel. Thorax deceleration and thorax deflection are less influenced by the intrusion. Thorax acceleration variation curves show some time lag, especially for the case of lower belts installation, and the curves also show some fluctuations when the intrusion is considered. Intrusion also increases neck forces, which are very important in the case of ISOFIX anchorages installation. Neck biomechanical injury predictors are higher for the ISOFIX installation when intrusion is considered. The model is now offering a lot of possibilities of improvement, development and exploitation and other developments aim to evaluate different child dummies responses in the case of various side impact and frontal collision configurations.

REFERENCES

Howard, A., Rothman, L., Moses McKeag, A., Pazmino – Canizares, J., German, A., Monk, B., Comeau, J.L., Hale, I., Mills, D. and Blazeski, S. 2003. "Children in Side Impact Motor Vehicle Crashes: Seating Position and Injury Mechanism." Proceedings of the Canadian Multidisciplinary Road Safety Conference XIII, Banff, Canada

Monclus-Gonzales, J., Eskandarian, A., Takatori, O. and Morimoto, J. 2001. "Development of Detailed Finite Element Models of Child Restraint System for Occupant Protection." Paper Number 126, 17th International Technical Conference on the Enhanced Safety of Vehicles, Amsterdam, Netherlands

National Highway Traffic Safety Administration. 1999. "New Car Assessment Program Side Impact Test Pontiac Grand AM 1999 Final Report. Report number SNCAP-CAL-99-03."
<http://www-nrd.nhtsa.dot.gov/database/nrd-11/asp/VehicleInfo.asp>

National Highway Traffic Safety Administration, Office of Regulatory Analysis and Evaluation Plans and Policy. 2002. "Preliminary Economic Assessment, Advanced Notice of Proposed Rulemaking (ANPRM) To Add A Side Impact Test to FMVSS No. 213."
<http://www.nhtsa.dot.gov/cars/rules/rulings/CPSUpgrade/CPSSide/PEA/toeI>

NHTSA Vehicle Crash Test Database,
<http://www-nrd.nhtsa.dot.gov/database/nrd-11/asp/TestTableDetails.asp?LJC=3629>

Stern, S.D. 1998. "Child Restraint Information in the National Automotive Sampling System Crashworthiness Data System." Paper No. 98-S10-O-21, p. 2306-2309, 16th International Technical Conference on the Enhanced Safety of Vehicles, Windsor, Canada

Sullivan, L.K., Willke, D.T., Brunner, J. 2001. "Comparison of European and U.S. Child Restraints in Lateral Grand AM Sled Tests." National Highway Traffic Safety Administration Vehicle Research and Test Center
http://dmses.dot.gov/docimages/pdf81/165824_web.pdf

TNO Automotive. 2003. "MADYMO Application Manual Version 6.1." Delft, Netherlands

TNO Automotive. 2003. "MADYMO Database Manual Version 6.1." Delft, Netherlands

Zaouk, A., Marzougui, D. and Kan C.D. 1998. "Development of a Detailed Vehicle Finite Element Model, Part I: Model Development." The 1st International Conference for the IJC, Detroit, MI, USA

THREE YEARS OLD CHILD NECK FINITE ELEMENT MODELISATION

Raphaël Dupuis
Frank Meyer
Rémy Willinger
Université Louis Pasteur
France
Paper Number 05-0081

ABSTRACT

Despite of recent progresses in occupant safety, the protection of children are not still optimal. To offer a better understanding of child injury mechanisms, the present study proposes a human-like finite element model of a three years old child's neck. The subject was scanned with a medical scanner. The images were first semi-automatically segmented in order to extract the soft tissues and the bones. In the second step, we separate the different bones slice by slice on the geometry previously reconstructed. The anatomic structures are identified and each vertebra is reconstructed independently with special attention for the articular process. In a second step, we have generated a original meshing on the previous geometry to obtain a finite element model of the child's neck. The anatomical structures incorporated are the head, the seven cervical vertebrae (C1–C7), the first thoracic vertebra (T1), the intervertebral discs and the principle ligaments which are modelled using non-linear shock-absorbing spring elements. The stiffness values used are taken from literature, and scaled down using scale factors from Irwin. This model incorporates 7340 shell elements to model the eight vertebrae, the head and 1068 solid 8-node elements to model the intervertebral discs. Contact between the articular surfaces is represented by interfaces permitting frictionless movement. Since this study does not aim to reproduce bone fractures, we have modelled the cervical vertebrae as rigid bodies.

A scaling factor for the intervertebral discs modulus of 0,705 is supposed by Yoganandan for the 3 year old child, this values conduce to disc modulus of the order of 100 MPa.

Given that validation data were not available, the model validation was conduced against Q3 dummy component sled tests. The accelerometric responses of the head model were similar with those recorded experimentally with a Q3 dummy neck in rearward, frontal and lateral impact direction.

INTRODUCTION

Each year, more than 700 children are killed on European roads and 80.000 are injured. The EC project CHILD (Child Injury Led Design) aims to improve the protection offered to children in cars by increasing the understanding about the injuries sustained and providing innovative tools and methods for improvement of Child Restraint Systems (CRS) in cars.

One of the tools developed is a three year old child head and neck finite element model. If some models are existing in the literature like Van Ratingen's [1] or Yoganandan's [2] model, they differ largely in term of purpose and methodology.

Multi-body Child Neck Model

Child multi-body neck finite element models are mainly models developed under MADYMO. Thus, TNO developed 3, 4, 5, 6, 8, 10 and 12 year old child models usable in automotive crash test reconstruction. The models are carried out by the assembly of cylinders, ellipsoids, parallelepipeds connected to each other by joints with one or more degrees of freedom and different stiffness according to mobility.

The models were validated by reproducing the tests carried out on Q serie dummies. A scaling was conduced on corridors resulting from the tests on volunteers and PMHS carried out by Mertz and Patrick [3] and Patrick and Chou [4]. Corridors of validation [1, 5] were then considered as the reference for the child (see figure 1).

The three year old child MADYMO model is most recent child model. It was developed by TNO in parallel of the Q3 dummy. Its validation was conduced within the framework of the EC CREST project. The Q3 model is directly issued from the dummy CAD. The head/neck elements were similar to those of the dummy.

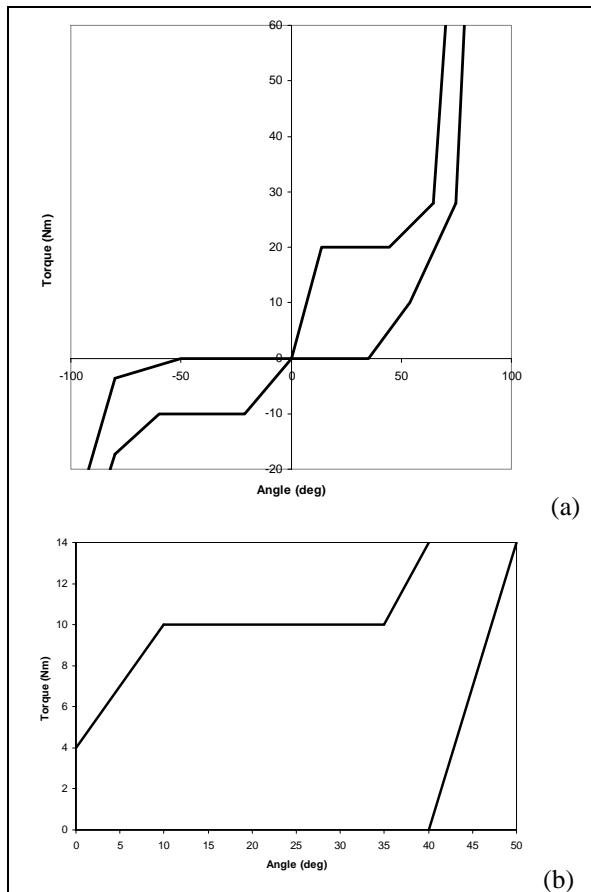


Figure 1. Corridor of behaviour of the Q3 neck dummy in term of moment/angle of flexion in flexion/extension (a) and lateral inflection (b) [1].

The validation was carried out by reproducing tests on the model similarly as previously realised on Q3 in frontal, rearward, lateral direction and of pendulum test. The stiffness and the damping coefficients of the various articulations were then tuned to adjust the dummy response.

Detailed Finite Element Models

Only two child human like cervical spine models were founded in the literature.

The first was that developed by Kumaresan and Yoganandan [2]. They developed three finite element models for three different ages: 1, 3 and 6 years. These models were limited to the cervical C4-C6 segment and resulted directly from the adult model [6-8]. It has to be noticed that this adult model was developed in order to realize static simulations. Three types of model construction were adopted: first a pure geometrical scaling, then the introduction of anatomical specificities without any scaling, and finally a method where the two preceding approaches were combined.

This first approach consisted in a pure geometrical scaling of the adult finite element model. No geometrical modification and no

anatomical specificity according to the age were introduced in the model. Comprehensive laws of the ligaments and the discs were not scaled, but maintained similar to those of adult.

For calculation and meshing reasons (divergence of the model), it was impossible to conduce a "scaling down" of the model, i.e. a scaling factor lower than 1. In order to solve this problem, they decided to realize a "scaling up" at 120%, 140%, 160% and 180%. The results were then extrapolated by supposing that the answer is linear according to the coefficient of scale and thus of the age.

With this methodology, they decided not to apply any scale factor to the geometry of the adult. Its dimensions were thus identical to those of the adult. In the other hand, some modifications of the mechanical characteristics of different the component was applied according to the age (see table 1).

Table 1.

Description of the geometrical specifications incorporated by Kumaresan [2] in the Yoganandan's adult model according to the age.

	1 year old	3 year old	6 year old
Spinous process	Growth cartilage present	Fused	Fused
Transvers process	Costal growth cartilage present	Costal growth cartilage present	Costal growth cartilage fused
Neuro-central cartilage	Present	Present	Missing
Growth cartilages of superior and inferior plate	Presents	Presents	Presents
Articular facets angle	60°	53°	48°
Unciform apophysis	Missing	Missing	Missing
Discal fiber percentage reported to the adult	80%	85%	90%
Nucleus volume compared to disc volume	90%	85%	80% (idem as adult)
Ligamentar stiffness compared to the adult's	80%	85%	90%

It should be noted that all anatomical specificities integrated in the finite element model result directly from medical observations. The ligament stiffness or the volume of nucleus were selected to study the influence of these parameters.

In this last approach, Kumaresan [2] coupled the two preceding approaches, i.e. to carry out a geometrical scaling, to modify the mechanical characteristics of the ligaments and discs, and to integrate anatomical specificities according to the age.

The comparison of the three types of models was done in static by applying either a compressive force (100N and 400N), or a couple (0,25Nm and 1Nm) at the top of C4, and by measuring the variation of principal mobility compared to that of the adult.

It appeared that there was a rigidification of the rachidian segment studied according to the age, the 1 year old child being much more flexible than the 6 year old child. Moreover, it has been noticed that the independent parameters which lead to the strongest increase in mobility were anatomical specificities and new comprehensive laws (approach 2), rather than simple dimensional scaling (approach 1), the combination of the two approaches (approach 3) being that which increased more mobility.

Nevertheless, even if the tendencies observed seemed to be in conformity with the experiment results on animals [9, 10], no experimentation on child is available to validate these results quantitatively, limitation which the authors concede readily. Even if these models were finally not validated, it should be retained that the inclusion of geometrical specificities of the child can offer comprehension of the injury mechanisms.

The other three year old child finite element model founded was that developed by Mizuno [11] by scaling from a Total Human Model for Safety (THUMS) AM50human finite element model to investigate the potential injury risks from restraints. The geometrical scaling factors were chosen so that λ_x , λ_y , λ_z have values as similar as possible, and the material properties scaling factors were determined in the literature [12, 13]. The model has been validated for thorax impact according to Hybrid III 3YO dummy requirements. No information are available on neck validation.

MATERIAL AND METHODS

Geometrical reference

A three year old male child was scanned with a ELSCINT Helix 3.0 (Elscint Ltd., Ma'alot, Israel) scanner, in order to realize a medical exam. The

slice thickness was 1.1 mm with a table feed of 1 mm (pitch 0.9). After insuring that no abnormality was detected, and after depersonalising the exam, the images were first semi-automatically segmented in order to extract skin and bones. This stage was conducted at IRCAD from software developed in partnership with the Epidaure project of INRIA for the automatic 3D patient reconstruction [14-16], and provided us a rapid and precise result [17] but no differentiation between the vertebrae was obtained (see figure 2).



Figure 2. Fully automatic reconstruction of the spine. All vertebrae are virtually stuck together, due to little thickness of the intra articular space..

In a second step, we separated the different bones slice by slice on the previously reconstructed model. Anatomical structures were identified (specifically the articular process) and each bone (i.e. the seven cervical vertebrae, the inferior part of the skull and the mandible) was reconstructed individually (see figure 3). The whole model was exported into a VRML format to be readable on any computer with freeware. The physical bone model was obtained using the FDM (fused deposition modelling) technology on a Prodigy Plus machine (Stratasys Inc., Eden Prairie, MN). The physical model realized in ABS polymer (see figure 4) was strong and durable, and the model accuracy compared with CT scan slices was inferior to 0.8 mm on the main dimensions.

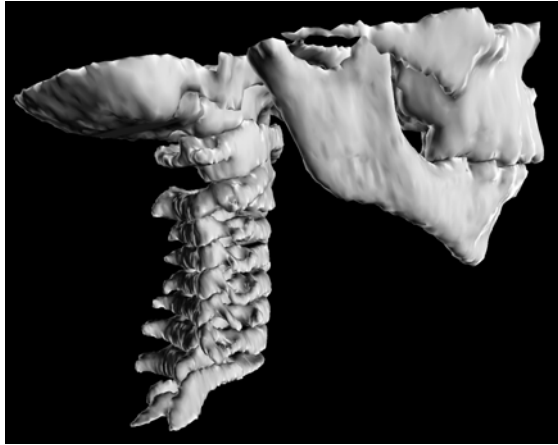


Figure 3. Complete reconstruction of the cervical spine of a three year old child: front and right view. All bones are separated and can be visualized independently.

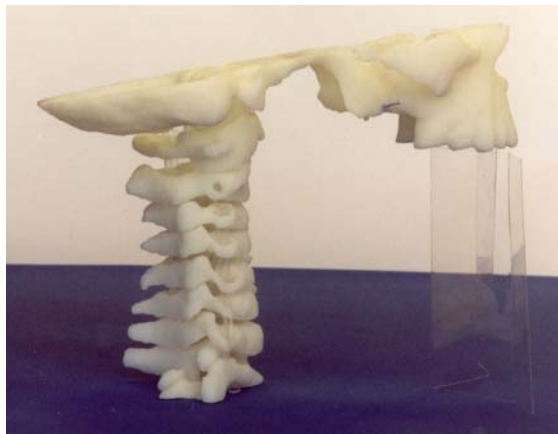


Figure 4. Physical model of the cervical spine of a three year old child. Global lateral view including skull base (C0).

Finite element modeling

In order to stick to our geometrical reference, we deformed and remeshed the geometrical meshing of an existing adult model [18]. The anatomical structures incorporated and illustrated in figures 5 to 8 are the head, the seven cervical vertebrae (C1–C7), the first thoracic vertebra (T1), the intervertebral discs and the principle ligaments, including the anterior longitudinal ligament (ALL), anterior-atlanto occipital membrane (AA-OM), posterior-atlanto occipital membrane (PA-OM), tectorial membrane (TM), posterior longitudinal ligament (PLL), flavum ligament (LF), supraspinous ligament, interspinous ligament (ISL), transverse ligament (TL), alar ligament (AL), capsular ligaments (CL) and the apical ligament (APL).

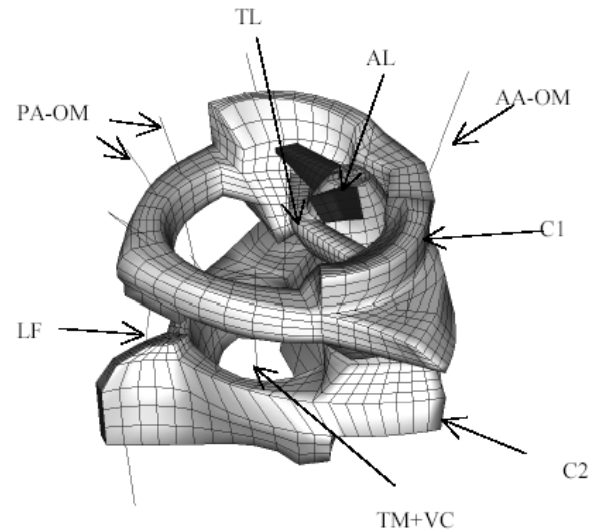


Figure 5. Ligamentary system of the upper cervical spine (C1-C2).

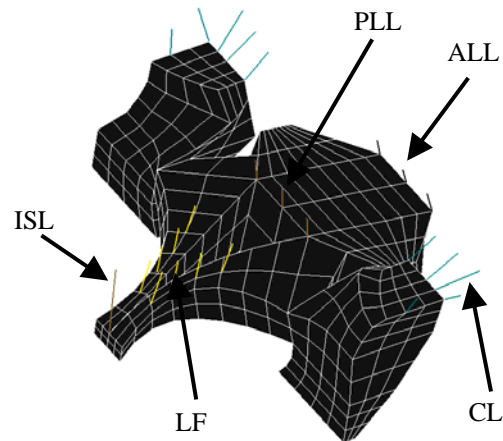


Figure 6. Ligamentary system of the lower cervical spine (C3).

These are modelled using non-linear shock-absorbing spring elements. The behaviour laws of each ligament in both the lower and upper cervical spines, are defined by referencing to three complementary studies: Myklebust [19], Chazal et al. [20] and Yoganandan et al. [21]. The Chazal et al. study [20] highlights the non-linear viscoelastic behavior of ligaments whereas Yoganandan et al. [21] gives information on their failure properties. The overall behavior of the ligaments can then be characterized by three pairs of coefficients α_1 , α_2 , α_3 determining the zone of low rigidity or neutral zone, the linear part, and finally the plastic behavior. The coefficients used for our model are described in Table 2 and a representation of the typical behavior of the five ligaments of the lower cervical spine is illustrated in figure 9.

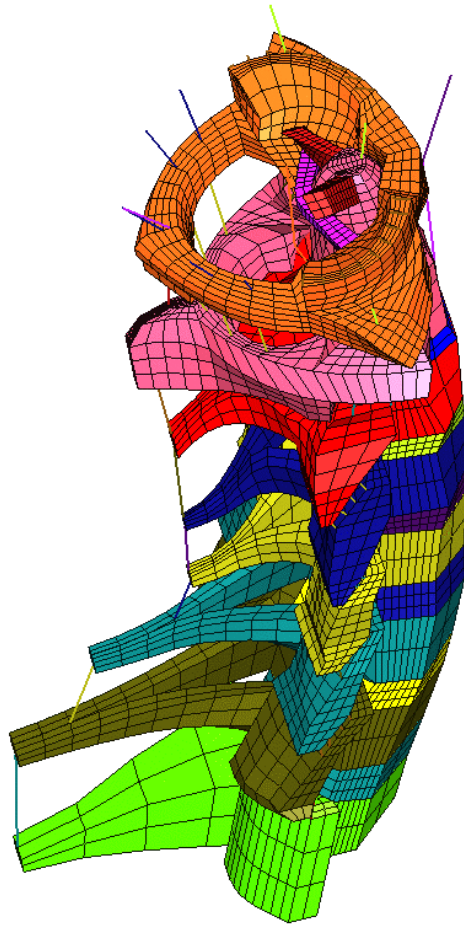


Figure 7. Surface meshing of the cervical spine (C1-T1), including its ligamentary system.

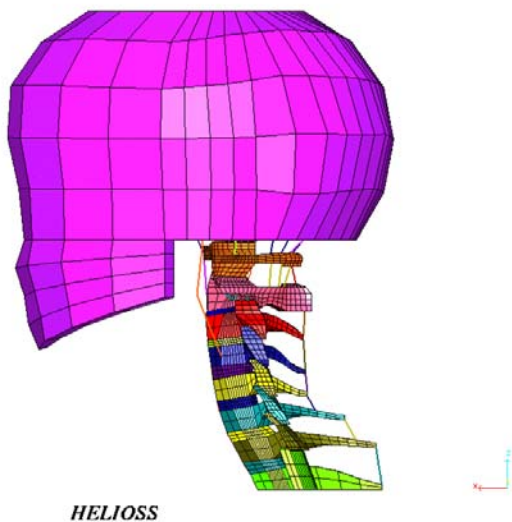


Figure 8. Complete finite element model of the head and neck complex of a three year old child.

Table 2.
Coefficients used to define the ligaments constitutive laws [20]. The rupture strengths are taken from Myklebust [19].

	A (α_1)		B (α_2)		C (α_3)
	$\varepsilon/\varepsilon_{\max}$	F/F_{\max}	$\varepsilon/\varepsilon_{\max}$	F/F_{\max}	ε_{\max}
ALL	0,21	0,11	0,78	0,87	0,58
PLL	0,25	0,12	0,77	0,89	0,45
FL	0,28	0,21	0,76	0,88	0,21
ISL	0,3	0,17	0,75	0,87	0,4
CL	0,26	0,15	0,76	0,88	0,41

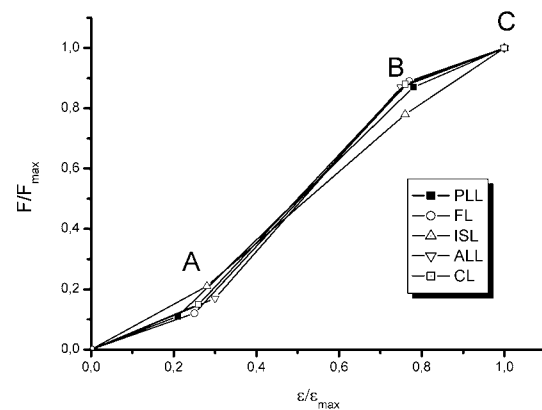


Figure 9. Behaviour laws of the anterior longitudinal ligament (ALL C2-C5), posterior longitudinal ligament (PLL C2-C5), flaval ligament (FL C2-C5), interspinous ligament (ISL C2-C5), capsular ligament (CL C2-C5) [20, 21].

In order to take into account the initial lengths of the ligaments in the model as well as those measured anatomically by Yoganandan et al. on the lower cervical spine [21] we calculated the laws as follows :

$$\begin{cases} d_i = L_0 * \alpha_{\max} * \alpha_i \\ F_i = F_{\max} * \alpha_i \end{cases} \quad i = 1, 2, 3 .$$

Where L_0 is the initial length of the ligament and d_i its deformation.

According to Irwin [12] and Yoganandan [25] scaling factors, all ligament behaviour laws were scaled in term of force.

The total height of the model is 17,3 cm and its weight is 4,57 kg. This model incorporates 7340 shell elements to model the eight vertebrae, the head and 1068 solid 8-node elements to model the intervertebral discs. Contact between the articular surfaces is represented by interfaces permitting frictionless movement. Since this study does not aim to reproduce bone fractures, we have modelled the cervical vertebrae as rigid bodies, taking their

inertial moments and masses from Deng [22] and scaled down using scale factors from Irwin [12] (see table 3).

Table 3.
Cervical vertebrae inertial properties applied to the center of gravity.

Name	Mass [g]	Ixx [g.mm ² * 10 ⁴]	Iyy [g.m ² * 10 ⁴]	Izz [g.m ² * 10 ⁴]
T1	78.5	0.846	0.626	0.129
C7	58	0.763	0.328	0.965
C6	58	0.763	0.328	0.965
C5	50	0.636	0.210	0.753
C4	56	0.773	0.221	0.897
C3	70	0.816	0.325	1.01
C2	86	0.902	0.662	1.24
C1	57	1.28	0.36	1.58

Most models use an elastic law for the intervertebral discs and a wide range of Young's modulus values has been observed, varying from 3,4 MPa in Yoganandan's [21] model to 4,3 MPa for that of Golinski [23] and 200 MPa for that of Dauvilliers [24]. A scaling factor of 0,705 given by Yoganandan [25] for the 3 year old child intervertebral disc is supposed, this values conduced to adopt a disc modulus of the order of 100 MPa.

Model validation

Given that validation data in term of acceleration were not available and that sled tests were only realized on full complete dummy, we were obliged to realize some Q3 dummy component sled tests (see figure 10). Therefore, the base of the Q3 dummy neck was fixed on the sled. A set of three accelerometers was attached to the dummy head to measure linear acceleration. The sled is accelerated in rearward, frontal and lateral direction.

In order to reproduce the experimentation with the numerical model, the model was controlled in terms of first thoracic vertebra speed (see figure 11 and 12).



Figure 10. Q3 dummy component sled test on head and neck.

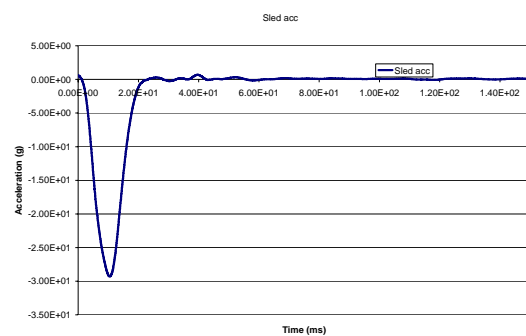


Figure 11. Sled acceleration in frontal impact.

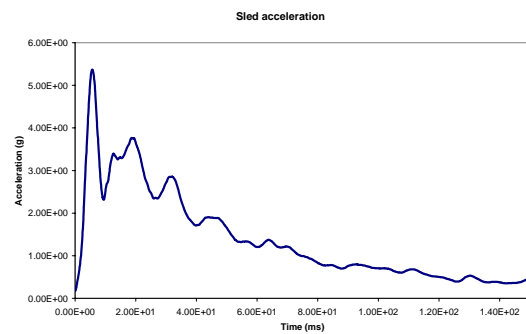


Figure 12. Sled acceleration in rearward impact..

Head linear acceleration values were computed and compared with those recorded experimentally.

RESULTS

The parameters of the model has been tuned in order to fit to the experimental results as shown in figure 13 and 14 for rearward impact, and in figure 15 and 16 for frontal impact. The results in lateral impact hasn't been presented as it will be discussed later.

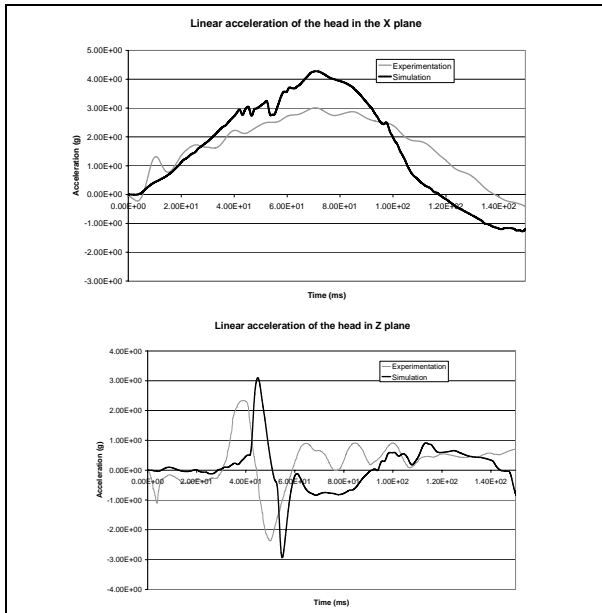


Figure 13. Linear acceleration of accelerometers in rearward impact: experimental data vs. numerical results.

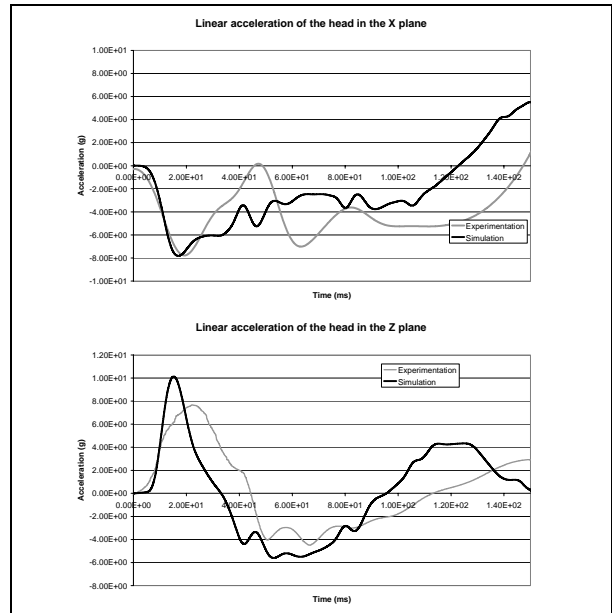


Figure 15. Linear acceleration of accelerometers in frontal impact: experimental data vs. numerical results.

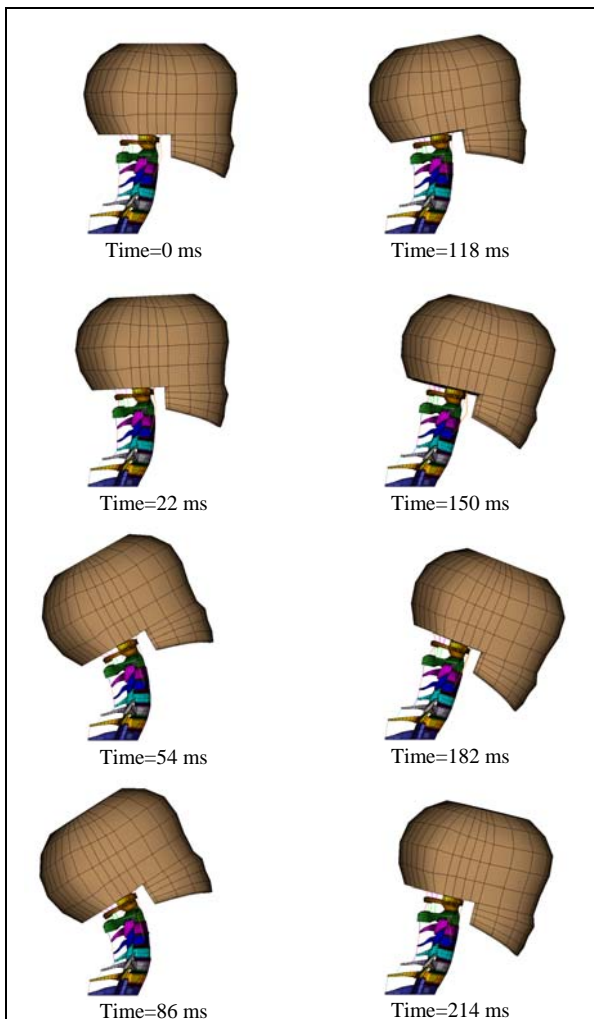


Figure 14. Model configurations in rearward impact

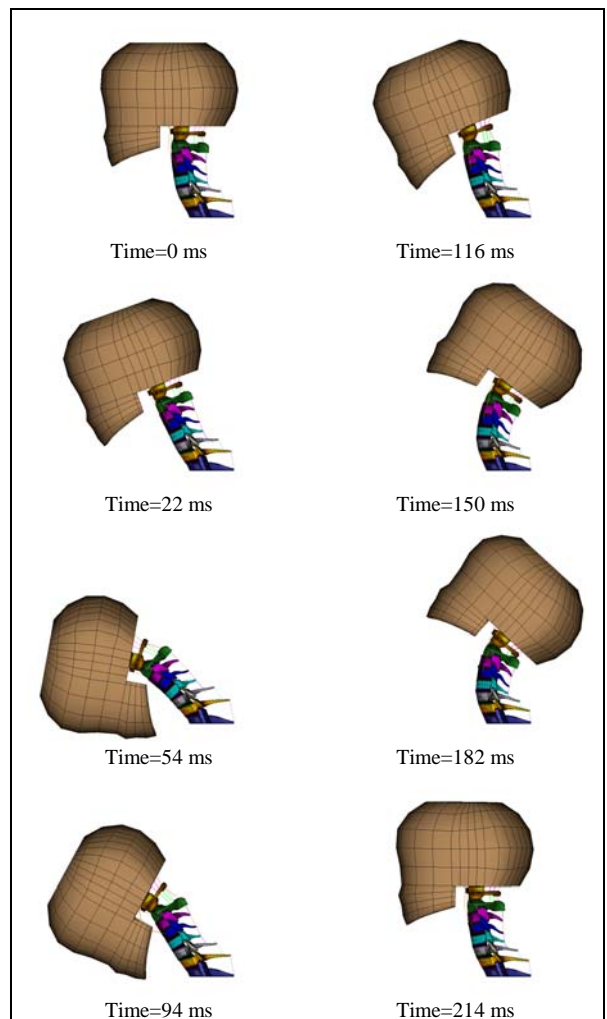


Figure 16. Model configurations in frontal impact

It can be observed that in rearward impact, the model correctly reproduce the acceleration of the head dummy center of gravity. The first peak amplitude present a good correlation in both the X axis and in the Z axis. The temporal position of this peak is also very near to the experimental's, with a little late on the Z axis.

In frontal impact, we can notice that in the first milliseconds after impact, the experimental and numerical curves are completely superposed, and that the peak amplitude is similar for the X axis.

However, the parameter set is not suitable to reproduce the behaviour in lateral impact. Indeed, if the results in term of acceleration are correct among X and Y axis during the first fifty milliseconds, the acceleration in Z direction is incorrect. No parameter set has been founded to reproduce at the same time the Q3 neck dummy comportment in frontal and rearward impact, and in lateral impact

DISCUSSION

The main discussion concerning the method is the validation of the model with regards to a dummy. In fact, no in-vitro or in-vivo experimentation on children neck has never been conducted. The data usable for infant finite element model validation are never "first hand" data, but only obtained by scaling adult results. The scaling coefficient of mechanical properties are based on three in-vitro tests (2 newborns and a 6 year old child) on parietal bone. With the inter-individual variation on human mechanical properties, we can wonder about the credibility of these scaling factors. That's why we decided to use the Q3 dummy as reference, because it proved its reliability in accident reconstructions that offers good correlation with injuries (EC CREST and CHILD program). We can notice that the methodology used by Mizuno [11] to validate its three year old child model is the same, even if it was on the torso. All this comfort us about our method.

The choice of the geometrical reference to realize our finite element model meshing can also be discussed. The medical scanner was realized on a three year old child, and because of anonymisation procedure, we didn't have information about its corpulence (weight, height...). However, it appeared us that it was a better solution to remesh a geometrical reference, than to apply a pure scaling on an adult model, moreover with similar scaling factor in the three direction as made Mizuno [11].

CONCLUSION

A three year old child human like neck finite element model was developed, based on a three

year old child medical scanner. The model include intervertebral discs and almost all intervertebral ligaments. It was compared with Q3 dummy neck that was validated with regards to scaled NDBL corridors. The three year old child neck finite element model validation was performed in frontal and in rearward impact. The model will be used for accident reconstruction in order to evaluate local injuries and to provide basis for injury criteria.

ACKNOWLEDGEMENTS

The authors would like to acknowledge the efforts of INRETS for their contribution in the validation of the three year old child neck finite element model.

The development and the validation of the model was funded by the European Community under the G3RD-CT-2002-00791 CHILD project.

REFERENCES

- [1] Ratingen, M. R. van; Twisk, D.; Schrooten, M.; Beusenberg, M. C.; Barnes, A.; Platten, G. 1997. "Biomechanically based design and performance targets for a 3-year old child crash dummy for frontal and side impact". Proc. 26th STAPP Car Crash Conf.: 243-260
- [2] Kumaresan, S.; Yoganandan, N.; Pintar, F. A. 1997. "Age specific pediatric cervical spine biomechanical responses: three dimensional nonlinear finite element models." Proc. 26th STAPP Car Crash Conf.: 31-61
- [3] Mertz, H. J. and Patrick, L. M. 1971. "Strength and response of the human neck." SAE710955.
- [4] Patrick, L. M. and Chou, . 1976. "Response of the human neck in flexion, extension and lateral flexion." VRI-7-3. Society of Automobile Engineers.
- [5] Lange, R. de; Made, R. van der; Feustel, J.R.; Subbian, T.; Hoof, J. van. 2001. "Development and evaluation of MADYMO child occupant dummy models". 4th North American MADYMO User's Meeting.
- [6] Yoganandan, N.; Kumaresan, S.; Voo, L.; Pintar, F. A.; Larson, S. 1996. "Finite element modeling of the C4-C6 cervical spine unit." Medical Engineering & Physics, 18 (7): 569-574.
- [7] Yoganandan, N.; Kumaresan, S.; Voo, L.; Pintar, F. A. 1997. "Finite element model of the human lower cervical spine." Journal of Biomechanical Engineering, 119 (1): 87-92.
- [8] Kumaresan, S.; Yoganandan, N.; Pintar, F. A. 1997. "Validation of nonlinear finite element model of human lower cervical spine." ASME Winter Bioengineering Conference, Dallas, TX, Nov: 16-21.
- [9] Mertz, H. J.; Driscoll G. D.; Lenox J.B.; Nyquist G.W.; Weber D.A. 1982. "Responses of

animals exposed to deployment of various passenger inflatable restraint system concepts for a variety of collision severities and animal positions.” Proc 9th International technical Conf on Experimental Safety vehicles, Kyoto, Japan.

[10] Prasad, D.; Daniel, R.P. 1984. “A biomechanical analysis of head, neck, and torso injuries to child surrogates due to sudden torso acceleration.” Proc 28th Stapp Car Crash Conf, Chicago, IL, Society of Automobile Engineers, 25-40.

[11] Mizuno, K.; Deguchi, T.; Furukawa, K.; Miki, K. 2004. “Development of three-year-old child human FE model.” IRCOBI Conference, Graz, September 335-336.

[12] Irwin, A.; Mertz, H.J. 1997. “Biomechanical basis for the CRABI and Hybrid III Child Dummies”, Proc. 26th STAPP Car Crash Conf.: 261-272.

[13] Curry, J. D.; Butler, G. 1975. “The mechanical properties of bone tissues in children.” *J. Bone and Joint Surg.* 57A, 6:810-814.

[14] Ayache, N. 1995. “Medical computer vision, virtual reality and robotics.” *Image and Vision Computing.* 13(4):295-313.

[15] Kass, M.; Witkin, A.; Terzopoulos, D. 1988. “Snakes: active contour models.” *International Journal of Computer Vision.* 1:321-31.

[16] Cotin, S.; Delingette, H.; Bro-Nielsen, M. 1996. “Geometric and physical representation for a simulator of hepatic surgery.” In: Weghorst SJ, Sieburg HB, Morgan KS, editors. *Health care in the information age. Future tools for transforming medicine. Medicine meets virtual reality: 4, studies of health technology and informatics* 29. Amsterdam, Oxford, Tokyo, Washington: IOS Press. 139-51.

[17] Soler, L.; Delingette, H.; Malandain, G.; et al. 2001. “Fully automatic anatomical, pathological, and functional segmentation from CT scans for hepatic surgery.” *Computer Aided Surgery.* 6(3):131-42.

[18] Meyer, F.; Willinger, R.; Legall, F. 2004. “The importance of modal validation for biomechanical models, demonstrated by application to the cervical spine.” *Finite Elements in Analysis and Design* 40: 1835–1855.

[19] Myklebust, J.; Pintar, F.; Yoganandan, N.; Cusick, J.; Maiman, D.; Myers, T.; Sances, A. 1988. “Tensile strength of spinal ligaments.” *Spine* 13 (5): 526–531.

[20] Chazal, J.; Tanguy, A.; Bourges, M.; Gaurel, G.; Escande, G.; Guillot, M.; Vanneuville, G. 1985. “Biomechanical properties of spinal ligaments and a histological study of the supraspinal ligament in traction.” *J. Biomech.* 18 (3): 167–176.

[21] Yoganandan, N.; Kumaresan, S.; Pintar, F. 2000. “Biomechanics of the cervical spine Part 2. Cervical spine soft tissue responses and

biomechanical modeling.” *Clinical Biomech.* 16: 1–27.

[22] Deng, Y.-C.; Goldsmith, W. 1987. “Response of a human head/neck/upper-torso replica to dynamic loading-II. Analytical/numerical model.” *J. Biomech.* 20 (5): 487–497.

[23] Golinski, W.Z. 2000 “3D-dynamic modelling of the human cervical spine in whiplash situations.” Ph.D. Thesis, Nottingham University.

[24] Dauvilliers, F. 1994. “Modelisation Tridimensionnelle et Dynamique du Rachis Cervical.” Ph.D. Thesis, LBM ENSAM, Paris.

[25] Yoganandan, N.; Pintar, F. A.; Kumaresan, S.; Gennarelli, T. A. 2000. “Pediatric and small female neck injury scale factor and tolerance based on human spine biomechanical characteristic”, IRCOBI Conference, Montpellier, September 21-23.

DEVELOPMENT OF BIOFIDELIC UPPER ARM FOR SID-IIS AND IMPROVEMENT OF THORACIC BIOFIDELITY WITH THIS ARM

Fumio Matsuoka

Mitsutoshi Masuda

Shunichi Katsumata

Toyota Motor Corporation

Japan

Paper Number: 05-0119

ABSTRACT

Side impacts present a severe collision mode from the perspective of occupant protection because there are relatively few vehicle structural components (such as a center pillar and door) and relatively little vehicle crush space exist. In recent years, technology has advanced including enhanced body structural integrity, torso air bags and curtain air bags. Further advances in these technologies are anticipated in the future. A dummy with excellent biofidelity is indispensable for such advanced technical development, and it is reported that the recently developed SID-IIs, exhibits better biofidelity compared with previous side impact dummies ES-1 and DOTSID.

However, when considering the compression characteristic of the upper arm of SID-IIs, it was found that the stiffness is excessively high compared with post mortem human surrogate (PMHS) data. It is thought that this characteristic can have considerable influence on thoracic rib deflection in side impacts because the upper arm transmits force from the door and/or the side airbag to the thorax.

In this study, a new upper arm component for SID-IIs has been developed to provide a better interaction with the thorax rib. According to the ISO guideline of side impact biofidelity evaluation, a series of tests with the new arm were conducted on the dummy.

It was shown that the biofidelity of the dummy with the modified arm, especially its thoracic responses, was improved by replacing the original arm with the newly developed one.

INTRODUCTION

Side impacts are a severe type of collision from the perspective of occupant protection. This is partially due to the fact that in the event of a side impact there are few vehicle structures for absorbing the energy from a side impact and little vehicle crush space in the event of a side impact as compared to other types of collisions.

Side impact tests are generally performed using a moveable deformable barrier (MDB) representing a passenger vehicle, which collide with a vehicle. In order to promote higher degree of occupant protection performance, an impact test using an MDB corresponding to an SUV is used for impact testing. A test method in which the side of a vehicle collides with a fixed pole-shaped object was also developed and put into practice.

Occupant protection technologies have also progressed in recent years, which can be seen by the application of technologies including vehicle structures with superior integrity, as well as curtain and torso side airbags. Further advances in these technologies are anticipated from these technologies in the future. In order to evaluate such new occupant protection technologies, a dummy with high biofidelity and injury measuring capabilities is essential.

The SID-IIs is a side impact dummy representative of a small human female. Development began in 1993 by the Occupant Safety Research Partnership (OSRP) with the intent of adding a high biofidelity dummy representative of small females. In 1995, the dummy was completed, and the structure and characteristics were announced [1]. The biofidelity of the SID-IIs was also evaluated by OSRP, which reported results showing superior biofidelity to other side impact dummies [2]. The evaluation method with target corridors for the biofidelity of side impact dummies is set forth in ISO 9790[3]. However, ISO 9790 defines corridors for the 50th percentile adult male (AM50), not a small female. Thus, a scaled corridor was used by OSRP to evaluate the SID-IIs. The results show a high score of 7.01 out of a total 10 possible points.

Furthermore, ISO 9790 includes biofidelity corridors regarding the head, neck, shoulders, thorax, abdomen, and pelvis. Although ISO 9790 covers most main parts of the body, it is still lacking on some points.

For example, observations of collisions between the dummy and the interior during side impacts and the

constraint posture resulting from the side impact airbag often showed the arms sandwiched between the chest and the door or the airbag. Based on these observations, it is reasonable to assume that arm characteristics influence both the dummy reaction force to the vehicle and dummy internal response. However, current biofidelity evaluations do not define characteristics of the arm itself, and no framework exists for defining the influence of arms from the two aspects mentioned above. Therefore, studying arm characteristics and their influence is considered essential to developing a dummy with higher biofidelity.

According to the literature of SID-IIs development [1], the structure and characteristics of the shoulder and arm of the SID-IIs are summarized as the following.

The shoulder is structured for lateral displacement, and the attached arm takes on a rounder shape than BIOSID with a higher stiffness than EuroSID-1. The arm length is 7 mm shorter than that of the AF05 Hybrid-III dummy, so as not to provoke deformation of the abdominal ribs. A pad corresponding to the height of the upper arm shoulder is used to control the initial impact pulse. The shoulder characteristics target a corridor that scales from the characteristics in ISO 9790.

It is not clear in the description whether the shape and characteristics of the arm itself were compared to an actual human arm.

Research regarding arm characteristics often focus on tolerance and characteristics such as three-point bending. However, there is little research on the lateral compression characteristic of the arm. Kanno (1993) has performed a study to obtain the lateral compression characteristic of the arm [4]. The study used an impactor with 152 mm diameter, 16 kg mass, and speeds of 2 and 4 m/s to impact two PMHS arms, respectively (Figure 1). Fixed to a flat plate, the circumference of these arms was 32cm. The arm's compression characteristic from the 4m/s test is shown (Figure2).

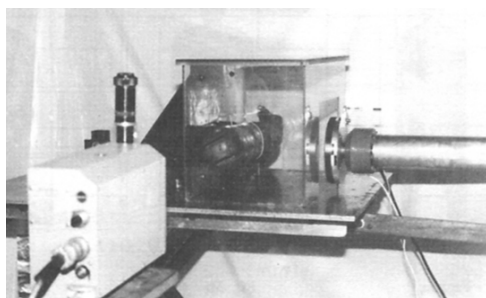


Figure 1. A dummy arm in pre-impact test position, actual tests unembalmed PMHS arms were used [4].

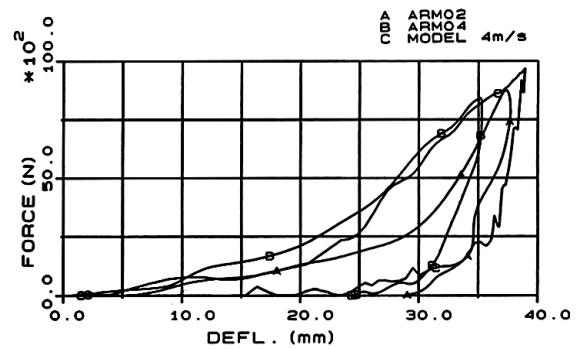


Figure 2. Force-deflection curves of PMHS arms (ARM02, ARM04) for 4m/s pendulum impacts [4].

Recently, another research was conducted at Virginia Tech by Kemper et al (2005) to evaluate the compressive response of human humeri with soft tissue [5]. These compression tests were also performed at 2.0m/s and 4.0m/s loading rates on 4 whole unembalmed fresh human humeri obtained from 2 matched pairs (Table 1) using a drop tower with a 16 kg impactor (Figure 3). The ends of the humeri were constrained in order to prevent the human humeri from rotating or translating during the impact event (Figure 3). The arm was placed on the support with a 152mm diameter and impacted. The arm's characteristics are shown (Figure 4).

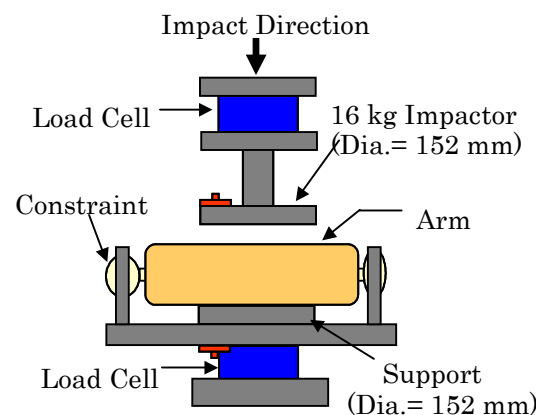


Figure 3. Humerus compression loading test setup (Front View).

Upon comparing the arm characteristics of SID-IIs under similar conditions, it was found that the arm of SID-IIs differed from that of the human (Figure 4).

In light of the above background, this paper explores improvements of the upper arm biofidelity and their influence on the dummy response for SID-IIs. The content of this paper focuses on the following three points: (1) development of an upper arm with excellent biofidelity for use in the SID-IIs; (2) verification of the biofidelity of the SID-IIs dummy in which this arm is used, and (3) determination of the influence on measured dummy injury values when using this arm.

Table 1. PMHS upper arm data for arm compressive tests [5].

Tests ID#	Test Speed (m/s)	Subject Number	Mass (kg)	Height (cm)	Breadth (mm)	Humerus Circumference with soft tissue (cm)
Arm 1	2.00	A	44.81	152.4	55.56	24.13
Arm 2	2.00	B	74.09	160.02	63.5	24.77
Arm 3	4.00	A	44.81	152.4	60.33	24.13
Arm 4	4.00	B	74.09	160.02	58.74	27.31

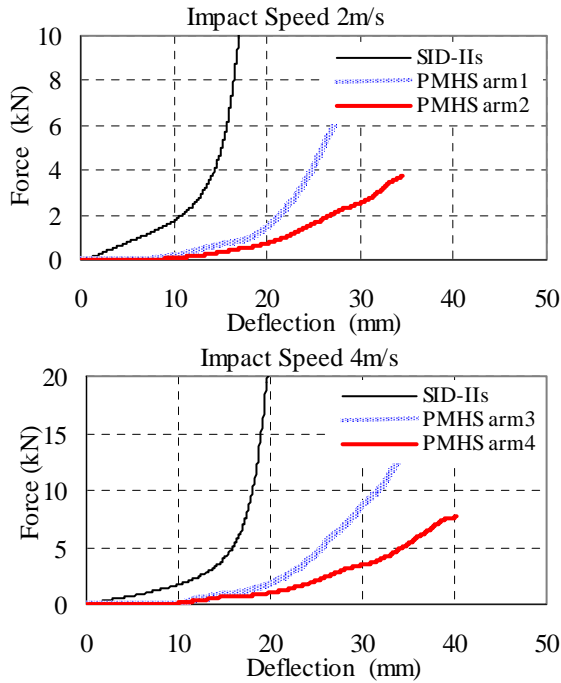


Figure 4. Comparison of Arm Force-deflection Curves Between PMHS and Dummies.

ARM DEVELOPMENT

Arm Design Targets and Test Method

The following items were used as design requirements for the upper arm of the SID-IIs.

Dummy Exterior Shape

The shoulder width dimension of the dummy was not changed.

Human Body Dimensions and Mass

Targets for arm thickness, width, length, and mass were set based upon data for the AF05's upper arm from UMTRI [6] (Table 2).

Upper Arm Lateral Compression Characteristic

The upper arm lateral compression characteristic of dummy was compared to that obtained from the PMHS test performed by Kemper et al. (2005).

Table 2. Dimensions and Mass of SID-IIs and Human Arms (AF05).

Arm	Mass (kg)	Breadth (mm)	Depth (mm)
SID-IIs	0.89	56	74
Human	1.12	67	89

Arm Development and Arm Biofidelity Test (Upper Arm Lateral Compression Characteristic) Results Upper Arm Shape and Mass

The major and minor axes of the elliptical cross section of the arm were matched to human dimensions (UMTRI). However, 9 mm were eliminated from the inner side of the arm. This is because the arm contacts the thorax rib and will not rest alongside the chest when the breadth (minor axis) is set to 67 mm without modifying the shoulder width (Table 3).

Table 3. Improved Arm Dimension and Mass.

Arm	Mass (kg)	Breadth (mm)	Depth (mm)
UMTRI	1.12	67	89
Modified	1.06	58	89
Original	0.89	56	74

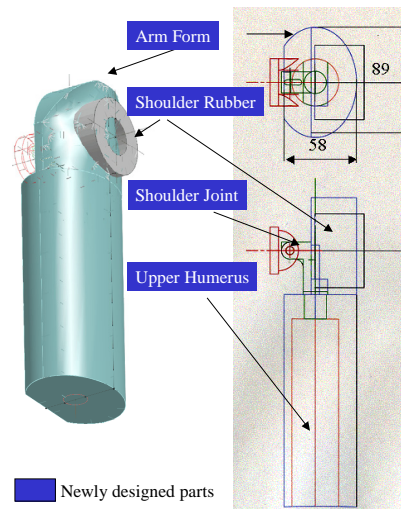


Figure 5. Modified SID-IIs Arm.

The cross section of the steel, representing bone, has a circular shape, and the position of the shoulder joint was displaced outward in order to set the bone at the center of the arm. In order for the arm mass to correspond to that of a human body (UMTRI AF05), the diameter of the steel bone was adjusted (Figure 5).

Selection of Arm Foam Materials

Of the three types of EPDM (ethylene-propylene rubber) arms with different compression characteristics the arm (Modified A) had a compression characteristic closest to the target characteristic was selected (Figure 6). As a result, an arm was developed with characteristics more closely resembling those in a human body than the characteristics of the arm prior to modification.

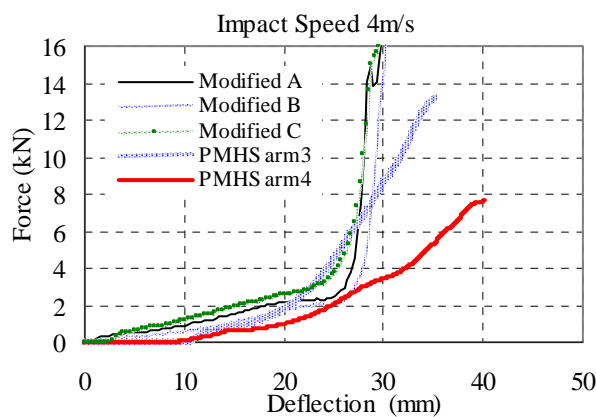


Figure 6. Force-Deflection Responses of Target and EPDM Arm.

DUMMY BIOFIDELITY EVALUATION

Dummy Biofidelity Evaluation Method

Biofidelity tests were performed mainly for the purpose of evaluating the influence of the new arm development on dummy response.

The evaluation method was based on the test method set forth in ISO 9790: 1990 (E) [3], which is employed as a general test method of side impact dummy biofidelity.

However, the small female (AF05) corridor necessary for evaluation is not given in ISO 9790[3]. Therefore, corridors scaled to the AF05 were developed [2] based upon ISO 9790.

Among the ISO test methods, those tests for the neck, shoulder and thorax, which are considered to be most affected by modifications of the arm, were performed. However, the tests listed below were not

conducted because the results are unlikely affected by the arm modifications.

Thorax Tests 1, 2: The test method consists of setting the arm at a 90-degree angle to the thorax and hitting the thorax with a pendulum. Therefore, the arm modifications would have no influence on the results.

Thorax Test 4: The special pad defined for use in this test cannot be obtained at present, thus the test could not be performed.

The tests performed and not performed are shown (Table 4).

Table 4 Biofidelity Test Matrix

Requirement	Test Description	Tested
Neck	Test 1 7.2G Sled Impact	Done
	Test 2 6.7G Sled Impact	Done
	Test 3 12.2G Sled Impact	Done
Shoulder	Test 1 4.5m/s Pendulum	Done
	Test 2 7.2G Sled Impact	Done
	Test 3 12.2G Sled Impact	Done
	Test 4 8.9m/s Padded WSU Sled	Done
Thorax	Test 1 4.3m/s Pendulum	Not tested
	Test 2 6.7m/s Pendulum	Not tested
	Test 3 1.0m Rigid Drop	Done
	Test 4 2.0mPaddeddrop	Not tested
	Test 5 6.8m/s Rigid Heidelberg Sled	Done
	Test 6 8.9m/s Padded WSU Sled	Done

Neck Biofidelity Tests

Neck Test 1

Method

The dummy was placed on a seat fixed perpendicular to the thrusting direction of the sled so that the dummy’s neck is vertical. The dummy was restrained by two wooden plates to suppress rotation of the arms and thorax, the shoulders and pelvis were restrained by belts. The upper ends of the plates were 50 mm below the top of the shoulders. The following items were evaluated: T1 acceleration (y-direction), relative movement of T1 with respect to the sled (y-direction), relative movement of head center of gravity position with respect to T1 (y- and z-directions), time of maximum movement of head center

of gravity position, head center of gravity acceleration (y- and z-directions), neck lateral bending angle, and neck torsion angle.

Results

The sled speed was 6.83m/s with the maximum acceleration of 6.8G inside of the corridor. The individual data and biofidelity score for this test are shown (Table A1 and A2). Other than the maximum horizontal displacement of the T1 rib, there are no substantial differences between the current arm and modified arm. Modified arm biofidelity is 7.4, and exceeds 7.15 of current arm in Test 1.

Neck Test 2

Method

A rigid seat, with its back inclined 15 degrees, was fixed perpendicular to the thrusting direction of the sled. A plate was fixed perpendicular to side surface of the seat, and the dummy was placed in the seat with its thorax and lumbar region contacting this plate. The upper end of the plate was 50 mm below the top of the shoulder.

A thorax cross belt, waist belt and horizontal thorax belt were also used for restraint. The following items were evaluated: neck lateral bending angle, neck lateral bending moment, neck anteflexio moment, neck torsional moment, neck lateral shearing load, neck longitudinal shearing load, and head composite acceleration.

Results

The sled speed was 5.79m/s and peak acceleration was 6.92G. The individual data and biofidelity score are shown (Table A3, A4 and Figure A1). There is a difference between the current and modified arms under tensile load. The biofidelity score of current arm is 3.99, and exceeds the score of 3.53 of modified arm.

Neck Test 3

Method

The dummy was restrained by two wooden plates to suppress rotation of arms and thorax. Belts were used to restrain the shoulders and pelvis. The following items were evaluated: T1 acceleration (y-direction), head center of gravity acceleration (y-direction), relative movement of head center of gravity position with respect to T1 (y-direction), neck lateral bending angle, and neck torsion angle.

Results

The sled decelerated at 7.0 m/s; its maximum deceleration was 11.44G within the corridor. The individual data and biofidelity score for this test are shown (Table A5, A6 and Figure A2). There are some differences between the current and modified arms for horizontal

acceleration and transversal deflection angle of T1 rib. The biofidelity score of modified arm is 5.34, which exceeds the score of 5.26 of current arm.

Shoulder Biofidelity Tests

Shoulder Test1

Method

A 150 mm diameter pendulum weighing 14 kg was targeted to impact the shoulder at 4.5 m/s, with the dummy arm in a resting state (down). The pendulum load and maximum displacement of the dummy shoulder rib were evaluated.

Results

For pendulum load, neither the SID-IIs current arm nor the modified arm fell into the standard corridor. The biofidelity score for both arms was 5 points.

Regarding the maximum displacement of the shoulder rib in a corridor of 22 to 30 mm, both the current arm and modified arm received no points. According to the biofidelity formula defined by ISO, they scored 5.0 points. The test results and scores are shown (Table A7, A8 and Figure A3).

Shoulder test 2

Method

Test method was similar to that of Neck Tests 1. T1 acceleration (y-direction) and relative movement of T1 with respect to the sled (y-direction) were evaluated.

Results

The individual data and biofidelity score are shown (Table A9 and A10). The biofidelity point of modified arm is 7.5, which is higher than 6.25 of current arm.

Shoulder test 3

Method

Test method was similar to that of Neck Tests 3. T1 acceleration (y-direction) was evaluated.

Results

The individual data and biofidelity score are shown (Table A11 and A12). The Biofidelity Point of current arm is 10.0, which is higher than 5.0 of modified arm.

Shoulder Test 4

Method

This was a padded Wayne State University (WSU) sled test performed at 8.9 m/s. The test setup is shown (Figure 7). The seat and seat back are Teflon-coated so that there is no effect on the dummy due to friction during sled motion. A load meter for the impact surface was fixed perpendicular to the sled direction. Regarding the dummy posture, the sagittal plane was set upright and the arm

angle was inclined 45 degrees forward of the thorax. The sum of shoulder and thorax loads was evaluated.

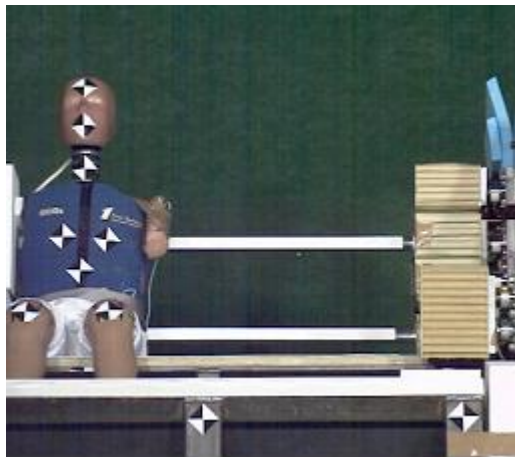


Figure 7. Shoulder and thorax test jig.

Results

For the sum of the shoulder and thorax loads, both the current and the modified arm received a biofidelity score of 5.0 points. In addition, evaluation of T12 movement was eliminated from the judgment factors because the human body corridor was not deemed reliable enough. According to the biofidelity formula defined by ISO, therefore both arms scored 5.0 points. The test results and overall scores are shown (Table A13, A14 and Figure A4).

Thorax Biofidelity Tests

Thorax Test 3

Method

The dummy was faced sideways and hung in a horizontal position, and the arm angle was inclined 20 degrees from the spine toward the front of the dummy. With this orientation, the dummy was dropped in free fall from a height 1.0 m above a rigid plate (impact surface). In this test, the load on the thorax rigid plate and maximum displacement of the thorax upper rib were evaluated.

Results

For the thorax plate load, both the current arm and modified arm were within ± 1 corridor, thus receiving a biofidelity score of 5 points. However, for the maximum displacement of the thorax upper rib, the current arm received 2.5 points from 2 out of 3 test results, whereas the modified arm received 5 points. According to the biofidelity formula defined by ISO, the current arm scored 5.0 points for an overall evaluation of “marginal”, and the modified arm scored 5.0 points. Test results and

overall scores are shown (Table A15, A16, A22 and Figure A5).

Thorax Test 5

Method

The test was performed in a similar format to the testing that was carried out at Heidelberg University (HU). A rigid plate was used as the impact surface at 6.8 m/s. The setup was similar to Shoulder Test 4 (Figure 7). The arm is at rest (down) in the test. The distance from the dummy to the impact surface was set to 0.35m. The following items were evaluated: shoulder/thorax plate load, T1 maximum acceleration, T12 maximum acceleration, and maximum acceleration of the thorax upper rib.

Results

Both the current and modified arm received 10 points with respect to the shoulder/thorax plate load. T1 (lateral direction) maximum acceleration responses in the lateral direction were within -1 corridor. Similar to T1, both arms received 0 points for T12 maximum acceleration responses in the lateral direction. For maximum acceleration in the lateral direction of the thorax upper rib, the current arm received 5.0 points, while the modified arm received 10.0 points. According to the biofidelity formula defined by ISO of one out of three tests, the current arm scored 3.75 points, and the modified arm scored 4.11 points. The test results and overall scores are shown (Table A17 and A18).

Thorax Test 6

Method

The test method was similar to that of Shoulder Tests 4. The sum of the shoulder and thorax plate force was evaluated.

Results

The individual data and biofidelity score for Thorax Test 6 are shown (Table A19, A20 and Figure A6). The biofidelity score of the current arm is 5.0 points, which is equal to that of the modified arm.

Biofidelity Evaluation Scores

Biofidelity scores based upon biofidelity tests with the current arm and modified arm are summarized (Table A21). The scores for the current arm regarding each measurement item and each test are compared with those of the modified arm. These results show that the modified arm leads to an increased score in Neck Tests 1, 3, Shoulder Test 2 and Thorax Tests 3, 5, and a reduced score in Neck Test 2 and Shoulder Test 3.

Summary of Biofidelity Evaluation

Some biofidelity tests were not performed because the results would not be affected by the arm modifications.

Due to the arm modifications, the thorax score increased, although the shoulder score decreased. The class designation by level was “good” for the thorax, while the shoulder and neck remained unchanged with a “fair” evaluation.

INFLUENCE ON INJURY VALUES ASSOCIATED WITH ARM MODIFICATION

In order to determine how dummy injury values (ex. Thorax rib deflection) changed, the biofidelity test analysis and full scale SUV MDB side impact tests were conducted.

Comparison of Thorax Injury Values in Biofidelity Tests

In the thorax biofidelity test 3, middle rib deflection and thorax plate force are the items used to evaluate biofidelity. However, in this test, thorax deflection and abdomen deflection were measured to determine the extent of the influence arm modifications have on injury values for the thorax and abdomen.

Results of Analysis on Biofidelity Test

The shoulder, abdomen and thorax injury values of SID-IIs in biofidelity test are shown (Figure 8).

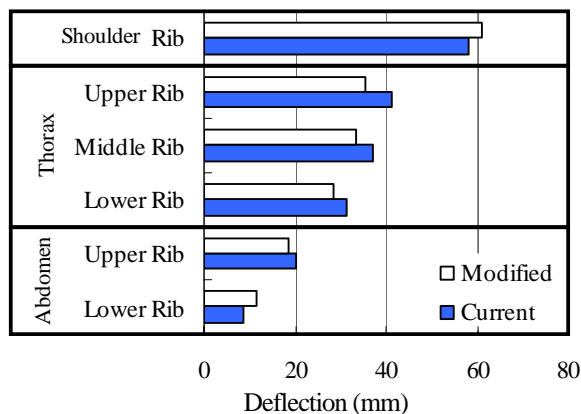


Figure 8. Dummy Injury Measurements in Biofidelity Thorax Test 3.

In the thorax biofidelity test 3 results, shoulder deflection increased. However, there was no significant change in plate force (Fig A5).

Furthermore, thorax deflection was reduced in the

case of the modified arm.

Full Scale SUV MDB Side Impact Test

In order to investigate how dummy injury values change due to the modifications of the SID-IIs arm, the dummy was evaluated in SUV MDB impacts to the side of a vehicle at 50 km/h performed by IIHS. The vehicle was a sedan sold in the U.S. market, which was equipped with curtain airbags in the front and rear seats, and side torso airbags in the front seats. SID-IIs dummies were placed in the front and rear seats on the impact side. The front seats were equipped with side airbags. The rear seats were not equipped with side torso airbags.

For comparison purposes, the test was performed twice: dummies having current arms were placed in one vehicle, and dummies with the modified arms were placed in the other vehicle.

Results of Full Scale SUV Side Impact

The front seats were equipped with side airbags. Thorax and abdomen deflection of the dummy are shown (Figure 9).

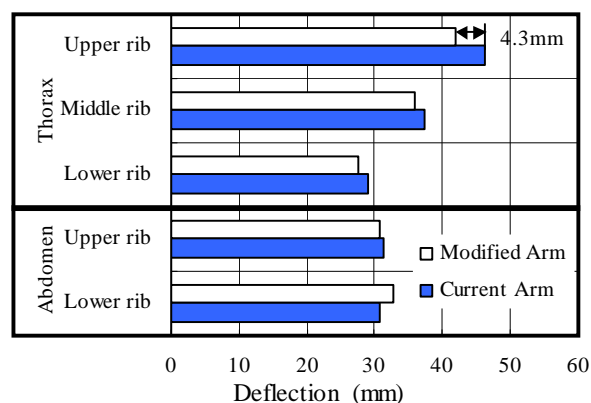


Figure 9. SID-IIs Driver Injury Measurements in IIHS SUV MDB Side Impact.

Compared to the current arm, the modified arm of the dummy in the driver position showed a decrease of 4.3mm in deflection of the thorax upper rib. Other thorax ribs showed approximately the same values.

The rear seats were not equipped with side torso airbags. Deflection of thorax and abdomen ribs of the dummy in the rear seat is shown (Figure 10).

Compared to the current arm, the modified arm of the dummy in the rear passenger position showed a 13.5mm decrease in thorax upper rib deflection, and a 7.6mm decrease in thorax middle rib deflection. There was no significant change in results for the abdomen. A comparison of the upper rib G waveforms in the impact is shown (Figure 11).

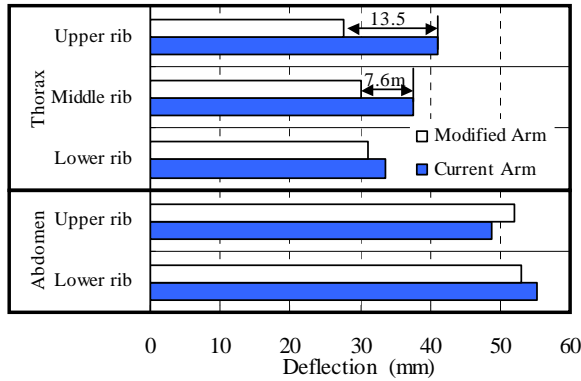


Figure 10. SID-IIs Rear Passenger Injury Measurements in IIHS SUV MDB Side Impact

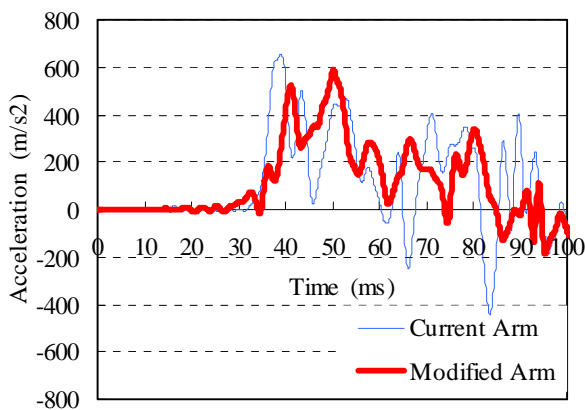


Figure 11. Rear Passenger Upper Rib Acceleration Response

DISCUSSION

Influence on Dummy Biofidelity

Biofidelity tests were performed in all conditions believed to be affected by modifications made to the arm. These results and the evaluation scores for all items are defined in ISO 9790

The results show a slight improvement in biofidelity due to the arm modifications without leading to deterioration in the overall biofidelity of the SID-IIs. The modifications are considered beneficial.

Influence of Arm Modifications on Thorax Injury Evaluation

By comparing thorax injury values in Thorax Test 3, shoulder deflection increased while thorax rib deflection decreased in the case of modified arm. However, there was no significant change in the impact load.

The decrease of thorax rib deflection is the result of softening arm skin characteristic, which led to a smaller reaction force from the thorax rib on the arm inner side and further deformation of the shoulder rib. A small reaction force from the rib on the arm means that the force of the arm pressing on the rib is also small, thus reducing thorax deflection.

Vehicle full-scale test results showed some differences between the current and modified arms in the front seat at which side airbags deployed. Compared to the current arm, the modified arm showed a slight decrease in deflection of the thorax upper rib. Other thorax ribs showed approximately the same values.

Furthermore, a notable difference was observed in the rear seat where airbags were not equipped. Compared to the current arm, the modified arm showed a significant decrease in thorax upper rib deflection, and also a decrease in thorax middle rib deflection. There was no significant change in results for the abdomen.

Accordingly, since the characteristic of the current arm is harder than a human arm, it appears that the thorax deflection value may be excessive in cases where the current arm and thorax rib come into contact.

CONCLUSIONS

1. The current SID-IIs arm does not accurately represent the human body in terms of compression characteristics, dimension, and mass. Thus, a modified SID-IIs arm was developed to more closely simulate these properties.
2. According to a series of tests, thorax biofidelity improved through the use of this modified arm. Although the shoulder became slightly worse, the overall biofidelity of the SID-IIs improved.
3. In cases where the arm came into contact with the thorax during a side impact, it was found that arm characteristics influence the thorax injury values. For this reason, dummy arm characteristics need to more closely represent a human arm.
4. The following were observed in full-scale vehicle tests, (IIHS SUV 50 km/h side impact test):
 - 4-1. No unique phenomena due to arm modifications were found.
 - 4-2. Small differences exist in thorax deflection due to arm modifications in driver seat, which was equipped with a torso airbag.
 - 4-3. Large differences in thorax deflection exist due to arm modifications in rear seat without torso airbag.

5. The modified arm increases the ability of the SID-IIs to accurately predict injury during side impact events.

REFERENCE

- [1]. Roger P. Daniel, Annette Irwin, John Athey, et al. 1995. Technical Specifications of the SID-IIs Dummy. Stapp Car Crash Journal, Vol. 39, 952735.
- [2]. Risa D. Scherer, Sarah L. Kirkish, Joseph P. McCleary, et al. 1998. SID-IIs Beta+-Prototype Dummy Biomechanical Response. Stapp Car Crash Journal, Vol. 42, 983151.
- [3]. ISO Technical Reports 9790:1999(E).
- [4]. Yoshihisa Kanno, Sohail Jamal, King H. Yang, Albert I. King, 1993. Mathematical Modeling of Human Thoracic Responses with and without Arms during Side Impact. Crashworthiness and Occupant Protection in Transportation Systems, Vol. 169, ASME.
- [5]. Kemper, A.K., Stizel, J.D., Duma S.M., Matsuoka, F., and Masuda M., 2005. Biofidelity of the SID-IIs and a Modified SID-IIs Upper Extremity: Biomechanical Properties of the Human Humerus. Proceedings of the 19th Enhanced Safety of Vehicles Conference, Washington, DC; 05-0123.
- [6]. L. W. Schneider, et al. 1983. Anthropometry of Motor Vehicle Occupants Volume 1-Procedures, Summary Finding and Appendices, P195, Appendix H P29, 30, UMTRI.

ISO 9790: 1990 Biofidelity Evaluation Results

The corridor used in the attachment is from SAE paper 983151.

Table A1: Neck Test 1 Current Arm Results (7.2G Sled)

7.2G Sled Weight factor $V_{2,1}=7$	Weight Factors $W_{2,1,k}$		Corridor		Current arm Results						Avg of Rating $R_{2,1,k}$	Test Rating
			Lower Bound	Upper Bound	Run 1	Rating	Run 2	Rating	Run 3	Rating		
Hori. Acc. of T1 (g)	W _{2,1,1}	5	10	15	9.0	5	8.8	5			5	7.15
Hori. Disp. of T1 Relative to Sled (mm)	W _{2,1,2}	5	38	51	36.9	5	38.3	10			7.5	
Hori. Disp. of Head C.G. Relative to T1(mm)	W _{2,1,3}	8	106	132	121.9	10	122.6	10			10	
Vert. Disp. of Head C.G. Relative to T1(mm)	W _{2,1,4}	6	63	96	48.2	5	51.2	5			5	
Head Excursion Time (s)	W _{2,1,5}	5	0.151	0.166	0.191	0	0.193	0			0	
Lat. Acc. of Head(g)	W _{2,1,6}	5	7	9	9.4	5	9.6	5			5	
Vert. (Downward) Acc. of Head (g)	W _{2,1,7}	5	7	8	7.5	10	7.6	10			10	
Flexion Angle(degrees)	W _{2,1,8}	7	48	65	53.3	10	54.3	10			10	
Twist Angle(degrees)	W _{2,1,9}	4	-45	-32	-36.3	10	-38.3	10			10	

Table A2: Neck Test 1 Modified Arm Results (7.2G Sled)

7.2G Sled Weight factor $V_{2,1}=7$	Weight Factors $W_{2,1,k}$		Corridor		Modified arm Results						Avg of Rating $R_{2,1,k}$	Test Rating
			Lower Bound	Upper Bound	Run 1	Rating	Run 2	Rating	Run 3	Rating		
Hori. Acc. of T1(g)	W _{2,1,1}	5	10	15	9.7	5	9.7	5	9.7	5	5	7.4
Hori. Disp. of T1 Relative to Sled(mm)	W _{2,1,2}	5	38	51	43.0	10	42.9	10	41.8	10	10	
Hori. Disp. Of Head C.G. Relative to T1 (mm)	W _{2,1,3}	8	106	132	126.6	10	123.8	10	123.9	10	10	
Vert. Disp. of Head C.G. Relative to T1 (mm)	W _{2,1,4}	6	63	96	54.6	5	56.2	5	54.5	5	5	
Head Excursion Time (s)	W _{2,1,5}	5	0.151	0.166	0.195	0	0.193	0	0.194	0	0	
Lat. Acc. of Head(g)	W _{2,1,6}	5	7	9	10.1	5	10.1	5	10.0	5	5	
Vert. (Downward) Acc. of Head (g)	W _{2,1,7}	5	7	8	7.7	10	7.7	10	7.7	10	10	
Flexion Angle(degrees)	W _{2,1,8}	7	48	65	55.9	10	56.0	10	56.0	10	10	
Twist Angle(degrees)	W _{2,1,9}	4	-45	-32	-39.2	10	-38.5	10	-38.7	10	10	

Table A3: Neck Test 2 Current Arm Results (6.7G Sled)

6.7G Sled Weight factor $V_{2,2}=6$	Weight Factors $W_{2,2,k}$		Corridor		Current arm Results						Avg of Rating $R_{2,2,k}$	Test Rating
			Lower Bound	Upper Bound	Run 1	Rating	Run 2	Rating	Run 3	Rating		
Flexion Angle (degrees)	W _{2,2,1}	7	44	55	51.6	10	54.7	10			10	3.99
Bending Moment of A-P Axis at O. C. (Nm) Mx	W _{2,2,2}	7	22	27	17.3	5	18	5			5	
Bending Moment of R-L Axis at O. C. (Nm) My	W _{2,2,3}	3	11	16	3.3	0	3.6	0			0	
Twist Moment (Nm) Mz	W _{2,2,4}	4	8	11	7.3	5	7	5			5	
Shear Force at O. C. (N)	W _{2,2,5}	7	500	567	353	0	351	0			0	
Tension Force at O.C.(N)	W _{2,2,6}	3	233	267	287	5	325	0			2.5	
P-A Shear Force (N)	W _{2,2,7}	4	217	250	79.2	0	84.7	0			0	
Resultant Head Acc.(g)	W _{2,2,8}	7	15	20	12.8	5	12.5	5			5	

Table A4: Neck Test 2 Modified Arm Results (6.7G Sled)

6.7G Sled Weight factor $V_{2,2}=6$	Weight Factors $W_{2,2,k}$	Corridor		Modified arm Results						Avg of Rating $R_{2,2,k}$	Test Rating	
		Lower Bound	Upper Bound	Run 1	Rating	Run 2	Rating	Run 3	Rating			
Flexion Angle (degrees)	$W_{2,2,1}$	7	44	55	54.3	10	50.5	10	54.5	10	10.0	3.53
Bending Moment of A-P Axis at O. C. (Nm) Mx	$W_{2,2,2}$	7	22	27	16.6	0	15.7	0	18	5	1.7	
Bending Moment of R-L Axis at O. C. (Nm) My	$W_{2,2,3}$	3	11	16	3.8	0	4.3	0	3.6	0	0.0	
Twist Moment (Nm) Mz	$W_{2,2,4}$	4	8	11	7.6	5	8.7	10	7.5	5	6.7	
Shear Force at O.C.(N)	$W_{2,2,5}$	7	500	567	359	0	359	0	362	0	0.0	
Tension Force at O.C.(N)	$W_{2,2,6}$	3	233	267	307	0	290	5	355	0	1.7	
P-A Shear Force (N)	$W_{2,2,7}$	4	217	250	77.1	0	81	0	80.5	0	0.0	
Resultant Head Acc.(g)	$W_{2,2,8}$	7	15	20	12.7	5	12.8	5	13.1	5	5.0	

Table A5: Neck Test 3 Current Arm Results (12.2G Sled)

12.2G Sled Weight factor $V_{2,3}=3$	Weight Factors $W_{2,3,k}$	Corridor		Current arm Results						Avg of Rating $R_{2,3,k}$	Test Rating	
		Lower Bound	Upper Bound	Run 1	Rating	Run 2	Rating	Run 3	Rating			
Lat. Acc. of T1(g)	$W_{2,3,1}$	5	14	19	18.8	10	18.5	10			10	5.26
Lat. Acc. of Head C.G.(g)	$W_{2,3,2}$	5	21	39	12.8	0	13	0			0	
Hori. Disp. of Head C.G. Relative to Sled (mm)	$W_{2,3,3}$	8	151	185	191	5	195	5			5	
Flexion Angle(degrees)	$W_{2,3,4}$	7	68	82	66	5	72.17	10			7.5	
Twist Angle (degrees)	$W_{2,3,5}$	4	62	75	48.52	0	51.23	5			2.5	

Table A6: Neck Test 3 Modified Arm Results (12.2G Sled)

12.2G Sled Weight factor $V_{2,3}=3$	Weight Factors $W_{2,3,k}$	Corridor		Modified arm Results						Avg of Rating $R_{2,3,k}$	Test Rating	
		Lower Bound	Upper Bound	Run 1	Rating	Run 2	Rating	Run 3	Rating			
Lat. Acc. of T1(g)	$W_{2,3,1}$	5	14	19	19.7	5	20.9	5	19.5	5	5	5.34
Lat. Acc. of Head C.G.(g)	$W_{2,3,2}$	5	21	39	13.5	0	13.8	0	13.3	0	0	
Hori. Disp. of Head C.G. Relative to Sled (mm)	$W_{2,3,3}$	8	151	185	201	5	206	5	206	5	5	
Flexion Angle(degrees)	$W_{2,3,4}$	7	68	82	75.4	10	76.7	10	75.8	10	10	
Twist Angle (degrees)	$W_{2,3,5}$	4	62	75	53.77	5	54.12	5	53.40	5	5	

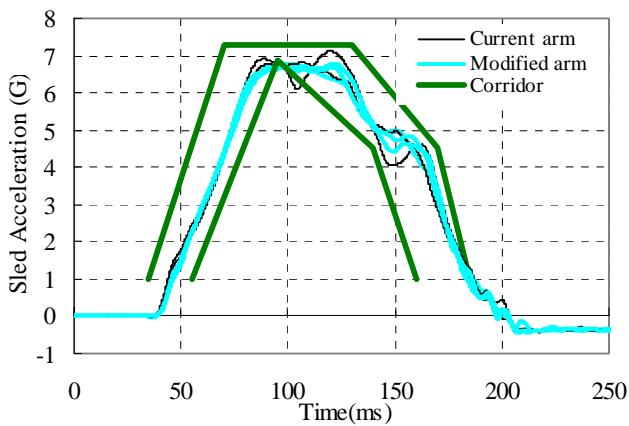


Figure A1. Sled Acceleration of Neck Test 1

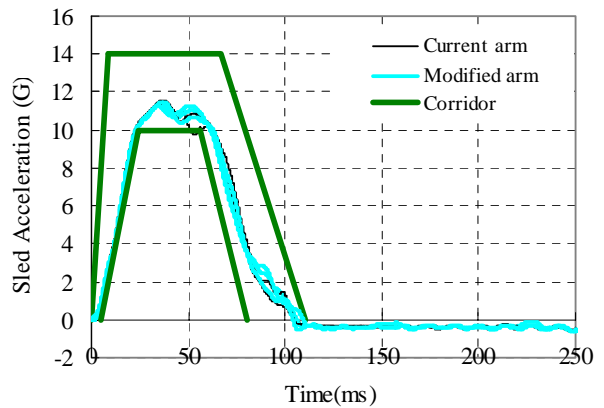


Figure A2. Sled Acceleration of Neck Test 3

Table A7: Shoulder Test 1 Current Arm Results (4.5m/s Pendulum Impact)

4.5m/s Pendulum Impact Weight Factor $V_{3,1}=6$	Weight Factors $W_{3,1,k}$	Corridor		Current arm Results						Avg of Rating $R_{3,1,k}$	Test Rating
		Lower Bound	Upper Bound	Run 1	Rating	Run 2	Rating	Run 3	Rating		
Pendulum Force(N)	$W_{3,2,1}$ 8	FigureA3			5		5		5	5	5.00
Shoulder Deflection(mm)	$W_{3,2,2}$ 6	22	30	36.7	5	36.7	5	36.4	5	5	

Table A8: Shoulder Test 1 Modified Arm Results (4.5m/s Pendulum Impact)

4.5m/s Pendulum Impact Weight Factor $V_{3,1}=6$	Weight Factors $W_{3,1,k}$	Corridor		Modified arm Results						Avg of Rating $R_{3,1,k}$	Test Rating
		Lower Bound	Upper Bound	Run 1	Rating	Run 2	Rating	Run 3	Rating		
Pendulum Force(N)	$W_{3,2,1}$ 8	FigureA3			5		5		5	5	5.00
Shoulder Deflection(mm)	$W_{3,2,2}$ 6	22	30	37.2	5	37.9	5	36.7	5	5	

Table A9: Shoulder Test 2 Current Arm Results (7.2G Sled)

7.2G Sled Weight factor $V_{3,2}=5$	Weight Factors $W_{3,2,k}$	Corridor		Current arm Results						Avg of Rating $R_{3,2,k}$	Test Rating
		Lower Bound	Upper Bound	Run 1	Rating	Run 2	Rating	Run 3	Rating		
T1 Horiz. Acc. (g)	$W_{3,2,1}$ 6	10	15	9.0	5	8.8	5			5	6.25
T1 Horiz. Disp. Relative to Sled (mm)	$W_{3,2,2}$ 6	38	51	36.9	5	38.3	10			7.5	

Table A10: Shoulder Test 2 Modified Arm Results (7.2G Sled)

7.2G Sled Weight factor $V_{3,2}=5$	Weight Factors $W_{3,2,k}$	Corridor		Modified arm Results						Avg of Rating $R_{3,2,k}$	Test Rating
		Lower Bound	Upper Bound	Run 1	Rating	Run 2	Rating	Run 3	Rating		
T1 Horiz. Acc. (g)	$W_{3,2,1}$ 6	10	15	9.7	5	9.7	5	9.7	5	5	7.50
T1 Horiz. Disp. Relative to Sled (mm)	$W_{3,2,2}$ 6	38	51	43.0	10	42.9	10	41.8	10	10	

Table A11: Shoulder Test 3 Current Arm Results (12.2G Sled)

12.2G Sled Weight factor $V_{3,3}=3$	Weight Factors $W_{3,3,k}$	Corridor		Current arm Results						Avg of Rating $R_{3,3,k}$	Test Rating
		Lower Bound	Upper Bound	Run 1	Rating	Run 2	Rating	Run 3	Rating		
T1 Horiz. Acc. (g)	$W_{3,3,1}$ 6	14	19	18.8	10	18.5	10			10	10.00

Table A12: Shoulder Test 3 Modified Arm Results (12.2G Sled)

12.2G Sled Weight factor $V_{3,3}=3$	Weight Factors $W_{3,3,k}$	Corridor		Modified arm Results						Avg of Rating $R_{3,3,k}$	Test Rating
		Lower Bound	Upper Bound	Run 1	Rating	Run 2	Rating	Run 3	Rating		
T1 Horiz. Acc. (g)	$W_{3,3,1}$ 6	14	19	19.7	5	20.9	5	19.5	5	5	5.00

Table A13: Shoulder Test 4 Current Arm Results (8.9m/s Padded WSU Sled)

8.9m/s Padded WSU Sled Weight factor	Weight Factors $W_{3,4,k}$	Corridor		Current arm Results						Avg of Rating $R_{3,4,k}$	Test Rating
		Lower Bound	Upper Bound	Run 1	Rating	Run 2	Rating	Run 3	Rating		
Shoulder+Thoracic Plate Force(N)	$W_{3,4,1}$ 9	Fig A4			5		5		5	5	5.00

Table A14: Shoulder Test 4 Modified Arm Results (8.9m/s Padded WSU Sled)

8.9m/s Padded WSU Sled Weight factor	Weight Factors $W_{3,4,k}$	Corridor		Modified arm Results						Avg of Rating $R_{3,4,k}$	Test Rating
		Lower Bound	Upper Bound	Run 1	Rating	Run 2	Rating	Run 3	Rating		
Shoulder+Thoracic Plate Force[N]	$W_{3,4,1}$ 9	Fig A4			5		5		5	5	5.00

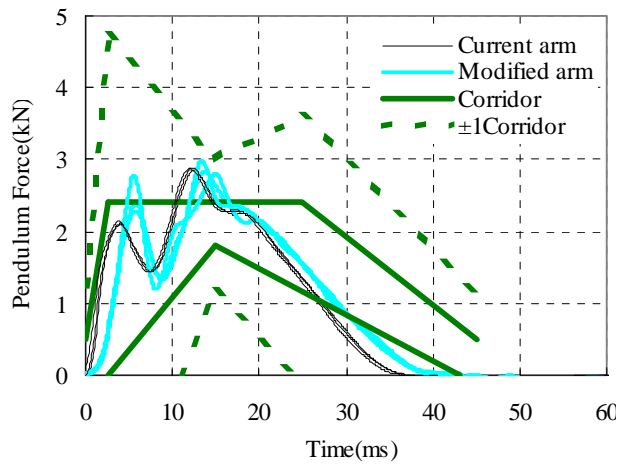


Figure A3. Pendulum Force of Shoulder Test 1

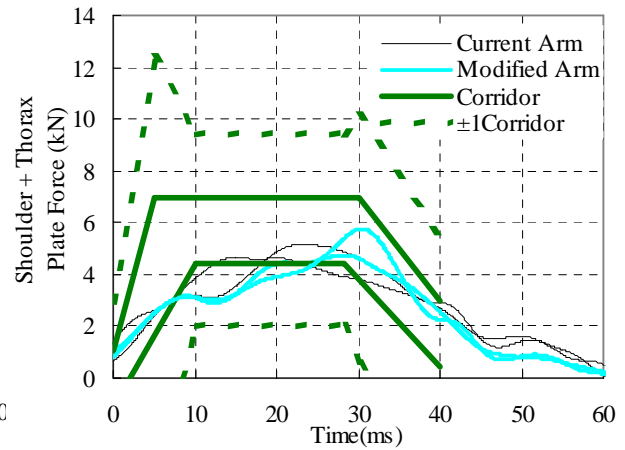


Figure A4. Shoulder Plate Force of Shoulder Test 4

Table A15: Thorax Test 3 Current Arm Results (Rigid 1.0m/s Lateral Drop)

Rigid 1.0m/s Lateral Drop Weight factor $V_{4,3}=6$	Weight Factors $W_{4,3,k}$	Corridor		Current arm Results						Avg of Rating $R_{4,3,k}$	Test Rating
		Lower Bound	Upper Bound	Run1	Rating	Run2	Rating	Run3	Rating		
Thorax Plate Force(N)	$W_{4,3,1}$	8	FigureA5		5		5		5	5.0	2.5
Deflection of Impacted Rib(mm)	$W_{4,3,2}$	8	24	32	42.1	0	40.6	0	41.3	0	

Table A16: Thorax Test 3 Modified Arm Results (Rigid 1.0m/s Lateral Drop)

Rigid 1.0m/s Lateral Drop Weight factor $V_{4,3}=6$	Weight Factors $W_{4,3,k}$	Corridor		Modified arm Results						Avg of Rating $R_{4,3,k}$	Test Rating
		Lower Bound	Upper Bound	Run1	Rating	Run2	Rating	Run3	Rating		
Thorax Plate Force(N)	$W_{4,3,1}$	8	FigureA5		5		5		5	5.0	5
Deflection of Impacted Rib(mm)	$W_{4,3,2}$	8	24	32	35.3	5	35.2	5	33.3	5	

Table A17: Thorax Test 5 Current Arm Results (6.8m/s Lateral Sled into Rigid Heidelberg type Wall)

6.8m/s Lateral Sled Rigid Heidelberg type Wall Weight factor $V_{4,5}=7$	Weight Factors $W_{4,5,k}$	Corridor		Current arm Results						Avg of Rating $R_{4,5,k}$	Test Rating	
		Lower Bound	Upper Bound	Run1	Rating	Run2	Rating	Run3	Rating			
Thorax Plate Force(N)	$W_{4,5,1}$	8	FigureA6		5		5		5	5.0	3.75	
Lat. T1Acc. (g)	$W_{4,5,2}$	7	99	133	61.3	0	62.9	0	60.3	0		0.0
Lat. T12Acc. (g)	$W_{4,5,3}$	7	105	143	71.2	5	71.1	5	70.8	5		5.0
Lat. Upper Thorax Rib Acc.(g)	$W_{4,5,4}$	6	87	117	128.2	5	135.0	5	132.3	5		5.0

Table A18: Thorax Test 5 Modified Arm Results (6.8m/s Lateral Sled into Rigid Heidelberg type Wall)

6.8m/s Lateral Sled Rigid Heidelberg type Wall Weight factor $V_{4,5}=7$	Weight Factors $W_{4,5,k}$	Corridor		Modified arm Results						Avg of Rating $R_{4,5,k}$	Test Rating	
		Lower Bound	Upper Bound	Run1	Rating	Run2	Rating	Run3	Rating			
Thorax Plate Force(N)	$W_{4,5,1}$	8	FigureA6		5		5		5	5.0	4.11	
Lat. T1Acc. (g)	$W_{4,5,2}$	7	99	133	59.6	0	64.7	0	58.7	0		0.0
Lat. T12Acc. (g)	$W_{4,5,3}$	7	105	143	75.2	5	80.5	5	74.4	5		5.0
Lat. Upper Thorax Rib Acc. (g)	$W_{4,5,4}$	6	87	117	78.6	5	84.0	5	94.3	10		6.7

Table A19: Thorax Test 6 Current Arm Results (8.9m/s Padded Sled WSU Type Wall)

8.9m/s Padded Sled WayneState typeWall Weight factor $V_{4,6}=7$	Weight Factors $W_{4,6,k}$	Corridor		Current arm Results						Avg of Rating $R_{4,6,k}$	Test Rating
		Lower Bound	Upper Bound	Run1	Rating	Run2	Rating	Run3	Rating		
Shoulder+Thorax Plate Force(N)	$W_{4,6,1}$	9	FigureA7		5		5		5	5.0	5

Table A20: Thorax Test 6 Modified Arm Results (8.9m/s Padded Sled WSU Type Wall)

8.9m/s Padded Sled WayneState typeWall Weight factor $V_{4.6}=7$	Weight Factors $W_{4.6,k}$		Corridor		Modified arm Results						Avg of Rating $R_{4.6,k}$	Test Rating
			Lower Bound	Upper Bound	Run1	Rating	Run2	Rating	Run3	Rating		
Shoulder+Thorax Plate Force(N)	$W_{4.6,1}$	9	FigureA7			5		5		5	5.0	5

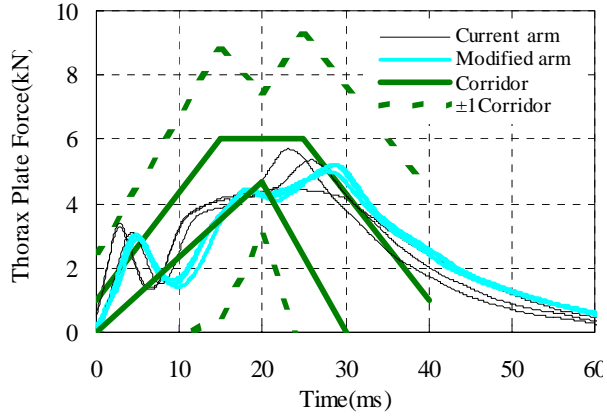


Figure A5. Thorax Plate Force of Thorax Test 3

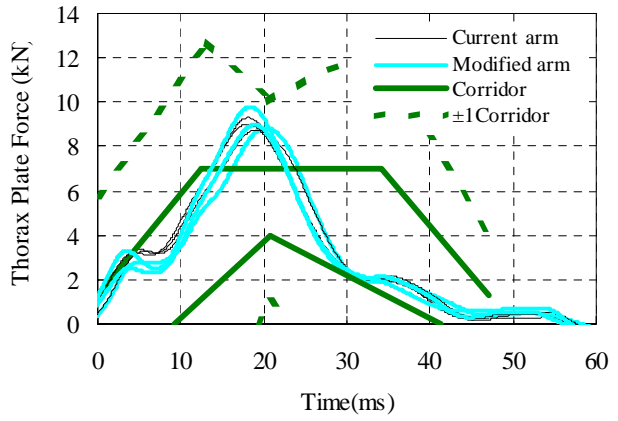


Figure A6. Thorax Plate Force of Thorax Test 5

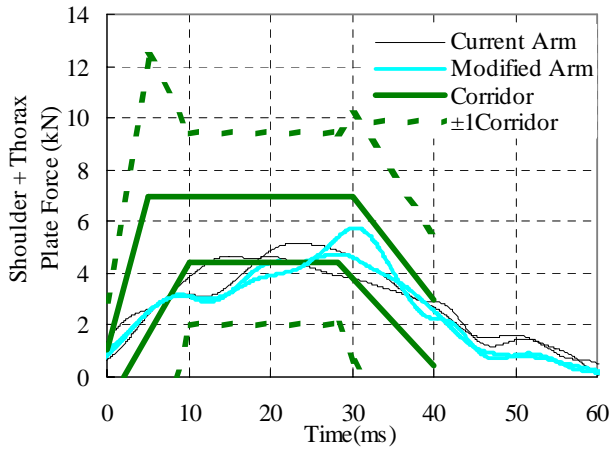


Figure A7. Thorax Plate Force of Thorax Test 6

BIOFIDELITY POINT

1. Neck, Shoulder and Thorax Biofidelity regulated by ISO 9790

- Arm modification gets the thorax biofidelity point up, the neck and shoulder ones down.
- Thorax biofidelity is good. Neck and shoulder biofidelities are fair. There is no change in biofidelity class.

Table A21 Biofidelity Point of Neck, Shoulder and Thorax

Body Region	Test condition	Weight Factors		Current Arm		Modified Arm	
				Test Rating	Biofidelity Rating	Test Rating	Biofidelity Rating
Neck	Test1-7.2G Sled	V2,1	7	7.15	5.61	7.40	5.56
	Test2-6.7G Sled	V2,2	6	3.99		3.53	
	Test3-12.2GSled	V2,3	3	5.26		5.34	
Shoulder	Test1-4.5m/s Pendulum Impact	V3,1	6	5.00	6.01	5.00	5.6
	Test2-7.2G Sled Impact	V3,2	5	6.25		7.50	
	Test3-12.2GSled Impact	V3,3	3	10.00		5.00	
	Test4-8.9m/s Padded WSU Sled	V3,4	7	5.00		5.00	
Thorax	Test1-4.3m/s Pendulum Impact	V4,1	9	10.00	6.74	10.00	7.2
	Test2-6.7m/s Pendulum Impact	V4,2	9	10.00		10.00	
	Test3- Rigid 1.0m/s Drop	V4,3	6	3.00		5.00	
	Test4-Padded 2.0m/s Drop	V4,4	0	0.00		0.00	
	Test5-6.8m/s Rigid Heidelberg	V4,5	7	3.75		4.11	
	Test6-8.9m/s Padded WSU Sled	V4,6	7	5.00		5.00	

Good: $6.5 \leq B < 8.6$

Fair: $4.4 \leq B < 6.5$

Marginal: $2.6 \leq B < 4.4$

2. Overall Biofidelity regulated by ISO 9790

- Arm modification gets the increase of 0.11 point about overall biofidelity.

(Notice※ :In ISO calculation method, weighting factor of the thorax is 10, and shoulder one is 5. So, thorax point has more contribution to overall than that of shoulder)

Table A22: Biofidelity Point (Body Region and Overall)

Body Regions	Weight Factors		Prototype		Current Arm		Modified Arm	
			Body region Rating	Overall Rating	Body region Rating	Overall Rating	Body region Rating	Overall Rating
Neck	U2	6	4.9	6.59	5.61	6.24	5.56	6.35
Shoulder	U3	5	6.2		6.01		5.60	
Thorax	U4	10	7.8		6.74		7.20	

Good: $6.5 \leq B < 8.6$

Fair: $4.4 \leq B < 6.5$

Marginal: $2.6 \leq B < 4.4$

Modified arm improved the over all biofidelity of SID-IIs as followings.

- (1) Overall biofidelity point
Current arm : 6.24 → Modified arm : 6.35 (up 0.11 points)
- (2) Thorax biofidelity point
Current arm : 6.74 → Modified arm : 7.2 (up 0.46 points)
- (3) Shoulder biofidelity point
Current arm : 6.01 → Modified arm : 5.6 (down 0.41 points)

BIOFIDELITY OF THE SID-IIs AND A MODIFIED SID-IIs UPPER EXTREMITY: BIOMECHANICAL PROPERTIES OF THE HUMAN HUMERUS

Andrew Kemper

Joel Stitzel

Stefan Duma

Virginia Tech – Wake Forest, Center for Injury Biomechanics
United States

Fumio Matsuoka

Mitsutoshi Masuda

Toyota Motor Corporation
Japan

Paper Number 05-0123

ABSTRACT

Accurate biofidelity for side impact dummies is crucial in order to accurately predict injury of human occupants. One such dummy is the SID-IIs, which represents the 5th percentile human female. A recent area of concern is the biofidelity of the upper extremity of side impact test dummies. Since the upper arm serves as a load path to the thorax, the response characteristics of the upper extremity can influence the thoracic response in side impact test dummies. However, there are currently no biofidelity evaluations with respect to the characteristics of the arm itself. The purpose of the study was to characterize the biomechanical properties of male and female humeri and to assess the biofidelity of the SID-IIs and a modified SID-IIs upper extremity. Results from two types of tests are presented. First, whole bone three-point bending tests were performed on eight isolated humeri from male and female human cadavers at static and dynamic loading rates 0.01 m/s and 3.0 m/s. Second, a series of compression tests were performed at two dynamic rates, 2 m/s and 4m/s, on a total of eight male and female humeri with all soft tissues attached. Then matched compression tests were performed on the SID-IIs and the modified SID-IIs humerus segment. The impact direction for all tests was from lateral to medial in order to simulate a side impact collision. All test results and biofidelity corridors are presented in the full paper. The test results show that for both the SID-IIs and modified SID-IIs, the force vs.

deflection response transitions from a linear response to an exponential response at deflections of approximately 15 mm and 25 mm, respectively. The male and female human humeri exhibited a similar trend but to a lesser extent. However, the force vs. deflection response of the modified SID-IIs upper extremity was more representative to that of the female human humeri than the original SID-IIs upper extremity. For example, the linear stiffness corridor from the 2m/s humerus compression tests was between 79.17 kN/m and 86.36 kN/m. For the same testing speed, the modified SID-IIs had a linear stiffness of 71.78 kN/m, while the SID-IIs had a linear stiffness of 183.9 kN/m. In summary, it is recommended that the modified SID-IIs upper limb should be used in place of the current SID-IIs upper limb in order to improve the biofidelity of the thoracic measurements of the SID-IIs.

INTRODUCTION

About 8,000 automobile occupants are killed and 24,000 seriously injured each year in side impact collisions [1]. The development of anthropometric test dummies specifically designed for side impact testing have helped to evaluate and improve new and evolving occupant protection technologies. One such dummy is the SID-IIs, which represents the 5th percentile human female. Accurate biofidelity for side impact dummies, such as the SID-IIs, is crucial in order to accurately predict injury of human occupants.

A recent area of concern is the biofidelity of the upper extremity of side impact test dummies. Since the upper arm serves as a load path to the thorax, the response characteristics of the upper extremity can influence the thoracic response in side impact test dummies. However, there are currently no biofidelity evaluations with respect to the characteristics of the arm its self. Even though, for all types of side impact accidents the second leading source of fatality, next to head injuries, is chest injuries (29%) [1].

Additionally, although airbags have reduced the risk of fatal injuries in automobile collisions, they have increased the incidence of some nonfatal injuries including upper extremity injuries [3]. Duma [3] found chondral and osteochondral fractures in the elbow joint for seven out of the 12 cadaver tests that had been subjected to upper extremity loading from a deploying seat mounted side airbag. Kallieris [8], who used the Hybrid III 50th percentile male dummy and male cadavers, found one humerus fracture out of five cadaver tests.

The first step in reducing these injuries is to determine applicable upper extremity injury criteria [6]. Duma [4] produced injury risk functions for the forearm and humerus fracture of the 5th percentile female based on mid-shaft bending moments. Duma [5] developed a multivariate risk function based upon the 5th percentile female that predicts a 50% risk of elbow fracture at a compressive elbow load of 1780 N and load angle of 30° superior to the longitudinal axis of the forearm. Duma [7] developed dynamic hyperextension injury criteria for the female elbow joint based on dynamic hyperextension tests on 24 female cadaver elbow joints.

The purpose of the study is to characterize the biomechanical properties of male and female humeri and to assess the biofidelity of the SID-IIs and a modified SID-IIs upper extremity. Results from two types of tests are presented. First, the results from whole bone three-point bending tests performed on eight isolated humeri from male and female human cadavers at static and dynamic loading rates, 0.01 m/s and 3.0 m/s, are presented. Second, the results from a series of compression tests performed at two dynamic rates, 2 m/s and 4 m/s, on a total of eight male and female humeri, with all soft tissues attached, and the SID-IIs and a modified SID-IIs upper extremity are presented.

METHODS

A total of 16 tests performed on fresh frozen human cadaver humeri in two parts. In part 1, 8 tests of 4 human humerus matched pairs were subjected to three-point bending using a hydraulic Material Testing System (MTS) at two impact rates. In part 2, 8 tests on 4 human humerus matched pairs and 6 tests both a Sid-IIs original and modified dummy arm subjected to compression loading on a drop tower at two dynamic impact rates.

Part 1: Humerus Three-Point Bending Tests

Dynamic humerus three-point bending tests were performed using a hydraulic Material Testing System (MTS 810, 13.3 kN, Eden Prairie, MN) at two loading rates on 8 unembalmed fresh human humeri obtained from 4 matched pairs.

Subject Test Data

Male and female matched pair humerus specimens ranging from 18 to 73 years of age were used for the three-point bending tests. For comparison with the standard population, Osteograms were performed on the left hand of each cadaver. The left hand of the cadavers was x-rayed and scanned by CompuMed incorporated (Los Angeles, CA). The BMD results are reported with respect to the normal population (Table 1). The t-score should be used to compare the cadaver's bone mineral density with that of the general population. In addition, the z-score can be used to compare the bone mineral density of the subjects with the average for their age. A t-score of -1 corresponds to one standard deviation below the mean for the general population (30 year olds), meaning the individual is at or above the -63rd percentile for bone mineral density, or close to normal. T-scores of 2 and 3 correspond to 97th and 99th percentiles, respectively.

Table 1.
Test subject data.

Subject Number	Gender	Age	BMD	T-Score	Z-Score
1	Female	46	93.7	-1.6	-1.6
2	Male	73	75.7	-3.2	-1.4
3	Male	18	138.3	3.2	3.2
4	Male	45	81.4	-2.7	-2.0

Experimental Setup

The primary component of the three-point bending test setup was a hydraulic Material Testing System (MTS 810, 13.3 kN, Eden Prairie, MN) (Figure 1). To stabilize the humerus in the test configuration, tissue was removed from the specimen and each end was inserted into a rigid square aluminum potting cup with polymer filler (Bondo Corporation, Atlanta, GA). During the potting process, care was taken to ensure the width between the supports for all specimens was 200 mm [8]. To maintain bending in the frontal plane, a pin was inserted through the left potting cup and a semicircular roller was attached to the right potting cup.

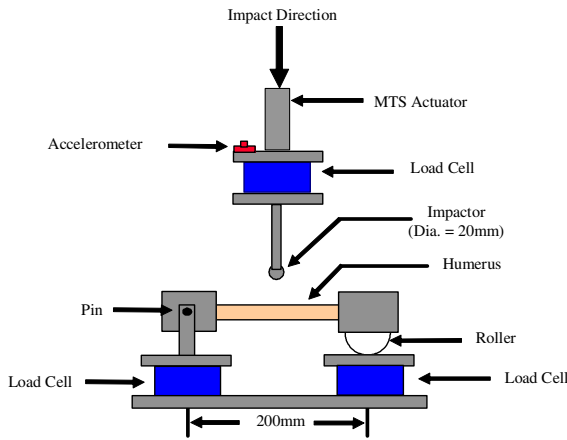


Figure 1. Humerus three-point bending test setup.

The humeri were randomly divided into two groups, where each group contained one specimen from each of the 4 matched pairs. The first group was subjected to a 0.01 m/s impact. The second group was subjected to a 3.00 m/s impact. Each humerus was instrumented with a uni-axial strain gage mounted to the mid-shaft bottom of the specimen (Vishay Measurements Group, CEA-06-062UW-350, Malvern, PA). The impactor assembly was instrumented with a five axis load cell (Denton 1968, 22,240 N, Rochester Hills, MI). Three axis load cells (Denton 5768, 11,120 N, Rochester Hills, MI) were mounted to each of the support towers. An accelerometer (Endevco 7264B, 2000 G, San Juan Capistrano, CA) was attached to the impactor head to allow for inertial compensation. Displacement was measured using the MTS internal LVDT. Data from the load cells and accelerometers were recorded at a sampling frequency of 30,000 Hz for the 0.01 m/s tests and 50,000 Hz for the 3.00 m/s tests (Iotech WBK16, Cleveland, OH). Pre and post test measurements were taken of each humerus three-point bending test specimen (Table 2).

Table 2. Humerus three-point bending pre and post test specimen data.

Tests ID#	Subject Number	Right/Left Humerus	Diameter M-L	Diameter A-P	Uncut Length	Distance form Fracture to Strain Gage
			(mm)	(mm)	(mm)	(mm)
Hum_S_1	1	Right	0.912	0.807	321	9.0
Hum_S_2	2	Left	0.952	0.950	327	0.0
Hum_S_3	3	Right	0.974	0.847	362	1.0
Hum_S_4	4	Left	0.816	0.881	350	10.0
Hum_F_1	1	Left	0.964	0.895	313	10.0
Hum_F_2	2	Right	0.863	1.010	330	6.0
Hum_F_3	3	Left	0.875	0.882	360	3.0
Hum_F_4	4	Right	0.764	0.960	355	4.0

Part 2: Humerus compression tests

Dynamic compression tests were performed at two loading rates on 8 unembalmed fresh human humeri obtained from 4 matched pairs using a drop tower with a 16 kg impactor. In addition to the human humeri, both a Sid-II's original and modified upper arm, provided by Toyota Motor Corporation, were tested at the same two loading rates using the same test setup in order to compare their responses to the responses of the human humeri.

Subject Test Data

Male and female matched pair humerus specimens, removed from subjects ranging from 56 to 87 years of age, were used for the tests (Table 3). The mass of the subjects ranged from 44.81 kg to 100.45 kg. The height of the subjects ranged from 152.4 cm to 180.34 cm.

Table 3.
Test subject data.

Subject Number	Gender	Age	Mass (kg)	Height (cm)
5	Male	56	81.37	170.18
6	Male	70	100.45	180.34
7	Female	61	44.81	152.40
8	Female	87	74.09	160.02

Experimental Setup

The primary component of the test setup was a drop tower with a 16 kg impactor (Figure 2). In order to simulate the response of the upper arm of a cadaver subjected to a side impact crash, the soft tissue was left on the human humeri for all compression tests. The ends of the humeri were constrained in order to prevent the human humeri from rotating or translating during the impact event (Figures 2 and 3).

The humeri were randomly divided into two groups, where each group contained one specimen from each of the 4 matched pairs. The first group was subjected to a 2.0 m/s impact (29.85 cm drop height). The second group was subjected to a 4.0 m/s impact (83.82 cm drop height). The impactor head and reaction plate were instrumented with single axis load cells (Interface 1210AF-22,240 N, Scottsdale, AZ). An accelerometer (Endevco 7264B, 2000 G, San

Juan Capistrano, CA) was attached to the both the impactor head and reaction support plate to allow for inertial compensation. A potentiometer (SpaceAge Control 62-60-8242- 2159mm, Palmdale, CA) mounted to the base of the drop tower was used to measure the displacement of the impactor. Data from the load cells, potentiometer, and accelerometers were recorded at a sampling frequency of 30,000 Hz for the slow tests and the fast tests (Iotech WBK16, Cleveland, OH).

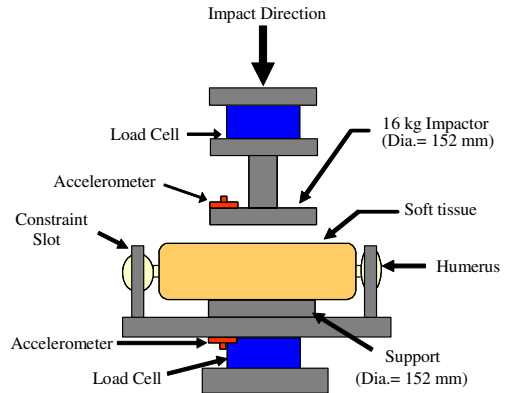


Figure 2. Humerus compression loading test setup (Front View).

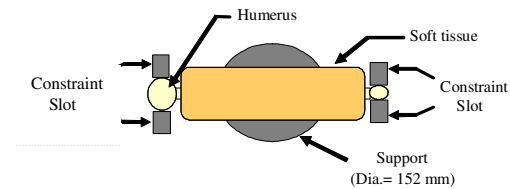


Figure 3. Humerus compression loading test setup (Top View).

Pre test measurements were taken of each humerus compression test specimen to document anthropometrical data (Table 4). The thickness of each specimen was measured after the specimen was placed on the support plate of the test setup.

Table 4.
Humerus compression test specimen data.

Tests ID#	Subject Number	Right/Left Humerus	Thickness (mm)	Humerus M/L Diameter (mm)	Uncut Length (mm)
Cad_1	5	Right	61.91	24.4	341.6
Cad_2	6	Left	46.04	22.9	335.3
Cad_3	7	Right	55.56	20.3	294.6
Cad_4	8	Left	63.50	22.9	325.1
Cad_5	5	Left	61.91	24.4	339.1
Cad_6	6	Right	46.04	22.9	335.3
Cad_7	7	Left	60.33	20.3	293.4
Cad_8	8	Right	58.74	22.9	321.3

The upper arm of the SID IIS, as well as automobile occupants, hangs vertically from the body when seated. Since the humeri tested were laid horizontally on a disc, the tissue flattened, causing the measured thickness to be less than when the arm hangs vertically.

In contrast, the dummy arm did not show any difference in thickness in the horizontal orientation. Therefore, the human humeri tests were not representative of a human occupant or similar to the dummy arm tests. To correct for this, the upper arms of 35 male and 35 female volunteers were measured (Table 5, Appendix A, and Appendix B). These measurements were taken with the arm in the vertical and horizontal positions, against surfaces representative of the tests in this report (Figure 4).

To measure the thickness of the arm in the vertical position, a flat plate was inserted between the body and the arm of a standing volunteer. The volunteer was asked to relax their muscles

and maintain contact between the plate and elbow joint with the arm hanging vertically in a relaxed position. The thickness was measured with a combination square, perpendicular to the plate, and from the plate to the midpoint of the arm. For measurements taken in the horizontal position, the volunteer laid their arm flat on a 152 mm diameter disk. The disk location was adjusted so it was centered in the middle of the humerus, and the volunteer adjusted the height of their shoulder until the humerus appeared flat on the disk. A combination square, perpendicular to the disk, was used to measure the thickness of the middle portion of the arm.

In addition to the vertical and horizontal thickness measurement, a third thickness measurement was taken by compressing the upper arm to a tolerable limit. This measurement was taken to give an indication of the toe region that would result from compressing the soft tissue.

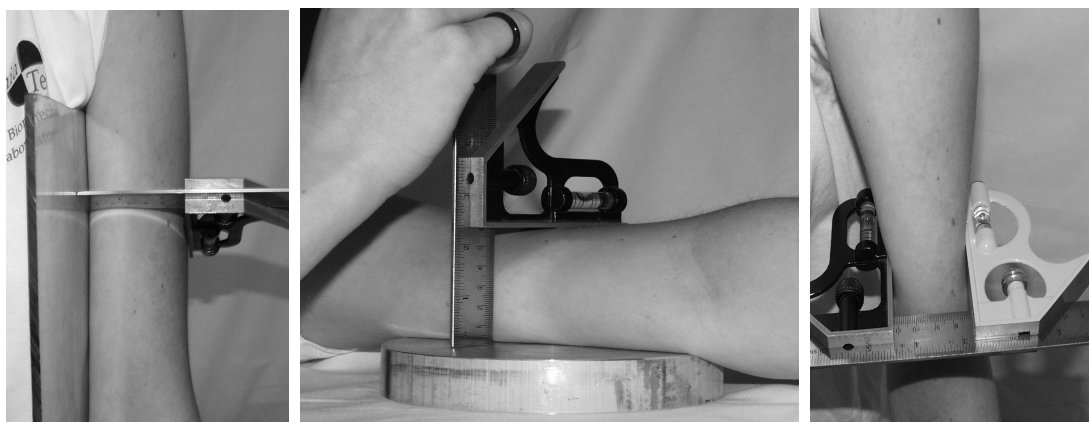


Figure 4. Upper arm thickness measurements taken on a volunteer, Vertically oriented (left), horizontally oriented (middle), and compressed to a tolerable limit (right).

Table 5.
Averages and standard deviations for 70 volunteer arm thickness measurements.

Gender	n	Average Height (m)	Average Mass (kg)	Vertical Thickness (mm)	Horizontal Thickness (mm)	Compressed Thickness (mm)	Ver -Hor (% diff)	Ver -Com (% diff)
Male	35	1.81 ± 0.07	82 ± 13	82 ± 8	72 ± 8	48 ± 6	14.7 ± 6.5	41.4 ± 5.9
Female	35	1.65 ± 0.07	61 ± 08	72 ± 6	64 ± 5	42 ± 5	12.3 ± 5.1	40.7 ± 4.5
Total	70	1.73 ± 0.11	71 ± 15	77 ± 9	68 ± 8	45 ± 6	13.5 ± 5.9	41.1 ± 5.2

RESULTS

The humerus data for both Task 2.1 and 2.2 is presented in the raw filtered form, as well as being mass scaled to the exact 5th percentile female and the 50th percentile male. This will allow for direct comparison to the dummy humerus values. All load cell and accelerometer data for both the three-point bending tests and compression tests was filtered at CFC 600. The potentiometer data for both compression tests was filtered at CFC 60 in order to eliminate excessive noise.

Part 1: Humerus three-point bending tests

The peak inertially compensated impactor force, peak deflection, peak strain, and the linear force increase for the 0.01 m/s and 3.00 m/s impact tests are presented (Table 6). The peak inertially compensated impactor force was mass scaled to either the 5th percentile female (Hum_S_1, Hum_F_1) or the 50th percentile male (Hum_S_2, Hum_S_3, Hum_S_4, Hum_F_2, Hum_F_3, Hum_F_4). The force vs. deflection data is presented in the raw filtered form, as well as being mass scaled to the exact 5th percentile female and the 50th percentile male (Figures 5-8). This will allow for direct comparison to the dummy humerus values.

Table 6.
Humerus three-point bending test results.

Tests ID#	Impactor Speed	Peak Bending Force (N)	Peak Moment (N/m)	Peak Deflection (mm)	Peak Strain (mstr)	Linear Force Increase (N/mm)	Scaled Peak Bending Force (N)	Scaled Peak Moment (N/m)
Hum_S_1	0.01 m/s	1347 *	134.7 *	7.72 *	16547.4	313.1	759 *	75.9 *
Hum_S_2	0.01 m/s	2889	288.9	10.38	23121.2	487.9	2745	274.5
Hum_S_3	0.01 m/s	4323	432.3	12.65	N/A	600.6	3673	367.3
Hum_S_4	0.01 m/s	3462	346.2	10.07	34548.9	566.5	3592	359.2
Hum_F_1	3.00 m/s	1574 *	157.4 *	4.79 *	7656.3	673.7	887 *	88.7 *
Hum_F_2	3.00 m/s	3684	368.4	8.22	14671.9	911.3	3501	350.1
Hum_F_3	3.00 m/s	4773	477.3	10.54	25876.2	959.0	4055	405.5
Hum_F_4	3.00 m/s	4460	446.0	9.67	20691.6	1441.9	4628	462.8

Note: * Designates that the maximum value was not at the time of fracture.

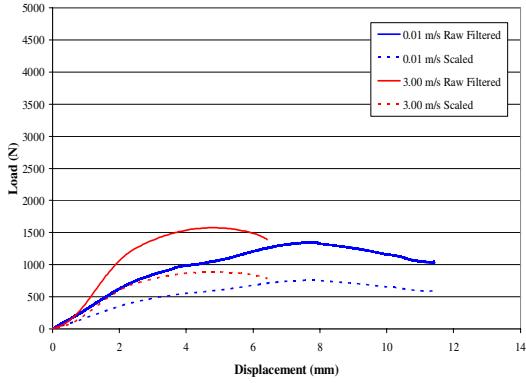


Figure 5. Subject 1 Three-Point Bending Force vs. Deflection
(Raw Filtered and Scaled to 5th Percentile Female).

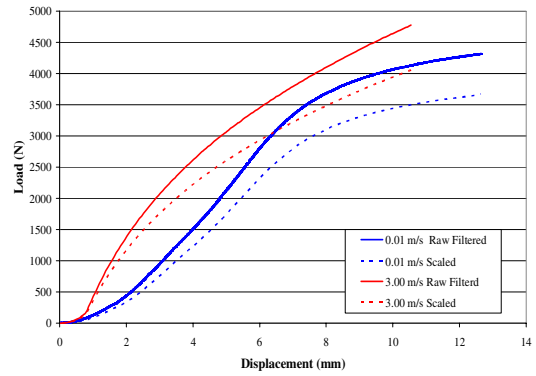


Figure 7. Subject 3 Three-Point Bending Force vs. Deflection
(Raw Filtered and Scaled to 50th Percentile Male).

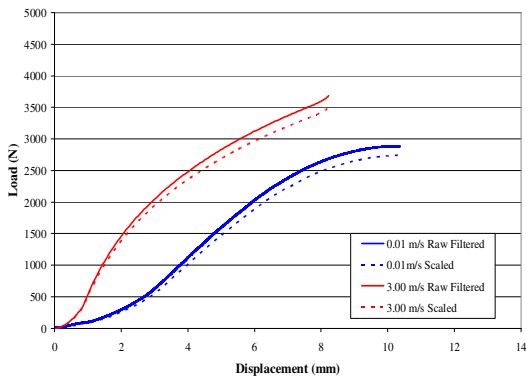


Figure 6. Subject 2 Three-Point Bending Force vs. Deflection
(Raw Filtered and Scaled to 50th Percentile Male).

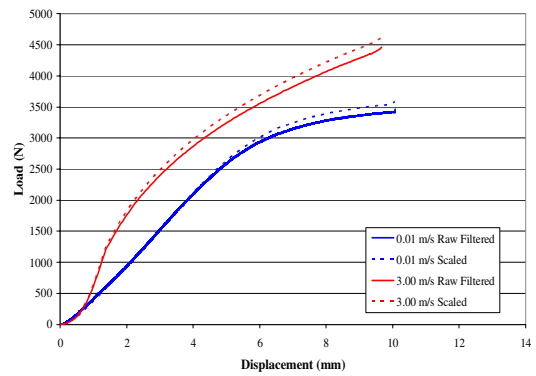


Figure 8. Subject 4 Three-Point Bending Force vs. Deflection
(Raw Filtered and Scaled to 50th Percentile Male).

Part 2: Humerus compression tests

The percent difference in thickness between the horizontal and vertical orientations for all volunteers was found to be 13.5%. In order to compensate for the loss in tissue thickness due to the horizontal testing orientation, the force versus deflection figures for the human humeri tests were shifted by 1.135 times the horizontal thickness measured when the humerus was placed on the test apparatus. The shifted force versus deflection responses of the human humeri for both dynamic compressive loading rates, 2.0 m/s and 4.0 m/s, were plotted along with the responses of the Sid-II's original and modified dummy arms (Figures 9 and 10).

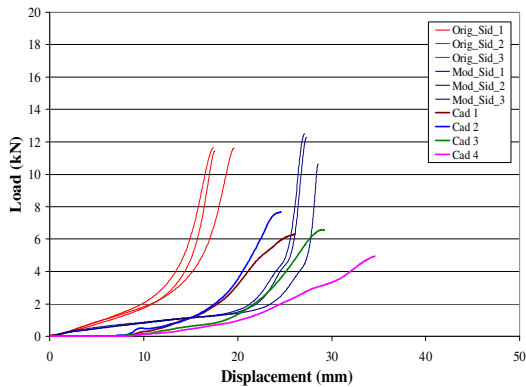


Figure 9. Shifted Dummy and Cadaver 2 m/s Compression Tests.

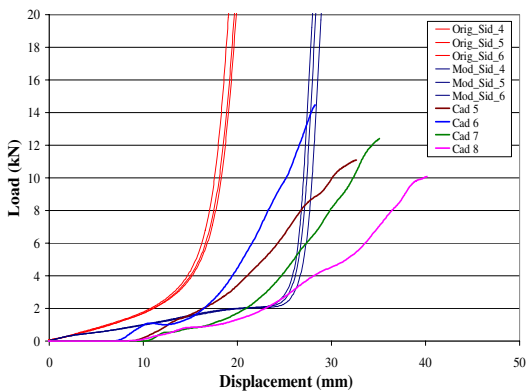


Figure 10. Shifted Dummy and Cadaver 4 m/s Compression Tests.

The shifted force versus deflection responses of the human humeri were then scaled to either the 5th percentile female or the 50th percentile male and plotted along with the responses of the Sid-II's original and modified dummy arms for both loading rates (Figures 11 and 12).

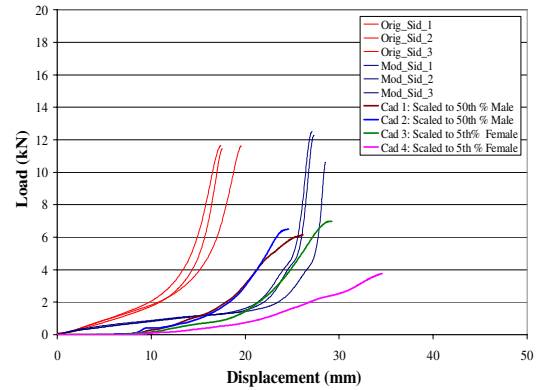


Figure 11. Shifted Dummy and Mass Scaled Cadaver 2 m/s Compression Tests.

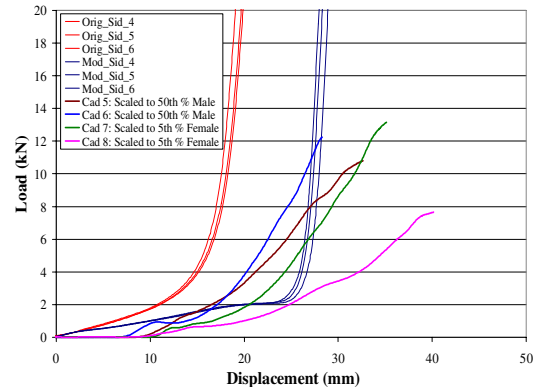


Figure 12. Shifted Dummy and Mass Scaled Cadaver 4 m/s Compression Tests.

CONCLUSIONS

Part 1: Humerus three-point bending tests

The scaled and non-scaled force vs. deflection responses for the 3.0 m/s impact tests both showed an increase in peak force and a decrease in peak deflection from the 0.01 m/s impact tests for all matched pairs. In addition, the male humeri exhibited a higher peak moment and peak strain than the female humeri.

Part 2: Humerus compression tests

The results show that for both impact rates, 2.0 m/s and 4.0 m/s, the modified Sid-IIs dummy arm force vs. deflection compression response is more representative to the scaled and non-scaled human humeri force vs. deflection compression responses than the original Sid-IIs dummy arm. Therefore, it is recommended that the modified SID-IIs upper limb should be used in place of the current SID-IIs upper limb in order to improve the biofidelity of the thoracic measurements of the SID-IIs.

REFERENCES

- [1] Cavanaugh J.M., Zhu Y., Haung Y., and King A.I. (1993) Injury and response of the Thorax in Side Impact Cadaveric Tests. 37th Stapp Carcrash Conference. pg. 199-221. Society of Automotive Engineers. Warrendale, PA.
- [2] Cesari, D, Rmaet, M., Bloch, J. (1981) Influence of Arm Position on Thoracic Injuries in Side Impact. Proc. Of 25th Stapp Conf., SAE Paper No. 811007.
- [3] Duma, S.M., Crandall, J.R., Hurwitz, S.R., Pilkey, W.D. (1998) Small female upper extremity interaction with a deploying side airbag. Proc. 42nd Stapp Car Crash Conference, pp. 47-63. Society of Automotive Engineers, Warrendale, PA.
- [4] Duma, S.M., Schrieber, P.H., McMaster, J.D.,Crandall, J.R., Bass, C.R., Pilkey, W.D. (1999) Dynamic injury tolerances for long bones of the female upper extremity. Journal of Anatomy. 194:463-471.
- [5] Duma, S.M., Boggess, B.M., Crandall, J.R., MacMahon, C.B. (2002) Fracture tolerance of the small female elbow joint in compression: the effect of load angle relative to the long axis of the forearm. Stapp Car Crash Journal: 46:195-210. Society of Automotive Engineers, Warrendale, PA.
- [6] Duma, S.M., Boggess, B.M., Bass, C.R., Crandall, J.R. (2003) Injury risk functions for the 5th percentile female upper extremity. SAE Paper No. 010166. Society of Automotive Engineers, Warrendale, PA.
- [7] Duma, S.M., Hansen, G.A, Kennedy, E.A, Rath, A.L, McNally, C.C., Kemper, A.R, Smith, E.P., Brolinson, P.G., Stitzel, J.D (2004) Upper Extremity Interaction with a Helicopter Side Airbag: Injury Criteria for Dynamic Hyperextension of the Female Elbow Joint. Stapp Car Crash Journal 48, pp. 1-22. Society of Automotive Engineers, Warrendale, PA.
- [8] Kallieris, D., Rizzetti, A., Mattern, R. (1997) Response and Vulnerability of the Upper Arm Through Side Air Bag Deployment. 41th Stapp Carcrash Conference. pg. 101-110. Society of Automotive Engineers. Warrendale, PA.
- [9] Kanno, Y., Jamal, S., Yang, K.H., King, A.I.(1993). Mathematical Modeling of Human Thoracic Responses with and without Arms during Side Impact. Crashworthiness and Occupant Protection in Transportation Systems. Vol. 169, ASME.
- [10] Kirkish, S., Begeman, P., Paravasthu, N. (1996) Proposed Provisional Reference Values for the Humerus for Evaluation of Injury Potential. Society of Automotive Engineers. Warrendale, PA.

APPENDICES

Appendix A. Male Volunteer Arm Thickness Measurements

subject	sex	age	height (m)	mass (kg)	vertical (mm)	horizontal (mm)	compressed (mm)	ver-hor % diff.	ver-com % diff.
1	m	25	1.70	68	80	67	43	19%	46%
2	m	24	1.93	84	80	69	47	16%	41%
3	m	28	1.75	73	76	74	47	3%	38%
4	m	22	1.73	94	93	83	54	12%	42%
5	m	23	1.83	75	75	65	50	15%	33%
6	m	22	1.80	75	77	68	43	13%	44%
7	m	26	1.80	84	91	78	51	17%	44%
8	m	25	1.88	82	78	65	51	20%	35%
9	m	27	1.88	98	87	82	53	6%	39%
10	m	26	1.83	91	84	73	43	15%	49%
11	m	19	1.73	75	95	76	48	25%	49%
12	m	23	1.85	98	86	83	62	4%	28%
13	m	22	1.73	91	91	83	56	10%	38%
14	m	21	1.85	86	86	80	55	8%	36%
15	m	19	1.85	96	92	82	57	12%	38%
16	m	18	1.80	84	87	72	48	21%	45%
17	m	18	1.75	70	83	73	46	14%	45%
18	m	24	1.70	65	77	67	46	15%	40%
19	m	21	1.90	109	92	78	56	18%	39%
20	m	19	1.75	61	69	59	40	17%	42%
21	m	20	1.83	88	86	84	60	2%	30%
22	m	20	1.88	93	89	69	48	29%	46%
23	m	24	1.85	75	74	65	53	14%	28%
24	m	21	1.75	91	87	79	46	10%	47%
25	m	22	1.93	118	88	81	47	9%	47%
26	m	19	1.83	68	67	59	43	14%	36%
27	m	18	1.88	75	76	62	44	23%	42%
28	m	19	1.88	70	68	62	40	10%	41%
29	m	20	1.80	78	92	74	44	24%	52%
30	m	19	1.83	84	86	79	48	9%	44%
31	m	20	1.80	77	75	64	44	17%	41%
32	m	18	1.68	63	69	61	38	13%	45%
33	m	19	1.75	73	76	64	44	19%	42%
34	m	21	1.83	75	76	62	39	23%	49%
35	m	22	1.88	82	88	72	47	22%	47%
<i>male ave.</i>		21.5	1.81	82	82	72	48	14.7%	41.4%
<i>male std.</i>		2.8	0.07	13	8	8	6	6.5%	5.9%

**Appendix B:
Female Volunteer Arm Thickness Measurements**

subject	sex	age	height (m)	mass (kg)	vertical (mm)	horizontal (mm)	compressed (mm)	ver-hor % diff.	ver-com % diff.
1	f	19	1.57	59	69	64	43	8%	38%
2	f	20	1.65	77	80	71	44	13%	45%
3	f	19	1.62	66	78	63	42	24%	46%
4	f	18	1.60	63	76	72	51	6%	33%
5	f	19	1.73	61	66	59	43	12%	35%
6	f	20	1.62	61	73	68	46	7%	37%
7	f	23	1.62	58	72	63	39	14%	46%
8	f	20	1.52	57	80	73	56	10%	30%
9	f	21	1.78	84	88	76	52	16%	41%
10	f	19	1.57	56	72	63	41	14%	43%
11	f	19	1.75	84	84	73	46	15%	45%
12	f	19	1.62	64	71	62	42	15%	41%
13	f	17	1.55	50	71	62	41	15%	42%
14	f	21	1.73	63	66	61	44	8%	33%
15	f	18	1.62	63	71	62	43	15%	39%
16	f	18	1.70	63	74	68	44	9%	41%
17	f	19	1.60	52	66	57	38	16%	42%
18	f	18	1.60	54	64	58	42	10%	34%
19	f	21	1.70	61	72	63	42	14%	42%
20	f	18	1.80	67	74	67	42	10%	43%
21	f	21	1.73	61	68	65	46	5%	32%
22	f	20	1.62	59	64	62	39	3%	39%
23	f	20	1.70	52	62	52	33	19%	47%
24	f	20	1.70	58	64	61	38	5%	41%
25	f	19	1.60	54	70	58	39	21%	44%
26	f	20	1.62	49	66	54	34	22%	48%
27	f	19	1.68	63	74	69	43	7%	42%
28	f	19	1.70	60	71	60	41	18%	42%
29	f	19	1.70	68	72	62	41	16%	43%
30	f	19	1.52	54	72	64	43	13%	40%
31	f	38	1.62	61	73	67	44	9%	40%
32	f	16	1.62	55	69	64	38	8%	45%
33	f	18	1.62	57	68	58	37	17%	46%
34	f	21	1.68	61	69	64	40	8%	42%
35	f	21	1.68	61	76	69	47	10%	38%
<i>female ave.</i>		19.9	1.65	61	72	64	42	12.3%	40.7%
<i>female std.</i>		3.4	0.07	8	6	5	5	5.1%	4.5%

A COMPARISON OF THE BIORID II, HYBRID III, AND RID2 IN LOW-SEVERITY REAR IMPACTS

A. Kim
A. Sutterfield
A. Rao
K.F. Anderson
J. Berliner
J. Hassan
A. Irwin
J. Jensen
J. Kleinert
H.J. Mertz
H. Pietsch
S. Rouhana
R. Scherer

Rear Impact Dummy Evaluation Task Group of the
Occupant Safety Research Partnership/USCAR
United States of America
Paper Number 05-0225

ABSTRACT

The BioRID II, 50th percentile Hybrid III and RID2 crash test dummies, all representing a mid-size adult male, were subjected to HyGE™ rear impact sled tests. Their measured and calculated responses were used to evaluate their sensitivity to sled velocity, head restraint position, and other test setup parameters. Three test series were conducted using different sled acceleration pulses and different types of seats. For conditions where three identical tests were conducted, repeatability was evaluated. In Series A, the effect of sled velocity on the Hybrid III and RID2 was evaluated. For the RID2, the effect of the initial backset was also evaluated in this series. In Series B, the head restraint position and the sled velocity were changed to see how the performances of the BioRID II, Hybrid III and RID2 were affected. In Series C, the effect of sled velocity changes and head restraint position on the Hybrid III and RID2 were again evaluated, and repeatability was assessed. Comments on the handling and durability of the dummies are also provided.

INTRODUCTION

The Occupant Safety Research Partnership (OSRP) of the United States Council for Automotive

Research (USCAR) evaluated the BioRID II (version C), the Hybrid III (FMVSS Part 572 Subpart E), and the RID2 (a prototype representative of production version 0.0). All three dummies represent the mid-size adult male. The Hybrid III was developed in the early 1970s [9, 21]. Although it has primarily been used in frontal impacts, it has also been used in rear, side and other types of impacts. Both the BioRID II [2, 7] and the RID2 [15] were developed more recently and were intended specifically for use in low-severity rear impacts.

In this study, the similarities and differences between these dummies were evaluated as well as the way each dummy was affected by changes in the test parameters. Three different test series were run in this evaluation. Series A examined the sensitivity to changes in sled velocity of the Hybrid III and RID2 when set to the same backset (the horizontal distance between the back of each dummy's head and the front the head restraint). The effect of varying the backset on the responses of the RID2 was also evaluated. In Series B, the effect of sled velocity and head restraint position on the responses of the Hybrid III, RID2 and BioRID II were evaluated. Additionally, the effect of varying the backset on the BioRID II was assessed. Series C further examined the sensitivity of the Hybrid III and RID2 to sled velocity and head restraint position and analyzed the repeatability of each dummy.

Each of the three different series of rear impact HyGE™ sled tests was run at a different test laboratory. The test matrix is shown in Table 1. The sled velocities ranged from 9 to 27 km/hr.

METHODS

General Setup

All the dummies were dressed consistently throughout the entire evaluation. The BioRID II was dressed in two pairs of shirts and shorts. The inner pair was made of Lycra® and the outer pair was made of cotton. The Hybrid III wore a cotton shirt and shorts. The RID2 was dressed in the provided neoprene suit.

**Table 1.
Test Matrix**

Test Series	ΔV (km/hr)	Dummies	Position	Head Restraint Position	# of Tests Per Dummy
A	9	Hybrid III, RID2, RID2 (105mm)	Driver	Fixed	1,1,1
A	9	Hybrid III, RID2, RID2 (105mm)	Passenger	Fixed	1,1,1
A	16	Hybrid III, RID2, RID2 (105mm)	Driver	Fixed	1,1,1
A	16	Hybrid III, RID2, RID2 (105mm)	Passenger	Fixed	1,1,1
A	24	Hybrid III, RID2, RID2 (105mm)	Driver	Fixed	1,1,1
A	24	Hybrid III, RID2, RID2 (105mm)	Passenger	Fixed	1,1,1
B	17	RID2, Hybrid III, BioRID II	Fore, Mid, Aft	Full Up	2,2,2
B	17	RID2, Hybrid III, BioRID II	Fore, Mid, Aft	Full Down	2,2,2
B	27	RID2, Hybrid III, BioRID II	Fore, Mid, Aft	Full Up	2,2,2*
B	27	RID2, Hybrid III, BioRID II	Fore, Mid, Aft	Full Down	2,2,2
C	10	Hybrid III, RID2	Driver	Full Up	1,2
C	10	Hybrid III, RID2	Passenger	Full Up	2,1
C	10	Hybrid III, RID2	Driver	Full Down	1,2
C	10	Hybrid III, RID2	Passenger	Full Down	2,1
C	24	Hybrid III, RID2	Driver	Full Up	1,2
C	24	Hybrid III, RID2	Passenger	Full Up	2,1
C	24	Hybrid III, RID2	Driver	Full Down	1,2
C	24	Hybrid III, RID2	Passenger	Full Down	2,1

* Only one of the BioRID II, 27 km/hr ΔV head restraint full up tests is included in the dummy comparison discussion for test Series B due to positioning issues.

The three facilities also used a standard set of minimum instrumentation for each dummy as listed in Table 2. The BioRID II used in this evaluation was not instrumented with a lower neck load cell. The transducers were oriented and the responses were filtered according to SAE J211 convention [19]. The dummies passed verification before and after each test series. The test facilities recorded the simulated rear impacts with high-speed film cameras at 500 and 1000 frames/second.

**Table 2.
Dummy Instrumentation**

	BioRID II	Hybrid III	RID2
Head CG 3-axis accelerometer	*	*	*
Upper neck 6-axis load cell	*	*	*
Lower neck 6-axis load cell		*	*
T1 single-axis (X) accelerometer		*	
T1 3-axis accelerometer	*		*

All the dummies were tested on production representative seats mounted to either a rigidized vehicle buck or a rigid platform buck. Each test series used a different type of seat. The dummies were restrained by 3-point safety belts in all the tests. The BioRID II and RID2 were positioned as recommended in their respective user manuals [2, 15]. The Hybrid III was positioned according to the FMVSS 208 seating procedure [8]. For each test, the backset was measured. The vertical height from the top of the head restraint to the center of gravity (CG) of the head was also measured. See Figure 1.

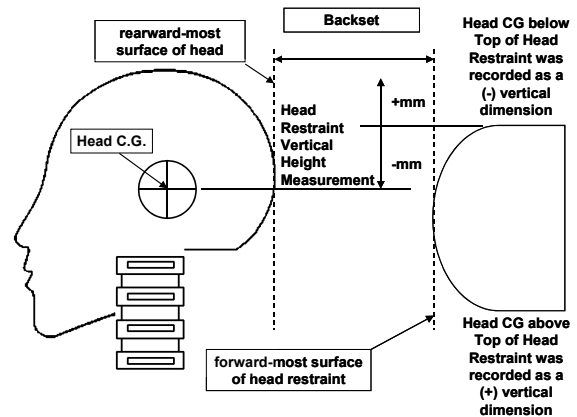


Figure 1. Head to head restraint backset and vertical height measurements.

The distances, formulas and methods for the following calculated responses are given in Appendix A. The external head impact forces were used to determine the contact forces with the head restraint. The tension-extension component of the Nij [13, 14, 1, 11, 12] and the NIC [23, 3, 4] were also evaluated.

The head restraint contact times were obtained by using a slope intercept approach, similar to the one described in SAE J2052 [20], on the external head impact force responses. The intercept value was calculated by taking the slope over a change of 50 N and extrapolating backwards to the point in time where the force level was zero.

Series A

In this test series, the Hybrid III and RID2 were subjected to simulated rear impacts with approximate sled velocity changes (ΔV s) of 9, 16, and 24 km/hr (Table 1). The sled acceleration pulses for each tested velocity are shown in Figure 2. The dummies were tested on identical bucket seats with integrated head restraints (Figure 3). The seats were replaced after each test. The seats were placed in the full rear seat track position. The seatbacks were set at 23°, measured between the seat frame and the vertical. The seating positions of the two dummies were switched from driver to passenger, and vice versa, for the repeat run of each test condition.

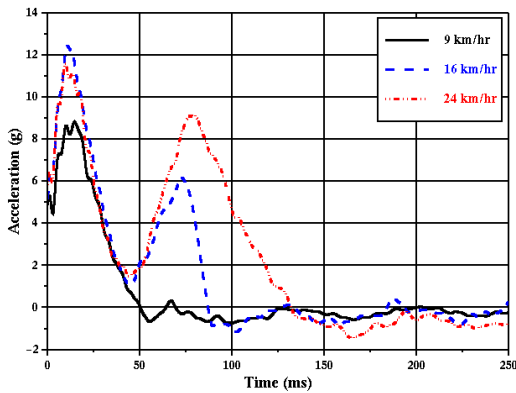


Figure 2. Series A: Sled acceleration pulses.

In its initial position, the Hybrid III backset was 55 mm. When the RID2 was first positioned according to its procedure [15], an average backset of 105 mm was obtained. In later tests using the same seating procedure, the RID2 was repositioned to match the 55 mm backset of the Hybrid III. Both dummies were positioned to the same H-point.

Figures 4 and 5 show the average and range of the backsets and the vertical distances from the center of gravity of the head to the top of the head restraint obtained for each test condition. The values obtained when the RID2 was at the 105 mm backset are labeled as "RID2 (105)". The RID2 initial setup tilt sensor readings are given in Appendix B Tables B1 and B2.



Figure 3. Series A: Test setup at 55 mm backset. Foreground – RID2, background – Hybrid III.

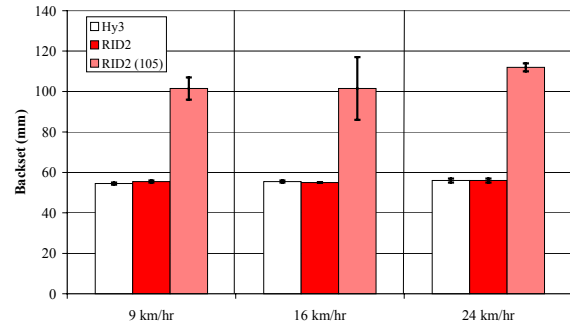


Figure 4. Series A: Backsets.

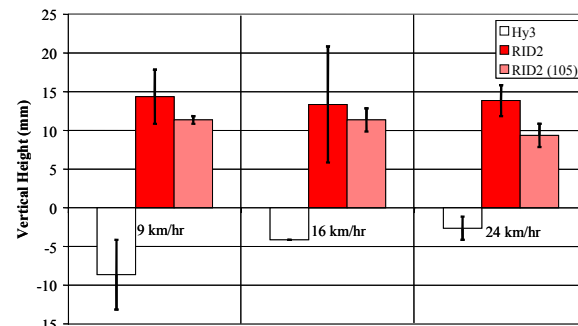


Figure 5. Series A: Vertical heights between the top of the head restraint and the head CG.

Series B

In the second test series, the Hybrid III, RID2 and BioRID II were tested concurrently (Figure 6) at ΔV s of 17 and 27 km/hr as shown in Table 1. The sled acceleration pulses are shown in Figure 7. Identical front bucket passenger seats with integrated 3-point belts were used and replaced after each test. The seats had adjustable head restraints and were also equipped with actuation devices that controlled head restraint movement (self-aligning head restraint mechanisms). The initial positions of the head restraints were either full up or full down. The seatbacks were set at an approximate angle of 16° .

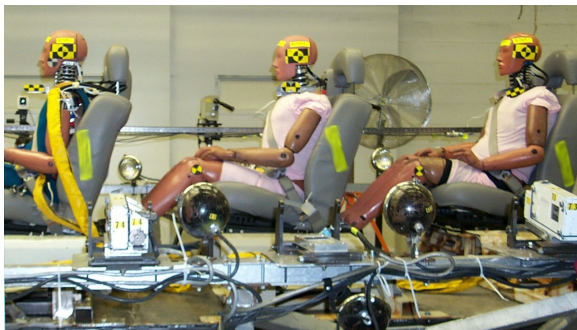


Figure 6. Series B: Test setup. From left-to-right, the RID2, Hybrid III, and BioRID II.

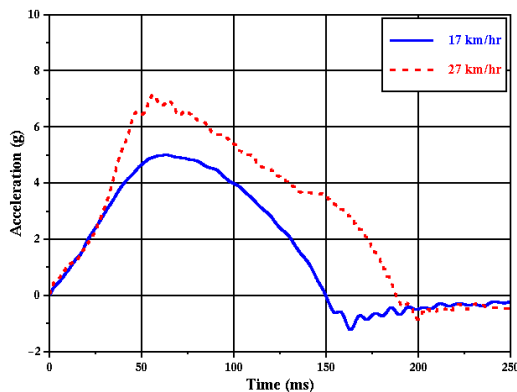


Figure 7. Series B: Sled acceleration pulses.

Figure 8 gives the average and range of the backsets for each test condition. The averages and ranges of the vertical heights from the top of the head restraint to the head CG, obtained by film analysis, are given in Figure 9. The RID2 tilt sensor angles at initial position are listed in Appendix B Table B3.

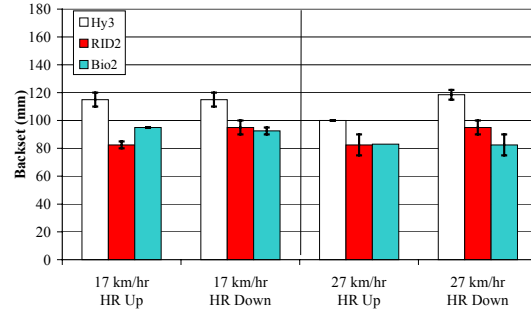


Figure 8. Series B: Backsets.

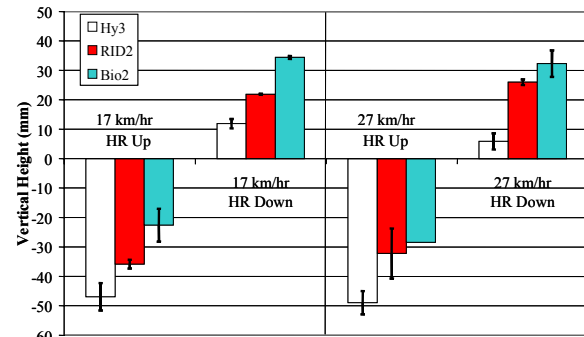


Figure 9. Series B: Vertical heights between the top of the head restraint and the head CG.

Series C

In the third series, a total of 12 sled tests were conducted with the Hybrid III and RID2 dummies (Figure 10). The sled tests were conducted at ΔV s of 10 and 24 km/hr (Table 1). Figure 11 shows the sled pulses used in this series. Identical front bucket seats with integrated 3-point belts were used. The same set of driver and passenger seats were used for the 10 km/hr tests, however, new seats were used for each of the 24 km/hr tests. The seats had adjustable head restraints that were set at either the full up or full down position. The seatbacks were set at an angle of 24° .

The dummies were seated side by side in bucket seats and their positions were switched in some of the tests (Table 1). Figure 12 gives the average and the range of backsets. From still setup photographs (Figure 13), it was observed that the tops of the head restraints in both the full up and full down positions were always above the CGs of the heads of the two dummies. This behavior was also seen for the RID2 in the 24 km/hr test setup. The initial RID2 angles are given in Appendix B Table B4.

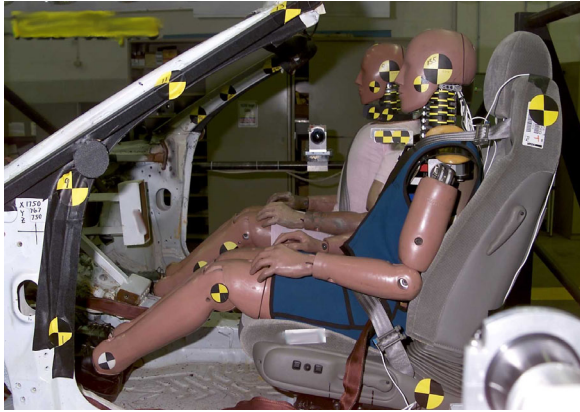


Figure 10. Series C: Test setup. Foreground - RID2, background - Hybrid III.

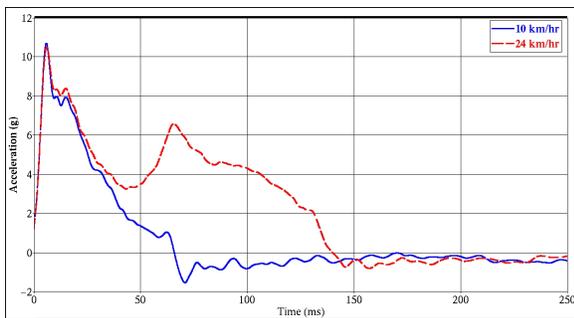


Figure 11. Series C: Sled acceleration pulses.

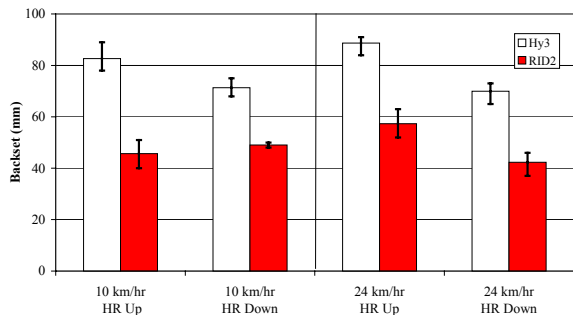


Figure 12. Series C: Backsets.

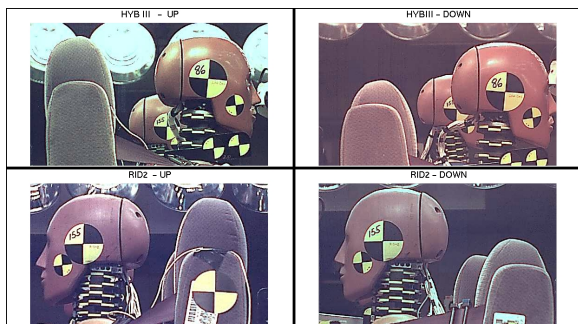


Figure 13. Test setup photographs. Top left - Hybrid III HR up, top right - Hybrid III HR down, bottom left - RID2 HR up, bottom right - RID2 HR down.

RESULTS AND DISCUSSION

The results of each test series are first discussed individually. Then, any observations that can be made by comparing two or more of the series are given. Lastly, there are comments on dummy handling and usability.

All bar chart graphs have the following format. Each bar represents the average of the peak responses for that test condition while the error bars represent the ranges.

Series A

This series examined the sensitivity of the Hybrid III and RID2 to sled velocity when both dummies were set to the same backset. Due to the difference in dummy seated heights, the effect of height was also indirectly observed. Although the following charts (e.g. Figure 14) show data for the Hybrid III, RID2, and RID2(105) only the Hybrid III and RID2 data will be discussed in the 55 mm Backset section. The RID2(105) data will be discussed in a later section on RID2 backset sensitivity.

55 mm Backset: Hybrid III and RID2

Resultant Head CG Accelerations

The averages of the peak head CG accelerations, obtained prior to the head losing contact with the head restraint due to rebound, are shown in Figure 14. The Hybrid III and RID2 have very similar peak resultant head CG accelerations. The average peak accelerations of both dummies increased between 9 and 16 km/hr but not between 16 and 24 km/hr. The increased seatback deformation seen at 24 km/hr (Figure 15), compared to that seen at 16 km/hr, limited the effect of this sled velocity increase on the head CG accelerations.

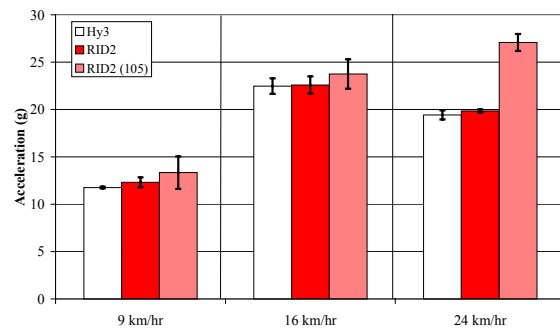
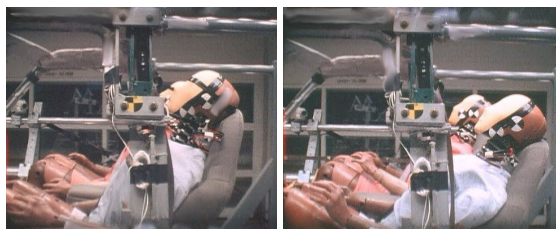


Figure 14. Series A: Resultant head CG accelerations.



a.) b.)
Figure 15. Series A: Maximum seatback deformation with a Hybrid III a.) 16 km/hr and b.) 24 km/hr.

T1 X-Accelerations

At each sled velocity, the average peak T1 X-accelerations of the Hybrid III and RID2 were within 2 g of each other (Figure 16). The peak accelerations of both dummies increased from 9 to 16 km/hr. At 24 km/hr, seatback deformation again limited the responses. The largest increase seen at this level was less than 1.5 g.

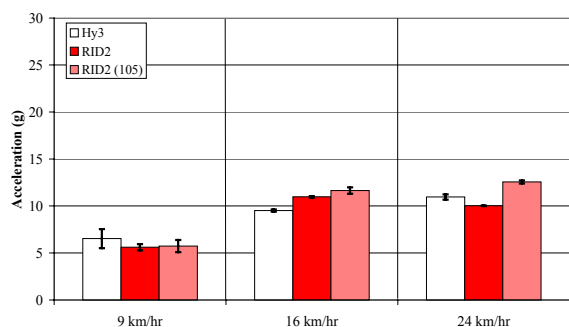


Figure 16. Series A: T1 X-accelerations.

Upper Neck Shear Forces

At 9 and 24 km/hr, the peak upper neck shear forces of the Hybrid III were greater than those of the RID2 (Figure 17). However, at 16 km/hr the peak responses of the dummies were similar. Due to the seatback deformation at 24 km/hr, the peak upper neck shear forces only increased between 9 and 16 km/hr.

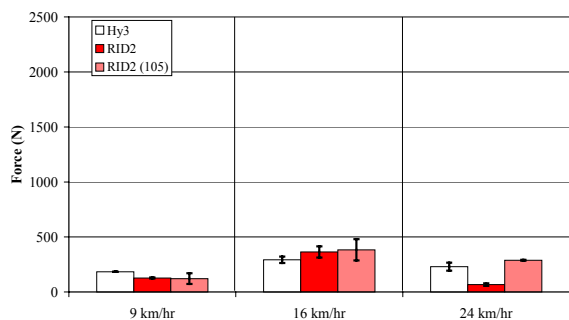


Figure 17. Series A: Upper neck shear forces, Fx.

Lower Neck Shear Forces

The Hybrid III and RID2 peak lower neck shear forces were comparable at each sled velocity (Figure 18). The lower neck shear forces of both dummies increased from 9 to 16 km/hr, but not at 24 km/hr. Like the upper neck shear forces, the seatback deformation occurring at this speed minimized the effect of the sled velocity increase on these responses. For both dummies, the shear forces at the lower neck were at least 35% greater than those at the upper neck.

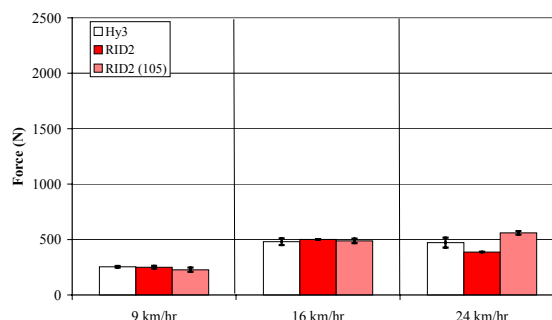


Figure 18. Series A: Lower neck shear forces, Fx.

Upper Neck Tensile Forces

In the axial direction, the peak RID2 upper neck forces were consistently greater than those of the Hybrid III (Figure 19). This is explained by the different seated heights of the two dummies. The head of the RID2, which had the greater seated height (Figure 5), hit higher on the head restraint than the Hybrid III. This resulted in the RID2 stretching over the head restraint more than the Hybrid III, resulting in higher tensile forces. The RID2 upper neck axial forces were more than double its respective shear forces. At 16 and 24 km/hr, the Hybrid III upper neck axial forces were also more than double its shear forces. The Hybrid III peak tensile responses increased with sled velocity across the entire range while those of the RID2 only increased from 9 to 16 km/hr. With respect to upper neck tension, the seatback deformation seen at 24 km/hr only limited the RID2's responses.

Lower Neck Tensile Forces

In general, the lower neck tensile forces of both dummies followed the behavior of their upper neck tensile forces. The RID2 lower neck tensile forces were consistently greater than those of the Hybrid III (Figure 20). At the lower neck, the RID2 axial forces were again more than double its respective shear forces; however, the Hybrid III axial forces were only greater than its shear forces at 24 km/hr. The Hybrid III peak tensile forces increased with each

increase in sled velocity, however, the RID2 forces only increased from 9 to 16 km/hr.

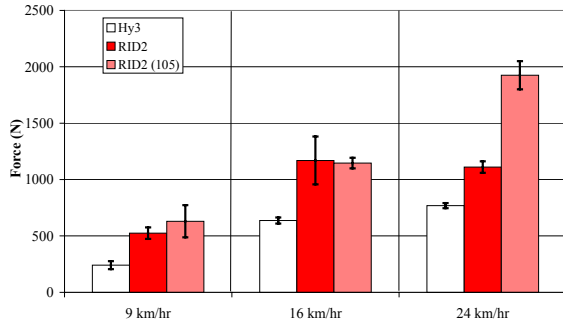


Figure 19. Series A: Upper neck tensile forces, Fz.

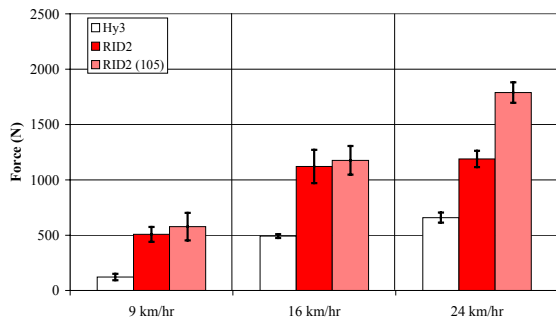


Figure 20. Series A: Lower neck tensile forces, Fz.

Occipital Condyle Extension Moments

The average extension moments at the occipital condyles are shown in Figure 21. Although the average Hybrid III extension moments were more than double those of the RID2 at each tested sled velocity, it should be noted that all the moments were less than 8 Nm. The differences between the dummies' responses were attributed to the lower bending stiffness of the RID2 neck [10].

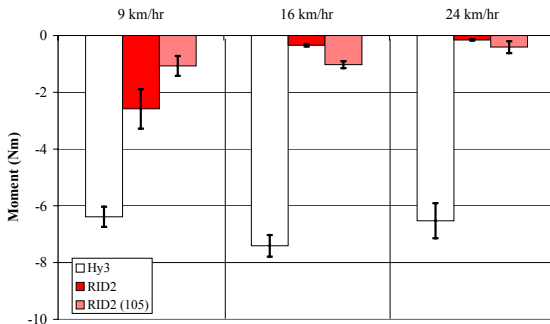


Figure 21. Series A: Occipital condyle extension moments, -My. (Note: The y-axis scale differs from that of Figure 22.)

C7/T1 Extension Moments

At the C7/T1 joint, the Hybrid III extension moments were approximately four times those of the RID2 (Figure 22). The lower bending stiffness of both the RID2 neck and thoracic spine, in comparison to the Hybrid III, contributed to this behavior [10]. The moments of both dummies increased from 9 to 16 km/hr, but it should be noted that the RID2 average moment only increased by 4 Nm. For the Hybrid III, the peak C7/T1 extension moments were at least five times greater than its occipital condyle moments.

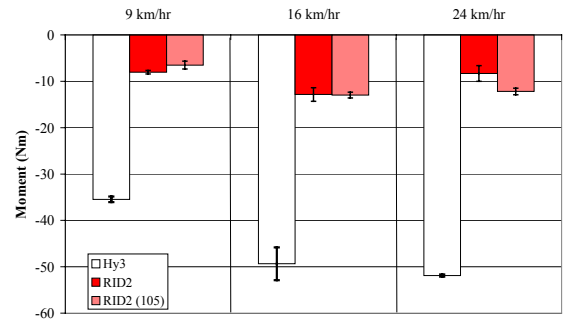


Figure 22. Series A: C7/T1 extension moments, -My. (Note: The y-axis scale differs from that of Figure 21.)

External Head Impact Fx Forces

The external head Fx forces were calculated and are shown in Figure 23. At the two lower sled velocities, the Hybrid III and RID2 responses were slightly different from each other. At 24 km/hr, the average Fx force of the RID2 was greater than that of the Hybrid III. The responses of both dummies increased from 9 to 16 km/hr. Again, the seatback deformation at 24 km/hr limited the effect of this increased sled velocity. At all three tested sled velocities, the RID2 neck also contacted the seat after initial head contact occurred. With the Hybrid III, this only occurred at the two higher velocities (16 and 24 km/hr).

External Head Impact Fz Forces

The RID2 external head Fz forces were greater than those of the Hybrid III (Figure 24). As with the upper neck tensile forces, this was due to the taller seated height of the RID2, which produced a different dummy to head restraint interaction. At 16 and 24 km/hr, the RID2 Fz forces had greater magnitudes than their corresponding Fx forces although the difference was less pronounced at the higher sled velocity. The peaks of both dummies increased from 9 to 16 km/hr. There were no

increases in the force responses when the sled velocity was increased to 24 km/hr.

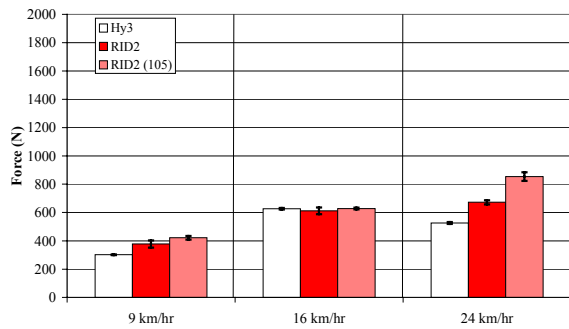


Figure 23. Series A: External head impact forces, Fx.

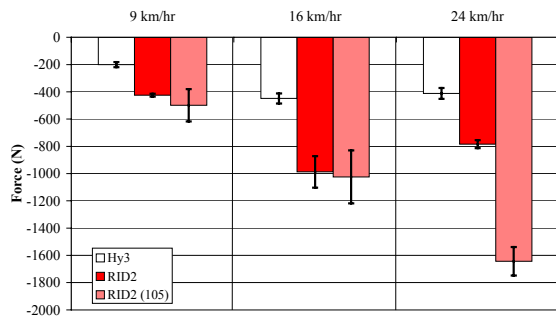


Figure 24. Series A: External head impact forces, Fz.

Head Restraint Contact Times

At 9 and 16 km/hr, the ranges of head restraint contact times for the Hybrid III and RID2 overlapped each other (Figure 25). Therefore, they were not considered to be different. At 24 km/hr, the ranges for each dummy were reduced, however the difference between the contact times of both dummies was no larger than it was at 16 km/hr. Neither the contact times of the Hybrid III nor those of the RID2 increased with sled velocity. One possible factor for this is that the dummies' interaction with the seat as the sled velocity was increased, caused more seatback deformation prior to contact. This would move the head restraint further rearward of the dummy's head, offsetting the effect of the increased sled velocity. Another factor may be the similarity of the sled acceleration pulses (Figure 2). All the pulses have very similar slopes, especially their onset slopes, and the dummies may be reacting the same way until they contact the head restraint.

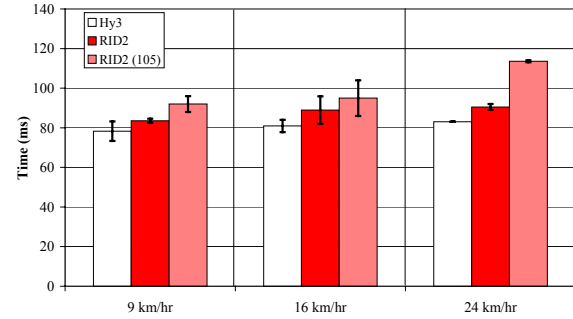


Figure 25. Series A: Head restraint contact times.

NICs

The average NIC values [23, 3, 4] of both dummies were equivalent at 9 km/hr as shown in Figure 26. At 16 and 24 km/hr, the RID2 average NICs were greater than those of the Hybrid III. Both the Hybrid III and the RID2 NIC values increased from 9 to 16 km/hr. At 24 km/hr, the effect of the sled velocity increase was countered by the effect of the seatback deformation and the NIC values did not increase.

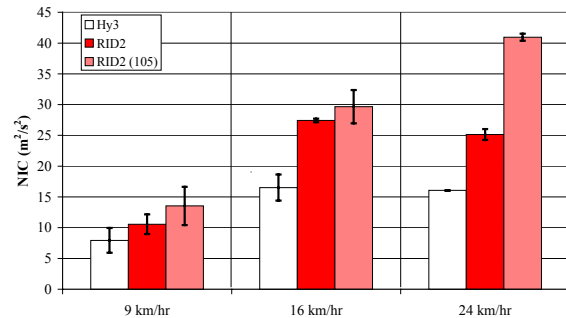


Figure 26. Series A: NICs.

Nij: Ntes

The average Nte values are shown in Figure 27. In this series, the Nte values were dominated by their tensile components. Since the RID2 had much higher tensile neck forces than the Hybrid III, due to its greater seated height, it also had greater Nte values. The Hybrid III Nte averages increased across the entire sled velocity range, while the RID2 Nte averages only increased from 9 to 16 km/hr. For the Nte, the seatback deformation that occurred at 24 km/hr limited the RID2's response but not the Hybrid III's response.

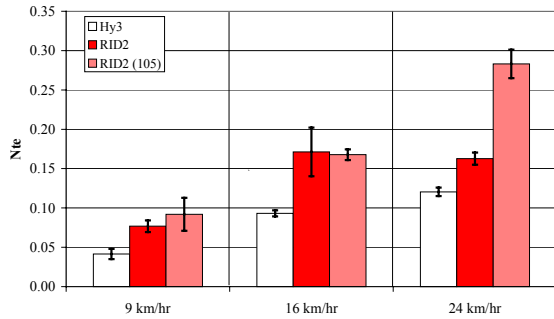
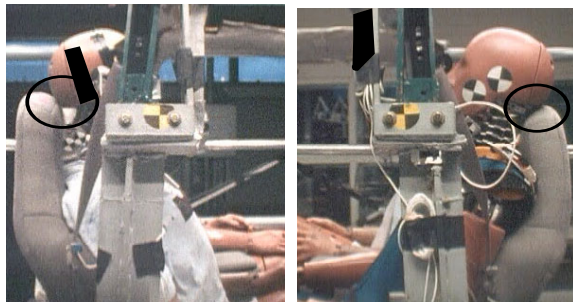


Figure 27. Series A: Ntes.

Seated Height

When set to the same backset of 55 mm, the RID2 sat higher than the Hybrid III with respect to the head restraint (Figure 5). This produced different kinematics. The Hybrid III initially struck the top front corner of the head restraint with the rear portion of its skullcap (Figure 28a). The RID2 initially struck the top of the head restraint more towards the bottom corner of its skullcap. The worst case is shown in Figure 28b. As a result, the RID2 stretched over the head restraint more and had greater axial forces (upper and lower neck tensile forces and external head impact Fz) than the Hybrid III.



a.) b.)
 Figure 28. Series A: Initial contact, 55 mm backset and 16 km/hr ΔV, a.) Hybrid III and b.) RID2.

RID2: Backset Sensitivity

As can be seen from Figures 14 through 27, the majority of the RID2 responses, including head restraint contact time, were insensitive to the backset change from 55 to 105 mm at 9 and 16 km/hr. However, at 24 km/hr, both the measured and calculated RID2 responses increased at the larger backset. As previously stated, more seatback deformation occurs at this velocity than at 16 km/hr (Figure 15). This, in addition to the larger backset of 105 mm, delayed the head restraint contact time by approximately 13 ms (Figure 25) allowing the head to head restraint contact velocity to increase. At approximately 123 ms, the head struck the internal

head restraint structure as indicated by the resultant external head impact force time-history traces (Figure 29). This resulted in the magnitude increases noted previously and caused many of the responses to increase with sled velocity across the entire tested range of 9-24 km/hr, rather than just between 9 and 16 km/hr. Five of these responses have been normalized by their respective values at the 55 mm backset and are shown in Figure 30.

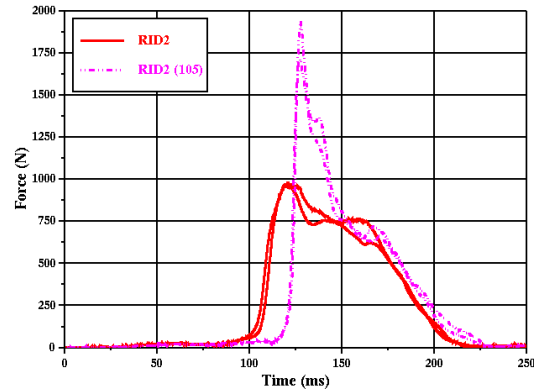


Figure 29. Series A: RID2 resultant external force time history curves, 24 km/hr ΔV.

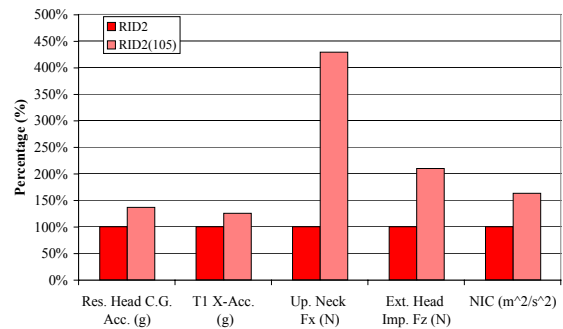


Figure 30. Series A: RID2 backset sensitivity, 24 km/hr. Normalized responses.

SERIES B

The responses of the RID2, the Hybrid III and the BioRID II in sled test Series B are compared in the following section. Each dummy was evaluated for its ability to differentiate between sled velocity (17 km/hr or 27 km/hr) and head restraint position (full up or full down). Two repeats of each test configuration were run. However, one of the BioRID II repeat tests was not used in the dummy comparison due to backset variance (see Table 1). These data were used to evaluate the BioRID II's sensitivity to backset. It should also be noted that the BioRID II version tested in this evaluation could not be

instrumented with a lower neck load cell. Therefore, it is not discussed in the lower neck response sections.

Resultant Head CG Accelerations

At 27 km/hr, the Hybrid III peak head acceleration was greater than that of the BioRID II, which in turn was greater than the RID2 value (Figure 31). At 17 km/hr, the dummy peak head accelerations were more similar. In all cases, the peaks increased with sled velocity. Similarly, the peaks increased as the head restraint position was changed from full up to full down. However, for the BioRID II at 27 km/hr, the difference between the two head restraint conditions was only 1.4 g.

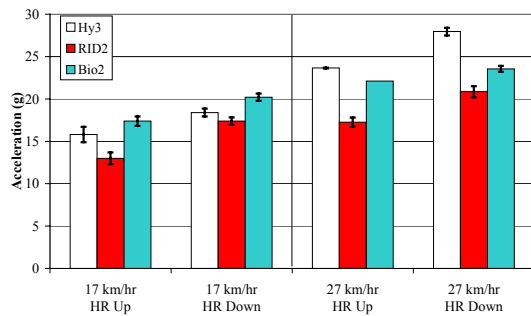


Figure 31. Series B: Resultant head CG accelerations.

T1 X-Accelerations

As shown in Figure 32, the Hybrid III peak T1 X-acceleration was consistently higher than the RID2 peak, however at 17 km/hr with the head restraint up, the difference was less than 1 g. All dummies increased peak T1 acceleration with increased sled velocity. Head restraint position did not influence the T1 X-accelerations.

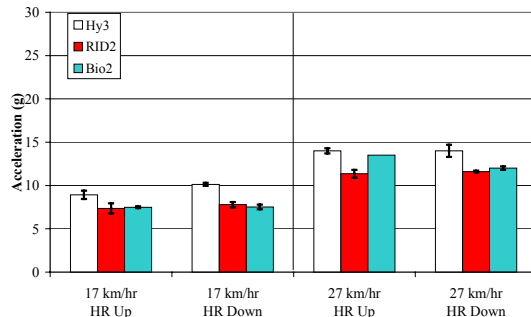


Figure 32. Series B: T1 X-accelerations.

Upper Neck Shear Forces

The Hybrid III peak upper neck shear forces were greater than those of the RID2 (Figure 33). This was due to the greater shear stiffness of the Hybrid III's neck [10] and its larger backsets. The Hybrid III peak upper neck shear forces were also greater than those of the BioRID II in the head restraint full up condition. At 27 km/hr with the head restraint full down, the BioRID II peak was greater than the RID2 and Hybrid III peaks. With respect to sled velocity, only the upper neck shear force of the BioRID II with the head restraint down increased from 17 to 27 km/hr. Only the BioRID II responses at 27 km/hr increased when the head restraint was moved from full up to full down.

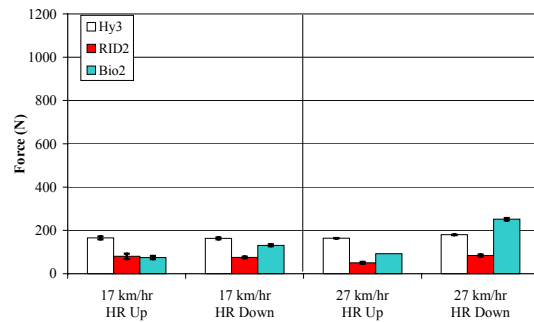


Figure 33. Series B: Upper neck shear forces, Fx.

Lower Neck Shear Forces

Similar to the upper neck shear forces, the lower neck shear forces of the Hybrid III were greater than those of the RID2 (Figure 34). This was due to the greater stiffness of the Hybrid III thoracic spine compared to that of the RID2 [10]. Only the Hybrid III responses and the RID 2 with the head restraint down increased consistently with sled velocity. Both the Hybrid III and RID2 responses increased as the head restraint was changed from up to down. For these two dummies, the peak lower neck shear forces were at least 2.5 times greater than the upper neck shear forces.

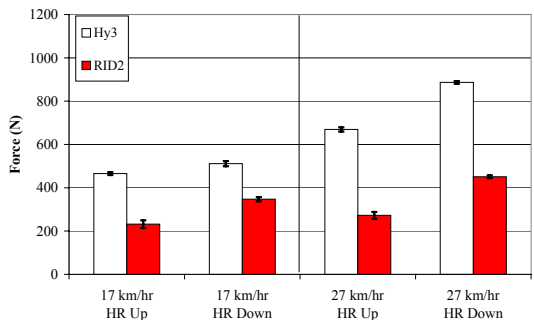


Figure 34. Series B: Lower neck shear forces, Fx.

Upper Neck Tensile Forces

The peak upper neck tensile forces of the BioRID II were greater than those of the Hybrid III and the RID2 except at 27 km/hr with the head restraint down, where all three dummies had similar peak values (Figure 35). At 17 km/hr with the head restraint down and 27 km/hr with the head restraint up, the Hybrid III peak was also greater than the RID 2 peak. For all the dummies, the peak upper neck tension increased with the increase in sled velocity. Similarly, all dummies measured a higher peak upper neck tension when the head restraint position was full down. The peak upper neck tensile forces ranged from twice to nearly ten times that of their respective upper neck shear forces.

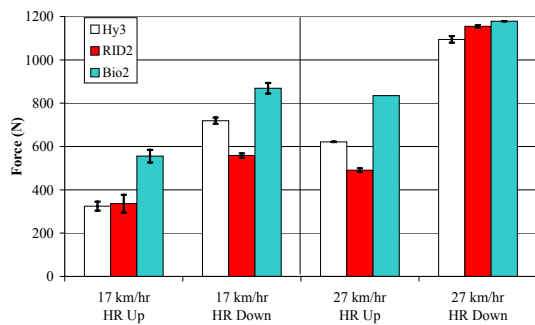


Figure 35. Series B: Upper neck tensile forces.

Lower Neck Tensile Forces

Figure 36 shows that the peak lower neck tensile forces of the RID2 were consistently greater than those of the Hybrid III. Additionally, the peak lower neck tension of both dummies increased with sled velocity and when the head restraint was lowered to the full down position.

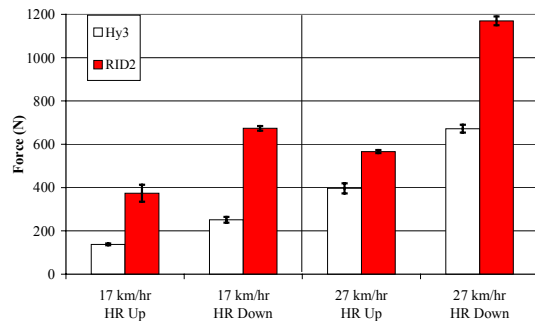


Figure 36. Series B: Lower neck tensile forces.

Occipital Condyle Extension Moments

At 17 km/hr with the head restraint full up, the peak extension moments of the Hybrid III were greater than those of the RID2 and BioRID II; however the difference between the Hybrid III and

RID2 values was less than 5 Nm. (Figure 37). At 24 km/hr with the head restraint full down, the peak BioRID moment was greater than that of the RID2, while the Hybrid III value fell between them. The extension moments of all the dummies increased with sled velocity, regardless of head restraint position. The BioRID II displayed the largest magnitude increase with sled velocity. The BioRID II response also showed the greatest increase between the head restraint full up and full down configurations at both sled velocities.

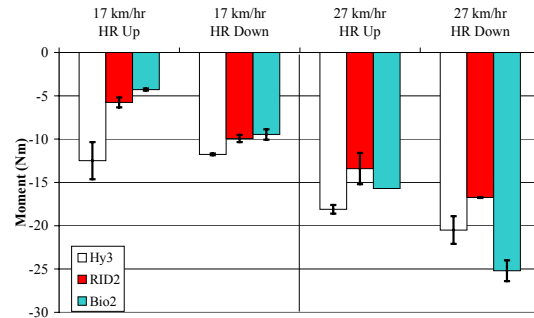


Figure 37. Series B: Occipital condyle extension moments, -My. (Note: The y-axis scale differs from that of Figure 38).

C7/T1 Extension Moments

Figure 38 shows that the C7/T1 extension moments of the Hybrid III were at least four times the RID2 values for all test conditions. The peak C7/T1 extension moments of the Hybrid III increased with sled velocity and with the change in head restraint position. The C7/T1 peak extension moments of the Hybrid III were at least three times higher than its occipital condyle moments.

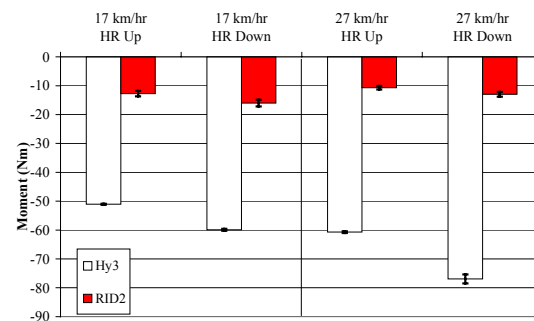


Figure 38. Series B: C7/T1 extension moments, -My. (Note: The y-axis scale differs from that of Figure 37.)

External Head Impact Fx Forces

At 17 km/hr with the head restraint full up, the external head impact Fx force of the BioRID II was

greater than that of both the Hybrid III and the RID2 (Figure 39). With the head restraint down, the Hybrid III response was lower than those of the RID2 and BioRID II. At the 27 km/hr with the head restraint down, the BioRID II peak external Fx force was lower than those of the Hybrid III and RID2. The peak external head Fx forces for all the dummies increased with sled velocity except for the BioRID II with the head restraint full down. The responses of all the dummies also increased as the head restraint was lowered, except for the BioRID II at 27 km/hr. The relatively low value of the BioRID II response in the 27 km/hr, head restraint down condition is explained by the dummy kinematics. In this condition, the head traveled over top of the head restraint, minimizing the shear force exerted on the head.

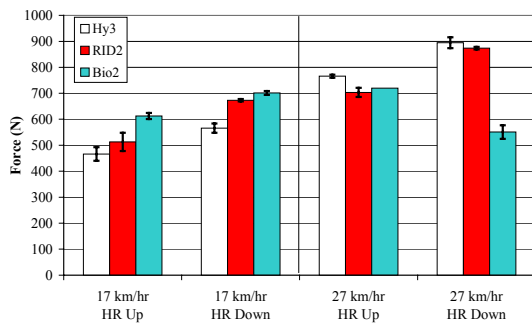


Figure 39. Series B: External head impact Fx forces.

External Head Impact Fz Forces

At 17 and 27 km/hr with the head restraint full up, the peak BioRID II Fz forces were greater than those of the Hybrid III, while the RID2 values fell between them (Figure 40). At 17 km/hr with the head restraint full down, both the BioRID II and RID2 peak Fz forces were greater than that of the Hybrid III. At 27 km/hr with the head restraint full down, the RID2 peak Fz force was greater than those of both the Hybrid III and BioRID II. Both the responses of the Hybrid III and RID2 increased with sled velocity when the head restraint was full down. The peak Fz forces for all three dummies increased when the head restraint was lowered, regardless of sled velocity. In this test series, the peak external Fz force was one of the responses most influenced by head restraint position. The peak magnitudes with the head restraint full down were 1.7 to 3.5 times greater than the peaks with the head restraint full up.

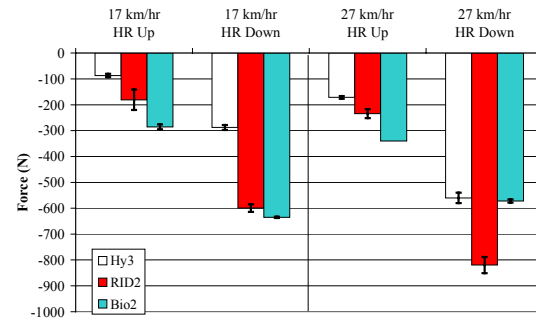


Figure 40. Series B: External head impact Fz forces.

NICs

The peak BioRID II NIC values were always greater than those of the Hybrid III and the RID2, regardless of sled velocity or head restraint position (Figure 41). At 27 km/hr with the head restraint full up, the Hybrid III also had a greater NIC than the RID2. The peak NIC values for all three dummies increased with increasing sled velocity. The NIC values did not change with head restraint position except for the RID2 and BioRID II at 27 km/hr.

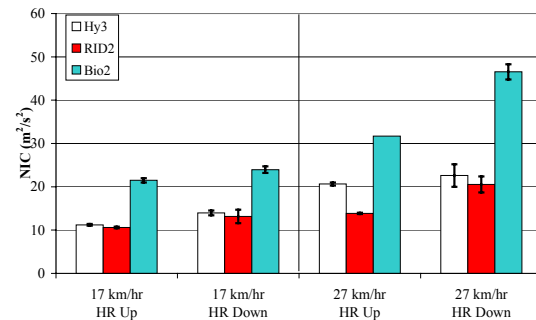


Figure 41. Series B: NICs.

In a previous evaluation program, the BioRID II was tested on rigid bench seats with no head restraints [10]. The same sled acceleration pulses were used in both programs. At the 17 km/hr ΔV , the average NIC value of the BioRID II on the rigid bench was $17.8 \text{ m}^2/\text{s}^2$ which was lower than the NIC values seen with the production seats, regardless of head restraint position. At the higher 27km/hr ΔV , the average NIC peak was 31.7 in the rigid bench seat condition. This was equivalent to the average NIC for the production seat with the head restraint full up but was still lower than the NIC with the head restraint full down. These results were counter-intuitive because the existence of a head restraint should decrease the risk of soft tissue neck injuries. However, the NIC values did not predict this, which means that the NIC may not be a good injury predictor.

Nij: Ntes

Figure 42 shows that at both sled velocities with the head restraint down, the BioRID II peak Nte values were greater than those of the Hybrid III and RID2. The peak Nte values for all three dummies increased with sled velocity and with the lower head restraint position. The BioRID II Nte peaks showed the largest change in magnitude both with sled velocity and head restraint position. For the RID2 and Hybrid III, the peak values of Nte at 17 km/hr with the head restraint full down were nearly identical to those measured at 27 km/hr with the head restraint full up.

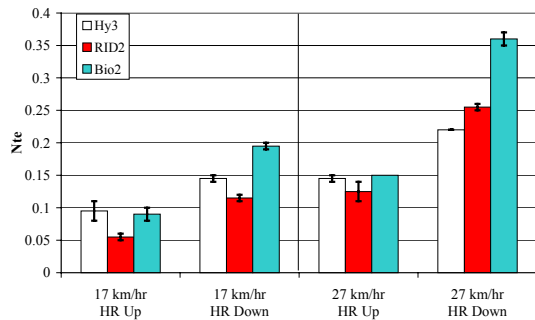


Figure 42. Series B: Ntes.

Head Restraint Contact Times

At both sled velocities with the head restraint full up, the RID2 contact times were less than those of the Hybrid III and BioRID II (Figure 43). This is attributed to the different bending stiffnesses of the dummy necks and to their different backsets (Figure 8). None of the dummies showed a change in restraint contact time with increased sled velocity. As explained in Series A, two possible factors for this may be the increased dummy/seat interaction prior to contact and the similarity of the acceleration pulses. The head restraint contact times of the RID2 increased with the lower head restraint position. The variations in these responses may be subject to the calculation method (see Methods section).

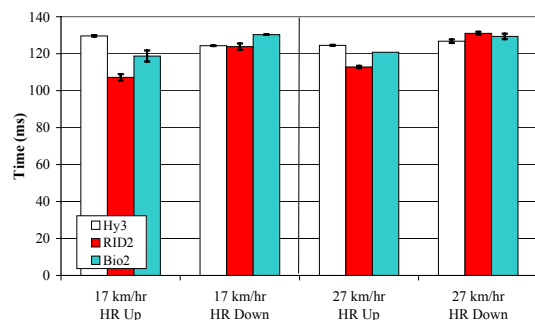


Figure 43. Series B: Head restraint contact times.

For all three dummies in Series B, the lowest peak responses were seen at the 17 km/hr ΔV with the head restraint full up. The highest peak responses occurred at the 27 km/hr ΔV with the head restraint full down. The peaks of the two other conditions, 17 km/hr with the head restraint full down and 27 km/hr ΔV with the head restraint full up, fell between those two extremes.

BioRID II: Backset Sensitivity

In one of the two 27 km/hr, head restraint full up tests, the backset of the BioRID II was 57 mm. In the other test, the backset was 83 mm. This difference in backset influenced both the measured and calculated responses, five of which are shown in Figure 44. Each individual response was normalized by its respective value at 57 mm. Another interesting point to note is the difference in the timing of the peak responses due to the change in backset. (Appendix C gives the time history curves for these responses.) At 27 km/hr, the peak responses of the 57 mm backset condition occurred on average 18 ms earlier, including a 20 ms shift in head restraint contact time, compared to the 83 mm backset responses.

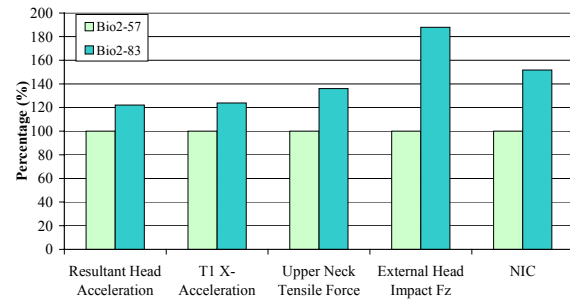


Figure 44. Series B: BioRID II backset sensitivity, 27 km/hr. Normalized responses.

SERIES C

In this series, the effect of sled velocity and the position of the head restraint on the responses of the Hybrid III and RID2 were studied. Sled tests were conducted at 10 and 24 km/hr.

Resultant Head CG Accelerations

The Hybrid III had higher peak resultant accelerations than the RID2 at 24 km/hr as shown in Figure 45. This difference may be due to the greater backset of the Hybrid III and the increased sled velocity. At 10 km/hr, this trend was not evident. The responses of both dummies increased with increasing sled velocity. The peak accelerations of the Hybrid III and the RID2 did not increase when the head restraint position was changed to full down. This may

be due to the fact that the head CGs of both dummies were below the top of the head restraint for both the full up and full down head restraint positions (Figure 13).

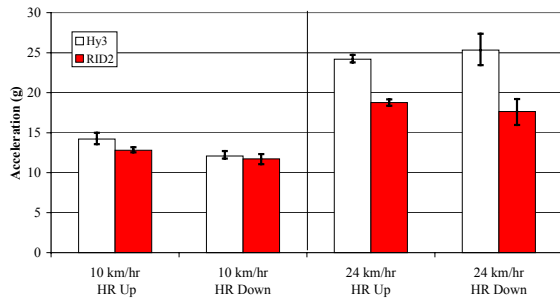


Figure 45. Series C: Resultant head CG accelerations.

T1 X-Accelerations

The T1 X-accelerations of the Hybrid III and RID2 showed the same trends as the head CG resultant accelerations. See Figure 46. The initial geometric factors, as described in the previous section, influenced the T1 X-accelerations in the same manner.

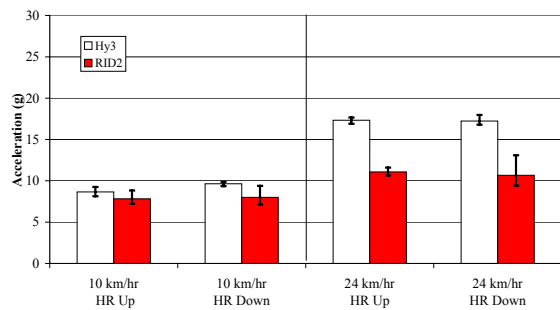


Figure 46. Series C: T1 X-accelerations.

Upper Neck Shear Forces

For both sled velocities, the Hybrid III upper neck shear forces were greater than those of the RID2 (Figure 47). This was attributed to the greater shear stiffness of the Hybrid III neck [10] and its larger backsets. The response of the Hybrid III with the head restraint full up increased with sled velocity. At the 24 km/hr ΔV with the head restraint full down, the Hybrid III peak shear force decreased as compared to the full up position. In the RID2, the upper neck shear forces were independent of sled velocity and head restraint position. This may have been due to the greater head restraint displacement at 24 km/hr as seen in Figure 48. The head restraint always deflected more in the full up position than in the full down position.

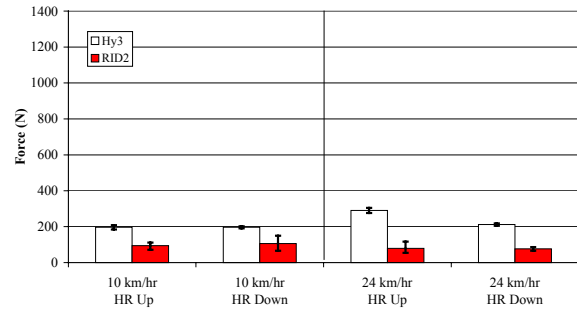


Figure 47. Series C: Upper neck shear forces, Fx.



a.) b.)
Figure 48. Series C: Maximum head restraint deflection with the RID2 a.) 10 km/hr and b.) 24 km/hr.

Lower Neck Shear Forces

Similar to the upper neck shear forces, the Hybrid III lower neck shear forces were greater than those of the RID2 (Figure 49) for all test conditions. This was attributed to the higher stiffness of the Hybrid III thoracic spine. The Hybrid III responses almost doubled with the sled velocity increase while the RID2 responses increased by at least 15%. The lower neck shear forces of both the Hybrid III and the RID2 were at least 80% greater than their upper neck shear forces.

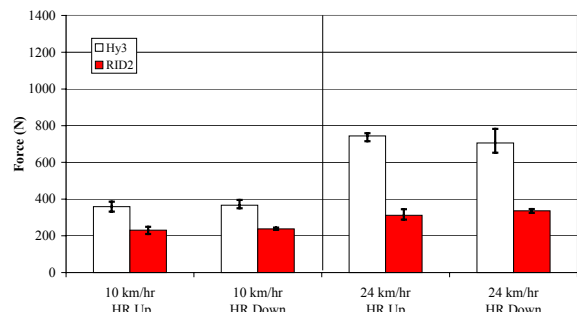


Figure 49. Series C: Lower neck shear forces, Fx.

Upper Neck Tensile Forces

In each test condition, the upper neck tensile peaks of the Hybrid III and RID2 were comparable to each other (Figure 50). The responses of both dummies increased with sled velocity by at least 80%. The upper neck tensile forces were at least double the shear forces for both dummies.

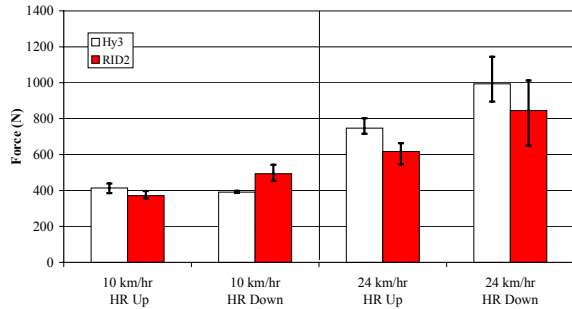


Figure 50. Series C: Upper neck tensile forces, Fz.

Lower Neck Tensile Forces

At 10 km/hr with the head restraint full down, the peak lower neck tensile forces of the RID2 were greater than those of the Hybrid III (Figure 51). With the head restraint full up, the difference between the Hybrid III and RID2 averages was less than 200 N. The Hybrid III tensile forces increased with sled velocity. The 24 km/hr RID2 lower neck axial forces were unavailable due to an instrumentation malfunction.

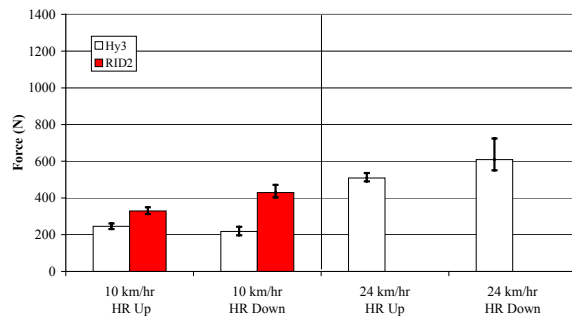


Figure 51. Series C: Lower neck tensile forces.

Occipital Condyle Extension Moments

At 24 km/hr with the head restraint full up, the peak Hybrid III extension moment was greater than that of the RID2 but the difference in the peak values was less than 5 Nm (Figure 52). In the other test conditions, the difference was even smaller and the moments were considered to be comparable. The Hybrid III extension moments increased with sled velocity, however, the magnitude change was less than 5 Nm.

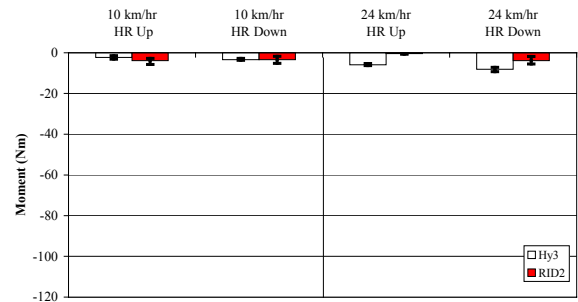
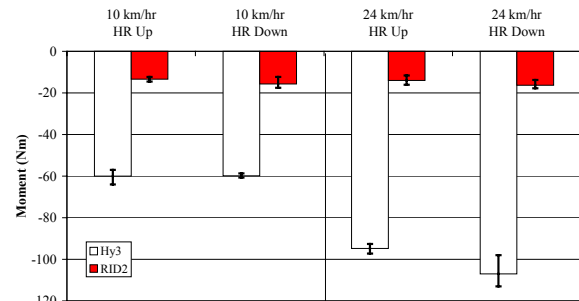


Figure 52. Series C: Occipital condyle extension moments, -My.

C7/T1 Extension Moments

The Hybrid III C7/T1 extension moments were more than three times those of the RID2 at both sled velocities (Figure 53). This was due to the higher bending stiffness of the Hybrid III neck compared to that of the RID2. The Hybrid III peak moments also increased with sled velocity. The C7/T1 peak extension moments of the Hybrid III were an order of magnitude higher than its occipital condyle moments. The RID2 C7/T1 moments were more than double its occipital condyle moments.



Figures 53. Series C: C7/T1 extension moments, -My.

External Head Impact Fx Forces

At 24 km/hr with the head restraint down, the peak Hybrid III external head impact Fx force was greater than that of the RID2 (Figure 54). In the other test conditions, the dummies' forces were comparable. Both the Hybrid III and the RID2 peaks increased with sled velocity.

External Head Impact Fz Forces

The peak external head impact Fz forces of both dummies were comparable for each test condition (Figure 55). With the head restraint full down, the Hybrid III peak forces increased with sled velocity.

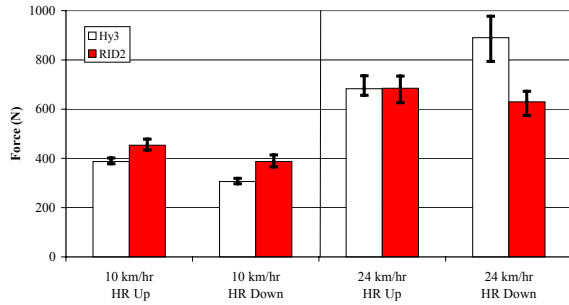


Figure 54. Series C: External head impact Fx forces.

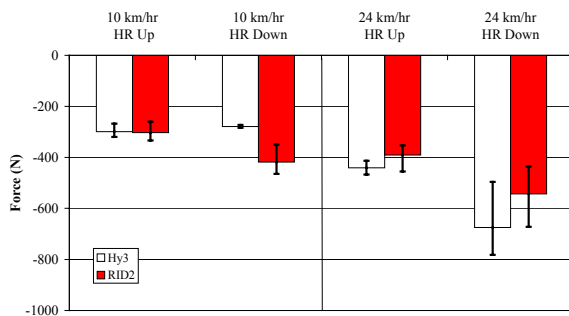


Figure 55. Series C: External head impact Fz forces.

Head Restraint Contact Times

With the head restraint in the full up position, the RID2 contacted the head restraint sooner than the Hybrid III (Figure 56). The contact times of the two dummies were more similar when the head restraint was full down. The head restraint contact times for both dummies did not change with sled velocity. Two possible reasons for this may be the increased dummy/seat interaction prior to contact, and the similar slopes of the acceleration pulses. The head restraint contact time was independent of head restraint position for both dummies.

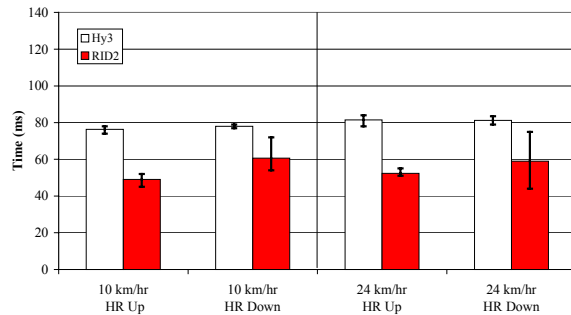


Figure 56. Series C: Head restraint contact times.

NICs

At 10 km/hr, regardless of head restraint position, and at 24 km/hr with the head restraint full down, the

Hybrid III and RID2 had similar NIC values (Figure 57). At the higher 24 km/hr ΔV with the head restraint full up, the Hybrid III peak NIC was greater than that of the RID2. Regardless of head restraint position, the Hybrid III NIC values increased with sled velocity while the RID2 NIC values did not increase.

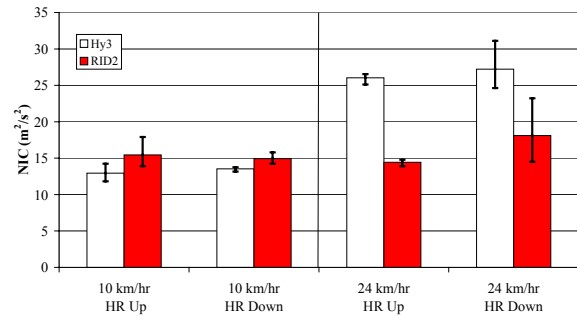


Figure 57. Series C: NICs.

Nij: Ntes

The Hybrid III and RID2 had comparable Nte values for each test condition (Figure 58). The peak Nte values of both dummies also increased with sled velocity. At 24 km/hr, the peak Nte values of both dummies increased when the head restraint was lowered.

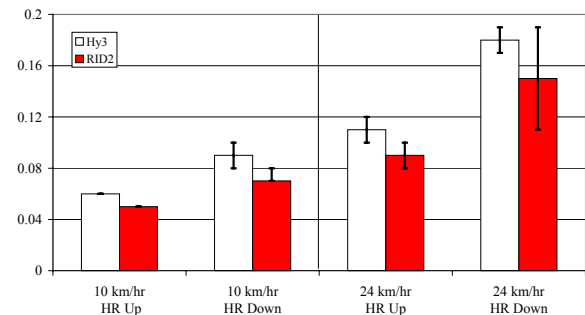


Figure 58. Series C: Ntes.

One result seen in Series C that was not seen previously was that none of the Hybrid III or RID2 responses distinguished the two head restraint positions.

Repeatability

In Series C, three repeat tests were conducted on both the Hybrid III and RID2 in each test condition. An analysis was conducted to determine the degree of repeatability of the dummy responses and how well they correlated with the impact conditions. Correlation analysis was done on the two main aspects of similarity between the repeated responses, namely, the magnitude and the characteristic shape.

Correlation coefficients with values of 1 indicate identical characteristics whereas values of 0 indicate orthogonality or lack of correlation.

Before analyzing the responses of the dummies, a coefficient of variance (CV) study was done for two test setup parameters: dummy position and sled pulse. The dummy H-point position and the peak sled pulse CVs were studied for each repeated test condition to confirm that there was minimal variation in the input. The results of that study are shown in Table 3.

Table 3.
Coefficient of Variation Table (%)

	Hybrid III				RID2			
	10 km/hr		24 km/hr		10 km/hr		24 km/hr	
	HR Up	HR Down	HR Up	HR Down	HR Up	HR Down	HR Up	HR Down
H-pt X	0.2	0.3	0.3	0.3	0.1	0.0	0.2	0.18
H-pt Z	1.8	1.4	2.3	0.5	1.2	1.9	0.4	0.54
Peak Sled Acc.	10.0	2.32	0.94	1.22	10.0	2.32	0.94	1.22

It is seen from Table 3 that the majority of the CVs were below 3%, which reflects a high degree of repeatability in the initial test setup. The peak sled pulse acceleration at 10 km/hr was the only parameter that was at 10%.

The correlation coefficients for the magnitude and shape for the majority of the measured dummy responses were computed using the formulas given by Xu et al. [25]. Due to space limitations, only the head and T1 X-acceleration responses of the Hybrid III and RID2 are presented here. The results of this analysis are shown in Figures 59-62. Appendix D, Tables D1-D4 give additional results.

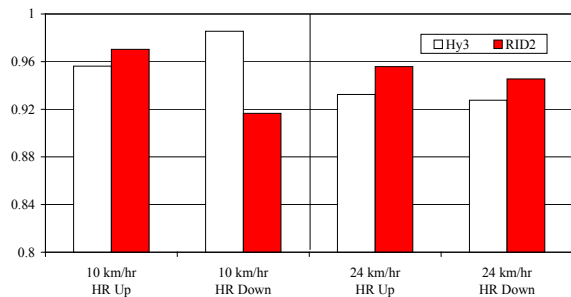


Figure 59. Magnitude correlation coefficient for the head acceleration response.

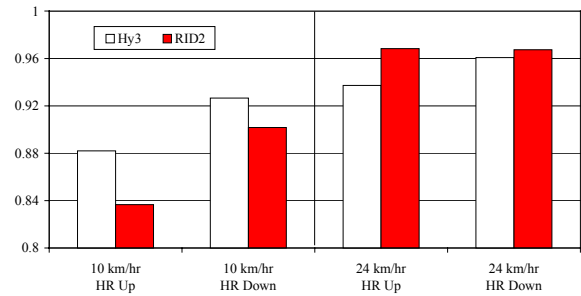


Figure 60. Magnitude correlation coefficient for the T1 X-acceleration response.

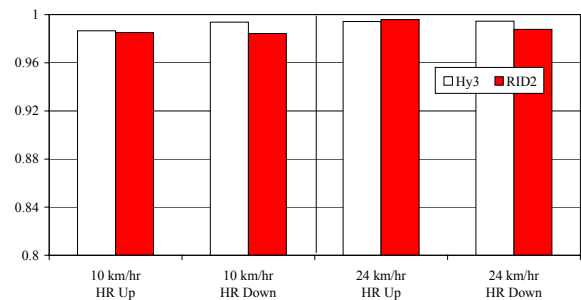


Figure 61. Shape correlation coefficient for the head acceleration response.

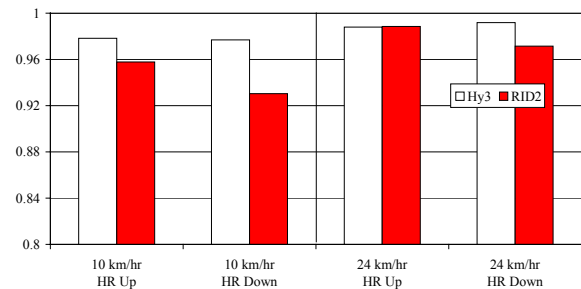


Figure 62. Shape correlation for the T1 X-acceleration response.

The repeatability of the dummy responses was classified according to Table 4.

Table 4.
Classification table for correlation coefficient

Correlation Coefficient	Classification
$0.97 \leq 1.00$	Excellent
$0.91 < 0.97$	Good
$0.00 < 0.91$	Poor

For both the Hybrid III and RID2, the bar charts show that the shape correlation coefficient values for both the head and T1 X-acceleration responses were consistently better than the magnitude values. The head had better correlation coefficients compared to the T1 for both magnitude and shape. Overall, the majority of the correlation coefficients were higher than 0.9, indicating an excellent to good degree of repeatability for both dummies. The only response with a correlation coefficient below 0.9 was the peak magnitude of T1 for the head restraint full up position at 10 km/hr. This may be attributed to the low CV value for the sled pulse in this test condition.

General Observations

In this section, any findings or trends that were observed in two or more of the test series are discussed.

Dummy Characteristics

Although all three dummies were intended to represent the 50th percentile male, their seated heights relative to the head restraint were different. In Series A, the Hybrid III head was more than 10 mm lower than that of the RID2 (Figure 5). In Series B, the Hybrid III head was at least 10 mm lower relative to the head restraint with at least 20 mm greater backset than the heads of the other two dummies, Figures 8 and 9. On the average, the head of BioRID II was consistently higher relative to the head restraint than those of the other dummies. In Series C, the vertical height measurements were not taken.

The difference in seated heights may also be explained by their designs. The Hybrid III, like the ATD 502, was designed for an automotive seated posture with an eye location that matched the 50th percentile adult male eyepoints [9, 24]. The RID2 design was revised to match the length of the WorldSID [15], and therefore matches the stature for a 50th percentile male as reported in Anthropometry of Motor Vehicle Occupants (AMVO) [22, 5]. The BioRID II was also designed to match the AMVO data [6, 22]. These differences in seated height, whether due to dummy positioning or design, may affect the way each dummy interacted with the head restraint/seat system and their responses.

One of the most noticeable differences between the Hybrid III and RID2 was the magnitudes of their C7/T1 extension moments. The Hybrid III moments were consistently at least three times greater than those of the RID2. This was due to the lower bending

stiffness of the RID2 neck and thoracic spine compared to those of the Hybrid III [10]. Throughout the series, the RID2 C7/T1 extension moments remained below 20 Nm. It should also be noted that the Hybrid III C7/T1 extension moments were at least three times greater than its occipital condyle moments. The BioRID II used in this evaluation was not equipped with a lower neck load cell; therefore, no comparison can be made.

Throughout the evaluation, there was one trend that was seen in both the Hybrid III and the RID2. The lower neck shear forces of both dummies were consistently greater than their respective upper neck shear forces by at least 35%.

A second trend that was observed was that the upper neck tensile forces of the BioRID II and RID2 were always greater than their respective upper neck shear forces. This was usually true for the Hybrid III as well; with the exception of the 8 km/hr Series A tests.

Dummy Responses to Sled Velocity

Overall, in each of the three test series, the tested dummies were found to be sensitive to sled velocity. Although there were many responses that increased as the sled velocity was increased, there were very few highly sensitive responses that were consistent across the entire evaluation. For the Hybrid III, only the lower neck tensile force increased in all three test series as the sled velocity was increased. For the RID2, it was the upper neck tensile force. The BioRID II was only tested in Series B. Its most sensitive responses were the upper neck extension moment, the Nte, and the NIC.

The head restraint contact times for each dummy, in all three test series, were insensitive to the sled velocities and acceleration pulses used in this evaluation. There are two possible contributors to this phenomenon. The first is that the dummies' interaction with the seat, as the sled velocity was increased, caused more seatback deformation prior to contact. This would move the head restraint further rearward of the dummy's head, offsetting the effect of the increased sled velocity. Another factor may be that within each test series, the sled acceleration pulses had very similar onset slopes, regardless of sled velocity, and the dummies may be reacting the same way until they contact the head restraint. The influence of these two factors may vary depending on the type of seat and sled acceleration pulses used.

With respect to the sled velocity change from 16 to 24 km/hr, the majority of the responses of the Hybrid III and RID2 did not increase in Series A.

However, at a comparable sled velocity change from 17 to 27 km/hr, the majority of the Hybrid III and RID2 responses did increase in Series B. This can be attributed to the different levels of seatback deformation between the two series.

Dummy Responses to Head Restraint Position

Series B and C both investigated the effect of head restraint position on the dummy responses. In Series B, the majority of the BioRID II, Hybrid III and RID2 responses increased when the head restraint position was changed from full up to full down. In Series C, the majority of the Hybrid III and RID2 responses did not change with head restraint position. (The BioRID II was not tested in Series C).

In Series B, when the head restraint was full up, the top of the head restraint was above the CG of the heads of all three dummies (Figure 9). When the head restraint was full down, the top of the head restraint was below the head CG. In Series C, the top of the head restraint was always above the CG of the dummies' heads, regardless if it was in the full up or full down position (Figure 13). This is illustrated in Figure 63. Once the top of the head restraint is above the CG of the dummy's head, either the Hybrid III or the RID2, increasing the height of the head restraint does not have a significant effect on the dummy responses.

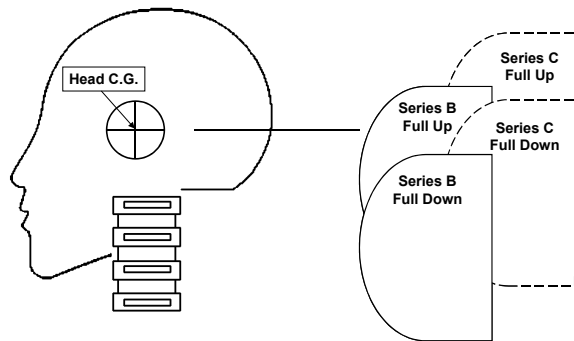


Figure 63. This graphic illustrates only the vertical height difference, relative to the CG of the head, between the full up and full down head restraint positions for Series B and C. (The backsets are not represented here).

For Series B, the external head impact Fz and the upper and lower neck tensile forces were the most sensitive Hybrid III responses to head restraint position. For the RID 2, the external head impact Fz, the Nte, and the upper neck tensile force were the three responses that increased the most when the head restraint was lowered. For the BioRID II, the

Nte, the upper neck shear force, and the external head impact Fz were the top three responses most affected by head restraint position. Across the three dummies, the external head impact Fz force was the most sensitive response to head restraint position while the T1 X-acceleration response was the least.

For Series C, none of the Hybrid III or RID2 responses distinguished between the two head restraint positions.

Backset Sensitivity

In Series A, the RID2 was tested at two different backsets: 55 and 105 mm. At the two lower sled velocities, 9 and 16 km/hr, most of the RID2 responses were insensitive to the change in backset. However, at 24 km/hr more seatback deformation occurred than at 16 km/hr, which combined with the larger backset, delayed the head restraint contact time by approximately 13 ms (Figure 25). The head gained more velocity and struck the internal structure of the head restraint (Figure 29), resulting in the majority of the RID2(105) responses increasing.

In Series B, the BioRID II was tested at 27 km/hr with backsets of 57 and 83 mm. Both the measured and calculated responses increased at the larger backset.

Handling Issues

Use of these dummies in a testing environment highlighted several areas where the dummies were already improved or could be improved further.

Hybrid III

The Hybrid III could benefit from the addition of tilt sensors to the head and pelvis regions to streamline the positioning process.

The Hybrid III is not designed for T1 target placement, requiring the test labs to fabricate something on site. Designated target locations on the lower neck would simplify this.

RID2

The lifting mechanism does not securely hold the dummy in place but allows it to slip sideways while suspended. This lifting method is difficult to use in a vehicle buck environment.

The neck positioning cable system requires improvement. It is complicated to use, difficult to adjust accurately, and also is not robust, because the cables slipped from their setting during testing and required readjustment more than once.

The neck is too soft to maintain its position in between testing, and requires a neck brace or removal of the head/neck, which is not practical for production environments. The brace that was supplied did not fit the dummy well and therefore did not provide optimal support for the neck, and also required removal of the T1 targets between consecutive tests. A system that is more customized for the dummy and easier to use is needed.

The use of tilt sensors for positioning the RID2 could streamline the positioning process, however the system provided requires some improvement. The tilt sensors should all be hard mounted in their appropriate locations to prevent slippage of the sensor inside the dummy.

BioRID II

The lifting mechanism must be removed for each test to prevent interaction with the lap belt, and the neck attachment also requires the T1 targets to be removed each time the dummy is lifted. The entire mechanism is difficult to use in a vehicle buck.

The use of a water bladder on a sled environment is a concern. Leakage could cause serious damage to sled equipment. Perhaps a fluid with a higher viscosity or gel like that used in the abdominal insert developed by Rouhana et al. [16] would minimize the damage caused by a leak.

Finally, the arm attachments do not securely attach the arms to the dummy. During sled tests the arms were seen to flail considerably, apparently causing damage to the chest jacket.

RID2 Neck Buffer Configuration

After this evaluation was completed, it was discovered that the RID2 neck buffer configuration was incorrect in both Series B and C. In Series B, the RID2 neck was missing a symmetrical pair of "D" buffers on neck level 1 (Figure 64). In Series C, a symmetrical pair of "C" buffers was missing on neck level 3 (Figure 65). To determine the effect of the missing buffers, 3 m/s pendulum tests were run with a RID2 neck that was configured as designed (correctly) and then configured to match each of the two tested configurations. Two repeat tests were conducted on each configuration in both flexion and extension. Due to the similar responses of all three neck configurations, see Appendix E, the effect of the missing buffers was judged to be negligible and does not invalidate the presented data.

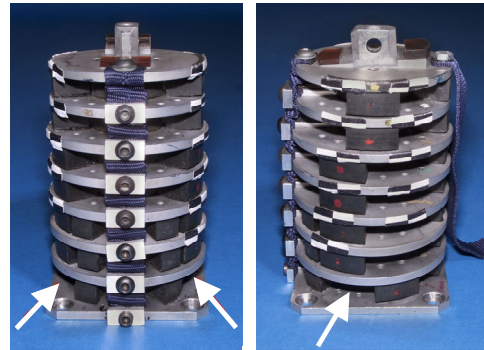


Figure 64. Series B: RID2 neck buffer configuration. The arrows point to the missing pair of "D" buffers.

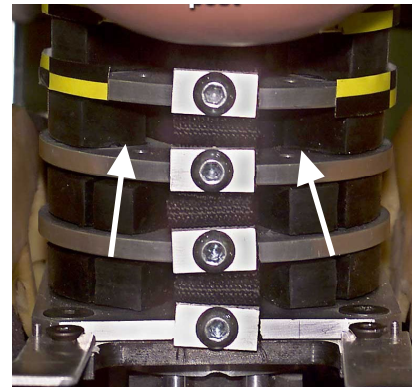


Figure 65. Series C: RID2 neck buffer configuration. The arrows point to the missing pair of "C" buffers.

CONCLUSIONS

- The C7/T1 extension moments of the Hybrid III were at least three times greater than those of the RID2. (The BioRID II was not instrumented with a lower neck load cell.)
- For the Hybrid III, the C7/T1 extension moments were at least three times its moments at the occipital condyles.
- For the Hybrid III and the RID2, the lower neck shear forces were always at least 35% greater than their respective upper neck shear forces. (The BioRID II was not instrumented with a lower neck load cell.)

- For the BioRID II and the RID2, the upper neck tensile forces were always greater than their respective upper neck shear forces.
 - For the Hybrid III, the upper neck tensile forces were usually greater than its upper neck shear forces.
- The BioRID II, Hybrid III and RID2 were all sensitive to sled velocity. (The BioRID II was only tested in Series B.)
 - The Hybrid III lower neck tensile force response was sensitive to sled velocity in all three test series.
 - The RID2 upper neck tensile force response was sensitive to sled velocity in all three test series.
- For all three dummies, the head restraint contact times were not sensitive to the sled velocity increases in these tests.
- In Series A, the seatback deformation that occurred at 24 km/hr limited the amount by which the Hybrid III and RID2 responses would have increased due to the sled velocity increase (16 to 24 km/hr) alone. (The BioRID II was not tested in Series A.)
- The BioRID II, Hybrid III, and RID2 dummies were sensitive to a head restraint position change from below their head CGs to above it.
- The Hybrid III and RID2 dummies were not sensitive to increases in head restraint height if the head restraint was already above their head CGs. (The BioRID II was not evaluated in this condition.)
- Neither the NIC nor the Nte, both of which are proposed injury criteria, provided additional information over the measured responses.
- The responses of the BioRID II and RID2 increased with larger backsets at approximate sled velocities of 24-27 km/hr.
 - At 9 and 16 km/hr, the RID2 responses were not affected by the change in backset from 55 to 105 mm. (The BioRID II was only tested at 27 km/hr.)

- As tested in Series C, both the Hybrid III and the RID2 had acceptable repeatability. (The BioRID II was not tested in this series.)

ACKNOWLEDGMENTS

The authors would like to thank Denton ATD, Inc. and Robert A. Denton, Inc. for providing the BioRID II and the necessary load cells for its use. Special thanks go to John Arthur and Mike Salloum for their technical support. We would also like to thank First Technology Safety Systems for providing the RID2 and the necessary load cells for its use and for hosting two RID2 technical sessions. Special thanks go to Steve Goldner and York Huang for their technical support. Special thanks also go to Mat Philippens, TNO Automotive, for sharing his technical expertise in support of this evaluation.

The authors would also like to thank Chris Addepalli, Charles Armstrong, Craig Hill, John Hills, James Howe, Theresa Reilly, and Kevin Taylor (DaimlerChrysler), the entire Ford SLD sled team, and Jan Morris (General Motors) for their contributions to this study.

REFERENCES

- [1] Alliance of Automobile Manufacturers. 1999. "Dummy response limit for FMVSS 208 compliance testing." Annex 2 of the Alliance of Automobile Manufacturers Submission to SNPRM, Docket No. 99-6407, December 22, 1999.
- [2] "BioRID II User's Guide." 2002. Robert A. Denton, Inc., February 27, 2002.
- [3] Boström, O., Svensson, M.Y., and Muser, M. 1999. "NIC measurement techniques and result interpretation." www.agu.ch/en/index.html, nic.calc.005.pdf.
- [4] Boström, O., Svensson, M.Y., Aldman, B., Hansson, H.A., Håland, Y., Lövsund, P., Seeman, T., Suneson, A., Säljö, A., and Örtengren, T. 1996. "A new neck injury criterion candidate- based on injury findings in the cervical spinal ganglia after experimental neck extension trauma." Proc. of 1996 International IRCOBI Conference on the Biomechanics of Impact, pp. 123-136.
- [5] Cesari, D., Compigne, S., Scherer, R., Xu, L., Takahashi, N., Page, M., Asakawa, K., Kostyniuk, G., Hautmann, E., Bortenschlager, K., Sakurai, M., Harigae, T. 2001. "WorldSID prototype dummy biomechanical responses." Stapp Car Crash Journal, 45: 285-318, 2001-22-0013.

[6] Davidsson, J., Flogård, A., Lövsund, P., Svensson, M.Y. 1999. "BioRID P3 – design and performance compared to Hybrid III and volunteers in rear impacts at $\Delta V=7$ km/hr." Proc. of 1999 Stapp Car Crash Conference, pp. 253-265. Society of Automotive Engineers, Warrendale, PA.

[7] Davidsson, J., Svensson, M.Y., Flogård, A., Håland, Y., Jakobsson, L., Linder, A., Lövsund, P., Wiklund, K. 1998. "BioRID I – a new biofidelic rear impact dummy." Proc. of 1998 International IRCOBI Conference on the Biomechanics of Impact, pp. 377-390.

[8] FMVSS 208. 2000. "Occupant Crash Protection." Docket of Federal Regulations 49, Part 571.208, US Government Printing Office, Washington, D.C.

[9] Foster, J.K., Kortge, J.O., and Wolanin, M.J. 1977. "Hybrid III – a biomechanically-based crash test dummy." Proc. 21st Stapp Car Crash Conference, pp. 973-1014. Society of Automotive Engineers, Warrendale, PA.

[10] Kim, A., Anderson, K.F., Berliner, J., Hassan, J., Jensen, J., Mertz, H.J., Pietsch, H., Rao, A., Scherer, R., and Sutterfield, A. 2003. "A biofidelity evaluation of the BioRID II, Hybrid III and RID2 for use in rear impacts." Stapp Car Crash Journal 47: 489-523.

[11] Mertz, H.J., and Prasad, P. 2000. "Improved neck injury risk curves for tension and extension moment measurements of crash dummies." Stapp Car Crash Journal 44: 59-75.

[12] Mertz, H.J., Prasad, P., and Irwin, A.L. 1997. "Injury risk curves for children and adults in frontal and rear collisions." Proc. 41st Stapp Car Crash Conference, pp. 13-30. Society of Automotive Engineers, Warrendale, PA.

[13] NHTSA. 2000. "Final rule on advanced airbags." Federal Register (FR), Vol. 65, 30680, May 12, 2000.

[14] NHTSA. 1998. "Notice of proposed rule making (NPRM) for advanced airbags." Federal Register (FR), Vol. 63, No. 181, September 18, 1998.

[15] Philippens, M.M.G.M. 2002. "RID2 v0.0 User Manual Draft." TNO Automotive, TNO report 01.OR.BV.048.1/MP, March 12, 2002.

[16] Rouhana, S.W., Elhagediab, A.M., Walbridge, A., Hardy, W.N., and Schneider, L.W. 2001. "Development of a reusable, rate-sensitive abdomen for the Hybrid III family of dummies." Stapp Car Crash Journal, Vol. 45: 33-59.

[17] SAE EA 23. 1998. "User's Manual for the 50th Percentile Male Hybrid III Test Dummy." Society of Automotive Engineers, Warrendale, PA.

[18] SAE J1733. 1994. "Sign Convention for Vehicle Crash Testing." Society of Automotive Engineers, Warrendale, PA.

[19] SAE J211. 1995. "Instrumentation for impact test – part 1 – electronic instrumentation." Society of Automotive Engineers, Warrendale, PA.

[20] SAE J2052 1997. "Test Device Head Contact Duration Analysis." Society of Automotive Engineers, Warrendale, PA.

[21] SAE PT-44. 1994. "Hybrid III: the first humanlike crash test dummy." Society of Automotive Engineers, Warrendale, PA.

[22] Schneider, L.W., Robbins, D.H., Pflüg, M.A., Snyder, R.G. 1983. "Development of anthropometrically based design specifications for an advanced adult anthropomorphic dummy family. Volume 1 (3)." U.S. Department of Transportation, National Highway Traffic Safety Administration, report No. DOT-HS-806-715 and UMTRI-83-53-1.

[23] Svensson, M.Y., Boström, O., Davidsson, J., Hansson, H.-A., Håland, Y., Lövsund, A., and Säljö, A. 2000. "Neck injuries in car collisions – a review covering a possible injury mechanism and the development of a new rear-impact dummy." Accident Analysis & Preventions 32: 167-175.

[24] Tennant, J., Jensen, R., Potter, R. 1974. "GM-ATD 502 Anthropomorphic Dummy – Development and Evaluation." SAE746030.

[25] Xu, L., Agaram, V., Rouhana, S., Hultman, R.W., Kostyniuk, G.W., McCleary, J., Mertz, H., Nusholtz, G.S., Scherer, R. 2000. "Repeatability evaluation of the pre-prototype NHTSA advanced dummy compared to the Hybrid III." Society of Automotive Engineers, Warrendale, PA. SAE 2000-01-0165.

APPENDIX A. EQUATIONS FOR CALCULATED RESPONSES

1. MOMENT TRANSFER EQUATION AND DISTANCES

$$M_{YCor} = M_Y + (F_X \bullet D_Z) + (F_Z \bullet D_X)$$

where F_X , F_Z , and M_Y are the measured loads and torques [17, 18].

Table A1.
Correction distances for the BioRID II, Hybrid III, and RID2

	D _X (mm)	D _Z (mm)
Occipital Condyle: BioRID II, Hybrid III, RID2	0.0	-17.8
C7/T1: Hybrid III	50.8	28.6
C7/T1: RID2	0.0	18.0

2. EXTERNAL HEAD FORCE EQUATIONS [20][†]

To calculate the inertia loads on the head (using a 50th percentile head mass, M = of 4.2 kg*):

$$F_{Xinertiaload} = M * A_{Xhead}$$

$$F_{Zinertiaload} = M * A_{Zhead}$$

To calculate the external head forces:

$$F_{Xhead} = F_{Xinertiaload} - F_{Xupperneck}$$

$$F_{Zhead} = F_{Zinertiaload} - F_{Zupperneck}$$

[†]The measured head CG accelerations and the measured upper neck loads were used to calculate the external head forces, not the corrected responses.

*4.2 kg represents the mass of the head above the measurement strain gage in the upper neck load cell.

3. NIC [23, 3, 4]

$$NIC = (0.2 * a_{rel}) + (v_{rel})^2$$

where $a_{rel} = T1a_x - C1a_x$,
 $v_{rel} = \int a_{rel} dt$,
 $T1a_x$ - T1 X-acceleration,
 $C1a_x$ - C1 X-acceleration[†].

[†]The head CG X-acceleration was used for C1a_x.

4. Nij - Nte [13, 14, 1, 11, 12]

$$Nte = (F_z/F_{Zc}) + (M_{OCV}/M_{Yc})$$

where $F_{Zc} = 6806$ N for tension and
 $M_{Yc} = 135$ Nm for extension.

APPENDIX B. RID2 TILT SENSOR READINGS AT INITIAL POSITION

Table B1.
Series A: RID2 55 mm backset

	Tilt Sensor 7 Head (Degree)	Tilt Sensor 6 T1 (Degree)	Tilt Sensor 5 Neck Bracket (Degree)	Tilt Sensor 3 Lumbar Bracket, Top (Degree)	Tilt Sensor 1 Lumbar Bracket, Left-Right (Degree)	Pelvic Reading* * (Degree)
9 km/hr, 1	0	6	-11	-1	-1	82.0
9 km/hr, 2	-1	6	-11	-1	0	83.9
16 km/hr, 1	-1	4	-9	-3	1	83.9
16 km/hr, 2	-1	6	-11	-1	0	83.2
24 km/hr, 1	1	6	-11	1	0	82.6
24 km/hr, 2	-1	6	-11	-1	0	83.0

*Tilt sensor 2 (Lumbar Bracket Bottom) and tilt sensor 4 (T12) were inoperative; the readings were not included.

**The pelvic angle was measured manually due to tilt sensor 2 being inoperative. A pelvic reading of 83° corresponded to 22.5°.

Table B2.
Series A: RID2 105 mm backset

	Tilt Sensor 7 Head (Degree)	Tilt Sensor 6 T1 (Degree)	Tilt Sensor 5 Neck Bracket (Degree)	Tilt Sensor 3 Lumbar Bracket, Top (Degree)	Tilt Sensor 1 Lumbar Bracket, Left-Right (Degree)	Pelvic Reading** (Degree)
9 km/hr, 1	2	12	-17	-9	0	82.6
9 km/hr, 2	1	12	-17	-5	1	83.8
16 km/hr, 1	1	12	-17	-7	-1	82.0
16 km/hr, 2	1	12	-17	-8	1	82.5
24 km/hr, 1	1	12	-17	-7	-1	83.0
24 km/hr, 2	1	12	-17	-7	0	83.8

*Tilt sensor 2 (Lumbar Bracket Bottom) and tilt sensor 4 (T12) were inoperative; the readings were not included.

**The pelvic angle was measured manually due to tilt sensor 2 being inoperative. A pelvic reading of 83° corresponded to 22.5°.

Table B3.
Series B: RID2

	Tilt Sensor 7 Head (Degree)	Tilt Sensor 6 T1 (Degree)	Tilt Sensor 5 Neck Bracket (Degree)	Tilt Sensor 3 Lumbar Bracket, Top (Degree)	Tilt Sensor 2 Lumbar Bracket, Bottom (Degree)	Tilt Sensor 1 Lumbar Bracket, Left-Right (Degree)
17 km/hr, HR up 1	-1	5	-1	-9	-1	0
17 km/hr, HR up 2	-1	2	-2	-10	1	0
17 km/hr, HR down 1	-1	5	-2	-10	1	0
17 km/hr, HR down 2	-1	4	-1	-10	0	0
27 km/hr, HR up 1	1	1	-2	-9	1	0
27 km/hr, HR up 2	-1	5	-1	-10	1	0
27 km/hr, HR down 1	0	3	-4	-9	0	0
27 km/hr, HR down 2	2	3	-2	-10	1	0

*Tilt sensor 4 (T12) was inoperative; the readings were not included.

Table B4.
Series C: RID2

	Tilt Sensor 7 Head (Degree)	Tilt Sensor 6 T1 (Degree)	Tilt Sensor 5 Neck Bracket (Degree)	Tilt Sensor 4 T12 (Degree)	Tilt Sensor 3 Lumbar Bracket, Top (Degree)	Tilt Sensor 2 Lumbar Bracket, Bottom (Degree)	Tilt Sensor 1 Lumbar Bracket, Left- Right (Degree)
10 km/hr, HR up 1	0	1	-2	1	13	-1	1
10 km/hr, HR up 2	0	0	-2	2	1	1	1
10 km/hr, HR down 1	0	-1	-1	-1	6	2	1
10 km/hr, HR down 2	0	1	-2	0	6	2	0
10 km/hr, HR up 3	0	1	-3	1	6	2	1
10 km/hr, HR down 3	1	0	-2	2	-1	2	1
24 km/hr, HR up 1	-1	0	-2	3	-1	-1	1
24 km/hr, HR down 1	0	1	-2	1	7	0	0
24 km/hr, HR up 2	0	1	-2	2	3	0	1
24 km/hr, HR up 3	0	-1	-1	0	3	1	1
24 km/hr, HR down 2	0	0	-1	1	1	1	1
24 km/hr, HR down 3	0	1	-2	0	0	2	0

APPENDIX C. SERIES B: BIORID II BACKSET SENSITIVITY TIME HISTORY RESPONSES.

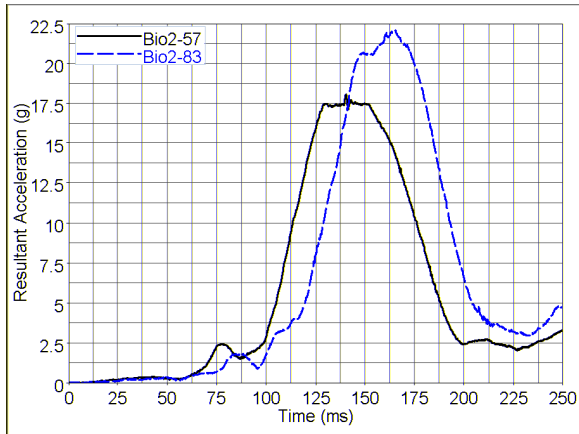


Figure C1. Series B: Resultant head acceleration. BioRID II at backsets of 57 and 83 mm.

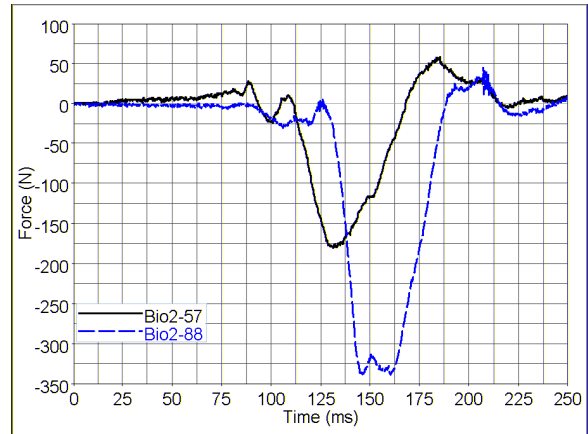


Figure C4. Series B: External head impact Fz. BioRID II at backsets of 57 and 83 mm.

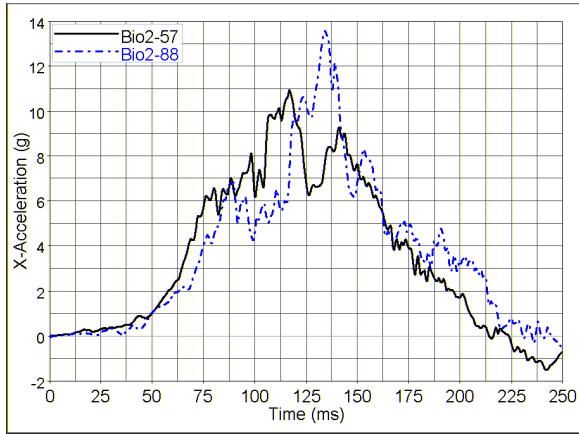


Figure C2. Series B: T1 X-acceleration. BioRID II at backsets of 57 and 83 mm.

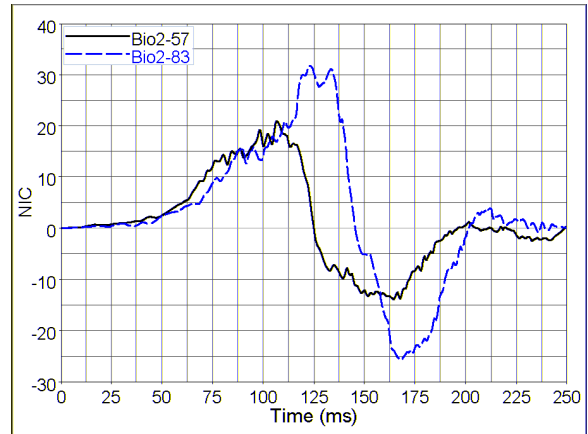


Figure C5. Series B: NIC. BioRID II at backsets of 57 and 83 mm.

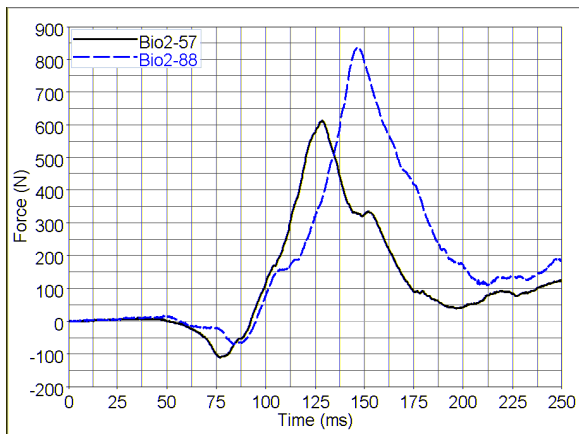


Figure C3. Series B: Upper neck Fz. BioRID II at backsets of 57 and 83 mm.

APPENDIX D. SERIES C: CORRELATION COEFFICIENTS.

Table D1.
Correlation coefficients for 10 km/hr, head restraint up

	Hybrid III			RID2		
	Magnitude	Shape	Phase	Magnitude	Shape	Phase
Head X-acceleration	0.9562	0.9866	1.4167	0.9704	0.9852	1.9
T1 X-acceleration	0.882	0.9783	2.5333	0.8366	0.9578	0.7833
T12 X-acceleration	0.8803	0.9929	2.1	0.9107	0.9478	0.35
Pelvis X-acceleration	0.9441	0.9953	2.3167	0.9386	0.9873	1.000

Table D2.
Correlation coefficients for 10 km/hr, head restraint down

	Hybrid III			RID2		
	Magnitude	Shape	Phase	Magnitude	Shape	Phase
Head X-acceleration	0.9855	0.9938	0.7667	0.9166	0.9844	0.4167
T1 X-acceleration	0.9266	0.9769	1	0.9017	0.9304	2.0667
T12 X-acceleration	0.9704	0.9727	1.3167	0.8590	0.9360	2.4833
Pelvis X-acceleration	0.8990	0.979	1.7167	0.9315	0.9826	8.5333

Table D3.
Correlation coefficients for 24 km/hr, head restraint up

	Hybrid III			RID2		
	Magnitude	Shape	Phase	Magnitude	Shape	Phase
Head X-acceleration	0.9324	0.9943	1.0833	0.9558	0.9959	2.600
T1 X-acceleration	0.9372	0.9880	1.8500	0.9684	0.9886	2.1167
T12 X-acceleration	0.9472	0.9858	1.5333	0.9145	0.9774	2.1168
Pelvis X-acceleration	0.9488	0.9877	4.0167	0.9659	0.9929	3.3833

Table D4.
Correlation coefficients for 24 km/hr, head restraint down

	Hybrid III			RID2		
	Magnitude	Shape	Phase	Magnitude	Shape	Phase
Head X-acceleration	0.9276	0.9946	0.2	0.9455	0.9879	4.8
T1 X-acceleration	0.9607	0.9918	0.0167	0.9674	0.9715	1.6167
T12 X-acceleration	0.9186	0.9910	0.2	0.9535	0.9751	2.1167
Pelvis X-acceleration	0.9205	0.9899	0.95	0.9521	0.9913	1.95

APPENDIX E. RID2 NECK BUFFER CONFIGURATION HEAD/NECK PENDULUM TESTS

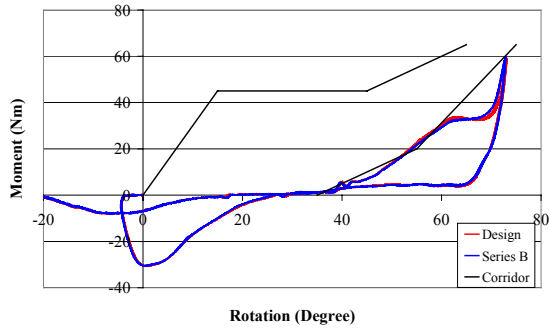


Figure E1. RID2 neck buffer configurations: Design and Series B. Flexion tests: Occipital condyle moment vs head/pendulum rotation.

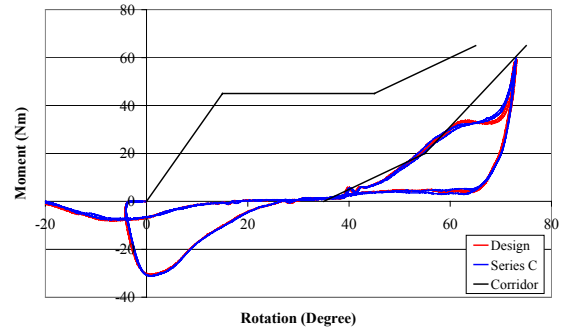


Figure E3. RID2 neck buffer configurations: Design and Series C. Flexion tests: Occipital condyle moment vs head/pendulum rotation.

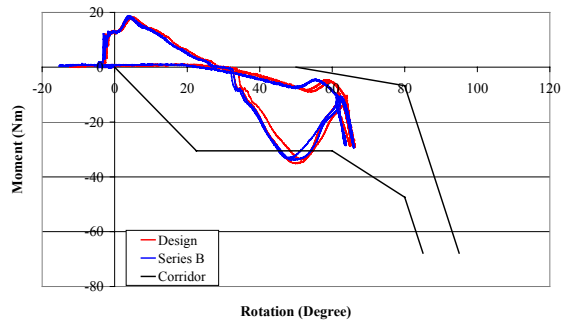


Figure E2. RID2 neck buffer configurations: Design and Series B. Extension tests: Occipital condyle moment vs. head/pendulum rotation.

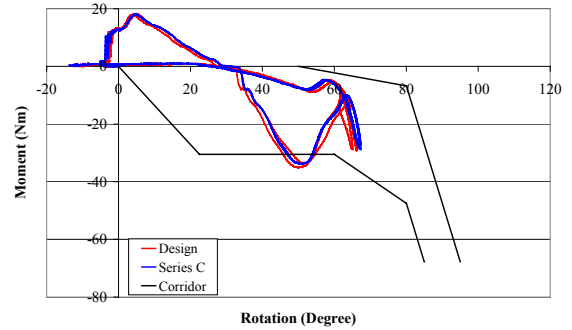


Figure E4. RID2 neck buffer configurations: Design and Series C. Extension tests: Occipital condyle moment vs head/pendulum rotation.

THE RESPONSE OF HYBRID III, EUROSID AND VOLUNTEER IN THE FIRST PHASE OF A ROLLOVER ACCIDENT

Norbert Praxl

Jiri Adamec

Holger Muggenthaler

Institute for Legal Medicine Munich

Germany

Paper Number 05-0254

ABSTRACT

In rollover crashes there is a high risk for occupants to suffer severe injuries. The number of rollovers tends to increase at present presumably because of the increasing number of cars with a relatively high COG (Minivans, MPVs). Therefore there is a great potential for injury reduction in that area. Available dummies are designed and validated for front, side or rear impacts but not for complex events like rollovers. So the question comes up which Dummy should be used to assess safety systems for rollover accidents.

The aim of the study was to get a detailed information of the dummy behaviour compared to human behaviour in the first phase of a rollover accident.

Series of measurements with volunteers and dummies (Hybrid III and EuroSID) were carried out by using a current car seat mounted on a sled with additional tilting mechanism. Two types of motion were imposed to the sled that represented different rollover scenarios: a pure translational motion and a pure rotational motion. Two different acceleration levels from the range found in real world crashes were used. The kinematics of dummies as well as kinematics and muscle activity of volunteers were analysed.

The results show a significant difference between the kinematics of dummy and volunteer. In the rotational sled motion the volunteer movement was directed to the opposite side compared to the dummy. Thus, the dummies do not represent human occupants very well. Furthermore, the kinematics of both dummies is very similar, so no preference regarding the dummy type can be recommended. The EMG revealed activity of all observed muscles in all test configurations, the muscle activity influences evidently the movement of human occupants. This results are supposed to be useful for the development of rollover dummies and advanced numerical occupant models.

INTRODUCTION

The objective of this work was to assess the kinematics of the occupant in the first phase of roll. The knowledge of occupant kinematics is essential for the design of new restraint systems or for the trimming of current systems for rollover accidents. Current restraint systems like curtain airbags and belt pretensioners have the potential to prevent severe injuries in rollover accidents. But these systems need a correct timing of triggering to be effective. If the occupant is already out of position when the restraint system is triggered the system may have no effect or even worse may lead to injuries of the occupant. This demonstrates the

importance of the occupant kinematics during the first phase of the roll for the assessment of possible out of position issues.

As opposed to most frontal, rear or side crashes the accelerations acting on the occupants in rollover accidents are usually lower and the duration of the crash is much longer (up to several seconds). Thus, the kinematics of the occupants can be influenced by muscular actions (both reflexive and voluntary).

Series of experiments with volunteers and dummies were carried out on a motion base that simulated the first phase of a roll. The kinematics were measured by a 3D motion capturing system, the activity of selected muscles of the volunteers was measured via surface EMG.

The experiments were designed to answer following questions:

- Do the occupants exert active muscle forces during the first phase of roll?
- In what regions are muscles activated?
- Is the muscle reaction side-specific (i.e. are there differences between the left and the right hand side of the same muscles)?
- Does the muscle activation clearly influence the kinematics of the occupant? How and to what extent?
- Does muscle activation (its level or time pattern) depend on the magnitude of the accelerations the body is exposed to?
- Does the occupant kinematics depend on the magnitude of the acceleration the body is exposed to?
- Are there interindividual differences in the occupant kinematics?
- Are there differences between the kinematics of volunteers and dummies (HybridIII and SID)?
- Which of the two used dummies is more suitable for the usage in rollover-like scenarios?

METHODS

Experimental Setup

In order to imitate the car motion in the first phase of roll a special sled facility with a mounted motion base has been constructed by TUG in co-operation with LMU. The sled was allowed to move on rails fastened firmly to the ground. A motion base (i.e. a steel frame with wooden platform) was anchored to the sled by a hinge so that tilting movement of the platform was possible. A current make of a car seat with

integrated seat belt was firmly screwed to the motion base. For safety reasons a safety frame with tight net was attached on both sides of the motion base (see Figure 1).

Two motion types were simulated by using the motion base that represent the dominant features of different rollover scenarios – translational movement (rollover scenarios with dominant lateral acceleration in the first phase – trip over, turn over, collision with another vehicle) and tilting movement (rollover scenarios in which the roll is not accompanied by significant lateral acceleration – flip over, fall over).

The translational movement was imitated by using the principle of inverse motion. It means that instead of inducing an initial velocity to the sled and braking it as it would be in the real car, the sled was exposed to the same lateral acceleration (originally deceleration of the car) in a resting position. The sled thus moved in the opposite direction than the (assumed initial) movement of the car, but the effects on the occupant are exactly the same. The translational movement of the sled was driven by a bungee rope, the acceleration of the sled was trimmed by adjusting the initial pull-strength of the rope.



Figure 1. The motion base with a seated volunteer.

The tilting movement of the motion base was driven by a pneumatic piston; the tilting velocity was determined by the initial air pressure. In this configuration the motion base stood still and only the tilting movement was induced.

The whole experimental set-up was designed to minimise all potential hazards for the volunteers. An approval of the ethics commission of the LMU was obtained in advance.

Prior to the experiment, each volunteer got an explanation of all procedures and signed an informed consent. His basic anthropometric data were collected and he put on a tight non-reflective dress.

The skin over chosen muscles was shaved and rubbed with EGM-preparation gel for better conductivity. The Blue Sensor® electrodes were positioned over the thickest part of the selected muscles (overview see Table 1).

Fourteen reflective markers for the kinematical analysis were positioned on the volunteers body as depicted in Figure 2. Please note that the list contents only the markers needed for the analysis, some more were used to facilitate the automatic tracking process. The same set of markers was used for the dummies as well.

Table 1. Muscles selected for the EMG analysis.

Muscle	Function
m. sternocleidomastoideus left	head rotation to the right, head tilt to the left
m. sternocleidomastoideus right	head rotation to the left, head tilt to the right
m. trapezius left	adduction, stabilisation of the shoulder girdle
m. trapezius right	adduction, stabilisation of the shoulder girdle
m. obliquus externus abdominis left	lateral flexion of the torso to the left
m. obliquus externus abdominis right	lateral flexion of the torso to the right
m. rectus femoris left	knee extension, hip flexion
m. rectus femoris right	knee extension, hip flexion

Based on the position of the real marker, the position of the so-called virtual markers was computed automatically. These points enhanced the analysis of the subjects movements.

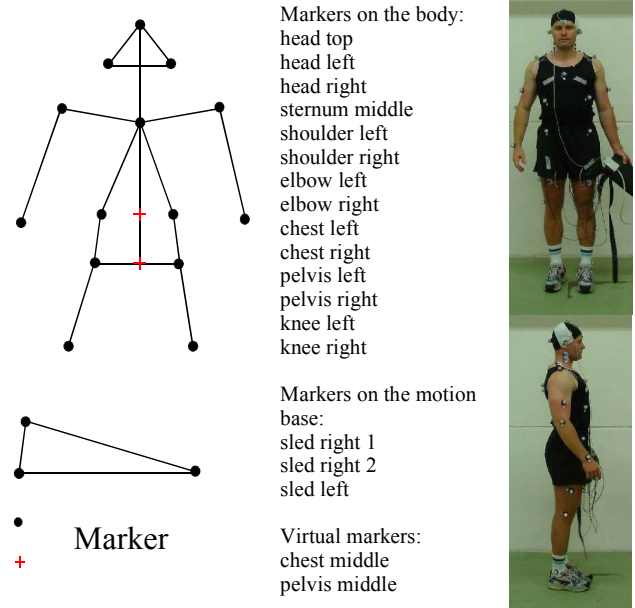


Figure 2. Positions of the reflexive markers on the volunteer's body.

Because of time and cost limitations, experiments were carried out with two volunteers, a HybridIII and a EuroSID dummies only. The test matrix showing the overview of experiments carried out in the movement science lab is depicted in Table 2.

The variants slow and fast in table 1 are stated in inverted commas because we were not able to reproduce exactly the quickness of the translational and rotational motion for all occupants. Though both bungee rope and pneumatic piston enabled the regulation of the motion to a certain degree, the

kinematics of the sled motion were not exactly reproducible. On the other hand, a construction of a sled facility with a high degree of reproducibility would have been much more consuming in terms of time and resources and the results achieved with our motion base proved to be meaningful. The acceleration levels in the experiments were chosen so that they comply with two requirements – they should represent the accelerations observed in the first phase of real rollover accidents and at the same time the experiment had to be safe for the volunteer. The peak lateral (inertial y-) accelerations achieved during the translational movement as well as the peak roll-rates achieved during the rotational movement are listed in table 3.

Table 2.
Experimental matrix.

Occupant	translational movement		rotational movement	
	„slow“	„fast“	„slow“	„fast“
volunteer 1	X	X	X	X
volunteer 2	X	X	X	X
Hybrid III	X	X	X	X
EuroSID	X	X	X	X

Table 3.
Peak accelerations/roll-rates of the motion base in the experiments.

Occupant	y- acceleration peak (g)		roll-rate peak (grad*s ⁻¹)	
	„slow“	„fast“	„slow“	„fast“
Volunteer 1	0.8	0.9	56	62
Volunteer 2	0.7	0.9	36	60
HybridIII	0.6	1.0	44	58
EuroSID	0.9	1.0	55	64

The peaks stated in table 3 were found from filtered kinematical data (low-pass filter with cut-off frequency 15Hz). It should be noted that acceleration data are computed as second derivative of marker positions and as such they are extremely sensitive to filtering. Different filter may have lead to different peak values.

Our experimental values are comparable to real data. However, one has to keep in mind that rollover accidents distinguish themselves with a very wide variety of kinematics (not only the heights of the accelerations vary in time, but also their directions) and as a result only a small part of possible scenarios has been dealt with.

The experimental peak values correspond well with the lower values of reconstructed accidents and are thus realistic. Higher accelerations and/or roll rates would have been dangerous for the volunteers.

In all experiments the occupant was seated and the seat belt properly fastened. After a check-up of all safety measures and a proper function of all measurement devices the propulsive devices were loaded (bungee rope pulled or pneumatic piston filled with air). The motion of the sled followed after a countdown, the volunteers were aware of the

motion onset.

For each occupant at least two measurements were carried out for each motion, i.e. the slower and the faster modus.

Instrumentation

The surface EMG was measured by using an 8-channel telemetric measurement device (NORAXON, Scottsdale, Arizona). The measurement was triggered simultaneously with the kinematical analysis system by the same external trigger.

For the kinematical analysis the EVA Real Time 2.1 (Motion Analysis, Santa Rosa, California) motion capturing system was used with 8 Falcon cameras. The recording frequency was set at 240Hz. The positioning of the cameras as well as the calibration of the measurement space was done according to the recommendations of the system manufacturer.

Evaluation and Analysis

The EMG Data were rectified and plotted at the same time and voltage scale in order to facilitate the assessment of the total amount of muscle activity. Because the position of the electrodes did not change between various test runs, it is possible to evaluate activation differences of the same muscles in various situations. However, a comparison between various muscles of the same subject is not possible because of likely differences in the amounts of muscle units recorded.

The trajectories of the markers on the subject’s body and on the motion base were tracked by using the EVA software and low-pass filtered with a cut-off frequency set at 15Hz. The positions of the virtual markers were computed in the system as defined by the investigator.

For the presentation of the occupant kinematics, screenshots from the animations have been made in the overall (near to frontal) view and in the top view (xy plane).

RESULTS

Translational Movement

Muscle Activity Analysis

Both subjects showed a considerable amount of muscle activity during the simulated first phase of roll in the slow as well as in the fast variant of the test. Active were apparently all the considered body regions – the neck, abdomen as well as the legs.

The onset time of muscle activity does most likely not depend on the quickness of the movement of the sled – we have found approximately the same values for the slow and the fast variants in both tested subjects. The fastest response show the neck muscles (sternocleidomastoideus) with the onset at approx. 0.1sec. A little bit slower reaction time has been found for the abdomen muscles and the upper leg muscles followed with a minor delay (reaction time up to 0.2sec). The response of the trapezius muscle was inconsistent and varied between 0.1sec and 0.2sec.

These findings correspond to our expectations – the neck muscles react first because the head is accelerated with respect to the torso and the muscular actions are presumably

aimed at its stabilisation. The stabilisation of the torso follows and because the legs are supported on the floor, no actions are needed until the torso has deviated from its upright position.

Though the translational movement of the sled was oriented from the left to the right hand side of the sitting subject, relatively little lateral differences in the muscle activation were found. The abdominal muscles showed about the same reaction on both sides in both subjects. It means that the muscles stabilise the torso regardless of the direction of acting forces (accelerations). The neck muscles showed concurrent activation as well. However, in the first subject there was completely the same activation onset time on both sides of the body whereas in the second subject there was a shift towards the right hand side (i.e. the right muscle was activated earlier and a concurrent activity followed, see Figure 3). It is apparent as well that there is more activation on the right hand side at the beginning of the movement – the muscle counteracts the tendency of the head to move to the left. After approximately 0.2sec there is no difference between the left and the right hand side of the neck musculature.

Also evident from Figure 3 is a higher amount of muscle activity in the faster variant of the movement. Though it is impossible to quantify the force exerted by the muscles (that is only to a certain degree possible in isometric contractions), the amount of muscle activity can be compared because the positions of the electrodes were exactly the same for both measurements. These results are also plausible, because higher sled accelerations bring about higher accelerations of the head and therefore more muscle force is required for stabilising.

Similar tendency (i.e. more muscle activation in case of higher accelerations) has also been observed in other muscles except for the upper leg muscles.

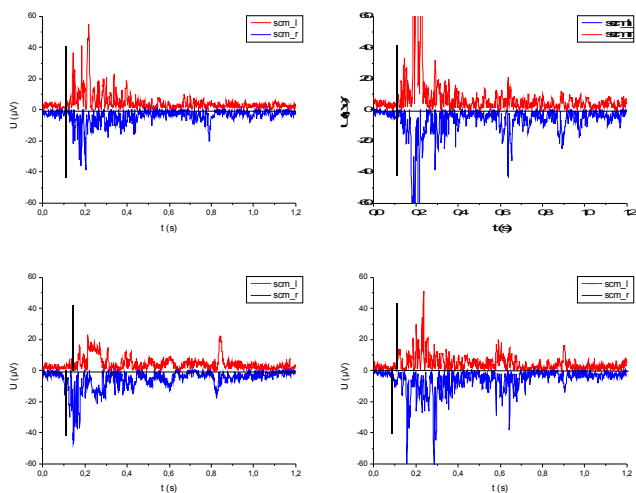


Figure 3. EMG of m. sternocleidomastioideus left (red) and right (blue); top row: Volunteer 1, slow (left) and fast (right) motion of the sled; bottom row: Volunteer 2; left column: slow (left) and fast (right) motion of the sled.

Occupant Kinematics Analysis

The kinematics of all measured occupants (volunteers as

well as dummies) recorded as 3D – Trajectories of selected points on the surface of various body segments is a very complex phenomenon. A simple synchronisation of all trials does not make sense because accelerations induced to the sled vary and the sled position as well as acceleration level in various trials differ one from another at the same point of time. Thus, two space locations of the sled were chosen and the positions of the occupant at these configurations were evaluated. The sled locations were chosen approximately at the beginning and at the end of the sled acceleration phase, the sled travelled 0.76m between the two screenshots. In the following, only the most interesting screenshots are presented, the complete set of pictures from all measurement runs can be found in the attachment.

It is apparent from the figures that only very little movement of the head and shoulder relative to the hip and chest occurs. Volunteer 1 as well as both dummies stayed with their trunk and head upright, only volunteer 2 showed some bending in the trunk. It means that there is most probably a high degree of interindividual variability in the response of human subjects to low lateral accelerations. Different kinematics of both volunteers corresponds well with the deviations found in the EMG signal as discussed above.

The dummy response met our expectations – both dummies are too stiff in the neck and shoulder region and tip over without bending the neck. With higher accelerations the trend observed in volunteer 2 would probably become more apparent in both volunteers whereas the dummy response would most probably stay the same. Because of safety reasons it was impossible to expose the volunteers to higher accelerations.

No noticeable rotation about the longitudinal axis was found in any of the evaluated segments in all occupants, no signs of movement forward or backward of the upper torso or the head were recorded. Thus, in this scenario the movement of the occupant can be considered planar in the frontal plane.

With respect to crash testing there is no preference regarding the dummy type to be used – both Hybrid III and EuroSID show the same (very stiff) behaviour.

Rotational Movement

Muscle Activity Analysis

Similarly to the translational movement, all the selected muscles responded to the rotational motion of the sled. However, some differences in the response have been observed.

The onset of the muscle activity corresponded roughly to the one found in the translational movement except for the upper leg muscles which were activated significantly later in the second volunteer. The most striking difference between the two volunteers has been found in the activation of the m. obliquus externus abdominis as shown in Figure 4.

Whereas the first volunteer activates the muscles on the left hand side of the body much sooner than on the other side, there is no lateral difference in the response of the abdominal muscles in the second volunteer. These reactions show two different strategies of the human subjects:

- An active effort to stabilise the trunk by means of concurrent muscular actions on both sides of the trunk

(the second volunteer).

- Bending of the torso actively back to the vertical position after its deviation due to the sled rotation (the first volunteer). The tilting motion of the sled was oriented clockwise from the point of view of the subject so the left hand side of the abdominal musculature was employed in the correction.

In spite of the huge difference between the left and right side found in the first volunteer in the abdominal muscles, all other muscles have shown exactly the same activation timing. The effort of the subject was possibly concentrated on the straightening of the torso whereas other body regions were stabilised.

The concurrent activity of abdominal muscles of the second volunteer was in turn followed by higher activity of the left hand side musculature of the neck (m. trapezius) and legs (m. rectus femoris). Thus, this subject corrected presumably the position of the head more in the shoulder region as opposed to the first volunteer.

A minor increase of the activation volume can be observed with higher sled acceleration in all measured muscles.

As mentioned above, it is impossible to assess quantitatively the amount of muscle activation in various muscles. Any conclusion regarding the exerted muscle forces and their influence on the kinematics of the subjects would therefore be misleading. However, the measurements provide valuable information about the response of human subjects to the movements in the first phase of roll.

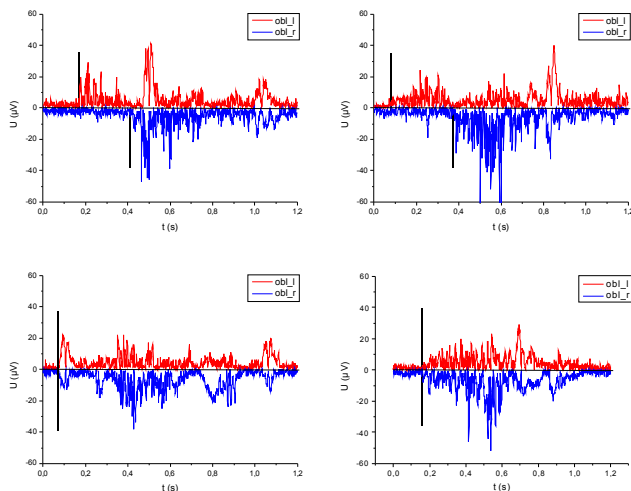


Figure 4. EMG of m. obliquus externus abdominis left (red) and right (blue); top row: Volunteer 1, slow (left) and fast (right) motion of the sled; bottom row: Volunteer 2; left column: slow (left) and fast (right) motion of the sled.

Occupant Kinematics Analysis

It is important to note that though the rotational movement of the motion base represented the first phase of other rollover types as discussed above, the overall rollover direction stayed the same (i.e. if a car would slide laterally as simulated by the translational movement, it would roll in the same direction as simulated by the rotational movement).

The kinematics of both dummies were according to our expectation the same as in the translational movement – their whole bodies just tipped over in the direction of the motion base rotation without any relative movement in the torso or neck regions. As apparent from the figures, there are no differences between the two dummies. Consequently, no preference regarding the usage in a rollover crash-testing can be recommended.

There were significant differences found in the kinematics of human subjects between the translational and rotational movement of the motion base. The bending of the torso and neck is oriented opposite to the one found in the translational movement. Figure 5 shows the comparison between the two movement types in volunteer 2.

In the fast variant of the test the bending of the upper torso and neck becomes even more pronounced.

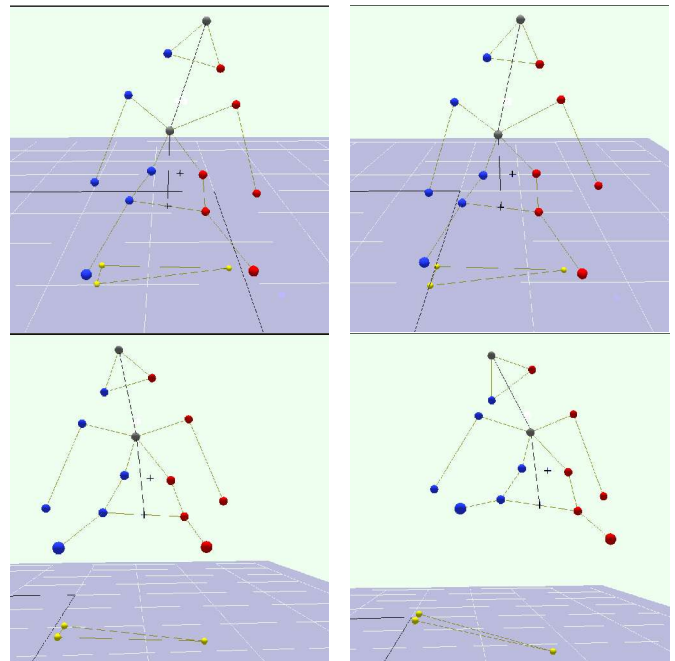


Figure 5. Bending in the torso and neck regions in volunteer 2 in the translational (up) and rotational (down) movement of the motion base, the early (left) and late (right) phase of the measurement, fast variant.

Though the above described lateral flexion of the upper torso and the neck occurs in both volunteers, the situation is similar to the one found in the translational movement, i.e. volunteer 1 tends to stay more in an upright position and the bending is only slightly indicated whereas volunteer 2 shows a much higher range of flexion. This fact is probably interrelated with the differences found in the muscle activation as described above and it indicates a huge interindividual variability of the response in human subjects.

The orientation of the shoulder, chest and hip regions did not change. The initial positions of the head markers were checked as well and deviations of the marker placement were excluded. The head of both volunteers rotates from the initial position and the rotation angle increases with time and/or rotation angle of the motion base.

Figure 6 shows the difference in the head/neck and upper

torso bending between the volunteers and the dummies in the late phase of the rotational movement. Evidently, the volunteers exert lateral flexion so that the head bends against the direction of the roll whereas the head of the dummies stays in parallel with the longitudinal axis of the body. The relative movement of the head shows thus opposite direction. Please note that for practical reasons the positions of the markers on the volunteers differ slightly from the dummies so the points on the top view do not overlap completely. However, the relative movement of the segments of interest is demonstrated very clearly.

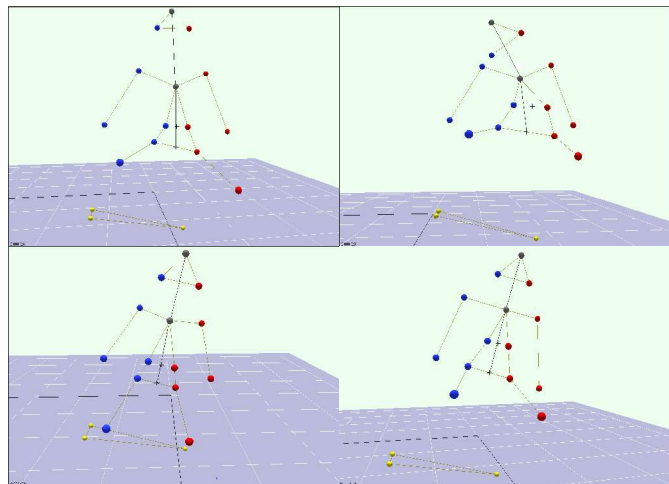


Figure 6. Difference in the lateral flexion of the head and upper torso of the volunteers and the dummies – late phase of the fast rotational movement. Top left volunteer1, top right volunteer 2, bottom left Hybrid III, bottom right EuroSID

CONCLUSIONS

- Both volunteers exerted in all tests active muscle forces, i.e. active movements of the occupants in the first phase of roll are very likely.

- Muscle activity was registered in all regions taken into account
- Differences between the activity of the left and the right hand side of the same muscles were found, i.e. the direction of the movement influences the muscle activation pattern.
- The muscle activity influences the kinematics of the occupant. The response to various movements (rotational versus translational movement) is different.
- With increasing accelerations the response pattern does not change significantly, but the volume of muscle activity increases.
- The relative movement of the shoulder and head/neck regions (i.e. lateral flexion) in the rotational and translational motion differ substantially from each other – the directions of the lateral flexion are opposite. The occupant kinematics is thus highly dependent on the rollover type.
- The occupant kinematics does not change substantially with increasing acceleration (i. e. the same trends can be observed), but the trends become more apparent.
- There is a high degree of interindividual variability in the occupant kinematics.
- Relevant differences were found between the kinematics of human subjects and the dummies.
- Both the Hybrid III and the SID dummies show the same kinematics in the first phase of roll. Therefore, there is no preference with respect to their usage in rollover scenarios.

ACKNOWLEDGEMENT

This work was performed within the Project „Improvement of Rollover Safety for Passenger Vehicles“ funded by the European Community within the 5th Framework-Programme “Growth” under the contract number G3RD-CT-2002-00802.

HUMAN BODY-CAR SEAT COUPLING UNDER REAR IMPACT

Nicolas Bourdet

Rémy Willinger

Strasbourg University, ULP/CNRS

2 rue Boussingault F-67000 Strasbourg

France

Paper Number 261

ABSTRACT

The development of new protective systems must be performed on reliable tools and representative of alive human. In an earlier study a simplified and realistic model of the head-neck system under moderate rear impact was performed.

It is clear and often addressed in the literature that under such an impact configuration, the deformation of the torso and the car seat, is of extreme importance and defines the initial conditions of the head-neck system.

In order to address this issue, an original lumped model of the human torso was developed in the present study and coupled to a car seat-head rest complex. The hypothesis of linear behavior was used for the torso being subjected to small deformations. The modal analysis of the human torso in a seating position conducted by Kitazaki and Griffin in 1992 was used in this study for both masses and mechanical properties identification.

In order to reproduce the four mode shapes identified experimentally the torso was divided in six segments to obtain the five degrees of freedom with the head neck system. This model of minimum complexity but able to reproduce the 5 first experimental vibration modes was validated in the frequency domain in terms of natural frequencies and damping as well as mode shapes. In addition to the lumped approach, an external geometry was implemented in order to couple the human body model to a finite element model of the car seat also developed in the present studies. Rear impact simulations for the two different configurations (flexible and rigid torso) showed an increase of about 35% for the maximum T1 acceleration and an increase of about 65% for the acceleration slope when a rigid torso is considered. Realistic body behavior and accurate T1 acceleration are essential aspects in real world accident reconstruction as well as for seat-head rest evaluation and optimization against neck loading.

INTRODUCTION

Despite advances in safety devices, neck injuries in traffic accidents, especially non-severe rear impact accidents, continue to be a serious and costly

social problem. The high cost of whiplash injury has been extensively documented in several countries (Szabo *et al* 2002 and 1996). The development of safety measures designed to decrease the incidence of whiplash injuries must be guided by meaningful and reliable human body surrogates. Most injury prevention strategies are based on impact analysis using anthropomorphic crash test dummies or mathematical models. Without proper evaluation of these experimental or computational models against the mechanical responses of the human body, it would not be possible to improve the current state-of-the-art neck injury prevention techniques. Unfortunately the spine is one of the most complex structures in the human skeletal system and its behavior during impact is still poorly understood.

At present there are no less than three crash test dummies dedicated for use in experimental rear impact analysis ; the Hybrid III dummy developed by Foster *et al* (1977), the BioRID II designed at Chalmers University Davidsson (1999) and the RID dummy proposed by TNO in the Netherlands Cappon *et al* (2001). A number of validation studies have been conducted on these dummies against volunteers and against post mortem subject neck responses (Davidson 1999, Cappon *et al* 2001, Davidson *et al* 1999, Prasad *et al* 1997, Seeman *et al* 1986 and Siegmund *et al* 2001) and have demonstrated the limited biofidelity of this human body surrogate under low speed rear impact. Optimization studies of the car-seat-head rest system were also described by Szabo *et al* 2002, Ishikawa *et al* 2000, Eichberger *et al* 1996 and Svensson *et al* 1993 and concluded that the safest protective system against whiplash depends on the dummy used.

The modeling of the human trunk began in the mid last century. Several kinds of models were developed either as a continuum or with lumped parameters. Most of these models do not have a realistic behavior compared to the human body. Either they are too detailed and involve a great quantity of not easily identifiable parameters with the existing experimental data, or they represent only one particular dynamic behavior of the trunk and cannot thus be used for other applications like simulations of rear impacts. Indeed, most of the

spine studies developed characterize the global dynamic behavior of the trunk-head unit under seat ejection for military application. Typically, the models can be divided into two categories:

- The continuous models (Hess and Lombard 1958)
- The lumped models (Vulcan and King 1970,).

However, none of them have been studying the kinematics behavior of T1 under rear impact.

Many multi body system human model have been developed in the MADYMO software (TNO 1997) for rear-end impacts. Jernström *et al* (1993) presented a two-dimensional human model. Jakobsson *et al* (1994) compared the head angle of this model with that of a volunteer at Δv 8 km/h. The upper thoracic spine curvature of the model and the time span for the head to headrest contact were not in accordance with the volunteer response. Next, as tests are not easy to be performed on volunteers that only can be exposed to non-injurious impacts, Eriksson (2002) developed a very simplified three-dimensional model with mechanical properties tuned in order to fit the BioRID I dummy response Davidsson *et al*. 1999 integrating a flexible spine. Cappon *et al*. 2001 also developed a dummy in a whiplash project with a flexible thorax called RID 2.

Typically, numerical or physical spine model validation is conducted against volunteers or postmortem human subjects (PMHS) by comparing the evolution of recorded mechanical parameters over time with the human response. This methodology is limited as it is very difficult to characterize a multiple degrees of freedom system under impact in the temporal domain. These difficulties are well illustrated by the large number of test dummy evaluation and comparative studies found in the literature. The number of prototype versions and contradictions between study conclusions illustrate how difficult it is to explain some phenomena that are masked within the time domain. An other illustration can be found in Philippens *et al* 2002 study where “realistic” dummy head kinematics can be observed, but T1 accelerations were out of corridors. The reason for this is that the dummy response has to remain within ranges or corridors with wide tolerance. The evaluation process in the temporal domain is not sufficiently accurate to extract initial ramps, local peaks and oscillations that can be of great importance.

Despite this critical issue, recent researches in spine biomechanics have improved our knowledge of this complex structure. The limitations listed above illustrate the need for further experimental and theoretical analysis. The purpose of this paper is to apply modal analysis techniques to characterize the human trunk system in vivo and to develop a lumped parameters model of this segment

in the sagittal plane.

Indeed modal analysis in engineering is non-destructive and used for identification of dynamic structures. In biomechanics the method has been used extensively for bone healing processing and for dynamic characterization of the human head (Hodgson *et al* 1967, Stalnaker *et al* 1971 and Willinger *et al* 1990). Contrarily to other studies, with respect to the spinal column, and in addition to impedance recording of a single degree of freedom, Kitazaki *et al* 1998 undertook a detailed experimental modal analysis of the whole column including the head. A total of 15 degrees of freedom were taken into account, 3 for the head, 10 for the spinal column and 2 for the frontal area of the abdomen. The seated subject was vibrated vertically. The transfer function in terms of the apparent mass between the input force and the different degrees of freedom accelerations enabled to extract the modal characteristics of the system in the modal domain, i.e. natural frequencies and eigen vectors or mode shapes. In this way, eleven vibration modes were identified between 1.8 Hz and 17 Hz due to back. The aim of Kitazaki's study was modal characterization and comfort. The modeling was therefore restricted to definition of the analytical transfer function rather than mechanical characterization of the human body.

In previous studies undertaken at ULP, the experimental modal analysis of the human head-neck system in vivo provided us with natural frequencies and mode shapes which constitute original validation parameters for dummy necks (Willinger and Bourdet 2002). A detailed description of the applied methodology can be found in Willinger and Bourdet 2004, demonstrating how this experiment provided the biomechanical background for dummy and numerical neck model evaluation (Meyer and Bourdet 2004).

In the present study, we used the results from Kitazaki *et al*. 1998 to identify a 5 degrees lumped torso model. In the following first section we will describe the modeling of the head-neck-torso unit and the identification methodology for the stiffness and damping parameters. We will then present the coupling of this model with a car seat model realistic boundary conditions to simulate low speed rear end impact.

Finally a “standard” rear impact is simulated with the new torso model. The results are then compared to the response computed with a rigid torso under similar loading condition.

MODELING OF THE HUMAN TRUNK

Experimental tests

The experimental data used in this study were completed in a context of ergonomics and comfort

by Kitazaki *et al* 1998. The task was to characterize the movements of the head and the torso when the body was subjected to a vibration. The final aim of this research was to determine the frequency behaviors of the human body in order to better understand the origin of pains at the lumbar level. They also aimed to analyze the glance stabilization of a subject driving a car. After a first experimental attempt of modal analysis on the human body *in vivo*, Kitazaki *et al* (1998) decided to propose a modal analysis of the head-neck-trunk unit.

The studied system is shown in figure 1b. It is about the head-neck-trunk unit whose position in the sagittal plan is characterized by 15 degrees of freedom: the head T_x , T_y , T_z and θ , recorded by an accelerometric device illustrated in figure 1a; and ten other sensors recording the accelerations of the five vertebrae T1, T6, T11, L3 and S2 in T_x and T_z .

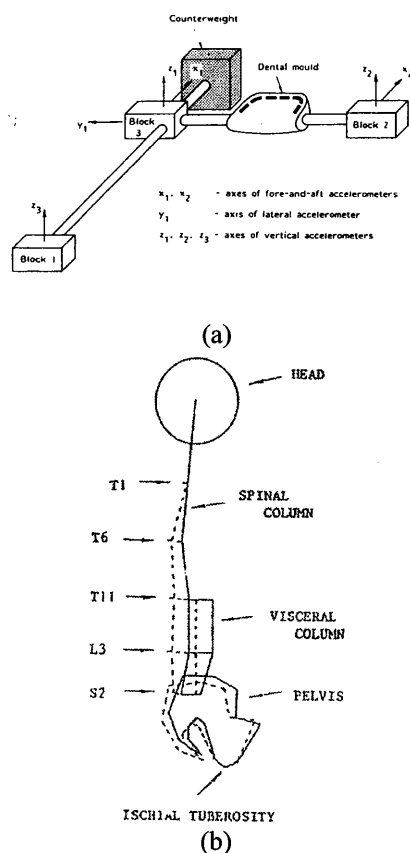


Figure 1. (a) Measurement device for kinematics recording, (b) degrees of freedom of the human body for modal analysis [Kitazaki *et al* (1998)].

The system was excited by a vibratory platform recording the transmitted force and accelerations. The frequency exciter was able to transmit up to 10kN with a maximum displacement of 1m. The vibratory test consisted of a Gaussian random excitation ($\Gamma=1.7 \text{ ms}^{-2} \text{ (rms)}$, $f=0,5 \text{ à } 35 \text{ Hz}$; during: 1 minute). Only one 32 years old male volunteer was subjected to the test. Thereafter, two types of

experimental responses were analyzed: the transfer functions in terms of:

$$\text{Apparent Mass : } A_{jk} = \frac{\Gamma_j}{F_k} \text{ and in terms of}$$

$$\text{Transmissibilitie : } T_{jk} = \frac{\Gamma_j}{\Gamma_k}$$

Where F_k et Γ_k are force and acceleration at the platform level (inputs).

This representation of the human body allowed the authors to write the transmissibility equations and to superimpose them with those recorded experimentally. The expression of the deformed mode shapes, illustrated in figure 2, and their quantitative description of table 1 was also described by this analytical transfer functions.

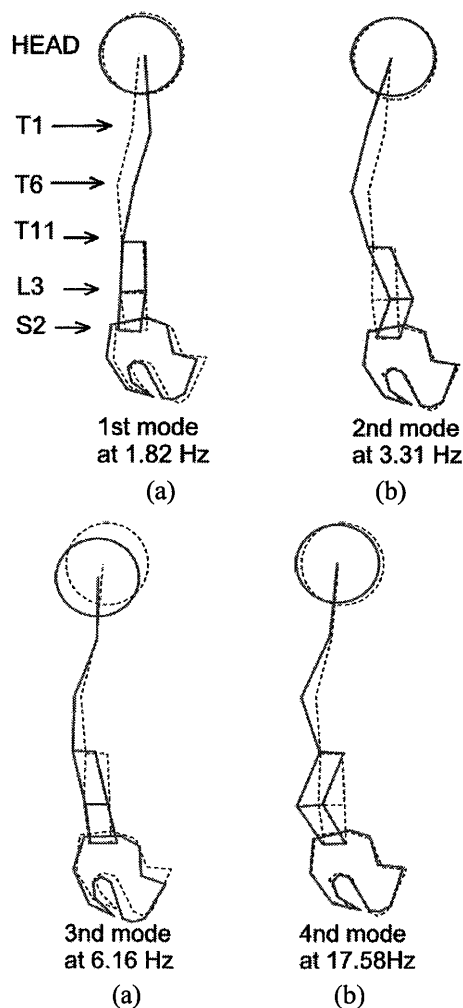


Figure 2. Representation of deformed mode shapes extracted by Kitazaki *et al* 1998, accordingly to the model.

While this study of high quality can be of very great interest in the analysis of car drivers' comfort, its applications in impact biomechanics are limited.

The limitations of this work, for a characterization of the spine column, are at two levels:

- the definition of the degrees of freedom is not adapted to a description of the cervical column,
- the analytical transfer function proposed not frequencies and modes shapes without mechanical parameters identification such as segment masses or rigidity and damping.

Four relevant deformed mode shapes are of interest for the spinal column modeling under rear end impact and will be considered in the following section.

Table 1. Quantitative results of the human body modal analysis.

Mode	Natural frequency [Hz]	Damping ratio
1	1.82	0.224
2	3.31	0.215
3	6.16	0.178
4	17.58	0.296

Lumped parameter model of the torso

In our study, we used the experimental data of Kitazaki (1992) and Kitazaki and Griffin (1998), to establish a minimum complexity lumped parameters model allowing the reproduction of a realistic dynamic behavior of the human torso. In order to obtain the deformed mode shapes given by Kitazaki, our model consists of five joints, as illustrated of figure 3. The head-neck joint remained blocked for this part of the study.

The model consisted of six segments respectively representing the lower and higher lumbar part, the lower and upper thorax, the neck and the head. Mass m_i and inertiae J_i from each part are concentrated at the gravity center G_i . Each joint has a stiffness k_i and damping c_i . We did approximate the angular functions to order 2 for all ψ_i angles around zero. The following functions are then obtained and reported in equation 1:

$$\begin{aligned} \sin(\psi_i) &= \psi_i + O(\psi_i^2) \\ \cos(\psi_i) &= 1 + O(\psi_i^2) \end{aligned} \quad (1)$$

The lengths, masses and inertiae were determined by anthropometric measurements and calculated using a geometrical model developed by Hanavan (1964). This model represents the human body by superimposition of ellipsoidal and cylindrical segments. The mass components are based on the regression equations reported by Clauser *et al* (1969).

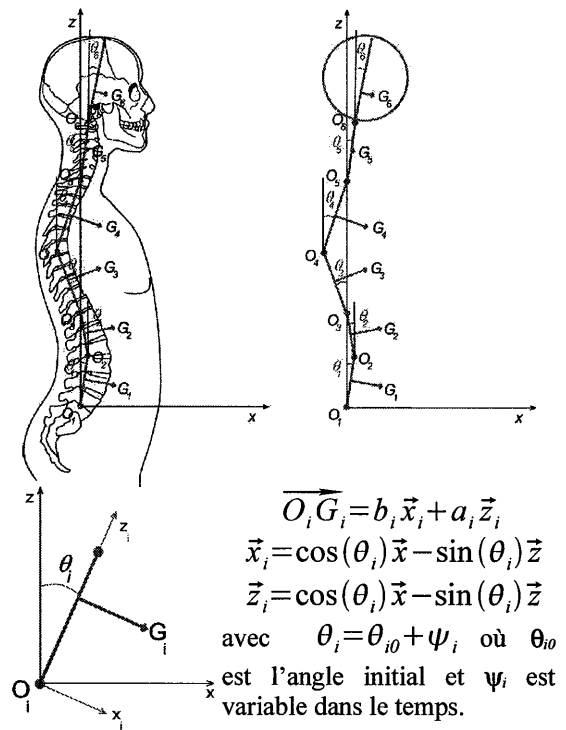


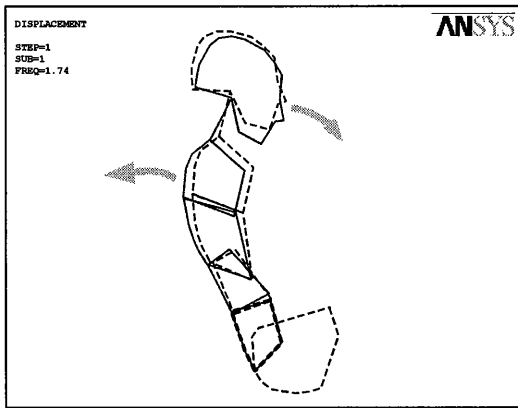
Figure 3. Representation of the lumped parameters model of the trunk.

In order to obtain the masses and inertiae of the five pivots model, we divided the trunk by an upper part and a lower part being the pelvic part. The values thus obtained, after having extracted from the literature the lengths necessary for calculation, are reported in table 2.

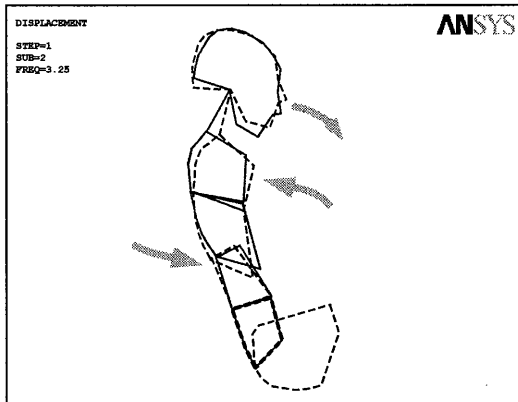
Table 2. Mass and inertial data of the trunk, the neck and the head.

Parts	Mass [kg]	Inertiae /y [kg.m ²]
Lower Lumbar	3.6	0.01
Upper Lumbar	7.3	0.0281
Lower Torso	8	0.0352
Upper Torso	10.5	0.0603
Neck	1.7	0.002
Head	4.5	0.04

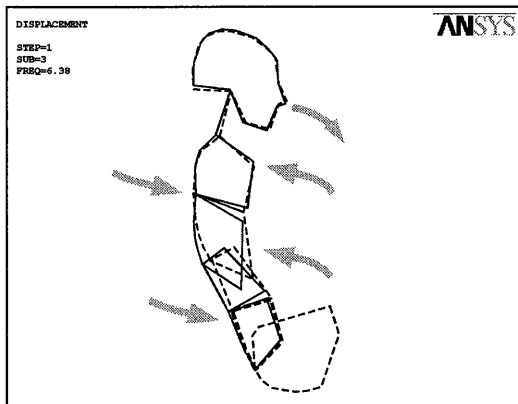
The lumped parameters model of the head-neck-trunk unit was introduced into the implicit finite element code ANSYS in order to calculate the natural frequencies and the deformed mode shapes of the system. The initial stiffness and damping values were selected so that the model presented the same deformed mode shapes as those obtained by Kitazaki at a similar natural frequency.



1st mode at 1.74 Hz

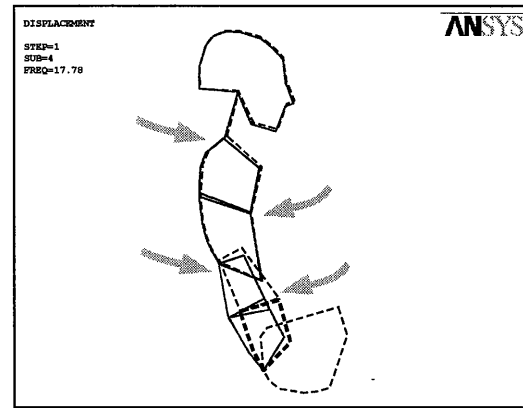


2nd mode at 3.25 Hz



3th mode at 6.38 Hz

Figure 4. Representation of the 3 first deformed mode shapes obtained under free vibration modal analysis with the proposed from the model.



4th mode at 17.78 Hz

Figure 5. Representation of the fourth deformed mode shapes obtained under free vibration modal analysis with the proposed from the model.

In order to be in the same configuration as in the experimental study provided by Kitazaki, we imposed a vertical displacement on all lower parts of the model including the legs and the feet. We also blocked the head-neck joint. Two types of analysis were carried out:

- a free vibration modal analysis, which permitted to distinguish the various deformed mode shapes accordingly to the natural frequencies for an elastic behavior;
- a harmonic analysis which permitted to determine the true values of the natural frequencies and the damping ratios.

The free vibration modal analysis enabled us to determine four deformed mode shapes with natural frequencies over 1 Hz, illustrated in figure 4 and 5. This deformed modes shapes can be compared with those obtained by Kitazaki and Griffin (1998) reported in figure 2. In fact, another natural frequency appears at 0.38 Hz which corresponds to a deformed mode shape not reported by Kitazaki.

The four modes presented are considered as sufficient to validate the model as only stiffness and damping in S2, L3, T11 and T6 are to be identified. Indeed, we already identified the T1 joint stiffness during a previous study on modal analysis of the head-neck system (Willinger and Bourdet 2004).

A parameter optimization of stiffness and damping was then carried out on the model in order to obtain a good accordance of the natural frequencies and the damping ratio with those extracted by Kitazaki *et al* 1998.

A total of 27 iterations were necessary to obtain these parameter optimization. Results are reported in table 3 together with the experimental ones.

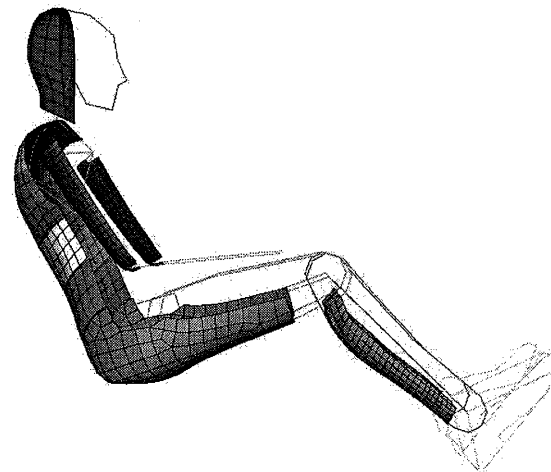
Table 3. Optimization model behavior compared with the experimental ones reported by Kitazaki *et al.*

Mode	Natural frequency [Hz]		Damping ratio	
	Exp.	Model	Exp.	Model
Mode 1	1.82	1.90	0.224	0.23
Mode 2	3.31	3.25	0.215	0.21
Mode 3	6.16	6.2	0.178	0.18
Mode 4	17.58	17.2	0.296	0.25

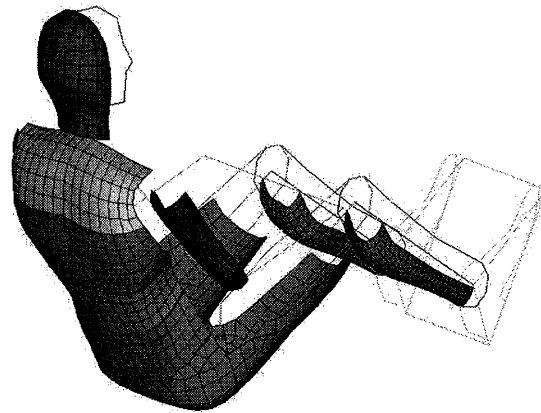
The model was then introduced into the explicit FE code RADIOSS (MECALOG). It is based on the lumped model presented previously. However the arms and the legs were added in order to take into account their the mass and inertial effects.

In order to reduce the number of elements, the model structure is defined with beam elements. An external shell representing the back of the car occupant was meshed and fitted to the human lumped model. The geometry of the surface is based on the volunteer's geometry by palpation of the back. Each segment is defined as a rigid body. Their mass and inertia are attached to the master node corresponding to the center of gravity of the considered torso part

Only surfaces in contact with the car seat were considered, as illustrated of figure 6. The considered surfaces are the following parts : torso surface (the upper thorax, the lower thorax, the upper and lower lumbar), the gluteal surface, the thighs, the legs, the arms and the head. The surface of the neck is related to the surface of the head. These considered surfaces were essential to carry out the coupling between human body and car seat, which is the subject of the following section.



(a)



(b)

Figure 6. Finite elements model of the human head-neck-trunk unit including surfaces in sagittal sight (a) and 3D sight (b).

CAR SEAT MODEL

The numerical modeling of a car seat aimed at giving realistic boundary conditions to the human model in the case of rear end impact. The car seat consists in various mechanical elements. The main parts of the seat were : the head-rest clamp, the head-rest foam , the foam of the backrest, the foam of seat base , the backrest spring, and the cover of the seat. The geometry of the seat was based on existing car seat and is illustrated in figure 7.

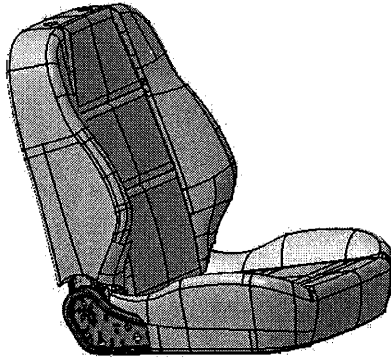


Figure 7. Representation of the car seat.

In this study, the material behavior laws for the foam and the cover were considered linear with material properties resulting from the literature.

The backrest was more detailed than base of the seat. Thus, a simplifying hypothesis consisted to model seat base with a flexible shell which aimed at limiting the movement of the thighs and pelvis. The mechanical properties of seat base have been extracted from a compression test and was considered with linear elastic shell elements and The Young modulus was of 1000MPa and the Poisson's ratio was 0.3. The thickness of the shell elements was of 1.5mm with a density of 500 g/l.

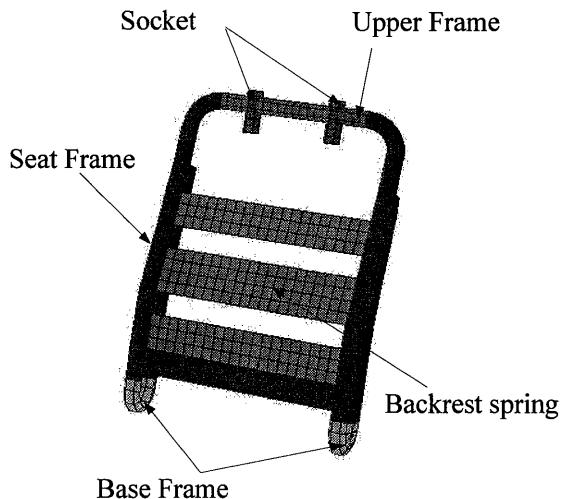


Figure 8. modeling of the backrest frame.

Special attention was paid to the backrest and headrest of the seat. The backrest frame was modeled with shell elements. The geometry was simplified as illustrated in figure 8. It was divided into three parts: the base frame considered as rigid body; the seat frame which can be deformable; and the upper frame also considered as a rigid body part. The seat base and the backrest frame were related by a spring fixed on the base frame. The

sockets were fixed on the upper frame.

The real backrest spring consisted of metal wire connected to the seat frame. At the model level, simplification led in a three meshed bands with shell elements as illustrated of figure 8. The sockets were modeled with shell elements and were considered as rigid segments. They were connected with the upper frame by springs. In the same manner as for the seat base, the material properties of the backrest spring were determined in order to have a qualitatively realistic behavior under static loading. We thus obtained a Young's modulus of 230MPa and a Poisson's ratio of 0.29. The density was of 7.8 kg/l and the thickness of the bands were of 2mm. The stiffness of the springs between the sockets and the upper frame were chosen very high to be considered as rigid.

The backrest foam is modeled with 3D brick elements. In order to homogenize meshing, it was necessary to simplify its geometry. The mesh is presented in figure 9. The foam is divided into three parts (upper, medium and lower) which can have different mechanical properties. The mechanical properties were extracted from modal analysis on several samples of 100x100x40 mm³. The material behavior law used was linear elastic with a Young's modulus of 80kPa and a Poisson's ratio of 0. The density of the foam is given by the manufacturer to be 40 g/l.

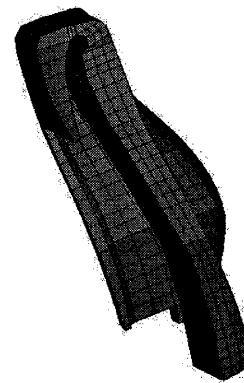


Figure 9. Modeling of the backrest foam.

In order to ensure numerical stability, a reinforcement shell was added on the back surface of the backrest foam. This is also covered with a fabric modeled with shell elements whose nodes coincide with those of the front external surface. The mechanical properties of the fabric have been extracted from static tensile tests. The value of the Young's modulus is then fixed at 1000MPa.

The head rest model consisted in the clamp and the headrest foam. The clamp is divided into two parts (figure 10): a deformable part which penetrates in the foam; and a rigid part which is

related to the sockets with a very stiff spring. The foam is meshed with 3D brick elements. The mechanical properties have been extracted from modal analysis, in the same manner as for the backrest foam. Thus the Young modulus was 50kPa, the Poisson's ratio is 0 and the density was of 36 g/l. The head-rest foam was also covered with a fabric meshed with shell elements. The mechanical properties of the fabric are the same as those used for the fabric of the backrest.

Finally, the seat base and the backrest frame are bound by a spring at the level of the base frame whose stiffness is of 3300 kNm/rad. A particular attention was made on the junction of the upper frame level with the clamp of the head rest. The sockets are connected both with the clamp and the upper frame by a very stiff spring.

HUMAN BODY-SEAT COUPLING

The coupling of the human model with the seat model was done by adjusting both model in geometrical position of the H-point. In order to have an ideal contact at the beginning of impact, we have moved several nodes of the human model by giving to the column a curve adapted to that of the seat (figure 11a).

In order to simulate a rear end impact, we applied an acceleration pulse from a EuroNCAP type at 16 km/h to the seat, as illustrated in figure 11b. The results are shown in figure 12. The purpose of this simulations is to compare the T1 kinematics obtained with a rigid thorax and the flexible thorax developed in the present study.

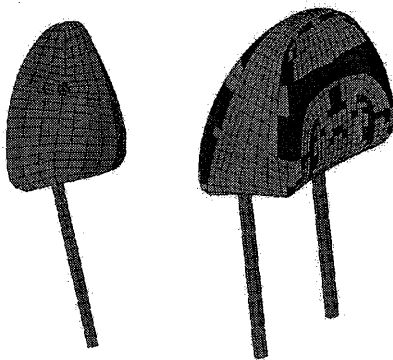


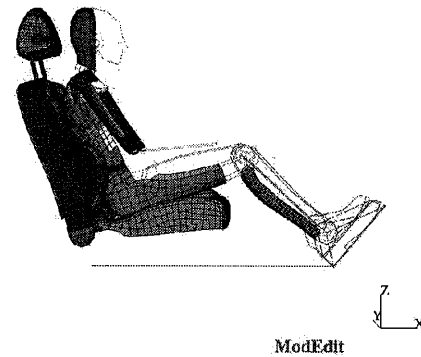
Figure 10. Modeling of the headrest.

To compare the flexibility influence of the thorax, we have to simulate two types of rear impacts.

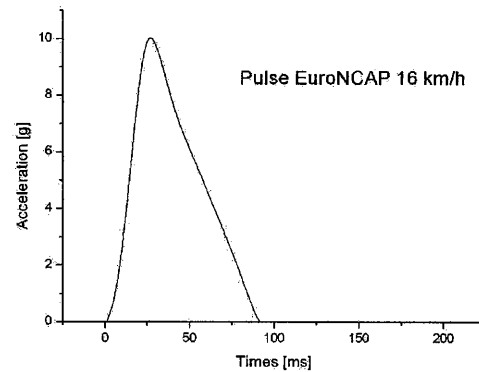
- a configuration with the torso model validated in the frequency domain called flexible torso;
- a configuration with the rigid thorax.

As represented in figures 13a and 13b, extracted at the same computing time (120 ms), an important differences in dynamic behavior can be observed

with an amplified head extension in the case of a rigid thorax (figure 13b) whereas figure 13a shows a marked retraction movement.



(a)



(b)

Figure 11. Positioning of the human model in the seat model (a), Representation of the EuroNCAP pulse at 16 km/h applied to the human-seat unit model (b).

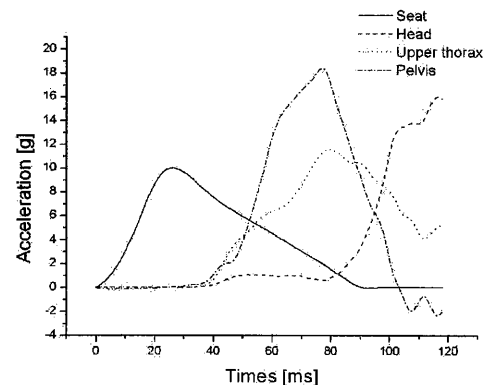


Figure 12. Results in terms of acceleration for several parts of the human-seat coupling model.

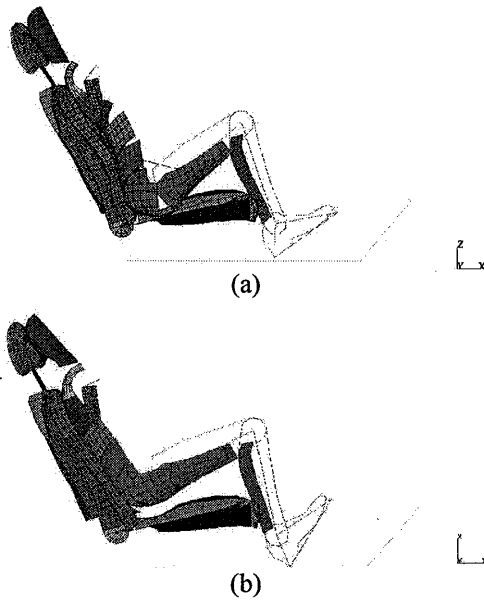


Figure 13. Simulation results under rear impact for a flexible column (a), and a rigid column(b).

Figure 14a shows the superimposition of the x-accelerations at T1 level, in the case of a rigid and flexible thorax. We clearly observe a difference of slope (62.5%) and amplitude (34.5%). Such a difference in T1 loading implies a radically different dynamic behavior of the head and neck, as shown in figures 15a, 15b and 15c for respectively C1-T1 relative displacement, head-torso angle rotation and C1-T1 relative velocity. The x-T1 displacement is more significant when the thorax is rigid, as illustrated in figure 14b. This is due to the fact that the backrest is loaded by all the trunk mass, while the borne mass by the backrest decreases with a flexible thorax. The same phenomenon is described in figure 14c for the Z-T1 displacement.

The effects of a various kinematics on the T1 level cause a relative displacement C1-T1 more significant for a rigid thorax (93 mm) than for a flexible thorax (77mm), as illustrated in figure 15a, with a gap of 20%. The relative velocity curves C1-T1 also shows a great variation up to a maximum of 45% (figure 15c). As for the head-torso relative rotation we can clearly see for the flexible thorax that the head has a retraction movement defined by the positive angles (figure 15b). On the other hand, a rigid trunk does not give the same behavior. Indeed, the head-torso relative rotation is first negative (extension movement) and then positive (retraction movement) caused by the head rest.

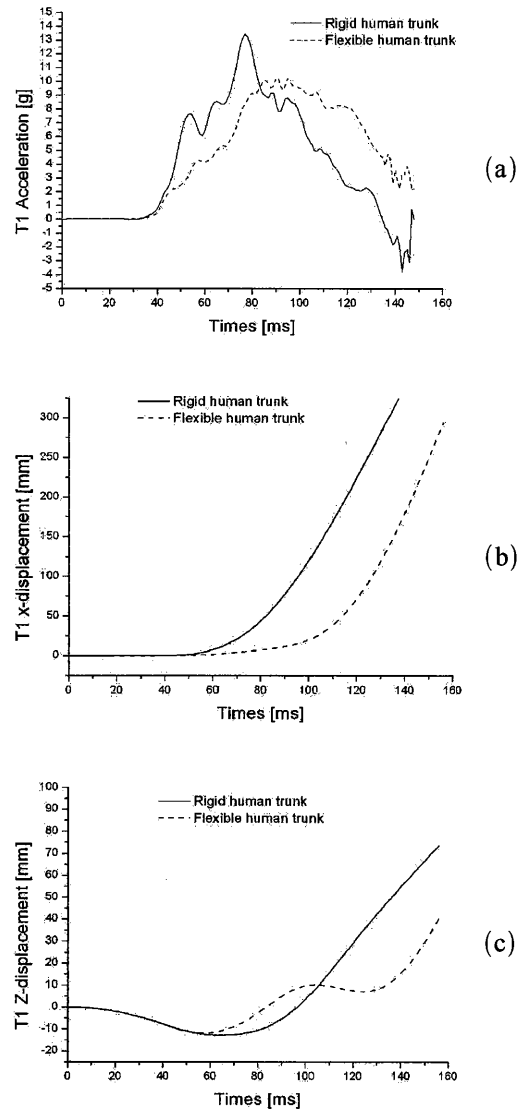


Figure 14. Superimposition of computed T1 acceleration for both rigid and flexible torso model under rear impact.

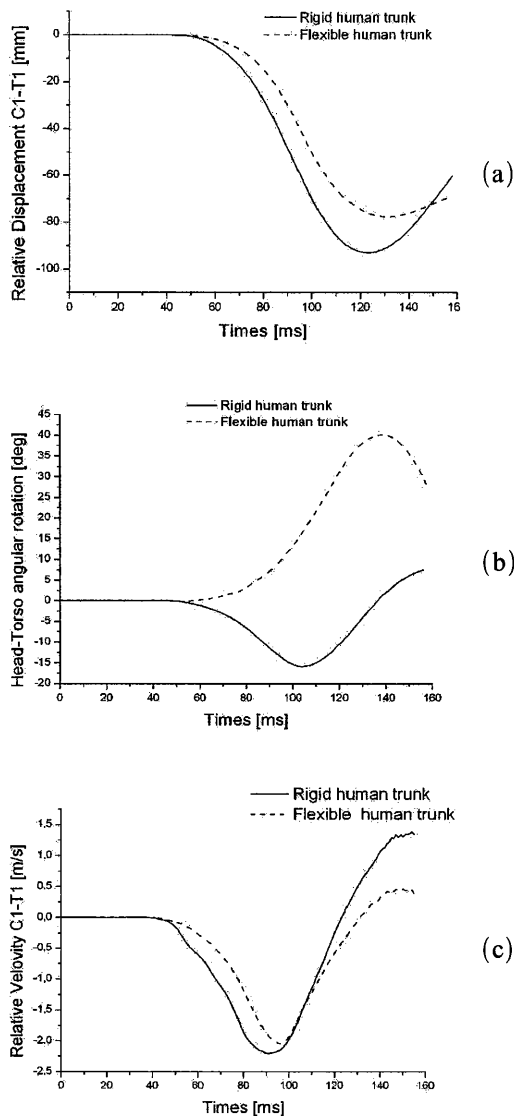


Figure 15. Superimposition of computed C1-T1 relative displacement (a), head-torso relative rotation (b) and C1-T1 relative velocity (c) computed with a rigid and non rigid torso model.

DISCUSSION

The discussion of this new human body-seat model is divided into two parts. The first one is the validation of the human torso model itself, and the second deals with the results at T1 level, the main parameters of the head-neck loading.

Most of the studies of the spine characterization were conducted in terms of intervertebral loading and kinematics of some vertebrae in the temporal domain (Kroell *et al* 1974, Stalnaker *et al* 1971 and Viano *et al* 1989). Kitazaki *et al* 1998 applied modal analysis technic and extracted deformed

modes which four of them correspond to the spinal column deformations. The linearity of the system was checked with the coherence function which remained close to 1. The superimposition of the numerical model analysis with the experimental results made it possible to define the stiffness and damping parameters for each joints of the torso model. Even if a more realistic modeling of the human torso behavior is proposed in the present study, it must be mentioned that the model validation is limited to the sagittal plane and based on one single 38 year old human male volunteer. Further analysis including female is therefore needed.

A number of validation and comparative studies of rear impact dummies are reported in the literature (Cappon *et al* 2001, Kim *et al* 2001, Siegmund *et al* 2001). All of them were conducted in the time domain. The main improvement observed using rear impact dummies was a more flexible spine than for Hybrid III dummy. Two recent comparative studies (Prasad *et al* 1997 and Philippens *et al* 2002) demonstrated that BioRID and RID2 had very similar responses under moderate impact although BioRID has a flexible thorax. Prasad *et al* 1997 concluded that Hybrid III is suitable for rear impact testing in the 8-24 km/h range when Philippens *et al* 2002 had the opposite position. This can be explained by a not enough accurate model evaluation in the time domain. In fact, The models are validated against volunteer and cadavers kinematics in the time domain in terms of corridors. This kind of validation is not accurate enough to extract all the dynamic behavior of the torso. Other contradictions were obtained in the time frame when Philippens *et al* 2002 found that for rear impact dummies head kinematics were acceptable whereas T1 kinematics were not. It is questionable here how the head can behave accurately when T1 does not, given that T1 is the input of the head-neck loading. In addition to the difficulty related to analyze in the time domain, authors often add complexity by considering seat and thorax effect to the neck validation. This is illustrated by Kim *et al* 2001 and Szabo *et al* 2002.

At the theoretical level Eriksson *et al* 2004 recently proposed a torso-seat coupling through a MADYMO BioRID I model coupled to a simplified seat model. The purpose was to reconstruct real world rear impacts and no in deep validation of the human torso was addressed in this study.

In our study we showed that a flexible thorax gave clearly different T1 responses compared to a rigid thorax. These boundary conditions applied to the head-neck system changes drastically the results in terms of head acceleration, head-neck relative rotation or displacement.

CONCLUSION

The experimental data extracted from the modal analysis of the human torso by Kitazaki *et al* 1998 enabled us to define a lumped model of the human torso with five degrees of freedom. This model is then able to reproduce the natural frequencies and deformed mode shapes of the column extracted by the preceding authors. Coupled with a car seat model, it can thus be used to simulate low speed rear end impact more realistically.

A comparative study contributed to show the influence of the thorax flexibility. The boundary conditions of the head-neck unit, imposed by T1 kinematics, showed a very different dynamic behavior of the head and neck when a flexible or rigid torso was considered. It then becomes very significant to have a realistic modeling of the dynamic behavior of the column, if we want to improve the protection systems for a car occupant under low speed rear end impact

In a further development it will be possible to conduct a parametric study on seat characteristics and optimize the seat against the biomechanical response of the human torso-neck-head complex.

REFERENCES

Clauser, McConville, and Young. (1969). Weight, volume and center of mass of segments of the human body. Ohio: Wright Patterson Air Force Base.

Cappon H., Philippens M., Ratingen v., and Wisnans J. (2001). Development and evaluation of a new rear-impact crash dummy: the RID2, Proc. 45th Stapp Car Crash Conference, Paper No 2001-22-0010, pp. 225-238.

Davidsoon J. (1999): BioRID II final report, Crash Safety Division, Department of Machine and Vehicle Design, Chalmers University of Technology, Göteborg, Sweden.

Davidsson, J., Lövsund, P., Ono, K., Svensson, M., and Inami, S. (1999). A comparison between volunteer, BioRID P3 and Hybrid III performance in rear impact. Paper presented at IRCOBI Conference in Bron, France.

Eichberger A., Geigl B., Moser A., Fachbach B., Steffan H., Hell W., and Langwieder K. (1996). Comparison of different car seats regarding head-neck kinematics of volunteers during rear end impact, Proc. IRCOBI Conference, pp. 153-164. Dublin, Ireland.

Foster, J.K., Kortge, J.O., and Wolanin, M.J. (1977). Hybrid III-a biomechanically-based crash test dummy. Paper presented at 21st Stapp Car Crash Conference.

Hanavan, E.P. (1964). A mathematical model of the

human body. Paper presented at AMRL-TR-64-102, AD-608-463. Aerospace Medical Research Laboratories in Wright-Patterson Air Force Base, Ohio.

Hess, J.L., and Lombard, C.F. 1958. Theoretical investigations of dynamic response of man to high vertical acceleration. *Aviat. Med.* 29.

Hodgson, V.R., Gurdjian, E.S., and Thomas, L.M. (1967). Determination of response characteristics of the head when impacting another body, with emphasis on mechanical impedance techniques. Paper presented at 11st Stapp Car Crash Conference.

Ishikawa T., Okano N., and Ishikura K. (2000). An evaluation of prototype seat using Biorid-P3 and Hybrid III with TRID neck, Proc. IRCOBI Conference, pp. 379-391. Montpellier, France.

Jakobsson, L., Norin, H., Jernström, C., Svensson, S.-E., Johnsen, P., Isaksson-Hellman, I., and Svensson, M.Y. (1994). Analysis of Different Head and Neck Responses in Rear-End Car Collisions Using a New Humanlike Mathematical Model. Paper presented at IRCOBI Conference in Lyon, France.

Jernström C., Nilsson G. And Svensson M. Y. (1993), A first approach to an implementation in MADYMO of a human body model for rear impact modeling. Proc of the 4th International Madymo User's Meeting, september 6-7, Eindhoven, The Netherlands.

Kim A., Anderson K. F., Berliner J., Bryzik C., Hassan J., Jensen J., Kendall M., Mertz H. J., Morrow T., Rao A., and Wozniak J. A. (2001). A comparison of the Hybrid III and BioRID II dummies in low-severity, rear-impact sled tests, Proc. 45th Stapp Car Crash Conference, Paper No 2001-22-0012, pp. 375-402.

Kitazaki, S. (1992). Application of experimental modal analysis to the human whole-body vibration. University of Southampton: ISVR.

Kitazaki, S., and Griffin, M.J. 1998. Resonance behaviour of the seated human body and effects of posture. *Journal of Biomechanics.* 31: 143-149.

Kroell, C.K., Schneider, D.C., Nahum, A.M. Impact tolerance and response of the human thorax II. SAE 741187 18th Stapp Car Crash Conference, 1974.

Eriksson L. (2004), Neck injury risk in rear-end impact – Risk factors and neck injury criterion evaluation with madymo modelling and real-life data. Thesis, Crash Safety Division, Department of Machine and Vehicle Systems, Chalmers University of Technology, Göteborg, Sweden 2004.

Meyer F., Bourdet N., Deck C., Willinger R., Raul

J.S. Human neck finite element model development and validation against original experimental data. 2004-22-0008, Stapp Car Crash journal, Vol. 48, pp. 177-206, Novembre 2004.

Philippens M., Cappon H., van Ratingen M., Wismans J., Svensson M., Sirey F., Ono K., Nishimoto N., and Matsuoka F. (2002). Comparison of the rear impact biofidelity of BioRID II and RID2, Proc. 46th Stapp Car Crash Conference, Paper No 2002-22-0023, pp. 383-399.

Prasad P., Kim A., and Weerappuli D. P. V. (1997). Biofidelity of anthropomorphic test devices for rear impact, Proc. 41th Stapp Car Crash Conference, Paper No 973342, pp. 387-415.

Seemann M. R., Muzzy W. H., and Lustick L. S. (1986). Comparison of human and Hybrid III head and neck response, Proc. 30th Stapp Car Crash Conference, Paper No 861892, pp. 291-312.

Siegmund G. P., Heinrichs B. E., Lawrence J. M., and Philippens M. (2001). Kinetic and kinematic responses of the RID2a, Hybrid III and Human Volunteers in low-speed rear-end collisions, Proc. 45th Stapp Car Crash Conference, Paper No 2001-22-0011, pp. 239-256.

Stalnaker, R.L., and Fagel, J.L. 1971. Driving point impedance characteristics of the head. Journal of Biomechanics. 4: 127-139.

Svensson, M., Lövsund, P., Håland, Y., and Larsson, S. (1993). The Influence of Seat-Back and Head-Restraint Properties on the Head-Neck Motion During Rear-Impact. Paper presented at

IRCOBI Conference in Eindhoven, Netherlands.

Szabo, T.J., and Welcher, J.B. (1996). Human Subject kinematics and electromyographic activity during low speed rear impacts. Paper presented at 40th Stapp Car Crash Conference.

Szabo T. J., Voss D. P., and Welcher J. B. (2002). Influence of seat foam and geometrical properties on BioRID P3 kinematic response to rear impacts, Proc. IRCOBI Conference, pp. 87-101. Munich, Germany.

Viano D.C., Lau I.V., Asburg C., King A.I. and Begeman P.; Biomechanics of the human chest, abdomen, and pelvis in lateral impact ; *Accid-Anal-Pev.* 1989 December ; Vol.21, No.6 : 553-574.

Vulcan, A.P., King, A.I., and Nakamura, G.S. 1970. Effects of bending on the vertebral column during +Gz acceleration. *Aerosp. Med.* 41: 294.

Willinger, R., and Cesari, D. (1990). Evidence of cerebral movement at impact through mechanical impedance methods. Paper presented at IRCOBI Conference in Bron, France.

Willinger R., Bourdet N., and Le Gall F. (2002) Characterization and modeling of the human head-neck in the frequency domain. Proc. Of the 5th Int. Conf. On Vibration Eng., Nanjing 2002, 167-173.

Willinger R. , Bourdet N., Fischer R and Le Gall F. (2004) Modal analysis of the human neck in vivo as a criterion for crash test dummy evaluation, *Journal of Sound and Vibration*, In Press, Corrected Proof, Available online 19 January 2005,

THE PROCESS OF EVALUTION AND DOCUMENTATION OF CRASH TEST DUMMIES FOR PART 572 OF THE CODE OF FEDERAL REGULATIONS

Daniel Rhule
Heather Rhule
Bruce Donnelly

National Highway Traffic Safety Administration
United States

Paper Number 05-0284

ABSTRACT

A candidate anthropometric test device (ATD), or crash test dummy, must undergo a rigorous evaluation and documentation process before it can be considered for incorporation into Part 572 of the Code of Federal Regulations. This process has been developed over many years and includes (1) thorough dummy and drawing inspection, (2) establishment of dummy certification criteria, (3) evaluation of the dummy's durability, biofidelity, repeatability, and reproducibility, and (4) the generation of a detailed manual for dummy assembly procedures. The evaluation process will be outlined and explained in detail. Recent dummy evaluations for the Thor Lx, the ES-2re and the Ten-year-old HIII dummies will be utilized as examples of the various parts of the process.

INTRODUCTION

The National Traffic and Motor Vehicle Safety Act of 1966 (the Safety Act) [1] authorizes the National Highway Traffic Safety Administration (NHTSA) to prescribe motor vehicle safety standards to reduce deaths and injuries resulting from traffic accidents. The Act requires that each Federal Motor Vehicle Safety Standard (FMVSS) shall be practicable, meet the need for motor vehicle safety, and be stated in objective terms.

NHTSA's FMVSSs generally consist of three groups of regulations: 1) the 100-series dealing with pre-crash avoidance requirements, 2) the 200-series dealing with crashworthiness requirements and 3) the 300-series dealing with post-crash requirements. Many of the 200-series crashworthiness standards specify dynamic crash tests, either full-scale vehicle crash testing or sled crash simulations, that replicate real-world crash scenarios. Anthropomorphic test devices (ATDs or test dummies) are used in these dynamic tests as measuring tools that render repetitive and correlative results under similar test conditions and to reflect the protective performance of a vehicle or item of motor vehicle equipment with

respect to human occupants. NHTSA enforces the FMVSSs by testing vehicles or equipment as described in the test procedures contained in the FMVSSs.

In 1970, NHTSA amended Federal Motor Vehicle Safety Standard 208 (FMVSS 208) to require automatic crash protection for all passenger cars as of July 1, 1973 and for most light trucks and vans as of July 1, 1974. Compliance would have been determined by a crash test with ATDs in the front outboard seats. Shortly after the March 10, 1971 final rule, Chrysler, et al. [2] filed lawsuits in the U.S. Court of Appeals for the Sixth Circuit challenging the automatic crash protection requirements. The plaintiffs argued that the automatic crash protection requirement were: (a) not "practicable," as required by the Safety Act, because the technology needed to comply with automatic protection was not sufficiently developed at the time; (b) did not "meet the need for motor vehicle safety," as required by the Safety Act, because seat belts offered better occupant protection than automatic protection; and (c) were not "objective," as required by the Safety Act, because an ATD built to the existing SAE Recommended Practice [3] did not produce consistent, reliable or repeatable test results.

In Chrysler v. DOT, the Sixth Circuit announced its decision on the lawsuits. The court ruled in favor of NHTSA on the first two arguments, but found in favor of the manufacturers on the third argument that the ATD specified by the standard did not meet the criterion of objectivity. The court remanded the case to NHTSA with instructions that further specification be made in objective terms to assure comparable results among test sites. The court further noted that, "The importance of objectivity in safety standards can not be overemphasized." Objective in the context of this case means that (1) the tests and dummies used to determine compliance or non-compliance with the standard produce identical results when the test conditions are duplicated (repeatability and reproducibility), (2) that the accuracy of the tools be demonstrable in a reasonable

test procedure and (3) that vehicle compliance be based upon instrument readings (crash test dummies) as opposed to the opinions of human beings.

NHTSA developed new specifications for the anthropometric test dummy following the Chrysler decision. In 1973, the agency created Part 572 under Title 49 of the Code of Federal Regulations [49 CFR 572], to be a repository for specifications of crash test dummies and similar test devices. At the same time, the agency issued much more detailed test dummy specifications for the ATD to be used in FMVSS 208 testing. That first crash test dummy was the Hybrid II Part 572 Subpart B, 50th Percentile Male.

Since the time of the Chrysler decision, NHTSA has sought to ensure that any candidate ATD considered for possible use in a Federal Motor Vehicle Safety Standard undergoes a rigorous evaluation and documentation process to determine the ATD's suitability for incorporation into Part 572 of 49 CFR. This process includes, as a minimum, the assurance that the dummy meets:

- dimensional, mass, and construction specifications as contained in a drawing set
- performance requirements based on test procedures, also called certification procedures, that assure the dummy responds accurately and repeatably under specified loading conditions
- documented procedures for the assembly, disassembly, and inspection (PADI) of the dummy such that any users performing an FMVSS crash test are able to prepare the dummy before and after testing
- documentation that the dummy is sufficiently durable, repeatable, reproducible, and biofidelic to be used as a test instrument, in combination with appropriate injury criteria, to assess the potential for injury in an FMVSS crash test.

Of these elements, the drawing part numbers as well as the certification test procedures and performance specifications appear in Part 572 of 49 CFR. The PADI and the supporting documentation are placed into the docket. Injury criteria, which are part of the FMVSS, appear in Part 571 of 49 CFR.

Every dummy must undergo a rigorous assessment process, often called "federalization," that incorporates these elements. Incorporation of a dummy into Part 572 includes a proposal stage through the publication of a notice of proposed rulemaking (NPRM) in the Federal Register, a public comment stage, and a publication of a final rule that

addresses the public comments. Publication of the final rule completes the addition of the ATD into the Part 572 regulation.

THE FEDERALIZATION PROCESS

The Federalization process requires a thorough inspection of the dummy and comparison to the drawings, certification and laboratory testing, sled testing and crash testing. Because of the high cost associated with crash testing and, to a lesser extent, sled testing, it is logical to perform those tests after the less expensive inspection and lab tests. Cost efficiency suggests a sequence of operations moving from inspection through lab testing to sled and crash testing. The various objectives of the Federalization process do not lend themselves to a sequential process because several requirements can only be fulfilled with multiple types of testing. For example, durability of a dummy is tested in the lab, on the sled and in crash tests. Figure 1 shows a chart cross-referencing the objectives of Federalization with the sequential operations of testing. In Figure 1 time and test operations progress from left to right while the functional objectives of Federalization are shown vertically on the left. This chart will be updated in each section of the following discussion indicating under which sequential task each Federalization requirement is met.

		TASKS			
		Dummy Inspection	Lab Testing	Sled Testing	Crash Testing
FUNCTIONS	Drawing Package				
	Certification				
	Durability				
	R & R				
	Biofidelity				
	PADI				
		TIME →			

Figure 1. Federalization objectives versus scheduled tasks matrix.

DRAWING PACKAGE

An engineering drawing package defining the physical dimensions of the dummy assembly, all sub-assemblies and detail drawings of all of the parts is a Federalization requirement and is incorporated into

Part 572.49 CFR by reference. The weight and center of gravity (CG) of the dummy component segments are also specified in the drawing package.

The actual physical drawings reside in the docket room at NHTSA headquarters in Washington, D.C. and are also available from the Docket in electronic graphics format (.pdf). The drawing package is intended to minimally specify the dimensional and mass properties of the dummy and all of the dummy parts.

The drawing package is usually produced by a dummy manufacturer and obtained by NHTSA during the dummy evaluation process. Most dummies are designed and developed in collaboration with national and international organizations such as the SAE, ISO, OSRP, EEVC, etc. Before the dummy is considered for incorporation into Part 572, the agency assures that the drawings and all associated information are accessible and freely available to the public without any restrictions, such as proprietary claims, patent rights, trade names, etc.

Inspection

Several dummies are acquired and completely disassembled and inspected. If more than one manufacturer supplies the dummy, at least one dummy from each supplier will be purchased for inspection and subsequent testing. Physical dimensions of each part of the disassembled dummy will be measured and compared to the drawing package and any discrepancies will be noted. This includes a check on the weights and CGs of component segments. In the case of flesh and foam parts with irregular shapes the critical dimensions are checked against the drawing, allowing for an appropriate tolerance on these soft parts.

The list of discrepancies is brought to the attention of the dummy manufacturer and the party responsible for the drawings. Often the discrepancy is a simple mistake in a drawing and easily corrected; however, sometimes a modification to the physical dummy is required. If a significant modification to the dummy is needed, the dummy may be returned to the manufacturer for correction. In many cases work can continue while the modified part is produced either by working with other dummy components that are not affected by the change or by substituting a prototype part that does not affect the dummy configuration or dynamic response. In the case when there are two, or more, manufacturers of a dummy who make a component part differently, a compromise on the discrepancy is sought. If

agreement cannot be reached, NHTSA will make a decision and incorporate a satisfactory design into the Part 572 drawing package.

The Federalization requirement for a drawing package is satisfied in the disassembly and inspection task (See Figure 2).

Modification

Before proceeding on to the testing phases of the evaluation process, the drawing and physical configuration issues must be resolved. Otherwise, it is likely that changes will be made to the dummy after testing has begun and these changes will invalidate the test results and require retesting. This process of examination and testing leading to

		TASKS			
		Dummy Inspection	Lab Testing	Sled Testing	Crash Testing
FUNCTIONS	Drawing Package				
	Certification				
	Durability				
	R & R				
	Biofidelity				
	PADI				

TIME →

Figure 2. Drawing package requirement satisfied by the dummy inspection task.

modifications continues throughout the evaluation process. It is a time consuming and frequently expensive iterative process. This examination and modification process is the principal reason that the evaluation proceeds from the least expensive to the most expensive type of examination, i.e., inspection, lab testing, sled testing and crash testing. It is quite possible at any point in the Federalization process that a shortcoming of the dummy will become apparent and modification will be required. If this occurs it is often necessary to back up and repeat some, or all, of the testing. This iterative, exacting and often expensive process results in a dummy that meets the Federalization requirements for durability, biofidelity, repeatability and reproducibility.

IIII Ten-year-old Child Dummy

The Ten-year-old Hybrid III child dummy (Figure 3) was developed under the direction of the SAE Hybrid III Dummy Family Task Force and in collaboration with First Technology Safety Systems (FTSS) and Denton Anthropometric Test Devices (DATD). NHTSA participated in this dummy design and evaluation. This dummy was divided into an upper half and a lower half and each half was designed and prototype parts fabricated by different manufacturers. Drawings and computer aided design (CAD) files were then exchanged, through the SAE committee, and each manufacturer then fabricated the other half of the dummy. The result was dummies manufactured by both suppliers that were nearly

identical. In the case of the Ten-year-old, NHTSA bought a whole dummy from each manufacturer and also bought the half of the dummy each had designed, assembling the two halves to make a third dummy.

The SAE committee provided the drawings and CAD files to NHTSA for the purposes of inspection. As would be expected under this collaborative design approach, the inspection process for the IIII Ten-year-old yielded only a small list of discrepancies between drawings and dummies. Table 1 shows the segment weight specifications and the actual weights of the dummies from each manufacturer indicating very good compliance with fairly tight tolerances.



Figure 3. The Ten-year-old IIII dummy.

Table 1.
Ten-year-old Segment Weights.

Segment	Part Number	Specification	Dummy 1	Dummy 2	Average
Head Assembly	880105-100X	8.23 +/- 0.10	8.25	8.16	8.21
Neck Assembly	420-2000	1.77 +/- 0.10	1.78	1.80	1.79
Upper Torso Ass'y	420-3000	17.94 +/- 0.30	17.82	17.82	17.82
Lower Torso Ass'y	420-4000	19.21 +/- 0.30	19.16	19.42	19.29
Upper Arm, Left	*420-7000-1	1.78 +/- 0.10	1.66	1.74	1.70
Upper Arm, Right	*420-7000-2	1.78 +/- 0.10	1.71	1.73	1.72
Lower Arm, Left	*420-7000-1	1.35 +/- 0.10	1.33	1.36	1.35
Lower Arm, Right	*420-7000-2	1.35 +/- 0.10	1.34	1.37	1.36
Hand, Left	420-7231-1	0.38 +/- 0.10	0.35	0.46	0.41
Hand, Right	420-7230-2	0.38 +/- 0.10	0.35	0.47	0.41
Upper Leg, Left	*420-5000-1	5.90 +/- 0.15	5.89	6.02	5.96
Upper Leg, Right	*420-5000-2	5.90 +/- 0.15	5.89	6.02	5.96
Lower Leg, Left	*420-5000-1	4.92 +/- 0.15	4.83	4.96	4.90
Lower Leg, Right	*420-5000-2	4.92 +/- 0.15	4.97	4.97	4.97
Foot, Left	420-5500-1	0.90 +/- 0.05	0.90	0.90	0.90
Foot, Right	420-5500-2	0.90 +/- 0.05	0.92	0.88	0.90
TOTAL WEIGHT	420-0000	77.61 +/- 2.00	77.15	78.08	77.62

CERTIFICATION

All regulated dummies are subjected to a series of tests in order to ensure that their components are functioning properly. These tests are typically conducted immediately before and after an FMVSS test is conducted to support the validity of the test results. The certification tests by and large evaluate the dummy's components that have important

consequences in their proposed FMVSS applications. With this in mind, the tests are generally designed to load the dummy at a range similar to what it is expected to undergo in the proposed application. The certification tests are also intended to monitor the responses of components that may have a tendency to deteriorate over time. Some typical certification tests include:

- head drop
- neck flexion and extension
- thorax impact
- knee/femur impact
- torso flexion

Generally, by the time the Agency begins the federalization process, a preliminary set of certification procedures have been developed. NHTSA must then acquire or fabricate any new equipment required to conduct the tests. The process of evaluating the certification test procedures can then be initiated. This includes assessing:

- Test procedures. Can the set-up be repeatedly achieved? Are the speeds realistic? Is the test user-friendly?
- Response corridors. Can the dummy meet the corridors? Are the corridors reasonable approximations of the loading that the dummy will experience in its intended application? Are the corridors within the dummy’s mechanical limits and the instrumentation capacities?
- Repeatability and reproducibility. Does each dummy provide repeatable responses? Do all of the dummies respond similarly?

In some cases, as with the Thor Lx and FLx advanced instrumented lower legs, the Agency has led the development of the design, independent of broad industry involvement. In this instance, there were no preliminary set of certification procedures and thus the Agency independently developed procedures and response corridors.

To establish certification procedures for the Thor Lx/FLx lower legs, the Agency developed preliminary test procedures based around the following biomechanical response requirements:

- quasi-static response characteristics for:
 - axial loading at the heel (force-deflection)
 - dorsiflexion/plantarflexion response (torque-angle)
 - inversion/eversion response (torque-angle)
- dynamic response characteristics for
 - axial loading at the heel (force-deflection)
 - dorsiflexion response (torque-angle)

After fabricating the necessary hardware, a preliminary test procedure was developed for each of these biomechanical requirements. Initial testing, however, revealed that the quasi-static testing was time consuming and difficult to set-up. Further development led to a dynamic inversion/eversion test procedure and thus the quasi-static tests were

relegated to the status of design guidelines, which are used in the development of the design, but not required for certification purposes. As a result, all of the certification tests would be dynamic impact tests – a heel of foot impact; a ball of foot impact; and an inversion/eversion impact.

After establishing the test procedures, the next step was to determine the response corridors. To accomplish this, multiple leg samples were acquired from several manufacturers and each leg was subjected to three repeats of the test procedures. From the data collected, the mean values of the significant responses were computed. Finally, the response corridors were constructed using a tolerance of 10% of the mean response value - the upper limits were set at 110% of the mean and the lower limits were set at 90% of the mean.

The final step is to document the certification test procedures in sufficient detail including:

- identification of the components included in each test
- a description of the test set-up geometry, speed, and orientation
- a diagram which supports the text description of the set-up
- definition of test probe properties including geometry and mass moment of inertia
- clearly stated response requirements

The Federalization requirement of developing certification procedures and response requirements is achieved through lab testing as shown in Figure 4.

		TASKS			
		Dummy Inspection	Lab Testing	Sled Testing	Crash Testing
FUNCTIONS	Drawing Package				
	Certification				
	Durability				
	R & R				
	Biofidelity				
	PADI				

Figure 4. Certification requirement is satisfied by the Lab testing.

DURABILITY

A dummy intended for use in an FMVSS crash test must be durable on several levels. To be valid as a regulatory test instrument that makes measurements to be used to pass or fail a vehicle it is desirable, although not necessarily mandatory, that the dummy survives the crash event intact and still be able to make accurate measurements. This durability is normally ascertained by performing dummy certification tests both before and after the crash test. It is important to recognize that a dummy used in FMVSS testing is intended to identify those vehicles having unacceptable occupant protection capability and to provide data to indicate whether or not the vehicle fails the crash performance test. The dummy needs to be durable at, and above, the failure injury criteria levels. This is likely to be at the upper end of the dummy's mechanical and electronic limitations. Further, the use of dummies in New Car Assessment Program (NCAP) testing at high crash energy levels requires a dummy to be durable well above the FMVSS crash test energy level. Finally, for cost reasons it is desirable that a dummy be sufficiently durable to be used for many years in many tests with only a reasonable level of maintenance and repair.

It is interesting to note that in addition to the durability requirements discussed in the previous paragraph, a dummy is expected to be sensitive to variations in crash loading ranging from low energy levels to high energy levels and to distinguish among good and poor restraint systems of widely varying design.

Certification Testing

Dummy durability assessment begins with certification laboratory testing. A typical thorax certification test setup is shown in Figure 5. The dummy designers generally provide certification test procedures and performance specifications, as was discussed in the previous section. These recommended test procedures serve as the starting point for assessment of dummy durability. The recommended certification tests will be performed repeatedly on several dummies, preferably made by different manufacturers. This testing will also serve as repeatability and reproducibility testing, as will be discussed in the next section.

As the evaluation progresses, the dummy will be visually inspected after each test for damage or excessive wear. Should a change in response data be observed, either sudden or gradual, the dummy will

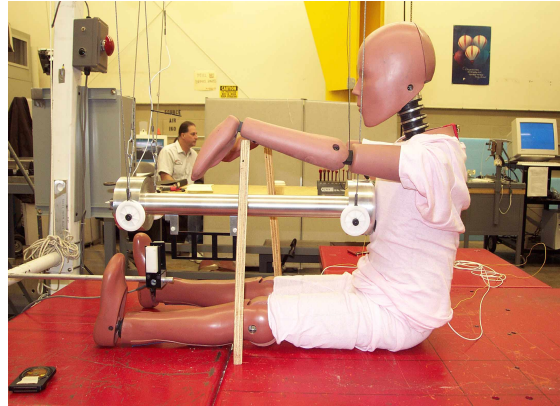


Figure 5. Ten-year-old dummy thorax impact.

be disassembled to ascertain if the reason for the change is breakage or wear. If breakage or wear of a dummy part is found, a decision must be made as to whether this is a tolerable situation and parts should be replaced as routine maintenance or an intolerable situation requiring either dummy modification or abandonment as a candidate test device.

When an intolerable durability problem is observed, the dummy manufacturer and the dummy designers are generally contacted in an effort to resolve the issue in the optimum manner: modification of the dummy, the test procedure or the maintenance procedure. With relatively new dummy designs it is not uncommon to discover durability problems due to extensive repeat testing of the dummy.

Note that at this point a modification to the dummy may be required and the certification testing will likely have to be repeated with the new part, which may be a prototype. This is the same iterative process discussed previously. When this occurs the NHTSA evaluation testing has effectively become part of the development process. It should also be noted that repeat certification tests with multiple dummies will provide repeatability and reproducibility data.

High-Energy Laboratory Testing

Following satisfactory performance in the certification testing, sets of high-energy certification tests are performed. These high-energy tests typically involve raising the kinetic energy of the impact in order to expose the dummy to impact severities slightly greater than those that might be expected in crash tests. Care must be taken in selecting which tests should be performed, e.g., a high-energy chest impact to the Ten-year-old dummy might be excessively severe for a dummy intended to

be loaded with a three-point belt restraint in a booster seat. Also, the process of careful inspection and possible modification is again followed with the possibility of iteratively repeating previous tests always present.

Out-of-Position Testing

In the case of small adult dummies or some child dummies, out-of-position (OOP) testing is performed. In these cases the OOP tests are performed with known aggressive airbag restraint systems to assure that the dummy can withstand severe loading to the head, neck and thorax. Figure 6 is an example of the Ten-year-old child dummy in the head-to-bag OOP position.

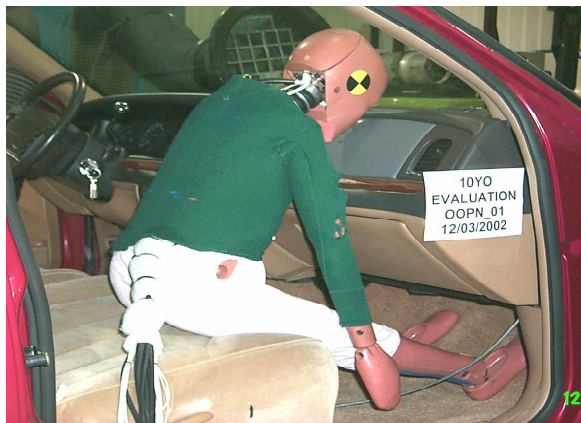


Figure 6. OOP testing for the Ten-year-old child dummy.

Sled Testing

Sled testing of the dummies is performed at FMVSS and at NCAP crash test energy levels. For frontal dummies sled testing is normally performed in a sled buck modeling a typical vehicle in the current fleet. For side impact dummies sled testing is normally performed in a flat wall sliding hard-seat type buck with and without wall padding. For child dummies the stylized FMVSS 213 bench seat is normally used with a Child Restraint System (CRS) or a booster seat. Note that the sled testing used to assess dummy durability may also be used to assess dummy repeatability and reproducibility.

Among other considerations, the typical sled testing matrix will be designed to subject the dummy to various seating positions and test conditions that may expose potential weaknesses of the dummy design.

Crash Testing

Crash testing in the anticipated FMVSS configuration is the final phase of durability assessment. If a dummy is to be used in NCAP testing, the higher energy crash test would be performed on the assumption that a durable dummy at NCAP speed would also be durable at the lower FMVSS crash speed.

Federalization Requirement

The Federalization requirement for dummy durability is satisfied by laboratory testing, sled testing and crash testing (See Figure 7).

		TASKS			
		Dummy Inspection	Lab Testing	Sled Testing	Crash Testing
FUNCTIONS	Drawing Package				
	Certification				
	Durability				
	R & R				
	Biofidelity				
	PADI				
		TIME →			

Figure 7. Durability requirement satisfied by the lab, sled, and crash testing.

REPEATABILITY AND REPRODUCIBILITY

Repeatability and reproducibility (R&R) are important considerations in the evaluation of a dummy. In the context of dummy evaluation, repeatability is defined as the similarity of responses from a single dummy when subjected to multiple repeats of a given test condition. Reproducibility is defined as the similarity of test responses from multiple dummies when subjected to multiple repeats of a given test condition. Any ATD that is to be used for federal regulatory testing must have an acceptable level of R&R to ensure confidence in the responses provided by the dummy.

R&R analysis requires the replication of tests on multiple samples of a dummy, preferably samples from multiple manufacturers. Clearly, the R&R results will depend largely on the dummy's ability to provide similar responses to each test. However,

several external factors may also play a role in the R&R results, such as the repeatability of the dummy's setup or the impact speed. In order to provide a meaningful R&R analysis, control of the test conditions must be exercised. Component tests, such as the certification tests, are more readily controlled and thus may be expected to provide the best estimates of a dummy's R&R. Sled testing provides an efficient alternative to vehicle crash testing and offers insight into the dummy's performance as a complete system. Full vehicle crash testing does not provide a desirable environment for R&R testing as the variation in structural materials of the crash vehicle are difficult to account for.

Additionally, the severity of the test conditions utilized for R&R assessment must also be considered. For example, if the test conditions are so severe that the responses are near or beyond the dummy's mechanical limits or electronic capacity, then the corresponding R&R analysis may not be meaningful. Consider a dummy that is mechanically limited to 50 mm of rib displacement. The rib is impacted repeatedly and the dummy measures rib displacements of 50 mm for each test. The analysis would indicate excellent R&R; however, due to the dummy's mechanical limitations, it is unknown whether this response is truly repeatable. A better evaluation might seek to impart, for example, 40 mm of rib deflection so that the mechanical limits are not approached.

A quantitative assessment of R&R is achieved using a statistical analysis of variance. The coefficient of variation (CV) is a measure of variability expressed as a percentage of the mean. CV is calculated according to the formula below:

$$CV = \frac{\sigma}{\bar{X}} \times 100\%$$

where

σ = standard deviation of responses

\bar{X} = mean of responses

Historically, NHTSA has categorized the CV scores according to Table 2.

There are several considerations that must be taken into account when CV scores are interpreted. One such consideration would be the relevance of the response. For example, the lateral shearing forces measured in a dummy designed for frontal impacts are generally considered to be of less significance. In

Table 2.
Assessment of CV Scores.

CV Score	Assessment
0 – 5%	Excellent
>5 – 8%	Good
>8 – 10%	Marginal (Acceptable)
>10%	Poor (Unacceptable)

this scenario, a poor CV score may not provide sufficient reason for concern. Consideration must also be given to the magnitude of the response. If the mean response is small, then even a small number for the standard deviation can result in a large CV. This consideration is closely related to the first one, in that responses which exhibit a low mean generally have less relevance to the given test condition.

As an example, the agency recently initiated an evaluation of the EuroSID-2re (ES-2re) dummy. To that end, the ES-2re was subjected to repeated certification and sled tests to establish its repeatability and reproducibility as a test tool.

To assess the ES-2re's R&R in certification tests, two sample dummies were each subjected to five repeats of each of the certification tests. The response data was collected and filtered according to the test procedures. Next, statistical analysis of the response criteria resulted in CV scores of repeatability for each dummy and reproducibility for both dummies. Table 3 presents a summary of the ES-2re's R&R analysis for certification tests. It is observed that the vast majority of the responses would be considered excellent, with only four CV scores falling in the 'good' range and just one score in the 'marginal' range.

The Federalization requirement for repeatability and reproducibility is satisfied by laboratory and sled testing (See Figure 8).

BIOFIDELITY

Biofidelity is a measure of how well a dummy replicates the response of a human. If a dummy replicates the human response quite well, it is said to have good biofidelity, or be quite biofidelic. Although not a requirement in Part 572, the dummy's biofidelity is an important consideration in the decision of whether or not the dummy is suitable for incorporation into Part 572.

		TASKS			
		Dummy Inspection	Lab Testing	Sled Testing	Crash Testing
FUNCTIONS	Drawing Package				
	Certification				
	Durability				
	R & R				
	Biofidelity				
	PADI				
		T I M E →			

Figure 8. The Lab and Sled testing satisfy the R & R requirement.

Until recently, NHTSA assessed dummy biofidelity based on subjective, qualitative analysis of dummy data fit within cadaver response corridors. Two methods are currently available for assessing the biofidelity of a dummy in side impact testing: 1) the ISO 9790 Biofidelity Classification System [4] and 2) the Biofidelity Ranking System developed by Rhule et al in 2002.

Although the ISO Biofidelity Classification System is well known and accepted within the biomechanics community, it contains several subjective features that limit its capability for impartial evaluation of the biofidelity of dummies that are to be considered for incorporation into Part 572. The ISO System utilizes

Table 3. ES-2re Certification Test R&R Analysis (ref. Docket # NHTSA-2004-18864-15).

Test/Criteria	Dummy S/N 070	Dummy S/N 071	Both
	CV (%)	CV (%)	CV (%)
Head Drop			
Peak Resultant Acceleration	1.1	1.6	5.4
Neck Flexion			
Flexion Angle	0.9	0.5	0.9
Time of Flexion Angle	2.3	2.7	2.4
A Angle	0.7	0.5	0.9
Time of A Angle	2.2	1.4	1.8
B Angle	0.7	0.5	0.9
Time of B Angle	1.6	2.6	2.5
Shoulder Impact			
Impactor Acceleration	2.7	9.3	6.9
Thorax – Rib Impacts			
Upper Rib Def. - 815 mm Drop Height	1.5	3.9	3.1
Middle Rib Def. - 815 mm Drop Height	0.3	0.3	0.3
Lower Rib Def. - 815 mm Drop Height	0.4	0.0	0.5
Abdomen Impact			
Maximum Impactor Force	2.1	2.0	1.9
Time of Max. Impactor Force	0.7	1.2	1.1
Maximum Abdomen Force	6.9	3.8	6.4
Time of Max. Abdomen Force	1.7	1.0	1.6
Lumbar Spine Flexion			
Flexion Angle	0.8	1.4	1.1
Time of Flexion Angle	1.7	1.9	1.7
A Angle	0.9	1.5	1.5
Time of A Angle	1.4	2.3	1.8
B Angle	0.3	1.3	0.9
Time of B Angle	1.8	.7	1.3
Pelvis Impact			
Maximum Impactor Force	3.5	1.3	2.8
Time of Max. Impactor Force	3.1	4.4	3.6
Max. Pubic Symphysis Force	4.0	1.1	3.1
Time of Max. Pubic Symphysis Force	3.4	4.6	4.2

assigned weights for the response measurements, test conditions and body regions. The weights were determined by averaging results of a poll of the ISO members. Since the responses of the poll may or may not be in line with the philosophies of the NHTSA, and since all body regions must pass their individual injury criteria in an FMVSS test, all body regions should be equally weighted when assessing dummy biofidelity. Moreover, the dummy responses are subjectively assigned a numeric value based on the qualitative assessment of the data fit within the cadaver corridors.

As the Biofidelity Ranking System [5] quantifies the biofidelity of a dummy in an objective manner, it was used by NHTSA to evaluate recent dummy biofidelity. The Biofidelity Ranking System is comprised of multiple tests of various types that have associated human response corridors. Each test is assigned a test condition weight in an objective manner that gives the highest weights to those tests that are most representative of the intended dummy test environment and that have response corridors developed from a large number of human subjects. For each measurement of each test, the dummy and human responses are compared over time and their differences quantified, where a lower number indicates better response similarity between the dummy and human. External and Internal biofidelity ranks, which are both deemed equally important for a dummy to possess, are computed to assess the overall biofidelity of a dummy.

As an example, the ES-2re dummy biofidelity was evaluated and found to be relatively good when compared to the SID-HIII, which is currently in Part 572. Tables 4 and 5 show the External and Internal Biofidelity ranks, respectively, for the ES-2re and SID-HIII.

Table 4.
External Biofidelity Ranks for the ES-2re and SID-HIII.
(ref. Docket NHTSA-2004-18865-8)

EXTERNAL BIOFIDELITY	ES-2re	SID-HIII
Overall Rank	2.6	3.8
Head/Neck Rank	3.7	1.0
Shoulder Rank	1.4	5.1
Thorax Rank	2.9	6.1
Abdomen Rank	2.6	3.0
Pelvis Rank	2.7	3.8
	re - rib extensions	

Table 5. Internal Biofidelity Ranks for the ES-2re and SID-HIII. (ref. Docket NHTSA-2004-18865-8)

INTERNAL BIOFIDELITY	ES-2re	SID-HIII
Overall Rank with abdomen	n/a	n/a
Overall Rank without abdomen	1.6	1.9
Head Rank	1.0	1.1
Thorax Rank	1.9 ¹	2.2 ²
Abdomen Rank	n/a	n/a
Pelvis Rank	2.0 ³	2.5 ³
n/a - not applicable (No human subject internal force data for comparison with the ES-2re; SID-HIII dummy does not make a measurement in the abdomen.)		
re - rib extensions		
1. Upper & lower thorax rib deflections & T-12 lateral acceleration		
2. TTI		
3. Pelvis lateral acceleration		

The biofidelity requirement is satisfied in lab and sled testing as shown in Figure 9.

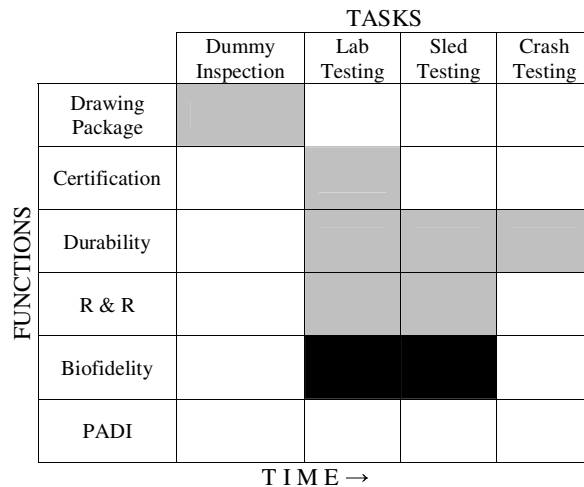


Figure 9. The lab and sled testing satisfy the biofidelity requirement.

PROCEDURES FOR ASSEMBLY, DISASSEMBLY AND INSPECTION

When a dummy is federalized it is necessary to document how the dummy is assembled, disassembled and inspected so that contractors who perform the FMVSS tests can put the dummy and its instrumentation together appropriately. This document, referred to as the Procedures for Assembly, Disassembly and Inspection, or PADI, is

incorporated by reference into Part 572. The PADI serves as a manual that illustrates how the dummy is put together and taken apart, as well as where and how the instrumentation is installed, and where to route the sensor cables within the dummy. It also includes procedures for inspection to aid in determining if certain parts are worn or damaged and need to be replaced.

Procedures for measuring external dimensions, segment weights and sensor output polarity for the dummy and free air resonant frequency and mass moment of inertia of the certification probes are also integral parts of the PADI.

If the dummy appears to be a reasonable tool for use in FMVSS and NCAP testing with regard to durability, biofidelity, repeatability and reproducibility, the documentation of the PADI becomes necessary. Since project engineers and technicians become expert at assembling and disassembling the dummy as the dummy evaluation progresses, it makes sense to document the procedures for assembly, disassembly and inspection after most of the evaluation is complete.

The PADI is organized into sections for each body segment: head, neck upper torso, lower torso, arms, legs and feet. Each section contains procedures for removal of the segment from the dummy, disassembly, inspection, assembly and attachment to the dummy. Exploded views of the body segment with its individual parts identified help to illustrate its construction. A table in each section identifies the parts of the body segment, with part number and title that match those of the Drawing Package. The dummy is disassembled from the head down in a piecewise fashion, with instructions, figures, and photographs shown to illustrate each step of the disassembly. Specific instructions on inspection of parts for wear and replacement are included, as well as procedures for assembling the segment and attaching it to the dummy.

Once the disassembly, inspection and assembly sections are complete, then the instrumentation installation and sensor cable routing sections of the PADI are written. These sections are also separated by body segment with photographs to illustrate specific steps to be taken.

Experience obtained during all phases of the evaluation process - inspection, lab testing, sled testing and crash testing - contributes to the development of the PADI (Figure 10).

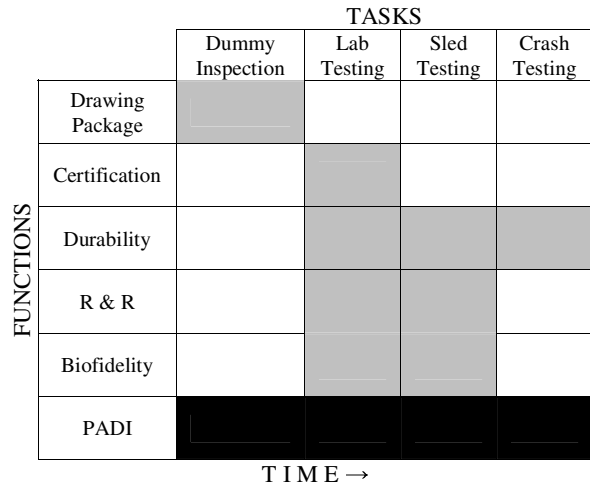


Figure 10. The experience gained in all phases of the evaluation process contributes to the PADI.

SUMMARY

A dummy that is a candidate for incorporation into part 572 49 CFR for potential use in a FMVSS performance standard must undergo a rigorous evaluation process: this process is often referred to as the Federalization process. This process is a standardized set of inspections and tests that result in quantified measures and corresponding documentation of the dummy's assembly and disassembly, drawing package, certification test procedures, durability, repeatability, reproducibility and biofidelity. Although no two dummy designs are identical and; therefore, no two dummy evaluation processes are identical, the skeleton of the process and the expectation for performance of the dummy remain constant.

It is important to recognize that a critical aspect of the evaluation process is the assessment of dummy suitability for the intended use. For example, a dummy designed for frontal impacts may not provide meaningful responses when tested in a side impact condition. This suitability evaluation is part of the entire process although it is not specified as an evaluation task. Further, it is important to be constantly aware of dummy behavior that is not suitable or human-like but may not be exposed in the scheduled testing. A recent example of this type of non-suitability was the lateral load path caused by the ES-2 back plate. This non human-like load did not become evident except after extensive crash testing with multiple vehicles.

Many new dummies are being developed by committee or consortium (HIII Ten year-old, SID IIs

and WorldSID) and it is important for those organizations to realize that the products of their extensive efforts must still undergo the rigorous Federalization process if the dummy is to be considered for use in the FMVSS. Further it is required that NHTSA possess, without restriction of any kind, an accurate and complete drawing package for the dummy for incorporation into part 572 by reference.

Similarly, vehicle manufacturers can be assured that a dummy that is incorporated into part 572 has been rigorously evaluated and is a dependable and reliable test tool that can be used in regulatory compliance testing (FMVSS), market incentive testing (NCAP) and will also be useful for research testing in other test configurations.

The details of the Federalization process outlined here will be continually updated as new techniques are developed and new biomechanical data becomes available. Examples of this are the Bio Rank approach [5] recently developed to quantify the assessment of biofidelity and the ongoing development of R&R procedures that are time history based rather than maximum value based. Nonetheless, the essential framework of Federalization will remain and the need to rigorously evaluate a dummy before it is used in testing will remain.

REFERENCES

- [1] Highway Safety Act of 1966, Public Law 89-564
- [2] Chrysler Corporation v. Department of Transportation, 472 F.2d 650 (1972), pg 659-693; United States Court of Appeals, Sixth Circuit, December 5, 1972.
- [3] Anthropomorphic Test Device for Dynamic Testing SAE J963, SAE Recommended Practice, Society of Automotive Engineers, June 1968.
- [4] International Standards Organization, "Technical Report 9790: Road Vehicles – Anthropomorphic Side Impact Dummy – Lateral Impact Response Requirements to Assess the Biofidelity of the Dummy," American National Standards Institute, New York, NY, 1999.
- [5] Rhule, H., Brunner, J., Bolte, J., Donnelly, B., Maltese, M., Eppinger, R., "Development of a New Biofidelity Ranking System for Anthropomorphic Test Devices," Stapp Car Crash Journal, Vol. 46 2002.

FIRST RESULTS FROM THE JAMA HUMAN BODY MODEL PROJECT

Tomiji Sugimoto

Japan Automobile Manufacturers Association, Inc.

Kunio Yamazaki

Japan Automobile Research Institute

Japan

Paper Number 05-0291

ABSTRACT

The number of fatalities from automotive traffic accidents in Japan is on a downward trend. However, the number of injuries is tending to increase. Consequently, there is a need for further safety measures to reduce the number of casualties. In order to achieve progress on vehicle safety measures, it is essential to develop human body models for use as tools to quantify injury parameters. The crash test dummies and impactors in common use, however, require consideration of durability and reusability. This gives rise to structural differences from the human body, and makes it difficult to evaluate any but preexisting injury parameters. Recent years, therefore, have seen the use of simulated models of the human body generated by computer. These models take advantage of the ability to model the structure of the human body and mechanical properties in minute detail, and are applied to explain the injury mechanisms and to evaluate vehicle collision safety. Joint cooperative projects have been initiated by automobile manufacturers, related research institutes, and other such organizations, particularly in the United States and Europe, bringing advances in development of models that more closely resemble the human body. Given these circumstances, the Japan Automobile Manufacturers Association, Inc. (JAMA) has initiated activities for development and research of computer-modeled human bodies in impact biomechanics, which can analyze pedestrian and occupant injury, through a system of cooperation between industry and academia for 3 years. This report introduces the substance of those activities, their status, and some initial results.

INTRODUCTION

The number of fatalities in automotive traffic accidents has, in the past few years, shown a decreasing trend, thanks in part to automotive safety technology. On the other hand, there has been an

increasing trend in the number of people injured, with more than a million people injured annually (Figure 1). Accordingly, further safety improvements are required, to reduce the number of fatalities and the number of people injured.

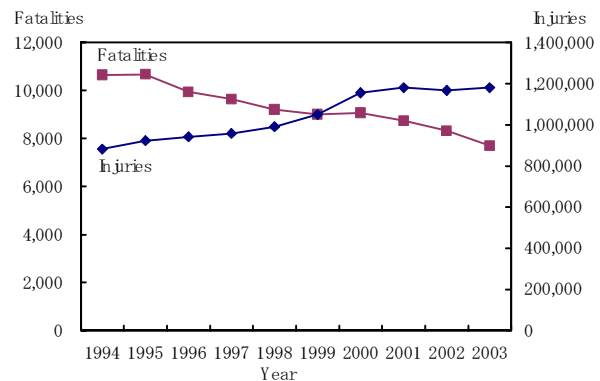


Figure 1 Trend of traffic accident fatalities and injuries in Japan

In order to make progress with safety improvements on the vehicle, research is being carried out into human body response to impact, to determine the mechanisms causing human body injury, and its limits. At the same time, in order to predict injuries to the human body, particularly during impact, and to prevent these injuries, it is necessary to estimate the effectiveness of safety devices and so on. As a tool to this end, development of a human body model is essential. For the human body model, volunteers or post-mortem human subjects (PMHS) could be considered, but generally, a human body simulation device (a crash test dummy that simulates the whole human body and impactor that simulates part of the human body) is used most frequently. However, the crash test dummy and impactor are structurally different from the human body because they must be equipped with devices to measure impact response and must be given to ease of use (durability, repetitive performance, etc.), so one concern has been the difficulty of evaluation outside of existing injury

parameters.

On the other hand, in recent years there has been a focus on human body simulation models using computers, as tools that push the boundaries of existing technology, to bring new possibilities. Human body simulation models utilize features that make possible detailed modeling of both the human body structure and mechanical properties. These models can be used in analysis of injury mechanisms, and in evaluation of vehicle crash safety (Figure 2). Concerning human body simulation models, conventionally modeling was carried out for each body regions being researched, but recently, development has been carried out for full-body models such as Total Human Model for Safety (THUMS, Toyota Central R&D Labs., Inc. and Toyota Motor Corporation)^[1] and H-Model (ESI)^[2]. In addition, cooperative projects have begun in the USA (Human Body Modeling Partnership) and in Europe (HUMOS: Human Model for Safety)^{[3][4]} between multiple automotive manufacturers and related research organizations, etc. These have led to the development of models that are closer to actual human bodies. This focus is on effective human body model research.

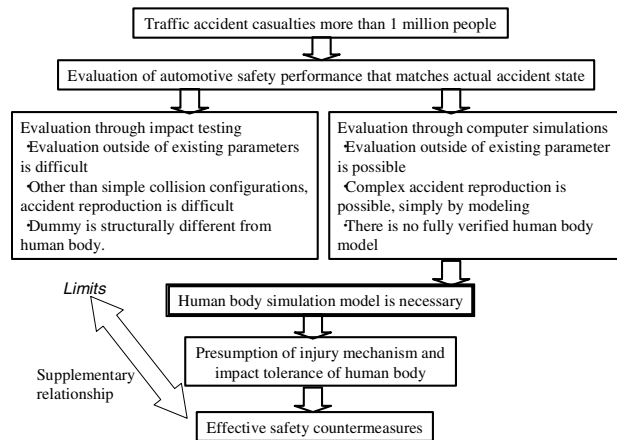


Figure 2. Necessity of human body model

Against this background, the Japan Automobile Manufacturers Association, Inc. (JAMA) has begun industry-wide activities aiming to improve research capabilities through technological interactions among automotive manufacturers and with academia, concerning human body computer model development (which has conventionally been carried out by individual automotive manufacturers) and research for this development (impact biomechanics research). This paper introduces the background of these activities, and their content.

FLOW OF AUTOMOBILE COLLISION SAFETY

DEVELOPMENT OF SAFETY IMPROVEMENTS

When adopting automotive collision safety improvements (test methods and protective devices), generally research in the flow shown in Figure 3 is necessary.

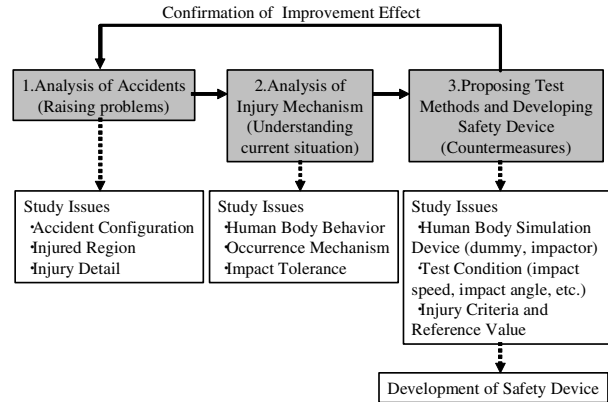


Figure 3 Flow chart of research of safety improvements

The first phase, “Analysis of Accidents”, is generally understood as the phase where problems are raised. From analysis of individual accidents and the results of statistical evaluation of accidents, the problematic accident configuration (vehicle collision direction, collision speed, passenger restraint conditions, etc.), injured body region, detail of injuries, etc. are understood, and if possible, cause analysis is carried out, to predict the items coming into contact with the human body.

The next phase, “Analysis of Injury Mechanism”, is the phase for understanding the phenomena themselves. In this phase, concerning the problems identified in the accident analysis phase, accident reconstruction, that is to say, vehicle and human body behavior assumptions are made, and impact conditions and impact load relating to the human body are predicted. Furthermore, from tests, etc., under impact conditions close to actual accident conditions and using the human body model, the injury occurrence mechanisms and human body impact tolerance are learned. At this time, depending on the type of human body model, it is not necessarily true that the impact conditions are equivalent to that of actual accidents without doubt. For example, in the case of actual tests using volunteers, it is necessary to estimate human body response that approximate actual accidents from data on impact conditions lower than those of actual accidents.

The phase “Proposing Test Methods and Developing Safety Devices” is the improvement phase. In this phase, the administrative side prepares test methods, and in the form of regulations or standards,

uniform safety improvements is determined for the product (automobiles). On the industry side vehicle design changes are made to meet the regulations and standards, and protective devices are developed according to in-house standards, leading to the development of a safer vehicle. In any case, test methods are necessary to evaluate safety performance, and for these tests, development of dummies or impactors, setting of test conditions (test vehicle or impactor collision speed and collision angle, etc.), and the selection of physical parameters for evaluation of injury and the injury reference values (impact tolerance) are all necessary.

When the improvement phase is complete, that series of research is complete, but confirmation of improvement effectiveness is necessary as continued work. This means a return to accident analysis, and the improvement is seen to be effective, then that issue is finished and identification of other problems is carried out. However, if the initially expected effect of the improvement is not sufficiently realized, once again it becomes necessary to understand the current situation and search for further improvements.

NECESSITY FOR HUMAN BODY COMPUTER MODEL

With the human body computer model, development of bones, internal organs, and outer skin, etc., has just begun, so it is not yet perfected. However, because it has the feature of being able to make detailed models of the human body structurally and of its mechanical properties, it is expected that it will be frequently used in the collision safety improvement flow outlined above. The following shows the items in which it is thought this model can be used.

Accident Reconstruction

At present, accident reconstruction is generally through impact tests using crash test dummies and actual vehicles. However, there are the problems that it is difficult to set test conditions for accidents where there are many vehicle behaviors, and that there are limits to the areas of the crash test dummy that can be measured, and to physical properties. Therefore, these issues can be resolved by utilizing the human body computer model and the vehicle model as a set. Although there are many problems in modeling the vehicle and human body, it can reproduce human body injuries and can help analyze vehicle body and human body collision reaction forces, so it is an important tool in accident analysis.

Analysis of Injury Mechanism and Impact

Resistance

Tests concerning this item generally use volunteers and PMHS. However, problems include the fact that there are limits to the physical properties that can be measured in these tests, and the fact that differences in properties due to individual physical differences (variations in shape and strength, changes in characteristics due to age, the presence of disease or illness, storage conditions, etc.) must be considered. Considering the physical properties that can be measured, the human body computer model is more effective in determining physical properties directly connected to human body tissue damage. In addition, because the model was built based on fundamental standard values, the problematic effect in the tests of individual physical differences is eliminated. On the other hand, it is possible to change, depending on the purpose of the test, the computer model's age or physique, and to analyze differences in impact resistance between the changed model and the standard model.

Crash Test Dummy and Impactor Development

When developing a crash test dummy or impactor that simulates specific parts of the human body, the problem is the biofidelity to the human body in the conditions used. In many cases, to confirm biofidelity, test data (drop test, impactor test, etc.) is used from tests implemented under simple impact conditions, to make a comparison for each human body part with volunteers or PMHS. However, if the human body computer model is used, it is possible to estimate human body response under a variety of condition, and it is possible to confirm dummy and impactor biofidelity with a wider variety of evaluation parameters.

Setting Injury Criteria

As for parameters to evaluate injury, the physical properties measured in tests using volunteers and PMHS, and the physical properties created using statistical models based on that data, are often used. However, parameters that are thought to be difficult to measure and have a low level of effect are often eliminated. With the human body computer model, it is possible to study many physical properties, and it is expected that it will be possible to select more appropriate injury evaluation parameters.

Confirming the Effectiveness of Safety Devices

When automotive manufacturers have implemented vehicle safety improvements and developed new safety devices, conventionally, evaluation is made from tests using crash test dummies and impactors simulating part of the human body. With crash test dummies, there is the problem of limits

to the areas and physical properties that can be measured. With the human body computer model, many physical properties can be measured, so it is possible to evaluate the effect on the human body in many aspects.

JAPAN AUTOMOBILE MANUFACTURERS ASSOCIATION, INC. (JAMA) ACTIVITIES

In the Japanese automotive industry, development of a human body computer model has been mainly carried out by individual automotive manufacturers. Research by JAMA has been carried out together with JARI (Figure 4), and the focus has been improving parts of the existing model, based on human body data.

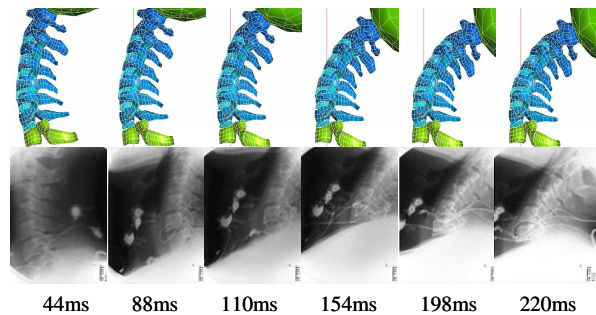


Figure 4 Simulation of cervical spine motion at rear-end impact (JAMA/JARI study)

In contrast, in the USA (Human Body Modeling Partnership) and in Europe (HUMOS), the joint research organizations (consortiums) have spanned automotive manufacturers, research organizations, and universities, etc., accelerating the development of the human body computer model.

Building on this situation, JAMA, too, has studied the promotion of a joint research organization involving automotive manufacturers, JARI, and universities, in order to strengthen human body model development.

Figure 5 is an outline of that concept. The aim is cooperation with research organizations related to the automotive industry and with universities, to implement research concerning human body characteristics and injury criteria and to build a human body computer model that can be used in automobile safety design. The plan is for an organization where research is carried out with the automotive manufacturers, JARI, and universities, etc., each having their own responsibilities for individual and joint research. Among the research items, there are some where cooperation is essential – for example, content such as human body characteristics that cannot be implemented without the cooperation of a medical university, content such as human body model

mechanism and function theory construction which requires the cooperation of an engineering university, or content requiring vehicle shape data for analysis using vehicle computer models which must be carried out by automotive manufacturers, etc. In addition, research organizations, such as JARI, are necessary, to carry out engineering analysis of medical data, or to assist in the development of the human body computer model. Moreover, there is a plan to enlist the help of software manufacturers who have the know-how concerning computer models to help with some of the work, when necessary.

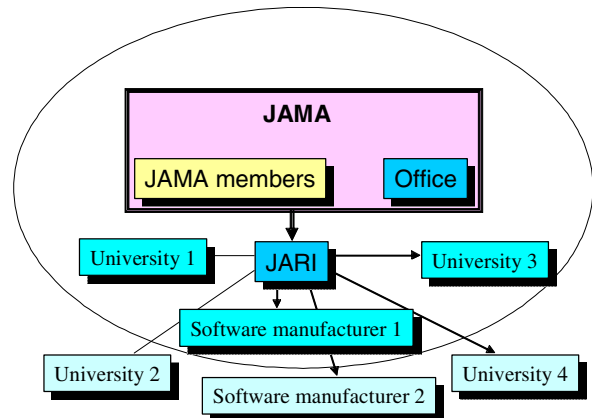


Figure 5 Outline of a joint research on human body modeling

As for the research schedule, we are starting in fiscal year 2004, and plan is to complete a human body computer model that can be used in pedestrian and passenger analysis within the next three years. In Japan, human body computer models such as THUMS and the pedestrian model based on the H-model^[5] already exist (Figure 6). This year, from the point of view of utilization of existing models, a pedestrian and passenger basic model (AM50 equivalent) that integrates the existing models will be developed. In the following two years, it is planned that the model will be modified based on the latest knowledge, and posture changing technology and scaling technology will be created. Through more rapid development of a human body computer model, it will be possible to undertake early initiatives to reduce the number of casualties in automotive traffic accidents in Japan, and at the same time, Japan will play a leading role in contributing to safety improvements around the world.

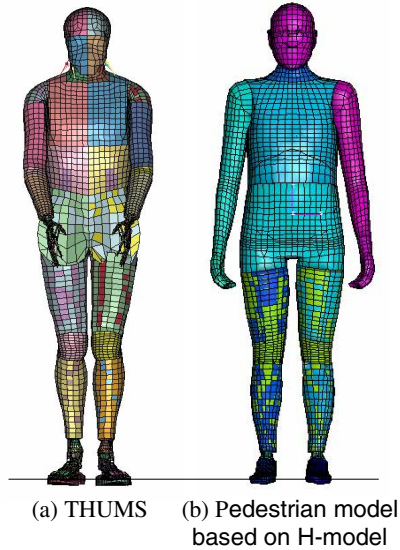


Figure 6 Existing human body models in Japan

The development of a human body computer model is also being tackled overseas, and JAMA would like to cooperate in those research organizations, too. However, from the point of view of taking safety improvements that match the situation in Japan, and of enhancing Japan's research base by contributing to the education of Japanese researchers, it is necessary to proceed with independent Japanese research activities.

STATUS OF DEVELOPMENT OF JAMA HUMAN BODY MODEL

JAMA has a plan to develop basic models for the pedestrian and passenger through the first half of 2005. These models will correspond to two kinds of solver (LS-DYNA and PAM-CRASH) respectively.

Development has almost been completed for the LS-DYNA version of a basic pedestrian model (Figure 7 and Figure 8). The basic pedestrian model has been developed based on both the THUMS and the pedestrian model based on the H-model. Concretely, the feature of each model was made the best use of, the THUMS was used for the upper half of the body, and the pedestrian model based on the H-model was used chiefly for the lower half of the body. The basic pedestrian model consists of 90,995 elements and 71,136 nodes, and the physique is near the AM50.

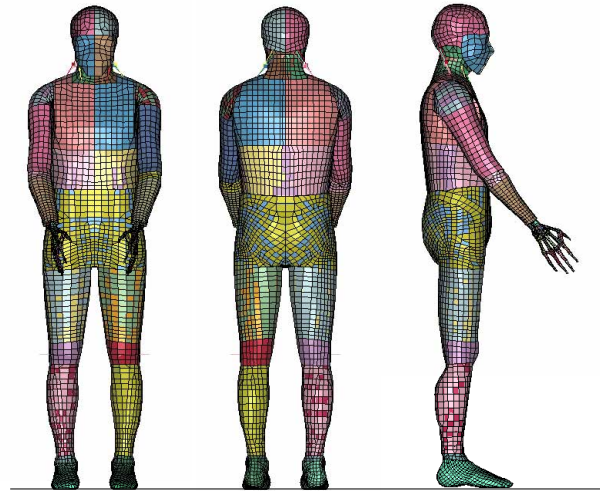


Figure 7 JAMA pedestrian model (externals)

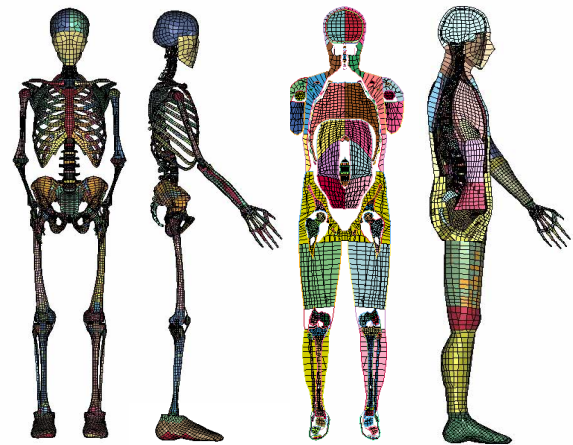


Figure 8 JAMA pedestrian model (internals)

The basic pedestrian model for PAM-CRASH will be developed by converting the model data of the LS-DYNA version. We will establish the conversion technology by accumulating experience and technology though it is difficult to convert the model for a different solver. The basic passenger model will be developed by changing the posture of the basic pedestrian model.

Basic models for the pedestrian and passenger will be improved based on the result of volunteer and PMHS tests during the next two years.

TRENDS IN OVERSEAS RESEARCH

As noted earlier, human body computer model research is being carried out in the USA and Europe, involving joint research organizations. The following is a brief explanation of their recent activities and situation.

In the USA, the Human Body Modeling Partnership began, with automotive manufacturers taking the initiative. The emphasis is on consortium style activities involving automotive manufacturers and research organizations, etc. including those outside the US. The aims are to modify injury evaluation parameters and criteria through the development of a human body computer model, and to expand accident reproduction research. In addition, through consortium type activities, it is expected that redundancy or incompatibility will be eliminated, development of the model will be accelerated, and costs will be reduced. Although full-scale activities will begin next year, in the first five years adult models of three physiques for both men and women (small frame, standard and large frame) will be created.

In contrast, in Europe, the consortium called HUMOS is already active. Participating members include five European automotive manufacturers, three software manufacturers, and seven research organizations or universities. Their goals and aims are basically the same as the Human Body Modeling Partnership noted above. Their research schedule is divided into phase 1 (HUMOS 1) and phase 2 (HUMOS 2). In phase 1, they were developing a passenger model of a European adult male 50th percentile size. This activity is complete. At present, phase 2 activities are being carried out, and with a target of the autumn of 2005, they are hurrying to build a model lineup of three models – a 5th percentile female, a 50th percentile male, and a 95th percentile male.

THE DIRECTIONS OF HUMAN BODY COMPUTER MODELS

Finally, the following is a discussion of the future directions for the human body computer model.

Detailed Modeling

The first human body computer models were based on multi-body dynamics. At that time, the aim was mainly analysis of the motion of human bodies during collisions. Later, for injury evaluation, it became necessary to have detailed modeling of each human body area, and so human body computer models were most often based on the finite element method (FEM). Models according to FEM were, at first, most often detailed models of the skeleton only. However, at present, there are also examples of modeling of internal organs or blood vessels. In the future, other human body systems (muscles, nerves, etc.) will also be modeled in detail.

Diversification of Injury Detail

In recent automotive accidents in Japan, there has been a reduction in the number of fatalities, with 8,000 people in 2003. In contrast, the number of people injured exceeded one million people in 1999, and has continued to grow since then with almost 1.2 million people the past few years.

Knowing this, vehicle safety improvements that have conventionally placed emphasis on reducing fatalities, have recently also begun to tackle reducing the number of people injured. For example, in the case of Japan, in safety standards that have existed for some time, the evaluation index was based on injury criteria in areas of the human body that cause death. However, in automotive assessment that aims at technology innovations that give better safety performance, the evaluation area extends into areas of the human body that have very little chance of causing death.

Accordingly, it seems that in the future research will focus on things other than large injuries causing grave damage such as death or severe injury. This means that detailed modeling of areas that have been omitted in the past will become important.

Improvements for the Elderly

In Japan, the number of deaths of elderly people is fewer over the past few years, but looked at as a portion of the whole, it is a rising trend. In 2003, there were 3,109 fatalities (of people 65 years old or older), and this accounted for approximately 40% of the total fatalities, including juveniles. In addition, in the case of the elderly in comparison with young people, it was learned that their rate of fatality is high, and when they are passengers in the vehicle cabin, they are more easily injured in the chest, etc. However there is not sufficient understanding of the causes of these phenomena. In Japan, the population of elderly people is rising dramatically, and in the future, there will even greater demand for research into collision safety for the elderly.

Enhancement of Surrounding Technology

With the latest human body computer model, each area of the human body is modeled in some detail, and even joint modeling, which traditionally had mathematical joint mechanisms, is now closer to actual human beings. Through this type of detailed modeling, position changing, which wasn't a problem with the first human body computer models, has become more difficult with recent models. Position changing technology is becoming increasingly important in actual analysis.

Furthermore, when evaluating vehicle safety, it is becoming necessary to ensure safety performance for passengers of a variety of physical types, other than the standard physique. When analyzing accident

reproductions, too, there is a requirement for technology that can freely change the physical type. Therefore, in the future, body frame scaling technology must be developed.

pp.119-125

CONCLUSIONS

In automotive safety performance research, vehicle and part impact tests are carried out using crash test dummies and impactors that simulate areas of the human body, and evaluations made of the safety performance, as to whether or not it meets human impact tolerance (injury criteria) as determined from tests using volunteers and PMHS. Impact biomechanics research, which is the foundation in determining these injury criteria, has mainly been implemented in Europe and the USA, with little contribution from Japan. However, in the future through the development of human body models, at the same time as comprehensively and systematically incorporating impact biomechanics research, a Japanese research system will be enhanced following the consortium organization system, raising the level of Japan's contribution, and creating an environment where comprehensive injury reduction improvements that match the Japanese situation will be tackled.

REFERENCES

- [1] Instruction Summary of Total Human Model for Safety (THUMS), Toyota Central R&D Labs, Inc.
- [2] H-Model Overview Description, ESI Group
- [3] Praxl, N. et al.: Simulation of Occupant Kinematics in Vehicle Rollover - Dummy Model Versus Human Model, Proceedings 18th International Technical Conference on the Enhanced Safety Vehicle, Paper Number 202
- [4] Robin, S.: HUMOS: Human Model for Safety – A Joint Effort towards the Development of Refined Human-like Car Occupant Models, Proceedings 17th International Technical Conference on the Enhanced Safety Vehicle, Paper Number 297
- [5] Dokko, Y.: Validation of the Human Head FE Model Against Pedestrian Accident and its Tentative Application to the Examination of the Existing Tolerance Curve, Proceedings 18th International Technical Conference on the Enhanced Safety Vehicle, Paper Number 322
- [6] Nishimoto, T.: The Current Situation surrounding Impact Biomechanics Research and JARI Initiatives, The Japan Society of Mechanical Engineers, M&M 2003 Materials and Mechanics Division Conference, OS-8
- [7] Ono, K.: Biomechanics for Occupant Protection Research, JARI Research Journal, Vol.26, No.3,

DUMMY TORSO RESPONSE TO ANTERIOR QUASI-STATIC LOADING

Greg Shaw
David Lessley
Rich Kent
Jeff Crandall

University of Virginia
Center for Applied Biomechanics
United States

Paper Number 05-0371

ABSTRACT

This study reviews the design targets that have determined the response of the frontal impact dummy torso to anterior loading. Test results are presented that include response to quasi-static loading of the anterior ribcage for NHTSA's THOR Alpha dummy. Sites on the anterior thorax of the THOR Alpha and Hybrid III frontal crash dummies were deflected 25.4 mm by a rigid rectangular indenter at six locations while external deflection measurements were taken at nine measurement locations. These tests were conducted to evaluate chest coupling, the degree to which locations away from the loading site are deflected for a given amount of loading site deflection, and regional stiffness of THOR Alpha relative to cadaver subjects tested in a prior study. THOR Alpha was found to be less coupled than the Hybrid III and generally more cadaver-like. THOR Alpha was found to be stiffer than the cadavers and the ratio of upper lateral to lower lateral ribcage stiffness was nearly twice that of the cadavers, a characteristic that may affect response to loading by occupant restraint belts. High torso stiffness under low rate loading reflects an historical priority for biofidelic response in the hub impact loading environment and the limited range over which the present ribcage construction can produce a biofidelic response. However, ribcage stiffness is one of several factors that determine the response of the human torso. A comprehensive understanding of human torso response to loading conditions such as those produced by contemporary and anticipated occupant restraint systems is required to advance the utility of the dummy torso as an injury prediction tool in priority crash conditions.

INTRODUCTION

Injuries to the thorax comprise 29 percent of all serious to fatal (AIS 3-6) injuries sustained by people involved in a crash (Ruan et al. 2003). Strategies to reduce thoracic injuries include the development of improved restraint systems, an effort that is facilitated

by a frontal impact dummy that responds in a biofidelic manner to loading of the anterior thorax.

This study reports the results of tests designed to assess the THOR Alpha dummy response to quasi-static loading of the anterior ribcage. THOR (Test device for Human Occupant Restraint), NHTSA's advanced frontal impact dummy, has demonstrated enhanced biofidelity relative to the Hybrid III, the frontal impact dummy currently used for vehicle compliance testing (Shaw et al 2000). The results are discussed relative to results from similar tests conducted on THOR's predecessor, the Prototype 50M, the Hybrid III, and cadaver subjects (Schneider et al 1992 a).

BACKGROUND

Biofidelic response to thoracic loading has long been an important performance criterion for frontal impact dummies. The response of current dummies has been optimized for a limited range of conditions due to technical limitations.

The thoracic loading response criteria for the Hybrid III dummy designed in the mid 1970s reflected the need for accurate evaluation of crash conditions involving anterior chest impact with the steering wheel hub (Foster et al 1977). Such impacts, unmitigated by energy absorbing steering columns and torso restraints, often caused life-threatening injuries (Voigt and Wilfert 1969).

The basis for the target crash dummy thoracic response to dynamic hub loading was provided by an extensive General Motors Research (GMR) effort that began in the mid 1960s (Kroell 1976). The effort included both sled tests and laboratory tests involving 48 cadavers. The laboratory impactor tests involved striking the seated subject's central sternum with a weighted, 152 mm diameter rigid flat disk similar in profile to a steering wheel hub. Chest deflection and impactor force were recorded (Kroell 1976) (Figure 1).

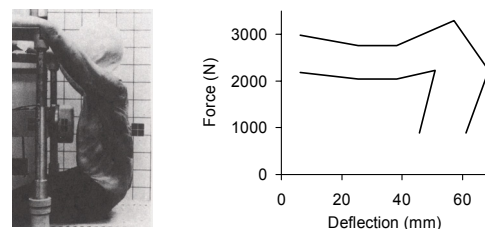
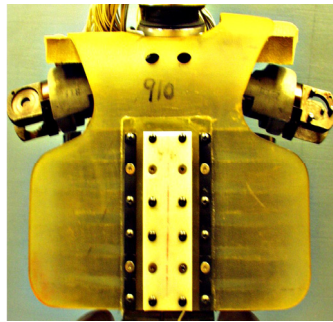
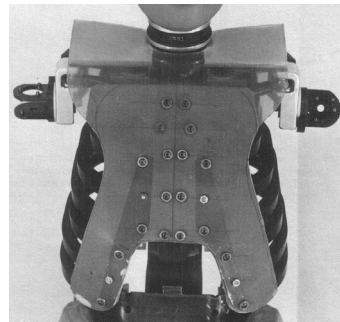


Figure 1. Kroell thoracic impact test condition and Kroell force – deflection response corridor for 4.3 m/s impacts.

The Hybrid III dummy thorax (Figures 2 and 3) was developed to match the force-deflection corridor based on the Kroell hub tests involving impactor



Hybrid III



Prototype 50M



THOR Alpha

Figure 2. Frontal impact dummy torsos. The 50M is shown without the upper abdomen.

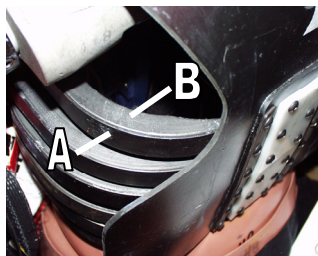


Figure 3. Hybrid III ribcage construction. Spring steel ribs (A) with visco-elastic damping material (B) to simulate the highly rate dependent response recorded for cadavers during Kroell hub impacts (Foster et al 1977). The damping material alone is insufficient to achieve the required stiffening under high-rate loading. Thus, increasing the elastic stiffness of the ribcage was required, which, however, compromises response at low loading rates, such as those generated by shoulder belts.

velocities of 4.3 and 6.7 m/s (Schneider et al 1989) (Foster et al 1977) (Figure 4). Biofidelic response under restraint loading was not a priority and the Hybrid III chest was found to be “considerably stiffer than that of the human” at lower loading rates and under quasi-static loading conditions (Schneider et al 1989).

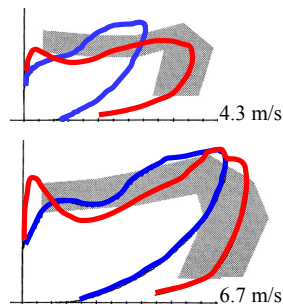


Figure 4. Kroell test responses relative to the 4.3 and 6.7 m/s Kroell force-deflection response corridors.

Red: 50M
Blue: Hybrid III

In the 1980s, increased restraint belt use required a reassessment of thoracic loading patterns (Kent et al 2001). In 1983, NHTSA began development of an improved frontal impact dummy, today known as THOR. The researchers, recognizing that belt and belt and air bag restraint systems could cause injuries especially to elderly occupants (Schneider et al 1989) (Schneider et al 1992 a), proposed that the new thorax be able to assess restraint loading in addition to hub loading:

The thorax/abdomen should be designed to provide humanlike response (i.e., biofidelity in response) and meaningful injury assessment for impact loading imposed by the following types of restraints and vehicle components:

1. Steering assembly (by unrestrained driver)
2. Instrument panel (by unrestrained passenger)
3. Shoulder/lap belt - i.e., three-point belt
4. Shoulder belt only - i.e., shoulder belt and knee bolster
5. Airbag
6. Belts plus airbag (Schneider et al 1989)

The priority of thoracic performance criteria seemed to evolve during the course of the NHTSA dummy development project. In a 1985 report, the priority loading conditions were listed in order of hub, shoulder belt, and air bag (Melvin 1988). In a 1992 report (Schneider et al 1992 a), the list was air bag, belt, and steering wheel loading. The 1992 report listed 4.3 m/s, quasi-static, and 6.7 m/s as priority loading conditions with 9 m/s as a secondary priority. The 4.3 and 6.7 m/s rates reflect Kroell hub impact velocities. The 9 m/s rate was considered typical of loading experienced by “out-of-position” occupants who are very close to the deploying air bag. In a report published in 1989, the researchers indicated that biofidelic performance under quasi-static loading may be the most important due to the increased use of restraint belts (Schneider et al 1989):

With the increased use of seat belts that has come about since the development of Hybrid III through state legislation; and the Federal requirement for passive restraint systems in all vehicles of the 1990s (i.e., FMVSS 208), it can be expected that higher loading rates will become less important and lower loading rates, resulting from

interaction with shoulder belts and airbags, will become increasingly important. For example, a preliminary analysis of chest loading rates to shoulder-belted cadavers and test dummies during 48-km/hr (30-mph) frontal impacts indicates that peak rates of chest deflection in the range of 1 to 4 m/s can be expected under these conditions. In the new thorax, designing to achieve humanlike biofidelity in response to low loading rates, and even quasi-static loading conditions, may be of equal or greater importance than designing to achieve biofidelity at higher loading rates. (Schneider et al 1989)

The Prototype 50M thorax (Figure 2), developed in the course of the University of Michigan Transportation Research Center (UMTRI) / NHTSA collaboration, defined the major design elements subsequently incorporated in the THOR dummy thorax. The response of this thorax was evaluated under the priority loading conditions described above. Results for the Kroell hub loading tests indicated that the 50M performed better than the Hybrid III dummy in the 4.3 m/s hub velocity test (Figure 4) (Schneider et al 1992 b). In acknowledgment of the increasing importance of lower velocity belt loading, a quasi-static anterior ribcage deflection test was conducted with an indenter that simulated a section of shoulder belt. The objective of this quasi-static test was to more fully characterize regional dummy thoracic response relative to the Hybrid III dummy and to cadavers, the best available live human surrogate. Achieving regional biofidelity was thought necessary to produce cadaver-like response to concentrated loading such as that from a shoulder belt (Schneider et al 1989). These tests, commonly known as the “Cavanaugh tests”, were supported by NHTSA, coordinated by UMTRI, and were conducted at Wayne State University Bioengineering Center and UMTRI (Figures 5 and 6) (Schneider et al 1989, Schneider et al 1992 a; Cavanaugh et al 1988). The tests were designed to measure coupling and regional torso stiffness. For these tests, coupling was defined as the relative deflection response of sites remote to the site that was deflected 25.4 mm downward by a gimbaled rectangular indenter.

The Prototype 50M performance in the Cavanaugh tests, while an improvement relative to the Hybrid III, was not as cadaver-like as it was in the Kroell tests. The Cavanaugh tests suggested that both the Prototype 50 M and the Hybrid III were much stiffer than the unembalmed cadavers. The 50M coupling relative to the cadavers’ was considered “generally good” (Schneider et al 1992 a).

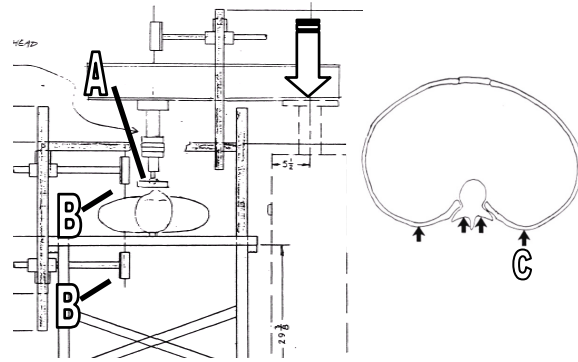


Figure 5. Cavanaugh test condition used for cadavers and Hybrid III dummy. Downward movement of a material test machine loading arm drives the gimbaled indenter (A) into the subject torso. Torso deflection is measured by uniaxial displacement sensors (B). Posterior measurements are possible when the torso is loaded centrally and no bilateral rib support (C) is used.

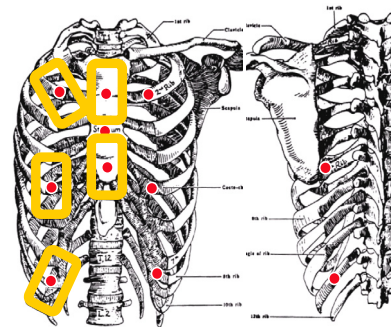


Figure 6. Cavanaugh loading sites (rectangles) and deflection measurement sites (red circles). Lateral sites were approximately 76 mm off the centerline at the level of the second, fifth, and eighth ribs.

The Prototype 50M, also known as TAD (Trauma Assessment Device), was followed by the development of the THOR dummy that began in 1994 (Rangarajan et al 1998). THOR Alpha was released by NHTSA in 2001. Although the THOR prototypes and THOR Alpha shared the basic thorax configuration of the 50M, the cross section of the THOR Alpha ribcage is more elliptical resulting in a smaller chest volume. In addition, minor changes were made to the shoulder to improve shoulder belt interaction (Xu et al 2000). In 2003 NHTSA directed UVA to conduct Cavanaugh tests on THOR Alpha in order to determine its performance relative to Cavanaugh cadaver subjects and, of secondary interest, its performance relative to the 50M and Hybrid III.

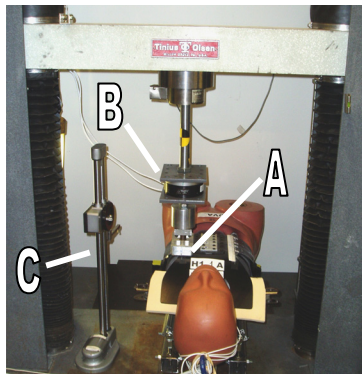
METHOD

The method for the tests reported in this study approximated the Cavanaugh tests of the Hybrid III and cadavers conducted at Wayne State University. A Tinius Olsen material testing machine was used to provide the anterior-posterior compression using the same “2 inch by 4 inch” (50.8 mm x 101.6 mm) indenter that was used for prior testing. The contact area of the indenter was intended to simulate a section of a shoulder belt.

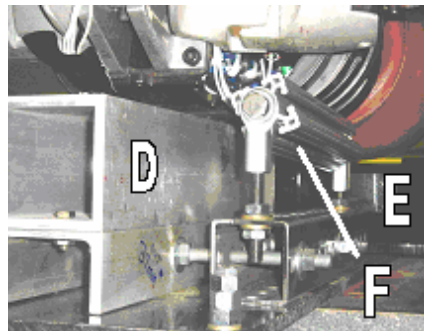
Tests began with the dummy supine under the indenter. All tests were performed with the torso

jacket (skin) removed, consistent with the procedure used in the Cavanaugh tests in which the dummy jacket was removed and the anterior skin and underlying soft tissue were removed from the cadaver torso. The subject was positioned so that the center of the indenter face coincided with one of the loading sites on the anterior ribcage. All six sites were loaded when the subject’s spine and ribs were supported (baseline condition). The three midline sites were loaded when only subject’s spine was supported.

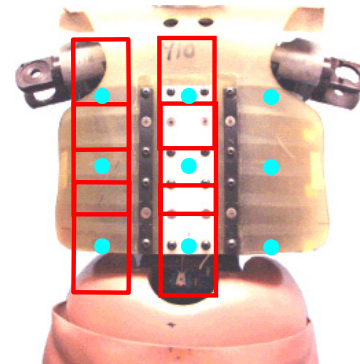
Figures 7 and 8 illustrate the test conditions for the Hybrid III and THOR dummies.



Hybrid III dummy under indenter (A) mounted to Tinius Olsen materials test machine. B – load cell, C – digital height gage

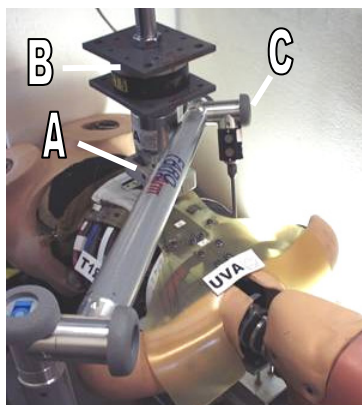


Posterior view looking from below dummy. D – Spine block, E – Pelvic block, F – Rib support (removable).

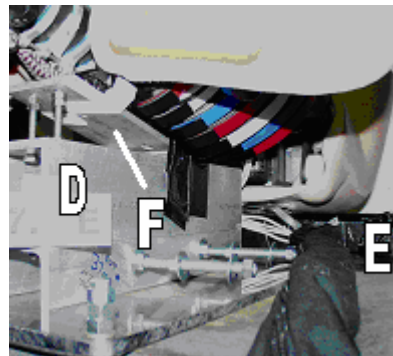


Loading sites (red rectangles) and measurement sites (blue dots).

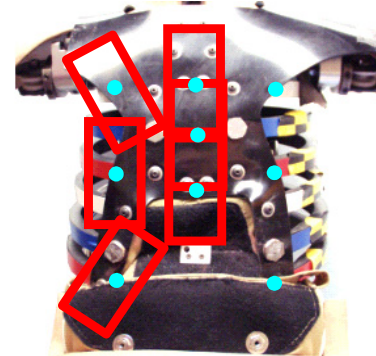
Figure 7. Hybrid III test conditions, hardware, and loading and measurement sites.



THOR dummy under indenter (A) mounted to Tinius Olsen materials test machine. B – Load cell, C – Faro Arm triaxial measurement tool.



Posterior view looking from below dummy. D – Spine block, E – Pelvic block, F – Upper spine support. Rib support not in place.



Loading sites (red rectangles) and measurement sites (blue dots). Three posterior sites mirrored the anterior lateral sites.

Figure 8. THOR test conditions, hardware, and loading and measurement sites.

Once the subject was positioned under the indenter, the indenter was lowered to contact the subject until the load cell recorded 25 ± 3 N. From the point of initial contact to the target preload value, the indenter face aligned itself with the local contours of the ribcage. This alignment was made possible by a ball joint above the indenter face. With the indenter in the pre-load position, the Tinius Olsen control software began the loading stroke at 102 mm/min and stopped at 25.4 mm.

Peak load was recorded when the indenter stopped. The indenter was held in the loaded position to allow deflection measurements to be taken at sites not obscured by the indenter using either a height gage (Hybrid III) (Figure 7) or triaxial displacement transducer* (THOR) (*Faro Arm ® Model B08-02 Rev. 07. Faro 125 Technology Park Lake Mary FL 32746-6204) (Figure 8). Both instruments were capable of accurate x-axis deflection measurement and trial tests indicated that x-axis deflection measured by the Faro Arm varied less than 0.3 mm from those measured by the height gage.

After measurements were recorded, the site was unloaded. A minimum time of thirty minutes was allowed between loading cycles to allow for sufficient recovery of the visco-elastic ribs.

RESULTS

Replicate tests on the Hybrid III suggested that test-to-test variation of deflection measurements was less than 1.3 mm (5 percent of the 25.4 mm indenter stroke). Variation in indenter force measurement was less than 5 percent (65 N).

Figure 9 shows the deformation of THOR's anterior ribcage in response to the 25.4 mm of indenter deflection at the six loading sites. In comparison to the Hybrid III, THOR Alpha was more cadaver-like in terms of both coupling and peak indenter load values. Results for the baseline tests in which both the spine and ribs were supported are presented in Figures 10 and 11 (coupling) and Figure 12 (indenter load).

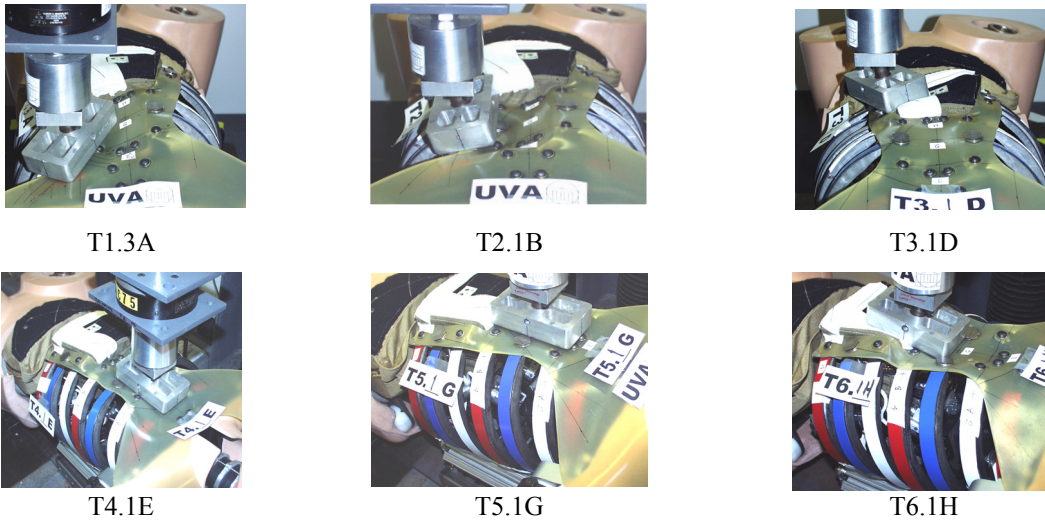


Figure 9. THOR's anterior ribcage deformation in response to 25.4 mm of indenter deflection for the six baseline tests.

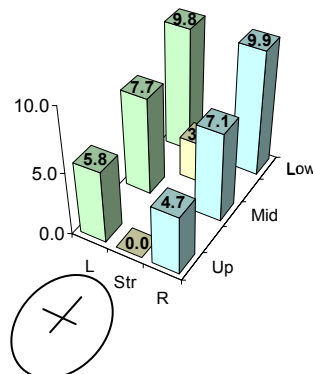
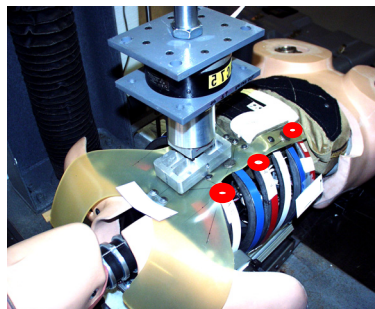


Figure 10. Presentation of coupling results. In this test the indenter loads the upper sternum. The red circles indicate loading/measurement sites. The colored columns in the plot indicate the relative deflection of each site in response to indenter loading. In this case, the indenter was centered on the upper sternum. Indenter displacement, 25.4 mm, is labeled a "0.0". A site that recorded no deflection would be labeled "10.0".

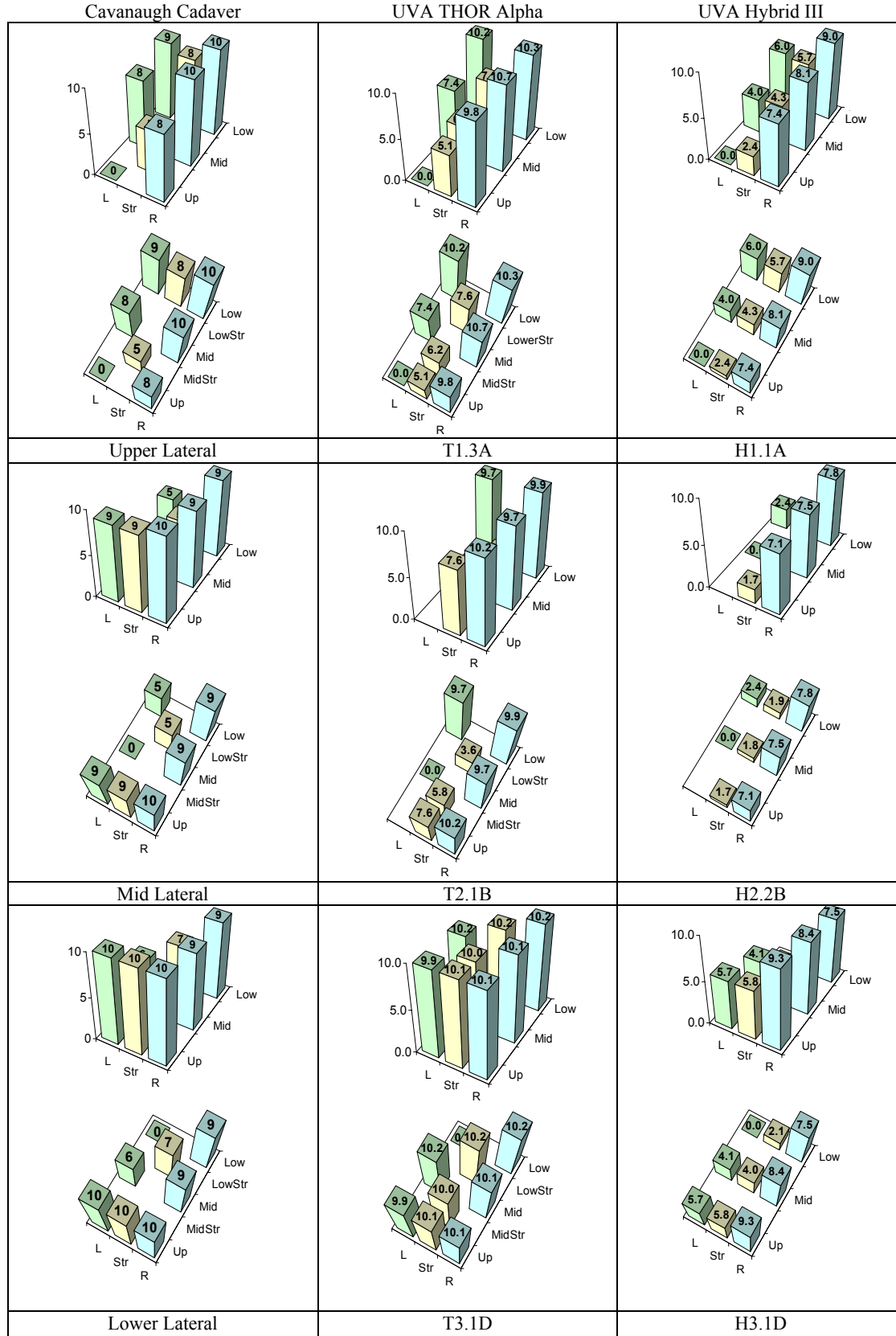


Figure 11. Coupling results. Str – sternum.

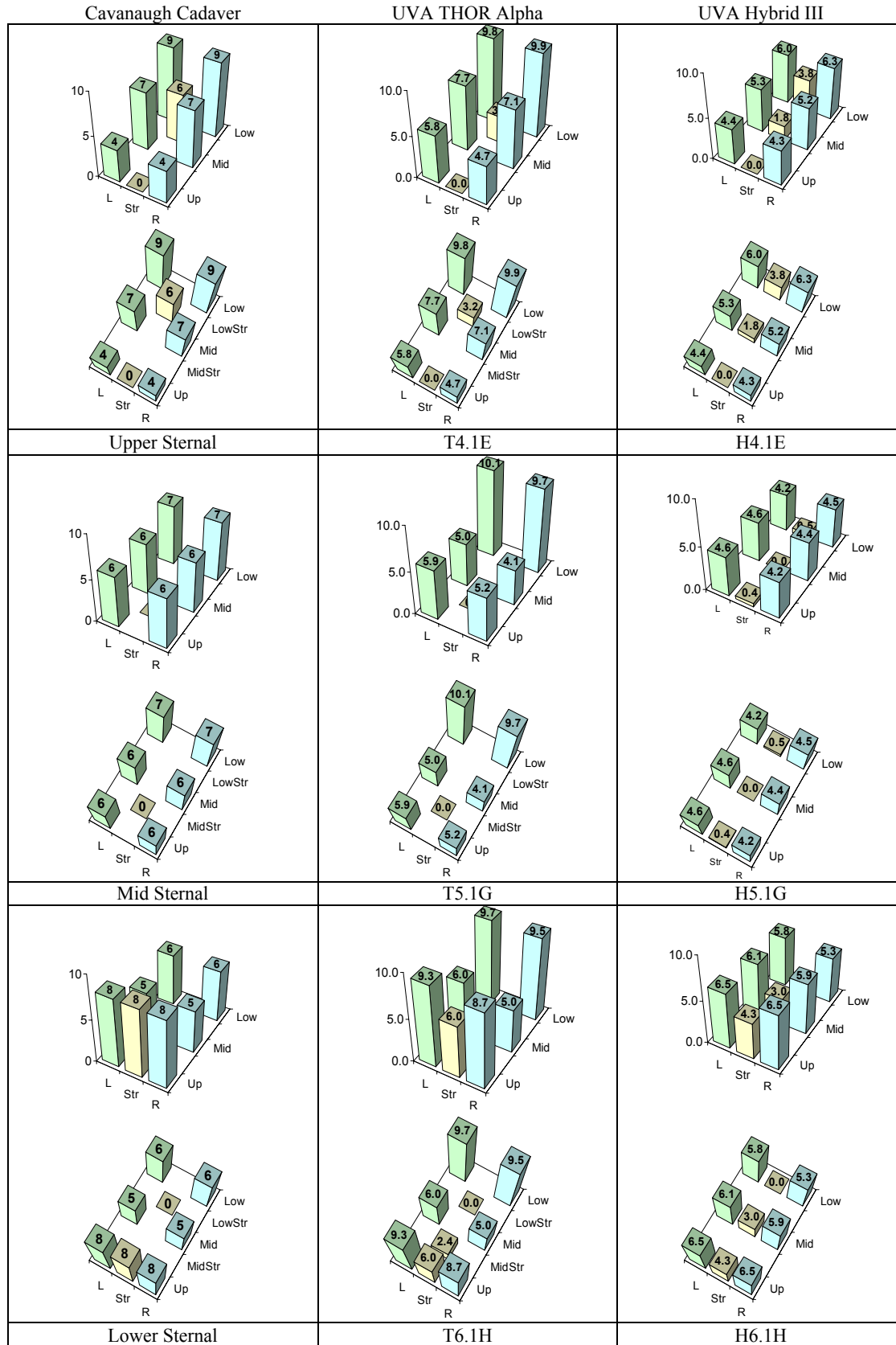


Figure 11. Coupling results continued.

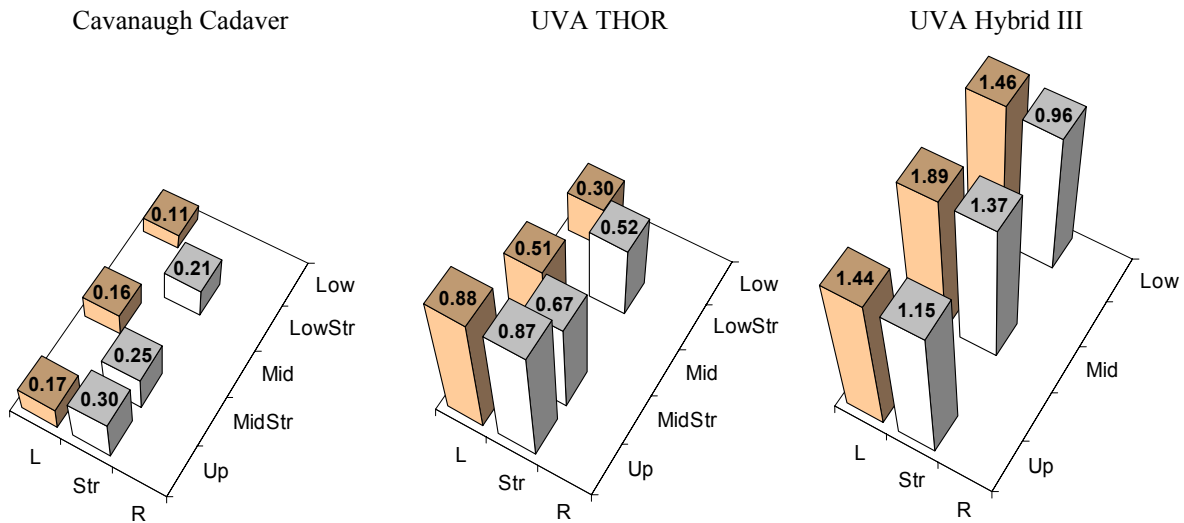


Figure 12. Comparison of cadaver, THOR, and Hybrid III indenter load results. Force in kN.

THOR Coupling

For some loading conditions, THOR was less coupled than the cadavers; for others THOR was more coupled. Figure 13 summarizes these findings. In general, THOR was less coupled than the Hybrid III, which, in turn, was more coupled than the cadavers for most sites.

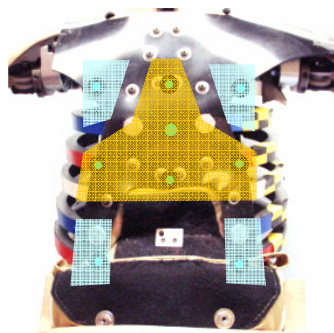


Figure 13. THOR coupling. The blue regions indicate less coupling than the cadavers; the orange region indicates more coupling.

In tests that loaded the mid and lower lateral and sternal sites, THOR Alpha's ribcage deflection pattern suggests that the lower lateral site moved independently and was minimally coupled to the rest of the ribcage. For example, when the lower sternum was loaded, THOR's lower lateral site deflected 5 percent while the average cadaver deflected 40 percent. When THOR's lower lateral site was loaded, no other sites deflected measurably. The average cadaver mid lateral site deflected 50 percent. THOR also was somewhat less coupled than the cadavers (and the Hybrid III) when the upper sternum was loaded.

Mid-sternal and mid-lateral loading results indicated that THOR's mid sternum was more

coupled to the lateral ribcage than were the cadavers'. THOR's upper and lower sternal sites were also more coupled than were the cadavers'. In general, the Hybrid III exhibited more lateral and longitudinal coupling than the cadavers. However, the Hybrid III recorded similar coupling between the lateral sites and the sternum when the sternum was loaded.

THOR Stiffness

The peak indenter load at 25.4 mm of deflection is an indicator of site quasi-static stiffness. Both the Hybrid III and THOR were much stiffer than the cadavers at all loading sites (Figure 12). The greatest difference for THOR was recorded for the upper lateral site where THOR was 5.2 times stiffer than the cadavers (0.88/0.17 kN). The elevated stiffness for the upper lateral site also produced a regional stiffness pattern that deviated from the cadavers. The ratio of the upper to lower lateral site stiffness was 2.9 for THOR, approximately twice that of the cadavers (1.5).

The Effect of Removing Posterior Rib Support

For sternal loading tests in which the bilateral rib supports were removed (Figure 8), the posterior rib deflection was recorded for three lateral sites that corresponded to the anterior lateral site locations, namely 76 mm from the subject centerline and directly below the anterior sites. Both the Hybrid III and THOR recorded little posterior rib deflection. The Hybrid III recorded deflection values that ranged from 2.1 to 2.8 mm. THOR recorded values that ranged from 0.4 to 2.1 mm. The highest values occurred at the upper lateral site for both dummies. These findings are similar to those reported by

Cavanaugh (1988) who found that the Hybrid III dummy ribs deflected posteriorly 2 to 2.5 mm when the sternum was deflected 25.4 mm and that the average cadaver deflected only about 1.3 mm. Removing the rib support had no meaningful effect on coupling for either dummy but did reduce stiffness. The Hybrid III and THOR sternal site stiffness was reduced by 12-18 percent and 7-16 percent respectively.

DISCUSSION

Test Limitations

The tests provide information regarding THOR Alpha's thorax response to regional quasi-static loading. However, interpretation of the results should consider study limitations. Although quasi-static loading may better approximate low rate restraint belt loading in comparison to hub impacts, belt loading is, nevertheless, a dynamic event that may alter both stiffness and coupling due to viscous effects.

The Cavanaugh test condition, in which the subject is stationary, does not reflect the dynamic interactions between the torso and restraints present in a frontal crash. The effect of subject posterior support, another departure from the crash environment, was not assessed.

The anterior ribcage was deflected a maximum of 25.4 mm in order to be able to compare with prior cadaver data (Schneider et al 1992 a). The 25.4 mm limit was adopted for the cadaver tests because the researchers found that greater deflection fractured ribs (Cavanaugh et al 1988). While evaluating THOR's response in the 0 to 25.4 mm range is valuable, a more complete characterization of ribcage response is necessary. For example, the generally linear response evident for 25.4 mm mid-sternal loading (Figure 14) may not represent the response for higher deflections. Further testing of both cadavers and THOR at deflection levels injurious to cadavers is required.

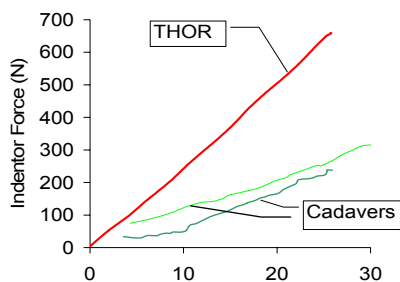


Figure 14. Mid-sternal deflection results for two cadavers tested by Cavanaugh et al (1988) and for THOR Alpha.

The design of the gimbaled indenter produced misalignment of the indenter with the target sites (Figure 15). The variation in misalignment and resulting deflection values was a function of indenter head tilt. In cases in which tilt was minimal such as for the mid and upper sternum, misalignment was minimal and the deflection at the loading site was nearly the same as that recorded for the indenter stroke. However, in cases in which the indenter tilted significantly, the misalignment could result in measured input deflection errors of approximately 2.5 mm (10 percent of the 25.4 mm indenter stroke).

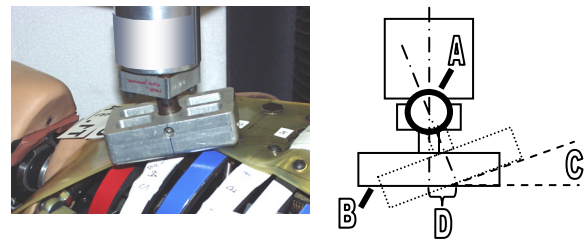


Figure 15. Indentor articulation. The ball joint (A) allows the indenter face (B) to tilt a maximum of 12 to 15 degrees (C) to align with the local contours of the indenter site. This produced as much as 14 mm of translation of the center of the indenter face (D).

THOR Alpha Comparison with Other Subjects

Although the indenter geometry increased the error bounds for deflection measurements, the study produced clear differences in torso response for the THOR Alpha and Hybrid III. Both subjects produced different responses relative to the cadavers tested by Cavanaugh. The THOR Alpha coupling and regional stiffness were more cadaver-like than the Hybrid III, a finding similar to that reported by Schneider (1992) for the Prototype 50M. The differences between THOR and the 50M were relatively minor; THOR was somewhat less coupled, less stiff in the lower ribcage, and stiffer in the upper ribcage.

This finding suggests that the THOR Alpha thorax response approximates that of the 50M. The 50M's developers claimed coupling to be acceptable relative to cadavers but found the 50M to be too stiff even if the dummy response was assumed to include the effects of muscle tensing (Schneider et al 1992 a). Likewise, while the THOR Alpha's coupling was generally cadaver-like, its stiffness at the loading sites was 2.4 to 5.1 times greater than the cadavers' (Figure 12).

Thorax Performance Priorities

Like the 50M, THOR Alpha's performance in the Kroell pendulum impact tests, is better than it is for the quasi-static Cavanaugh tests. In the hub impacts, both the Prototype 50M and THOR Alpha demonstrate force-deflection responses similar to those of cadavers (Figures 4 and 16) (Schneider et al 1992 b). These results suggest that performance in simulated steering wheel hub impacts (conducted at 4 to 7 m/s) was a higher priority than performance under quasi-static / low speed (1 to 4 m/s) loading for both the 50M and for the THOR Alpha despite the recognized need for improved response to restraint loading (Schneider et al 1989).

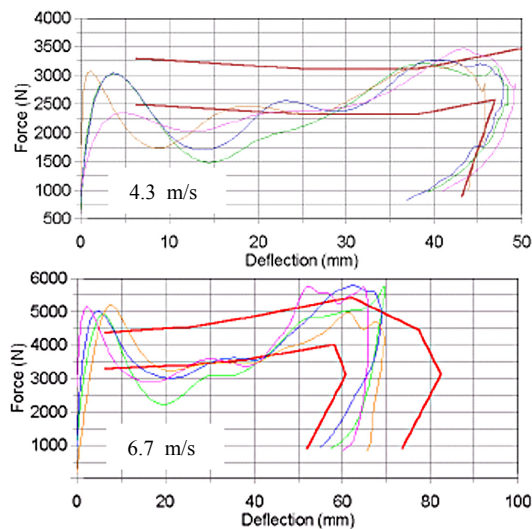


Figure 16. Results for multiple THOR Alpha Kroell impacts. (Tariq Shams personal communication 2004)

Review of the material documenting the development of the 50M suggests that the developers of the 50M attempted to create a novel torso that promised be able to respond biofidelically under both low and high speed loading (Figure 17).

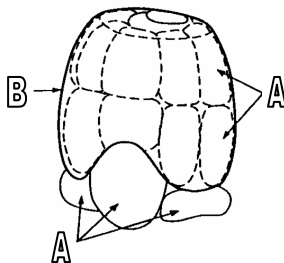


Figure 17. UMTRI torso concept using fluid-filled bladders (A) in an elastic shell (B).

Despite many attempts to realize the concept with physical models, none achieved the desired response characteristics and all would have required considerable effort to develop into a viable dummy

component. Constraints of time and money forced the 50M developers to adopt the traditional damped spring steel rib construction and, given the results of the Cavanaugh tests, its response limitations also. In turn, the results of the UVA Cavanaugh tests suggest that THOR Alpha shares the same response limitations.

GESAC, THOR's developer, modified the ribcage in light of the UVA test results. Unfortunately, only a modest reduction in upper ribcage stiffness produced an unacceptable force-deflection response in the hub impact tests. In addition, the softer ribcage threatened to "bottom out" against the spine under severe anterior loading creating both an unrealistic response and durability concerns (Tariq Shams personal communication 2004). Given the inability of both UMTRI and GESAC to successfully achieve both low and high-rate loading response targets, we question whether this goal is achievable with present ribcage construction methods.

Limitations of Poor Response Biofidelity in Low Rate Loading

The decision to produce a torso with priority biofidelity in Kroell hub impacts may have compromised THOR Alpha's response to low speed loading characteristic of belt restraints. In UVA frontal sled tests with standard and force-limited three-point belt systems, the location of peak chest deflection was different for THOR Alpha and cadavers for tests in which the subjects were seated in the right front passenger position. The location of peak chest deflection for THOR Alpha was consistently in the lower chest (Kent et al 2003), while for the cadavers it occurred in the upper chest. This result may be due, in part, to the difference in stiffness ratio between upper and lower ribcage between the dummy (2.9) and cadavers (1.5) recorded in the Cavanaugh tests. Recent studies, acknowledging the limitations of current frontal impact dummies and injury criteria for assessing injury from restraint loading, have advocated a shift in focus away from the Kroell corridors and toward a lower-rate, non-impact environment (Kent et al. 2004, Shaw et al. 2005).

However, further study is required to fully understand which factors are critical to biofidelic response and to accurately assess dummy performance. In the UVA sled tests, the difference in location of peak deflection was not observed for the driver position and may be characteristic of conditions particular to this test series. Moreover, the relative importance of peak deflection location,

deflection magnitude, and mechanical coupling has not been determined.

Biofidelic dummy response to restraint loading is influenced by factors other than regional stiffness. THOR Alpha's coupling response and ribcage geometry, both clearly more cadaver-like than the Hybrid III, are other parameters that influence deflection response. Structures adjacent to the ribcage also determine response to anterior loading. These include the shoulder/clavicle structure, the spine, and the pelvis which have been designed to be more cadaver-like for THOR Alpha (Schneider et al 1992b). However, there is insufficient cadaver response information to determine how cadaver-like a dummy torso must be in order to respond

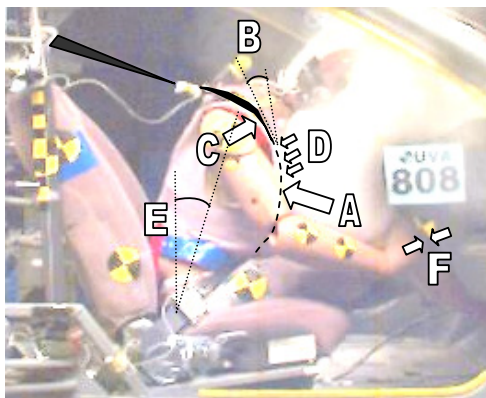


Figure 18. Factors external to the ribcage that affect ribcage deflection in a frontal crash.

A – Normal shoulder belt loading is determined, in part, by shoulder geometry and angle of the belt over the shoulder (B).

C – Portion of normal belt force born by shoulder.

D – Distribution of air bag loading.

E – Torso angle. Torso angle, defined by the relative movement of the upper spine with respect to the pelvis, is influenced by pelvic restraint by the seat cushion, lap belt, and interaction with the instrument panel (F) as well as upper torso movement, a function of shoulder belt characteristics and air bag loading. The torso angle influences factors A, B, C, and D.

CONCLUSIONS AND RECOMMENDATIONS

THOR Alpha's responses in the Cavanaugh tests were more cadaver-like than the Hybrid III as were the responses of its predecessor, the Prototype 50M. Like the 50M, THOR Alpha's torso was, however, stiffer than that of the cadavers, a characteristic that could affect response to loading by occupant restraint systems. The excessive torso stiffness under low rate loading reflects an historical priority for biofidelic response in the hub impact loading environment and the inability of current mechanical torsos to mimic a human equally well over a wide range of loading rates and environments.

Excessive stiffness and non biofidelic relative regional stiffness may have contributed to THOR Alpha's lack of cadaver-like response to restraint loading in tests conducted by UVA. However, there are several other factors that influence response to restraint loading, but the significance of their contribution, individually or in combination, is poorly understood. Therefore the effect of changing a single factor, such as torso stiffness, is difficult to predict. Reducing torso stiffness to match that of the cadavers, either by modifying the present ribcage to

biofidelically. For example, although the THOR Alpha shoulder is more human-like than the Hybrid III, the shoulder joint and clavicle are more anterior than the corresponding structures of the human. Whether this difference is enough to significantly affect shoulder shielding of the anterior chest (and reducing upper chest deflection) is unknown. Therefore, while the Cavanaugh tests identify a substantial difference in stiffness between THOR Alpha and cadavers, and while stiffness may contribute significantly to restraint loading response, it is only one of several factors influencing response (Figure 18).

the detriment of impact response, or designing a new ribcage capable of biofidelic response over a wide range of loading rates, is but one of several changes that may be needed to improve response.

Prior to modifying or redesigning the dummy torso, we recommend a thorough study to define the human torso response to loading to injurious levels by contemporary and anticipated occupant restraint systems. Although further quasi-static tests may be valuable, the study should include a dynamic crash environment in order to more comprehensively identify and quantify critical factors (and their interaction) that determine torso deflection. We also recommend a comprehensive review of dummy thoracic performance criteria and priority of loading conditions and anticipate that biofidelic response to restraint systems will merit a higher priority than steering wheel hub impacts.

In summary, significant improvement in the biofidelity of frontal crash dummy torso response to restraint loading can be realized if there is a better understanding of the factors that determine the human response. Although this information is critical to developing an improved torso, the technology does not exist to exactly replicate a human occupant and

human response for the wide range of loading conditions possible in a frontal crash. For the foreseeable future, dummies will involve compromises regarding the range of loading conditions and/or accuracy of response. Therefore, the need to prioritize loading conditions, reflected in the development and performance of the present frontal impact dummies, will be a prerequisite for future dummy development.

ACKNOWLEDGMENTS

The authors acknowledge the support and guidance of Mark Haffner, Rolf H. Eppinger, Nopporn Khaewpong, and Peter Martin of the Biomechanics Research and Development Group of the National Highway Traffic Safety Administration (NHTSA), U S Department of Transportation. This study was supported by DOT NHTSA Grant DTNH22-93Y-07028. All findings and views reported in this manuscript are based on the opinions of the authors and do not necessarily represent the consensus or views of the funding organization. Larry Schneider, University of Michigan Transportation Research Institute (UMTRI), provided the indenter use for the tests. John Cavanaugh provided information necessary to help recreate the test conditions he used for the cadaver subjects. GESAC prepared the THOR Alpha and provided Kroell test results.

REFERENCES

Cavanaugh J, Jespen K, King A. (1988) Quasi-static frontal loading to the thorax of cadavers and Hybrid III dummy. Proceedings of the 16th International Workshop on Human Subjects for Biomechanical Research., Atlanta, GA. pp 3-18.

Foster, J, Kortge, J, Wolamin, M. (1977) Hybrid III-A Biomechanically Based Crash Test Dummy. Paper 770938, Society of Automotive Engineers.

Kent, R, Bolton, J, Crandall, J, Prasad, P, Nusholtz, G, Mertz, H, Kallieris, D. (2001) Restrained Hybrid III dummy-based criteria for thoracic hard-tissue injury prediction. IRCOBI Conference on the Biomechanics of Impact.

Kent, R, Lessley, D, Shaw, C, Crandall, J. (2003) the utility of Hybrid III and THOR chest deflection for discriminating between standard and force-limiting belt systems. Paper 2003-22-0013, Society of Automotive Engineers.

Kent, R, Lessley, D, Sherwood, C (2004) Thoracic response corridors for diagonal belt, distributed, four-

point belt, and hub loading. Stapp Car Crash Journal 48: 495-519.

Kroell, C (1976) Thoracic response to blunt frontal loading in The Human Thorax – Anatomy, Injury, and Biomechanics, Society of Automotive Engineers publication P-67, pp 49-77. Reprinted in Biomechanics of Impact Injury and Injury Tolerances of the Thorax-Shoulder Complex, Backaitis (ed.), Society of Automotive Engineers 1994 publication PT-45, pp 51-79.

Melvin, J (1988) The Engineering Design, Development, Testing and Evaluation of an Advanced Anthropometric Test Device, Phase 1: Concept Definition. DOT HS 807 224. February 1988.

Rangarajan, N, White, R, Shams, T, Beach D, Fullerton, J., Haffner, M, Eppinger, R, Pritz, H, Rhule, D, Dalmotas, D, Fournier, E (1998). Design and Performance of the THOR Advanced Frontal Crash Test Dummy Thorax and Abdomen Assemblies. Proceedings of the 16th International Technical Conference on the Enhanced Safety of Vehicles.

Ruan, J, El-Jawahri, R, Chai, L, Barbat, S, Prasad, P. (2003) Prediction and analysis of human thoracic impact responses and injuries in cadaver impacts using a full human body finite element model. Stapp Car Crash Journal, 47: 299-321.

Schneider L, King A, Beebe M (1989) Design Requirements and Specifications: Thorax-Abdomen Development Task. Interim Report: Trauma Assessment Device Development Program. DOT HS 807 511. November 1989.

Schneider, L, Ricci, L, Salloum, M, Beebe, M, King, A, Rouhana, S, Neatherly, R. (1992a) Design and Development of an Advanced ATD Thorax System for Frontal Crash Environments. Final Report Volume 1: Primary Concept Development. Trauma Assessment Device Development Program. DOT HS 808 138. University of Michigan Transportation Research Institute. June 1992.

Schneider L, Haffner M, Eppinger R, Salloum M, Beebe M, Rouhana S, King A, Hardy W, Neatherly R (1992b). Development of an Advanced ATD Thorax System for Improved Injury Assessment in Frontal Crash Environments. Paper 922520, Society of Automotive Engineers.

Shaw, G, Crandall, J, Butcher, J. (2000) Biofidelity Evaluation of the THOR Advanced Frontal Crash Test Dummy. IRCOBI Conference on the Biomechanics of Impact.

Shaw, G, Lessley, D, Crandall, J., Kent, R (2005) Elimination of thoracic muscle tensing effects for frontal crash dummies. Paper 05B-81, Society of Automotive Engineers World Congress April 11, 2005.

Voigt, G, Wilfert, K (1969) Mechanisms of injuries to unrestrained drivers in head-on collisions. Paper 690811, Society of Automotive Engineers.

MODELING OF THE MATERIAL PROPERTIES AND FLUID-STRUCTURE INTERACTION IN THE TRAUMATIC RUPTURE OF AORTA

Sang-Hyun Lee

Kurosh Darvish

Center for Applied Biomechanics

University of Virginia

United States

Libor Lobovsky

Department of Mechanics

University of West Bohemia

Czech Republic

Paper Number 05-0390

ABSTRACT

Traumatic rupture of the aorta (TRA) is a leading cause of fatality in motor vehicle crashes. However, its injury mechanisms are still unknown since it is difficult to replicate and evaluate such ruptures experimentally. In this study, the mechanisms of aortic rupture in dynamic pressure loading were investigated using Finite Element (FE) Analysis.

A hyperelastic material model with linear viscoelasticity was used to characterize the mechanical behavior of aorta based on oscillatory biaxial tests and literature data. It was shown that the previous data led to contradictory uniaxial and biaxial responses. A set of new material properties were identified which closely described all the available experimental data.

Furthermore, a Finite Element model of aortic arch was studied under pressure impulse as seen in cadaveric sled tests. Four approaches were used to model the fluid namely, Lagrangian, Eulerian, Arbitrary Lagrangian-Eulerian (ALE), and Smoothed Particle Hydrodynamics (SPH). The Eulerian approach, in which the mesh is fixed in space through which the material flows, was the most complete one in terms of modeling the flow and interaction with the wall, though it required relatively large computational time. In the ALE approach, a Lagrangian material deformation was considered followed by an advection cycle for smoothing the mesh. The result of the ALE approach compared to the Eulerian approach showed less flow and localized deformation. In the SPH formulation, the fluid was represented by particles which interact with one another and the surroundings through specific potential energy functions. The SPH approach exhibited rather idealized behavior of the fluid flow with less computational time. The TRA models were validated against *in vitro* tests and predicted the most probable location of rupture at the isthmus as indicated in the experiments.

INTRODUCTION

Traumatic rupture of the aorta (TRA) is a major cause of fatality in automobile accidents. According to the previous studies, aortic injuries continue to be present in about 20 percent of motor vehicle crash fatalities [1, 2]. The injury mechanism of TRA is still unknown and it is difficult to replicate and evaluate such ruptures experimentally, though different hypotheses have been proposed. The TRA due to pressure was the focus of this study. Other proposed mechanisms of TRA include relative motions and osseous pinching [3, 4]. The primary site of the TRA is reported at the isthmus region with the probability of 75-85%, which is the transition between a relatively mobile heart and a relatively fixed descending aorta [1, 5].

Before failure aorta undergo large deformations due to the internal pressure, the inertial forces, and the contact forces acting upon aorta from the surrounding tissues. Simulation of aorta in impact loading using finite element (FE) analysis was conducted to improve the understanding of the mechanisms of aortic injury. The biofidelity of the results of the FE model is in part dependent on the choice of material constitutive model. The uniaxial and biaxial experimental data of Mohan and Melvin (MM) showed that the mechanical behavior of aorta is rate dependent and failure occurs at stretch ratios more than 60% [6, 7]. Previous FE studies simplified aortic blood with linear elastic fluid model which is incapable of sustaining large deformations [8, 9]. Complicated and more realistic flow interaction with the aortic wall can be accomplished by applying such techniques as Arbitrary Lagrangian Eulerian method (ALE) or Smoothed Particle Hydrodynamics (SPH).

METHODS

Material Model

A representative rectangular piece (20.5 mm x 18.4 mm x 1.36 mm) of human aorta, sample HA41, was subjected to biaxial oscillatory stretch at 20 Hz

superimposed on a constant stretch, using the test setup described in [10] (Figure 1). The sample was excised from the arch of aorta of a 27 year-old subject and was connected to two shakers and two load cells using 12 silk sutures. The oscillatory deformation was determined based on the measured accelerations of the two shakers moving in the circumferential and longitudinal directions. The biaxial forces were measured using two load cells mounted opposite to the shakers. The displacement offsets and the time history of the state of strain in the central quadrilateral region, PQRS, were determined based on motion analysis of high speed (1000 frames/sec) video photography of the sample deformation.

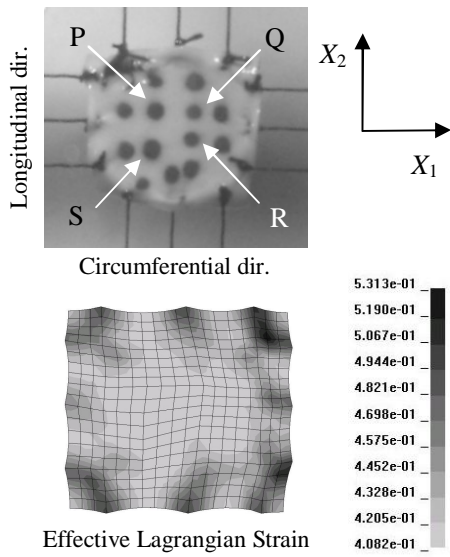


Figure 1. HA41 aorta sample and its FE model for biaxial testing at 20Hz

A second-order Mooney-Rivlin (MR) constitutive model of the following form, for an isotropic material, was assumed for aorta:

$$W = C_{10}(I_1 - 3) + C_{01}(I_2 - 3) + C_{11}(I_1 - 3)(I_2 - 3) + C_{20}(I_1 - 3)^2 + C_{02}(I_2 - 3)^2 \quad (1)$$

in which, W is the strain energy function, C_{ij} are the material properties and I_i are the invariants of the left Cauchy-Green strain tensor. The above equation is compatible with material 77 in LS-DYNA [11]. Viscoelasticity of the material was approximated by adding a one-term Prony series, $G(t) = 2m_0 \exp(-bt)$, to the hyperelastic shear modulus, where $m_0 = 2(C_{10} + C_{01})$ is the linear shear modulus and b is the decay rate. The factor 2 in $G(t)$ was chosen based on the ratio between the dynamic and quasi-static result given in [6]. The hyperelastic material properties were

determined by least-squares optimization of an analytical solution for the biaxial forces subject to a general biaxial deformation. The viscoelastic decay rate was determined based on the phase shifts between the oscillatory displacements and forces. For the quasi-static and dynamic uniaxial test data (MM Static and MM Dynamic) given for a 25 year-old subject, MR models were characterized. Analytical solutions for uniform biaxial deformation were compared with the experimental biaxial data given in [7] to validate the quasi-static MR models. Finally, the MR material models for HA41 and MM Static were implemented in LS-DYNA (ver.970) and the model results were compared with the experimental oscillatory biaxial data.

Fluid-Structure Interaction

A simplified FE model of aorta (Figure 2a) was developed based on the geometry and dimension from a human aorta used in the biaxial tests [10]. The aortic wall was modeled with one-layer solid elements. Four approaches were used to model the fluid namely, Lagrangian, Eulerian, Arbitrary Lagrangian-Eulerian (ALE), and Smoothed Particle Hydrodynamics (SPH). In the Lagrangian method, the mesh is attached to the body and it transforms according to the deformation of the material. The Eulerian approach is solving the problem with a fixed mesh in space through which the material flows. Therefore, some initially void elements, representing the environment, are needed. In the ALE approach, in each time step, a Lagrangian material deformation is considered followed by an advection for fluid calculations. In the SPH formulation, the fluid is represented by particles which interact with one another and the surroundings through specific potential energy functions. Computations were performed using LS-DYNA (ver. 970) for the Lagrangian, Eulerian and ALE models, and PAM-CRASH (ver. 2002) for the SPH model.

To perform the pressurization simulation, particularly for the ALE and SPH models, a reservoir tube and a piston were used to create the fluid inflow boundary condition at the inlet of the tube. A linear ramp representative of cadaveric sled tests was taken as the pressure input (Figure 2b). The model was symmetric with respect to the X-Y plane and fixed boundary conditions (no flow) were defined at the other end. For fluid-structure interaction (FSI) in LS-DYNA, coupling of the Lagrangian mesh of aorta with the Eulerian mesh of the fluid was used. For this purpose in PAM-CRASH, the node to segment contact was implemented. A friction coefficient of 0.08 was assumed in the ALE and the SPH model between fluid and structure, which created flow characteristics consistent with the Eulerian model.

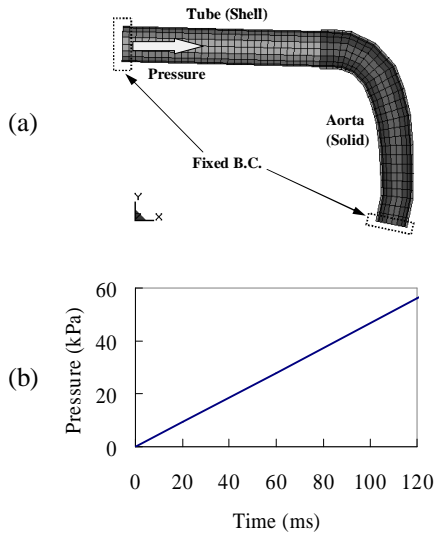


Figure 2. Simplified FE aorta model and pressure history

RESULTS AND DISCUSSION

The material parameters determined for the MM Static, MM Dynamic, and HA41 models are summarized in Table 1. For HA41, the experimental strains were all below 40%. Therefore, any result of this model for higher strains is merely speculative. The MR material model was able to closely match the uniaxial MM Static and MM Dynamic data (Figure 3). The behavior of the model for HA41, which was characterized based on the biaxial oscillatory results, in uniaxial deformation, was close to the MM Static data particularly at strains below 40%. In uniform biaxial deformation (Figure 4), the response of the MM Static model was significantly stiffer than the reported biaxial data. However, the response of the HA41 model, at strains below 40% was closer to the experimental biaxial data.

Table 1. Material properties (in kPa) of the MR models for the quasi-static and dynamic results of Mohan and Melvin and the hyperelastic response of the biaxial test of HA41

Test	MM Static	MM Dynamic	HA41
C_{10}	1.16E+01	1.67E+02	1.96E+01
C_{01}	7.17E-01	-4.83E+01	9.25E+00
C_{11}	-2.64E+03	-3.82E+03	-5.73E+01
C_{20}	1.06E+03	1.81E+03	5.46E+01
C_{02}	1.71E+03	2.00E+03	1.41E+01

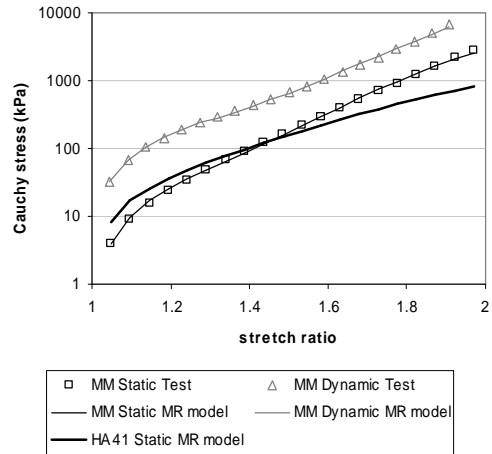


Figure 3. Responses to uniaxial loading. Experimental and MR model results for the quasi-static and dynamic tests of MM, and FE model results for the HA41 sample

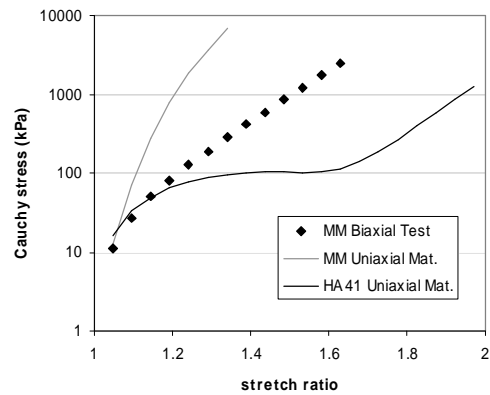


Figure 4. Responses to uniform biaxial loading. Experimental and MR model results for the quasi-static test of MM and MR model results for the HA41 sample

FE simulation of the oscillatory biaxial deformation with HA41 model showed that forces and strains were closely following the experimental data (Figure 5 and Figure 6 respectively). The stiffness hourglass coefficient (type 4) for this simulation was $HG=0.1$ and the ratio of hourglass energy to internal energy was less than 5%. The fact that E_{22} in the experiment was larger than the model showed that the tissue was anisotropic. For the FE simulation with MM Static material model, with $HG=0.1$ the ratio of hourglass energy was 40% and the forces were significantly higher than the experimental data. With $HG=0.001$, the forces were close to the experimental data, but the strains were

low and excessive deformation occurred in the boundary (Figure 6). Therefore, the MM Static and biaxial data led to contradictory uniaxial and biaxial responses. The HA41 material properties closely described the experimental data for strains below 40%.

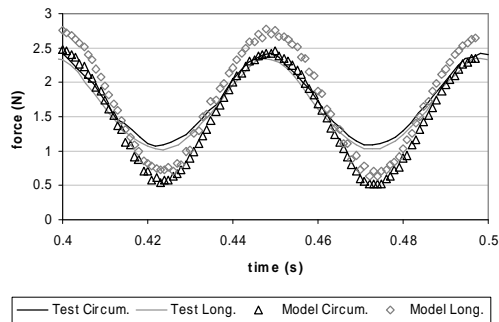


Figure 5. Comparison of forces in the circumferential and longitudinal directions between biaxial test data and FE results with HA41 MR material model

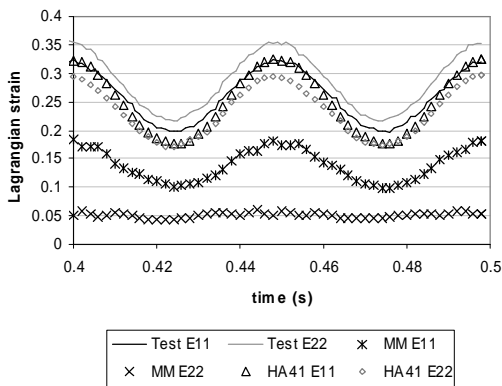
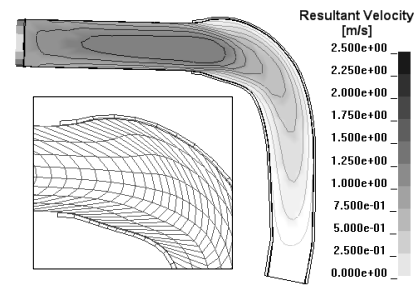


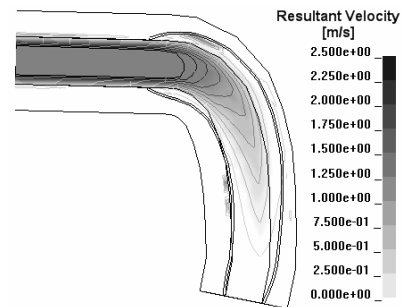
Figure 6. Comparison of strains between biaxial test data and FE results with MM static and HA41 MR material models

Based on the material parameters of HA41, the FSI models were used to simulate the *in vitro* pressure tests described in [10]. The velocity profile and pressure distribution in the fluid were considered as the main factors representing the flow characteristics which were measured at the isthmus region. Although all approaches predicted a parabolic velocity profile which is expected for Poiseuille-like flows, the Lagrangian method showed excessive mesh distortion which caused rapid drop of the time-step during simulation (Figure 7). All three FSI models predicted generation of vortices at the isthmus only when the loading rate was increased to 20 kPa/ms. For the test loading condition (0.5 kPa/ms) no vortices occurred. The maximum

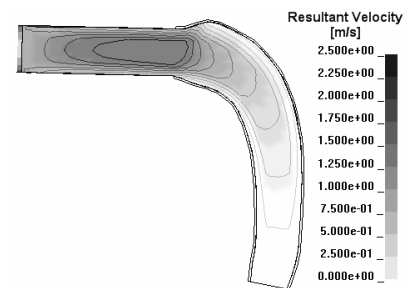
velocity was in the range of 2.5 to 3.0 mm/ms at 120ms. The pressure distribution was uniformly decreasing along the tube with about 60% of the input pressure at the isthmus.



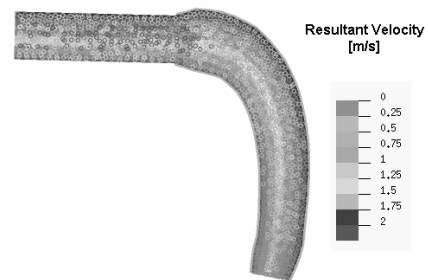
(a) Lagrangian fluid



(b) Eulerian fluid



(c) ALE fluid



(d) SPH fluid

Figure 7. Comparison of velocity profiles of FSI models (at 100ms)

The trend of stretch ratios and stresses measured in the circumferential and longitudinal directions were consistent in the three FSI models. However, the results of the SPH model were higher than the two other models (Figure 9). In the SPH model, the identical material model was not used as only the first-order Mooney-Rivlin was available in the PAM-CRASH solver and it resulted in slightly different behavior. In the ALE model, the flow could not propagate as much as in the Eulerian and SPH models and the deformation of aorta was more concentrated in the ascending region. The maximum principal stress was predicted at the inner arch of the wall, close to the isthmus, in the range of 250 to 275kPa in the circumferential direction (Figure 8). The results were compared with the uniaxial failure tests [6] and the pressurization tests [10] (Figure 10). The material models used in this study were characterized based on sub-failure deformations (maximum strain about 15%). As a result, the stress-stretch ratio curves predicted from the models were almost linear and did not show the nonlinear trend observed in the experiments in large stretch ratios. However, the maximum values of stress and strain were located within the experimental data range. Neither in LS-DYNA nor in PAM-CRASH there is a material model that can handle both the nonlinearity and anisotropy that is observed in the aorta tissue. In the Eulerian method, because of the void elements, the total number of elements was higher than the others and also required the largest CPU calculation time (Table 2). For the SPH approach, the initial time step was the largest and the CPU time was the smallest in this simulation. However, as the number of elements grows, calculation time may increase dramatically.

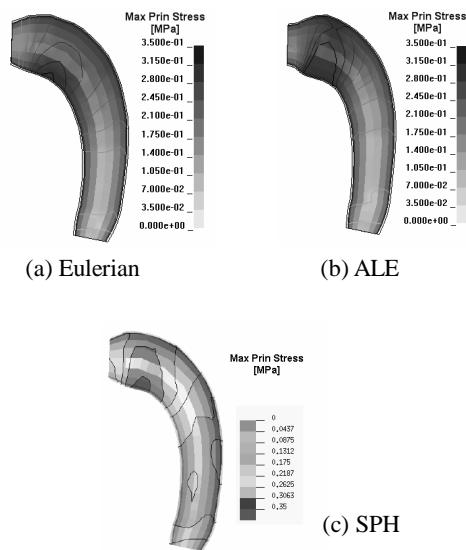


Figure 8. Maximum principle stress distribution

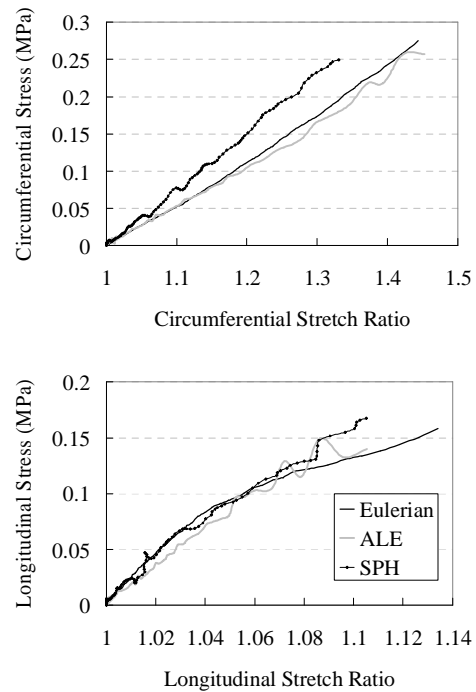


Figure 9. Aorta wall stress-stretch ratio at isthmus

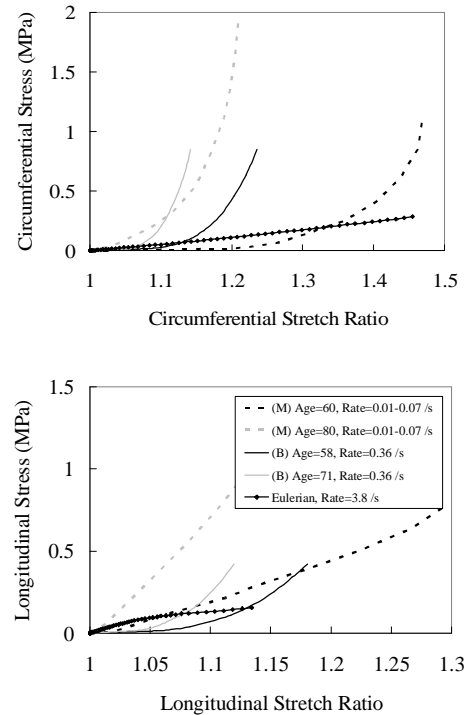


Figure 10. Stress vs. stretch ratio at isthmus and comparison with experiments

Table 2.
Computational aspects of the models

Element formulation	Eulerian	ALE	SPH
Elements	6544	1904	2016
Δt_i (μ sec)	0.97	0.97	1.75
CPU time (sec)	11238	5626	3940
Solver	LS-DYNA	LS-DYNA	PAM-CRASH
CPU Clock	Intel® Pentium®4 2.8GHz		

CONCLUSIONS

Three TRA models with material properties determined from dynamic biaxial tests were validated against *in vitro* tests and predicted the most probable location of rupture at the isthmus as indicated in the experiments. The Eulerian approach was the most complete one in terms of including the flow and interaction with the wall, though it required relatively large computational time. The ALE approach resulted in less flow and more localized deformation in the aorta. The SPH approach exhibited rather idealized behavior of the fluid flow but the results in the aorta wall were close to the Eulerian approach with less computational time.

REFERENCES

- [1] Katyal, D., McLellan, B.A., Brenneman, F.D., Boulanger, B.R., Sharkey, P.W., Waddell, J.P. 1997. "Lateral impact motor vehicle collisions: significant cause of blunt traumatic rupture of the thoracic aorta." J. Trauma, No. 42 (5): 769-772.
- [2] Richens, D., Field, M., K., Neale, M., Oakley, C. 2002. "The mechanism of injury in blunt traumatic rupture of the aorta." Eur. J. Cardiothorac Surg., No. 21: 288-293.
- [3] Lundewall, J. 1964. "The mechanics of traumatic rupture of the aorta." Acta. Pathol. Microbiol. Scand., No. 62: 34-36.
- [4] Crass, J. R., Cohen, A.M., Motta, A.O., Tomashefski, J.F., Wiesen, E.J. 1990. "A proposed new mechanism of traumatic aortic rupture: the osseous pinch." Radiology, No. 176: 645-649.
- [5] Symbas, P. N., Tyres, D.H., Ware, R.E. 1973. "Traumatic rupture of the aorta." Ann. Surg., No. 178 (6).
- [6] Mohan, D., Melvin, J.W. 1982. "Failure properties of passive human aortic tissue I- Uniaxial tension tests." J. Biomechanics, No. 15 (11): 887-902.
- [7] Mohan, D., Melvin, J.W. 1983. "Failure properties of passive human aortic tissue II- Biaxial tension tests." J. Biomechanics, No. 16 (1): 31-44.
- [8] Shah, C. S., Yang, K.H., Hardy, W., Wang, H.K., King, A. 2001. "Development of a computer model to predict aortic rupture due to impact loading." Stapp Car Crash Journal, No. 45.
- [9] Richens, D., Mark, F., Shahrul, H., Michael, N., Charles, O. 2004. "A finite element model of blunt traumatic aortic rupture." Eur. J. Cardiothorac Surg.
- [10] Bass, C. R., Darvish, K., Bush, B., Crandall, J.R. 2001. "Material properties for modeling traumatic aortic rupture." Stapp Car Crash Journal, No. 45.
- [11] Hallquist, J. O. 1998. "LS-Dyna Theoretical Manual."

DEVELOPMENT OF A HUMAN BODY FINITE ELEMENT MODEL FOR RESTRAINT SYSTEM R&D APPLICATIONS

Jay (Zhijian) Zhao, Gopal Narwani

TAKATA – Automotive Systems Laboratory, Inc.

Paper Number 05-0399

ABSTRACT

A human body finite element model for an average adult male was developed. The model is based on the integration of finite element models of body regions of the thorax, abdomen, shoulder and head-neck, previously developed at Wayne State University. The model includes details of the human skeleton and major soft tissues in these body regions, including the skull, spinal column, neck muscles, joint ligaments, ribcage, clavicle and shoulder bones and joints, lungs, heart, aorta, vena cava, esophagus, liver, spleen, and kidneys, and various connective arteries and veins, and pelvis.

Extensive validations of the human body model have been made against Post Mortem Human Subjects (PMHS) responses for the frontal and side impacts, as well as belt and surrogate airbag loading under various conditions of fifteen sets of pendulum tests performed and published by various researchers. The force-deflection characteristics of shoulders, thorax, and the abdomen are in good agreement with the experimental data.

The model was further validated against the chest band data of belted PMHS 30mph sled test (NHTSA bio-mechanics database, test #2860). The model predicts the histories of chest deflections and shapes of the fourth and eight rib sections. Robustness study in sled test simulations was made. The model performed well under the impact severities of 15-35 MPH in frontal and side impacts.

Stress analysis was made on the clavicle under lateral pendulum impact, on the abdominal solid organs under rigid bar impacts, and on the chest ribs under the 30mph belted PMHS sled test. Comparisons of the analysis results with autopsy results showed that the model can estimate possible locations of the bone and organ failures, consistent with the experimental observations.

INTRODUCTION

Research and development of next generation advanced automotive restraint systems presents a unique set of challenges.

A recent survey by MLIT/JAMA/JARI on ITARDA Traffic Accident data in 2000 [1] showed that in Japan 76% of occupant fatalities were involved in frontal crashes, and 20% in side crashes. Among the frontal accidents head injuries accounted for 40% of the total fatalities, followed by chest injuries 25%, abdomen injures 11%, and neck injuries 7%. This survey also showed that belt usage reduced fatalities of occupants in all-direction auto accidents, but was not effective for reduction of the serious injury rates of occupants. In the United States also, similar trends of occupant fatality percentages classified by automobile accident types and injured body regions of occupant, have been reported in various publications by Mulligan et al. [2], Cavanaugh et al. [3], Elhagediab and Rouhana [4], and Lee and Yang [5], etc..

We studied the NASS/CDS database from 1993 to 1999. 59,426 cases of the thoracic and abdominal soft tissue injuries of occupants involved in the frontal accidents (PDOF=11-1 o'clock, AIS=2+) were analyzed. We found out that the unrestrained occupants had more organ injuries: about 72% for aorta, 52% for liver, 49% for spleen, 48% for kidneys, 47% for lungs, and 25% for heart, among all the cases. Comparatively, the percentages of organ injury in the total injured occupants restrained with seat belt only were: 17% for aorta, 40% for liver, 37% for spleen, 39% for kidneys, 32% for lungs, and 68% for heart. For the occupants restrained with both seatbelt and airbag the organ injury rates were, 5% for aorta, 8% for liver, 12% for spleen, 12% for kidneys, 11% for lungs, and 6% for heart. These findings tell us that the seatbelt combined with airbag provided better protection for occupants.

It is a challenge to develop safer and more advanced restraint systems, maximizing the protection performance for all the human body regions while to eliminate or to minimize their possible side effects, especially on the thoracic and abdominal organs. To optimize the restraint load distribution on the human body, particularly to properly distribute load through the shoulder and upper thorax of occupant, we need to better understand the shoulder's mechanical response and transmission of load to the thorax in frontal, oblique, and lateral impacts.

Protection of elderly people is expected to get increased attention in the next generation restraint system designs. The population continues to age worldwide. It was estimated that by 2030, 25% of the population will be age 65 or older [6]. Older people in general are more susceptible to injury, primarily thoracic injury, and that the morbidity, mortality, and treatment costs for a given injury are typically higher for old people. Kent et al. [7] found that the chest deflection threshold for rib fractures is strongly dependent on age. To better protect occupants of all age groups, especially elderly people, we should look to improve methods and tools for system performance evaluation.

The efficacy or performance of restraint systems is assessed using a variety of tools. Anthropomorphic test devices (ATDs), or dummies, are often used. ATDs are instrumented to measure various mechanical parameters, including accelerations at the center of gravity (CG) of head, chest, pelvis, chest deflection, and neck & femur forces etc. These mechanical parameters, or combinations thereof, correlated with presence of injury in similar cadaver tests to some extent, are used as "predictors" of injury risk. However, ATDs have certain limitations. The shoulder complex and the abdomen body parts of ATDs have poor biofidelity. ATDs have no or very limited capability for assessment of injury of the soft tissues (internal solid organs, ligaments, tendons, facet joint, etc.) in the human body. As supplemental tools, Post Mortem Human Subjects (PMHS) or animal tests may be performed to provide additional biomechanical information. Because these tests are very expensive, laborious, and have limited repeatability, they are not often used in laboratory for restraint systems evaluation.

Computer aided engineering (CAE) plays an important role in restraint systems R&D. Human body model emerges as an important tool for assessment of occupant injury and restraint system

performance. Specifically, a well-developed human body model helps in understanding injury mechanisms of the bony skeleton and soft tissues/organs of the restrained occupant under complex loading conditions in laboratory and real car crashes. The human body model, by taking into account changes of the anatomical structures and material properties due to aging, can be used to study aging factors to help evaluate restraint concepts for elderly occupant protection. The sled test simulations using the human body model, combined with a few PMHS component tests, will play an important role in assessment of restraint system performance and side effects. These tasks are impossible or very difficult to be conducted by using the current ATDs.

With the rapid advances in computer technology, sophisticated finite-element models of the human body have been developed in recent years. There currently are few published human body models. However, all of them have some limitations for the system R&D applications to our knowledge. Toyota Central R&D Lab., Inc. has developed the Finite Element Model of the Total Human Model for Safety (THUMS-AM50 version 1.52) [8]. This model has detailed human skeleton structures. But the model treats the thoracic and abdominal soft tissues as lumped masses. The vertebrae were defined as rigid bodies. These modeling methods limited the model usage for injury estimation of the soft tissues and thoracolumbar spine. Ford Motor Company constructed a human body model for an average adult male and validated its thoracic impact responses against a few sets of PMHS tests [9]. This model includes details of the skeleton and major thoracic and abdominal solid organs. However, it is not clear from the paper [9] that how much details of the anatomical structures in the shoulder complex were modeled in this model and that how reliable it is applied in sled test simulation applications. The other mid-sized human male body models commercially available, have similar deficiencies.

During past decades Bioengineering Center of Wayne State University (WSU) has published a human thorax model [10], a human abdomen model [11], a human shoulder model [12], a human neck model [13], and a human head model [14, 15]. These models were validated to some extent against data obtained from the PMHS pendulum tests. We used these models extensively and concluded that development of a human body model based on integration of these body part models should meet our needs and expectations.

The purpose of this research was to develop a robust and reliable human body model for our restraint system R&D applications. The basis of this work were finite element models of the body regions of the thorax, abdomen, and shoulder, developed at WSU. In order to achieve our goal we have made great efforts on improvement of the modeling methods and integration to achieve computation robustness and efficiency, as well as its validations.

METHODS AND MODEL DESCRIPTION

Model Improvement and Description

The whole human body model numbering scheme was designed as follows:

The first two digits of nodes and elements (numbered in millions), parts and materials (numbered in thousands) coincide with the sequence number for the following eighteen body parts: 1-brain, 2-skull, 3-neck, 4-shoulders, 5-left arm, 6-right arm, 7-thoracic bony structures, 8-thoracic soft tissues, 9-aorta, 10-lumbar spine, 11-abdominal soft tissues, 12-pelvis, 13-left femur, 14-right femur, 15-left knee, 16-right knee, 17-left tibia & foot, and 18-right tibia & foot.

To obtain better quality of finite elements, the model were remeshed particularly for the bodies of the torso skin, the pelvis flesh, the kidneys and the renal artery and vein, the abdominal hollow organs walls, the shoulder scapula, the Supraspinatus and Infraspinatus muscles. All the interfaces between or among anatomical sub-structures, basically modeled as tied nodes or surfaces, were reorganized. All the interactions among the anatomical structures, modeled as interface contacts, were redefined. The detailed finite-element models for the body parts of head and neck, and the rigid body models for the lower extremities were integrated.

Our new 3D FE model of the human body represents an average adult male with weight of 75Kg. It contains about 45,656 solid elements, 52,565 shell elements and 268 1-D elements, with total about 80,000 nodes and 99,000 elements. The minimum element mesh size is about 1.3mm (in the aortic arch region). Figure 1 shows this model. A description of the model by body regions is given below.

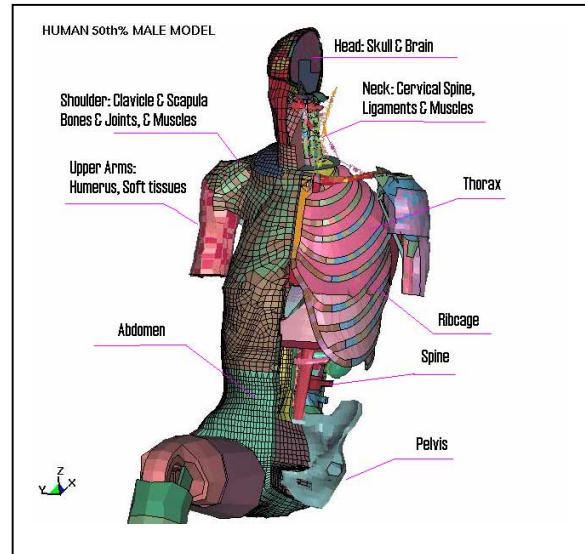


Figure 1. The human model model

The head model consists of scalp, skull, dura, falx, tentorium, venous sinuses, ventricles, cerebrum (gray and white matter), and cerebellum. The parts and material data are based on published information [14].

The neck model, consisting of the vertebrae from C1 through T1 including the intervertebral discs and anterior and posterior ligaments, synovial facet joints, and muscles, developed and validated against the data of PMHS free head-neck drop tests performed at Duke University [16] and PMHS pendulum rear impact to T1 conducted at WSU [13].

The shoulder model included three bones, the humerus, the scapula and the clavicle, and four joints, the glenohumeral, the acromioclavicular, the sternoclavicular joint, and the scapulothoracic articulation. Various muscles, tendons and ligaments in the shoulder complex are modeled. The modeling methods for the four joints were explained in the publication [12]. In this shoulder model, we redefined the bone-muscle-bone contacts for the Scapulo-thoracic Articulation and for the interactions between the ribcage and the posterior shoulder (Supraspinatus, Infraspinatus, Latissimus dorsi, Trapezius, and Deltoid) muscles. The material properties of the shoulder ligaments (those modeled as nonlinear elastic membrane) and muscles (those modeled as viscoelastic solid) were updated based on the latest experimental data from the dynamic loading tests for the human bone-ligament-bone

specimens of acromioclavicular, coracoclavicular and sternoclavicular joints [18].

The thorax model consists of the ribcage (spine, sternum, 12 pairs of ribs, and external and internal intercostals muscles) and internal soft tissues (heart, lungs, aorta, pleural, diaphragm, and the blood vessels and the air passages) [10]. In this model, the material model of the lungs is modeled using MAT_LUNG_TISSUE in the LS-DYNA code version 970 (LSTC, Livermore, California), in which the material coefficients were determined by fitting the experiment data of Michael Yen's bi-axial tests on excised specimens of human lung parenchyma [17]. The material model for the cortical bone (modeled as shell elements) and spongy bone (modeled as solid elements) uses elastic viscoplastic model combined with continuum damage mechanics (MAT_DAMAGE_2 in LS-DYNA). The intersection between parietal pleura and diaphragm was defined by tied-nodes. The left and right ventricles of the heart and the inside of the Aorta, Vena Cava and Esophagus were pressurized by airbag models.

The abdomen model contains the liver, spleen, kidneys, abdominal aorta, and inferior vena cava. A description of the original WSU abdomen model can be found in the paper [11]. Taking into considerations of better modeling of the anatomical interfaces among the solid and hollow organs and regional variation of the stiffness in between the midabdomen and the lower abdomen, we made some changes to the abdomen model. Instead of using one set of membrane elements to represent the whole cavity between the subcostal plane and the pelvic cavity [11], we defined a compressible solid in the cavity coupled with a set of membrane in a closed volume pressurized by an airbag. Additional arteries and veins (common iliac veins, external iliac artery, left and right renal veins, and veins and arteries connecting main vessels to the lumbar spine) were modeled. The density and the material properties of the liver, kidneys, and spleen were also updated based on the latest published experimental tests on the porcine liver, spleen and kidney specimens [19].

The thoraco-lumbar spine model is fully deformable. Twelve thoracic and five lumbar vertebrae were connected through discs and ligaments. We have conducted simulations using the sub-model of the lumbar spine to correlate the experimental data of the human cadaver lumbar tests under six different loading conditions of anterior and posterior shear, tension, compression, flexion

and extension [20]. The responses of the lumbar spine model agree with the experimental data under all the loading conditions except for the flexion loading case. Adjustment of the material properties of the bones and ligaments of the spine was made.

The models for the lower extremity and lower arms and hands are relatively simple. The Hybrid-III legs were attached to the human body torso. To do so the pelvic bones of acetabulum and iliac were defined as rigid bodies. The anatomical data of the arms and hands were not included. Lumped mass were added to the upper arms to take into account their inertia effects.

Material Properties

Fourteen material models (constitutive laws) are used in the human body model. The material properties for some important tissues are listed in table A-1 in the appendix of this paper.

MODEL VALIDATION

PMHS Pendulum Impact Test Simulations

In our first round of the model validations, fifteen tests of PMHS pendulum impacts to three body regions of thorax, abdomen, and left shoulder were simulated. Table 1 summarizes the impact conditions and the sources of experimental data.

Thoracic Force-Deflection Responses

To validate the response of the thorax body region, five cases (case 1-5 as listed in Table 1) of the PMHS pendulum impact tests were simulated. The chest deflections were calculated from the displacement of the impact center point on the chest skin relative to the thoracic spine. In Cases 1-2, the forces were obtained from the anterior pendulum-body contact forces, while in Cases 3-5, the forces were from the posterior body-backplate contact. Comparisons of the force-deflection responses between the model and the test data are shown in Figures 1 to 5.

Table 1.
PMHS pendulum impact tests for the model validation

Case No.	Description of the test conditions	Ref. No.
1	23.4 Kg 150mm disk at 6.5 m/s to center of thorax	[21]
2	23.4kg 150mm disk 30 degree oblique impact to thorax at 6.5 m/s	[22]
3	UVA hub loading to thorax	[23]
4	UVA diagonal belt loading to thorax	[23]
5	UVA distributed loading to thorax	[23]
6	32Kg rigid bar impact to midabdomen at 6.1 m/s	[24]
7	48Kg rigid bar impact to midabdomen at 9.0 m/s	[25]
8	23.4kg disk 30 degree oblique impact to right side of upper abdomen at 6.5 m/s	[22]
9	Close-proximity surrogate airbag impact to midabdomen	[25]
10	Belt loading to midabdomen	[25]
11	23.4Kg disc lateral impact to left shoulder at 4.5 m/s	[12]
12	23Kg 200X150mm ram lateral impact to left shoulder at 4.4 m/s	[26]
13	The 23Kg ram 15 degree oblique impact to left shoulder at 4.4 m/s	[26]
14	The 23Kg ram 30 degree oblique impact to left shoulder at 4.4 m/s	[26]
15	The 23Kg ram 30 degree oblique impact to left shoulder at 7.6 m/s	[26]

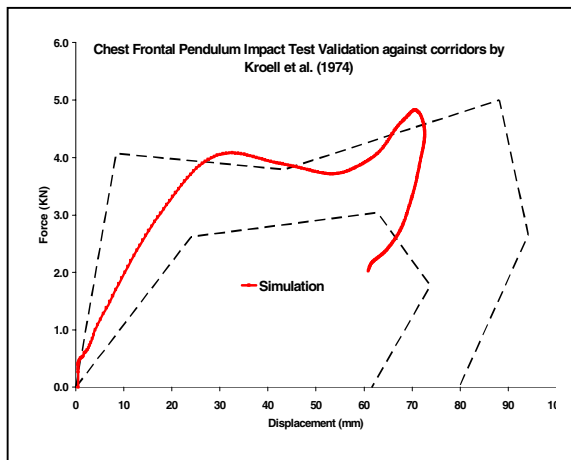


Fig.1 Force-deflection comparisons of Case 1

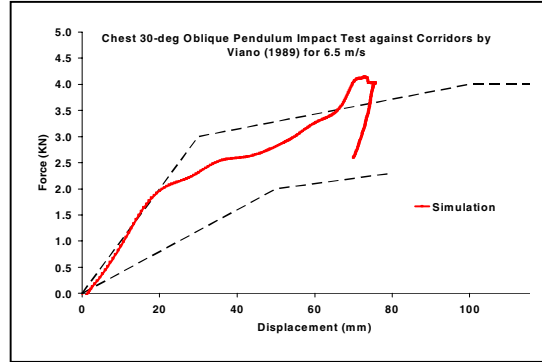


Fig. 2 Force-deflection comparisons of Case 2

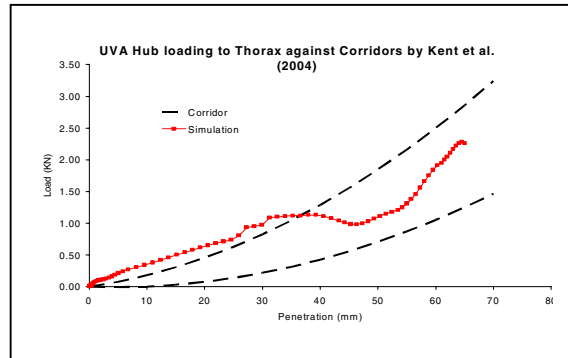


Fig. 3 Force-deflection comparisons of Case 3

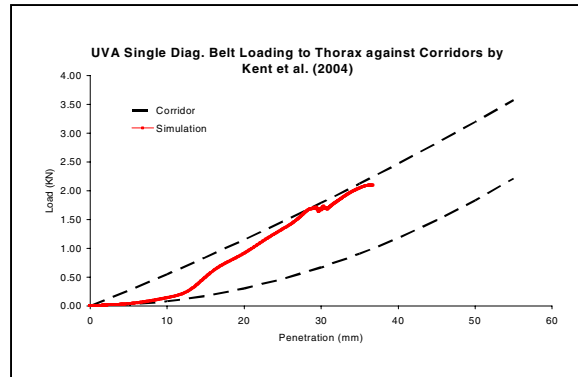


Fig.4 Force-deflection comparisons of Case 4

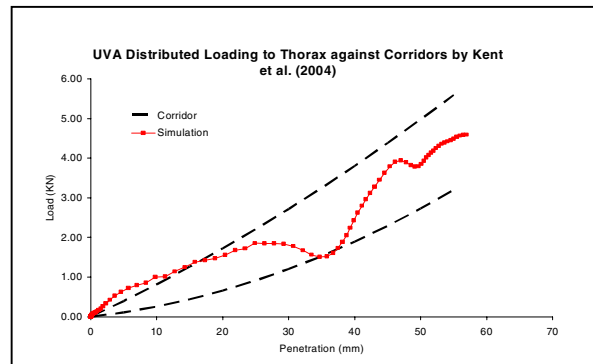


Fig.5 Force-deflection comparisons of Case 5

All these figures show that the calculated chest force-deflection responses are basically in the corridors of the test data by Kroell [21], Viano [22], and Kent et al. [23].

These results verified the model's predictions of the chest force-deflection responses to change of impact directions (cases 1 & 2) and types of loading (cases 3-5).

Abdominal Force-Deflection Responses

Cases 6 to 10 were set up to validate the model's abdominal responses to different impact mass and speed, loading type and impact directions. The abdominal deflections were calculated from the displacement of the impact center point on the abdomen skin relative to the lumbar spine.

Figure 6 to 10 show correlations between the calculated and measured forces-deflection responses of the midabdomen or the upper abdomen for cases 6-10. We see that overall the model predicts the abdominal responses reasonably.

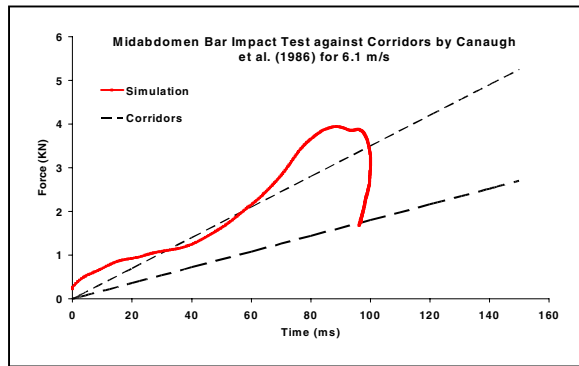


Fig. 6 Force-deflection comparisons of Case 6

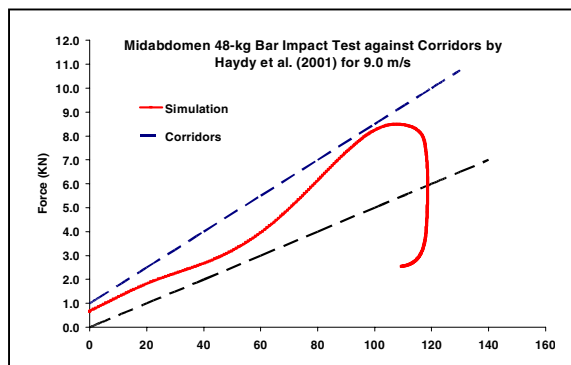


Fig. 7 Force-deflection comparisons of Case 7

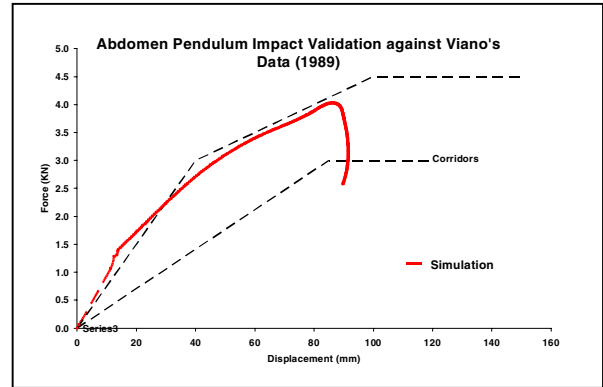


Fig. 8 Force-deflection comparisons of Case 8

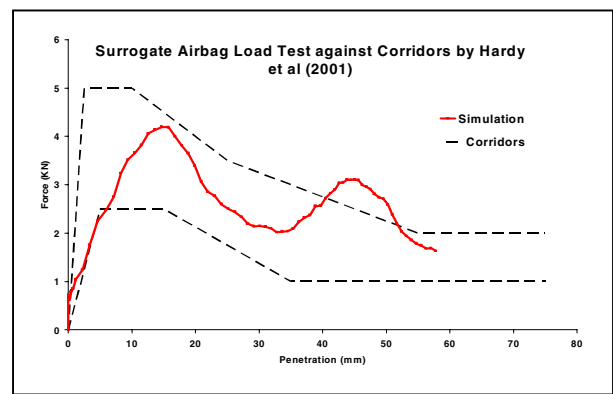


Fig. 9 Force-deflection comparisons of Case 9

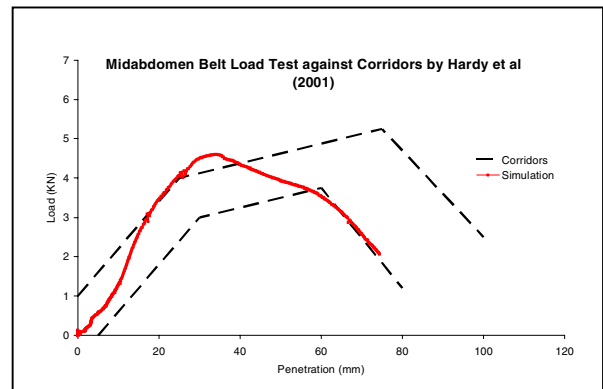


Fig. 10 Force-deflection comparisons of Case 10

Shoulder Force-Deflection Responses

Cases 11 to 15 were chosen to validate the responses of the shoulder. The shoulder deflections were calculated from the relative displacements of acromion-to-acromion. Comparisons of the forces-deflection responses between the model and the PMHS pendulum test data are shown in Figures 11 to 14. In the oblique impacts (Case 12-14), the responses in both y (the lateral direction) and x (the

anterior-posterior direction) were correlated with the data by Bolte et al [26].

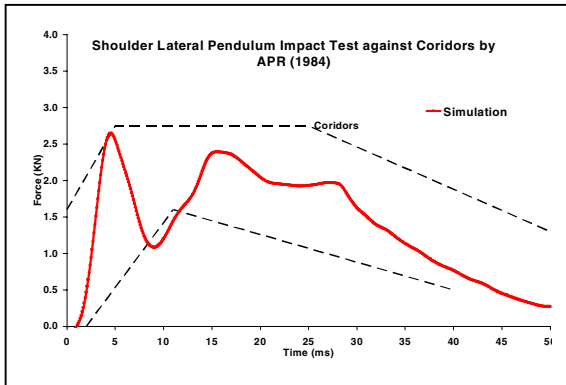


Fig. 11 Force-deflection comparisons of Case 11

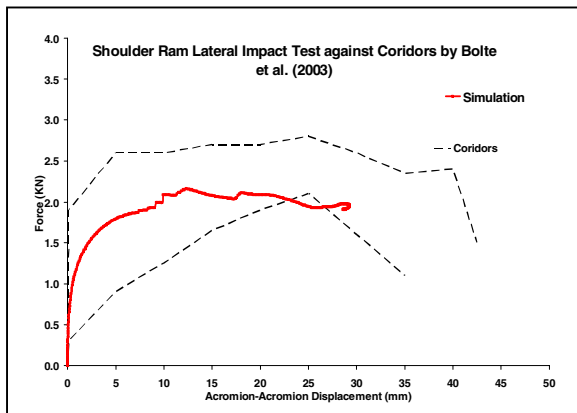


Fig. 12 Force-deflection comparisons of Case 12

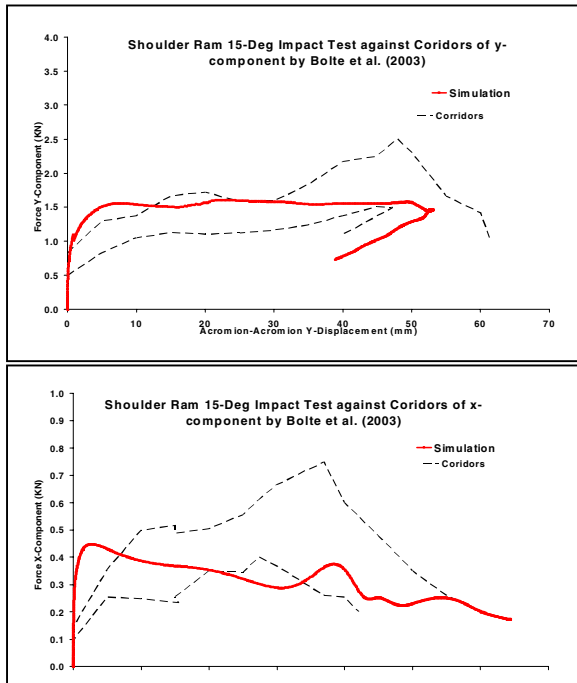


Fig. 13 Force-deflection comparisons of Case 13

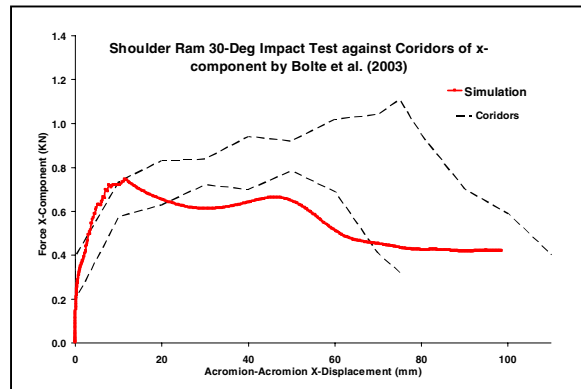
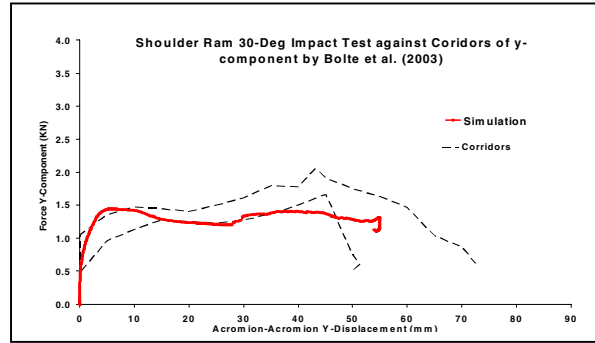


Fig. 14 Force-deflection comparisons of Case 14

PMHS Sled Test Simulation

For using the model as effective system evaluation tool, it is important to validate it under dynamic crash conditions. A set of PMHS sled test data in the NHTSA biomechanics database (test# 2860) was selected for such model validation. The test #2860 run at University of Virginia in 1992, used a 30.7 mph frontal crash pulse for a 3-point belted PMHS seated in a Tempo buck. The subject was an embalmed cadaver of 68 years old male with weight of 67Kg and height of 171cm. The test made use of two 40-gage chest bands, one on the fourth and one on the eighth rib to measure chest deformation during the impact event. The experimental data also included shoulder and lap belt forces, accelerations at T1 & T12 vertebrae and sternum.

The human body model was positioned in the test buck described in test report [27]. The belt system was modeled approximately in absence of details in the report. The sled crash pulse per this test report was used in the model.

The computed shoulder and lap belt forces were correlated with the test data. The model's predictions of the chest deflections were compared with available chest band measurement data.

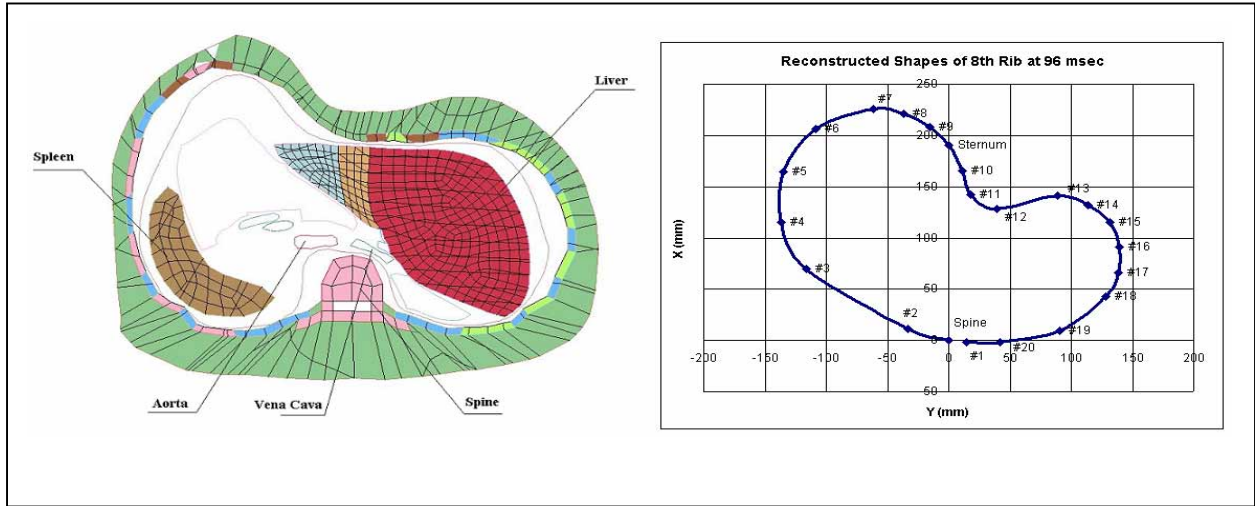


Fig. 17 Comparison between the simulated and experimental chest shapes at rib #8 at 96 msec

Figure 15 & 16 compare the model-predicted and measured histories of the chest deflections at rib #4 and #8 sections.

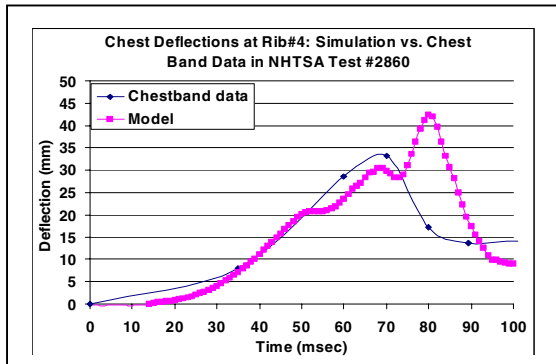


Fig. 15 Histories of the chest deflections at rib #4

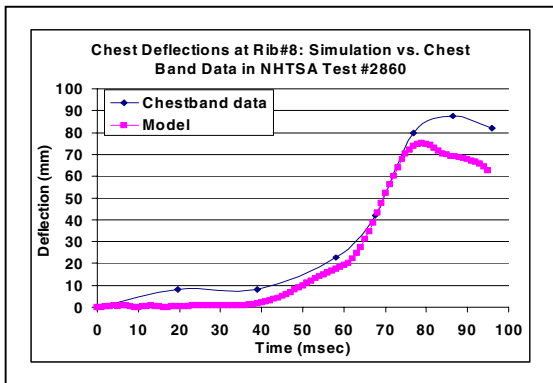


Fig. 16 Histories of the chest deflections at rib #8

The simulation results and the chestband data of chest deformation shapes within the time period

of 120msec were also compared. Figure 17 shows such a comparison of the chest band shapes in the rib#8 transverse section plane at 96 msec. The computed profile is the transverse section view cut through the rib#8. The experimental shape was reconstructed from the chestband signals at 96 msec. The shapes are similar to each other.

These results give us some confidence in the human body model chest response estimations similar to PMHS under dynamic crash simulations.

Robustness Study in Sled Tests Simulations

To serve the needs of restraint system R&D applications, the human body model must be tested under various sled tests conditions. The motivation of this study was to assess robustness of the model in sled test simulations under a variety of restraint environments and crash conditions.

We set up a matrix that consisted of 12 runs, in which variations of crash severity (15 mph to 35 mph) and restraint systems (3-point & 4-point seatbelts, with or without driver & passenger airbags) were considered, as shown in Table 2.

All the simulations in the matrix were completed successfully. Robustness of such defined human sled test models was confirmed. Quantification of all of these model's results is in process.

Table 2.
Matrix of the human body sled tests for model robustness study

Run #	Occupant & Restraint Systems	Crash Pulse or Speed
1	Driver, 3pt-belted.	30mph
2	Driver, airbag only.	30mph
3	Driver, 3pt-belt + airbag.	35mph
4	Driver, 4pt-belt + airbag.	35mph
5	Driver, airbag only.	15mph
6	Passenger, 3pt-belted.	30mph
7	Passenger, airbag only.	30mph
8	Passenger, 3pt-belt +	35mph
9	Passenger, 4pt-belt +	35mph
10	Passenger, 3pt-belted.	15mph
11	WSU rigid wall side impact to a free occupant.	6.9 m/s
12	WSU rigid wall side impact to a free occupant.	9.1 m/s

INJURY ANALYSIS

Injury assessment and analyses were made for the simulation cases through the analysis of model predicted stress-strain field of hard and soft tissues in the shoulder, thorax and abdomen body regions. Comparing the injuries observed in the PMHS tests with model-predicted stresses should be helpful for us to understand the injury mechanism and to assess the model's capability and weakness for injury estimation at tissue level. In this section, the results of such analyses are presented.

Thoracic Rib Fracture Estimation

The sled test simulation case (NHTSA Test #2860 as analyzed above) was taken as a sample for this study.

The subject suffered multiple rib fractures in the sled test. In the right plot of Figure 18, white elliptic circles marks the approximate rib fracture locations reconstructed according to the published rib fracture report [27]. For comparison, the model-predicted stress contours of the ribcage at 100msec are shown in the left plot of Figure 18. We see that those high-stress areas concentrate around the

observed fracture locations. The maximum Von Mises stresses of the ribs exceed 70MPa, while chest compression is more than 35%, indicating rib failures as compared the values (threshold of von Mises stress of 75-137 MPa) discussed in the publication [9].

Abdominal Organ Injury Estimation

Hardy's autopsy reports [25] of the rigid bar impacts to midabdomen of free-back cadavers were analyzed. Among the seven PMHS subjects under such test conditions five suffered liver injury and two had spleen injury. Table 3 summarized Hardy's findings particularly for the post-impact liver injuries.

Stress analysis was made on the liver based on the results of simulation case 7 from Table 1. Figure 19 gives anterior and posterior view of the Von Mises stress contours on the liver. We can see that in the high-stress concentrated areas the maximum Von Mises stresses are above 200KPa, exceeding the ultimate compressive stress thresholds in the range of 127-192 KPa [19]. These areas are most likely the origination of the tissue failures at those locations observed from the experiments described in Table 3.

Shoulder Injury Estimation

The tests data of ram impact to left shoulder of cadavers by Bolte [26] were analyzed. Among their fourteen tests reported, only one subject (Lat03) was found to have distal clavicle fracture. The test conditions were a lateral impact to the left shoulder of 84 years-old male subject of 64Kg weight at 4 m/s. The published radiograph showed the fracture location is on the clavicle close to Acronio-clavicular joint [26].

The model predicts the possible clavicle fracture locations which are in agreement with the experimental observation. As shown in Figure 20 left plot, the high-stress concentration areas are on the left clavicle around the Acronio-clavicular joint. The maximum Von Mises stresses of the clavicle are above 25 MPa..

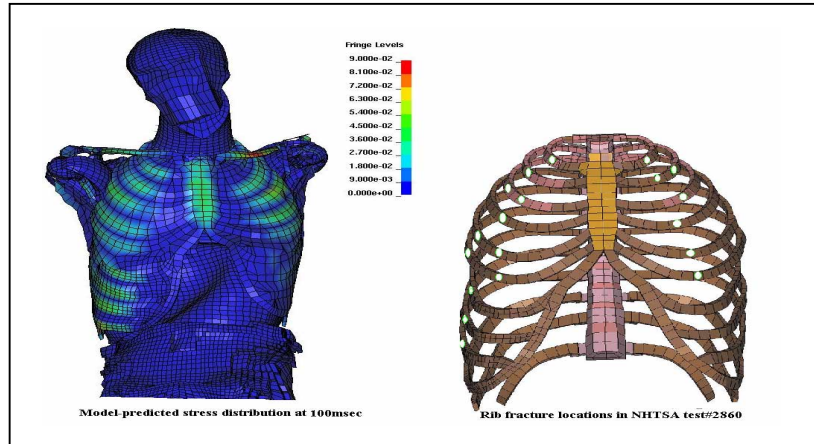


Fig. 18 Comparison between the simulated and experimental chest shapes at rib #8 at 96 msec

Table 3.

Hardy's autopsy results for liver injury from the cadavers subject to midabdomen rigid-bar impacts [25]

Test	Test Subject and Impact Speed	Liver Injury Description
GI1	Female, 73Y, 175cm, 36Kg. 4.3m/s.	NA
GI3	Male, 87Y, 173cm, 73Kg. 6.3m/s.	Vertical tear of right lobe, 7.5cm anteriorly, 9cm posteriorly.
GI4	Male, 93Y, 165cm, 58Kg. 6.6m/s.	Right capsule tear, 11cm anteriorly. Tear of left lobe, 3.5cm posteriorly.
GI6	Male, 85Y, 165cm, 91Kg. 6.1m/s.	Vertical tear of inferior edge, 2.5cm.
GI7	Male, 74Y, 181cm, 77Kg. 9.1m/s.	No liver injury.
GI8	Male, 71Y, 182cm, 64Kg. 9.0m/s.	Tear of inferior edge, 3cm. Multiple lacerations of left lobe posteriorly. Multiple lacerations of right lobe inferiorly.
GI9	Female, 85Y, 155cm, 51Kg. 9.6m/s.	Vertical tear of right lobe of liver, 5.0cm. Transverse tear of right lobe. Multiple irregular tears of right lobe posteriorly.

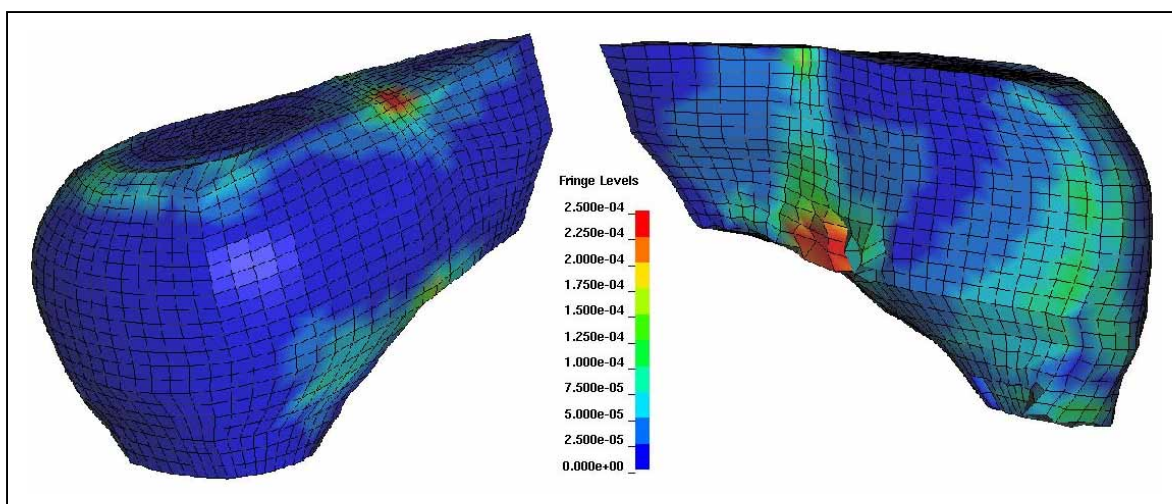


Fig. 19 Stress Contours of the liver at 48 msec at 9.0 m/s impact to midabdomen (simulation case 7)

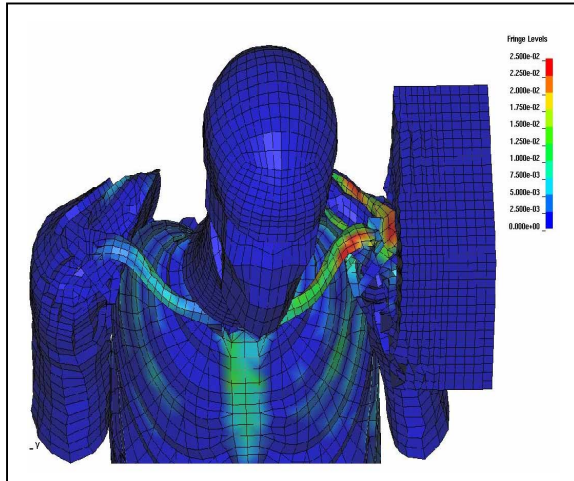


Fig. 20 Stress contours of the shoulders under ram impact at 4.4 m/s

CONCLUSIONS

A human body finite element model was developed for an average adult male with detailed bony and soft tissues in the body regions of the head-neck, shoulder, the thorax, and the abdomen.

Extensive validations of the human body model against Post Mortem Human Subjects (PMHS) responses for the frontal and side impacts, as well as belt and surrogate airbag loading under various conditions of fifteen sets of pendulum tests performed and published by various researchers were carried out. The force-deflection responses of shoulders, thorax, and the abdomen due to change of impact energy and directions, and types of loading are in good agreement with the experimental data.

This model was further validated against the chest band data of belted PMHS 30mph sled test. The model predicts the histories of chest deflections and deformed shapes of the fourth and eighth rib sections. This study demonstrated that the model is applicable in sled test simulations under the impact severities of 15-35 MPH in frontal and side impacts.

Stress analysis made on the clavicle under lateral pendulum impact, on the abdominal solid organs under rigid bar impacts, and on the chest ribs under the 30mph belt PMHS sled test indicate that qualitatively this human body model can provide us very useful information about the possible failure locations of the skeletal and soft tissues in the body regions of the shoulder, the thorax and the abdomen under our considered loading conditions. However,

accurate predictions of damage of the tissues are not possible by using the current model version. More work needs to be done both experimentally and analytically at the tissue level.

ACKNOWLEDGEMENT

The authors would like to gratefully acknowledge Bioengineering Center of Wayne State University for providing us their base models for the development of finite element human body model reported in this paper. Special thanks to Dr. King Yang for his guidance and support for this research.

The authors also wish to acknowledge Dr. Jialou Hu at ASL/Takata for his helpful discussions regarding some material models.

REFERENCES

- [1] MLIT/JAMA/JARI, "Proposals for Activities on International Harmonization Advanced Frontal Impact Dummies." IHRA BIO-WG in Washington D.C., USA, July 16, 2004.
- [2] Mulligan, G.W.N., Pizey, G., Lane, D., Anderson, L., English, C., Kohut, C., "Thoracic Trauma Assessment Formulations for restrained Drivers In Simulated Frontal Impact." SAE Paper 942206, 1994.
- [3] Cavanaugh, J., "The Biomechanics of Thoracic Trauma." In *Accidental Injury Biomechanics and Prevention*, Ed. By A. Nahum and J. Welvin, Springer-Verlag, New York, pp. 362-390, 1993.
- [4] Elhagediab, A.M. and Rouhana, S.W., "Patterns of Abdominal Injury in Frontal Automotive Crashes." In *Proceedings of the 16th International Technical Conference on Experimental Safety Vehicles*, NHTSA, Washington D. C., Paper 98-S1-W-26, pp. 327-337, 1998.
- [5] Lee, J.B. and Yang, K.H., "Abdominal Injury Patterns In Motor Vehicle Accidents: A Survey of NASS Database From 1993 to 1997, *J. of Traffic Injury Prevention*, Vol. 3, No. 3, pp. 241-246, 2002.
- [6] Kent, R., Sherwood, C., Lessley, D., Overby, B., Matsuoka, F., "Age-Related Changes In The Effective Stiffness of The Human Thorax Using Four Loading Conditions." in *Proceedings of RCOBI Conference*, 2003.
- [7] Kent, R., Patrie, J., Matsuoka, F., Mullen, C., "Development of an Age-dependent Thoracic Injury Criterion for Frontal Impact Restraint Loading." in

Proceedings of the 18th Technical Conference on the Enhanced Safety of Vehicles, Nagoya, Japan, 2003.

[8] Iwamoto M., Kisanuki Y., Watanabe I., Furusu K., Miki K. and Hasegawa J., "Development of a Finite Element Model of the Total Human Model for Safety (THUMS) and application to injury construction, in Proceedings of IROCOBI, pp31-42, Munich, 2002.

[9] Ruan, J., El-Jawahri, R., Chai, L., Barbat, S., Prasad, P., "Prediction and Analysis of Human Thoracic Impact Responses and Injuries in Cadaver Impacts Using a Full Human Body Finite Element Model." Stapp Car Crash Journal, Vol. 47, Paper #2003-22-0014, 2003.

[10] Shah, C.S., Yang K., Hardy, W., Wang, H.K., King A.I., "Development of a Computer Model to Predict Aortic Rupture Due to Impact Loading." Stapp Car Crash Journal, Vol. 45, Paper #2001-22-0007, 2001.

[11] Lee, J.B. and Yang K., "Development of a Finite Element Model of Abdomen." Stapp Car Crash Journal, Vol. 45, Paper #2001-22-0004, 2001.

[12] Iwamoto, W., Miki, K., Mohammad, M., Naif, A., Yang K., Begeman, P.C., and King, A.I., "Development of a Finite Element Model of the Human Shoulder." Stapp Car Crash Journal, Vol. 44, Paper #2000-01-SC19, 2000.

[13] Yang K., Zhu, F., Luan, F., Zhao, L., Begeman, P.C., "Development of a Finite Element Model of the Human Neck." Stapp Car Crash Journal, Vol. 42, Paper #983157, 1998.

[14] Zhou, C., Khalil, T.B., and King, A.I., "A New Model Comparing Impact Responses of the Homogeneous and Inhomogeneous Human Brain." Stapp Car Crash Journal, Vol. 39, Paper #952714, 1995.

[15] Zhang L., Yang K., Dwarampudi, R., Omori, K., Li, T., Chang K., Hardy, W., Khalil, T.B. and King, A.I., "Recent Advances in Brain Injury Research: A New Human Head Model Development and Validation." Stapp Car Crash Journal, Vol. 45, Paper #2001-22-0017, 2001.

[16] Winkelstein, B.A., Nightingale, R.W., and Myers, B.S., "Impact Neck Injury Dynamics: Relationships between Impact Surface, Cervical Spine Kinetics, and Injury Risk." Proceedings of the 6th Injury Prevention through Biomechanics, pp. 85-95, 1996.

[17] Yen, Michael, R.T., "Development of Thorax Model Sub-project-C: Mechanical Properties of Human Heart, Lung and Aorta." Ph.D. Thesis of the Department of Biomedical Engineering of University of Memphis, September, 1999.

[18] Koh, S.W., Cavanaugh J.M., and Leach J.P., "Mechanical Properties of the Shoulder Ligaments under Dynamic Loading." Stapp Car Crash Journal, Vol. 48, Paper #2004-22-0006, 2004.

[19] Tamura, A., Omori, K., Miki, K., Lee, B.J., Yang, K.H., King, A.I. "Mechanical Characterization of Porcine Organs." Stapp Car Crash Journal, Vol. 46, Paper #2002-22-0003, 2002.

[20] Demetropouloa, C.K., Yang, K.H., Grimm, M.J., Khalil, T.B., and King, A.I. "Mechanical Properties of the Cadaveric and Hybrid III Lumbar Spines." Stapp Car Crash Journal, Vol. 42, Paper #983160, 1998.

[21] Kroell, C.K., Schneider, D.C. and Nahum, A.M., "Impact Tolerance and Response of the Human Thorax II." Stapp Car Crash Journal, Vol. 18, Paper #741187, 1974.

[22] Viano, D.C., "Biomechanical Responses and Injuries in Blunt lateral impact." Stapp Car Crash Journal, Vol. 33, Paper #8922432, 1989.

[23] Kent R. Lessley, D. and Shrewood, C., "Thoracic Response to Dynamic, Non-Impact Loading from a Hub, Distributed Belt, Diagonal Belt and Double Diagonal Belts." Stapp Car Crash Journal, Vol. 48, Paper #2004-22-0022, 2004.

[24] Cavanaugh, J.M., et al., "Lower Abdominal Tolerances and Responses." Stapp Car Crash Journal, Vol. 30, Paper #861878, 1986.

[25] Hardy, W., Schneider, W. and Rouhana, S.W., "Abdominal impact Response to Rigid-Bar, Seatbelt, and Airbag Loading." Stapp Car Crash Journal, Vol. 45, Paper #2001-22-0001, 2001.

[26] Bolte IV, J.H., Hines, M.H., Herriot, R.G., McFadden, J.D., and Donnelly, B.R., "Shoulder Impact Response and Injury Due to Lateral and Oblique Loading." Stapp Car Crash Journal, Vol. 47, Paper #2003-22-0003, 2003.

[27] Klopp G.S., "Test ASTS79, Using A Cadaver Utilizing A Three Point Seat Belt—A Report on a Test Run for NHTSA." Automobile Safety Laboratory of the University of Virginia, September 7, 1992.

APPENDIX

Table A-1.
Material properties for some important tissues

Tissues	Material Model	Density kg/m ³	Young's Modulus(GPa)	Poison Ratio	Yield Stress (GPa)	Tangent Modulus (GPa)
Cervical vertebrae	Elastic	2500	0.354	0.3		
Cervical Intervertebral disc	Elastic-Plastic	1000	0.253	0.3	0.0014	0.00265
Face-neck skin	Viscous foam	1090	E1=0.02 N1=5.0 V2=55.0 E2=0 V2=1.2 PR=0.45			
Clavicle sponge bone	Elastic-plastic	1000	1.6	0.3	0.021	0.055
Clavicle cortical bone	Piecewise-plastic	2000	11	0.3	0.22	3.66
Clavicle cartilage	Elastic-plastic	1000	0.02071	0.45	0.0062	0.001
Clavicle cortical bone	Elastic-plastic	2000	11.5	0.3	0.123	4.17
Spongy bone for thoracic ribs	Damage_2	1000	0.04	0.45	0.0018	0.032
Coastal cartilage	Damage_2	1500	0.04901	0.4	0.00484	0.0156
Cortical bone for thoracic ribs	Plasticity with Damage	2000	10.18	0.3	0.0653	2.3
Rib cartilage	Elastic-plastic	1000	0.0227	0.35	0.0062	0.001
Costal muscle	Elastic-plastic	1000	0.0103	0.4	0.073	0.00103
Esophagus	Elastic	1200	0.005	0.4		
Lung	Lung Tissue	700	K=0.05, C=3.88E07, $\alpha=5.85$, $\beta=-3.21$ C1=1.265E-8 C2=2.71 (in kg-mm-msec unit)			
Heart	Low Density Foam	1000	0.003	TC=0.01 HU=0.95 Loading/unloading compression function specified.		
Pulmonary trunk	Elastic	1200	0.005	0.4		
Pulmonary veins	Elastic	1200	0.01	0.4		
Mediastinal pleura	Elastic	1200	0.015	0.4		
Trachea	Elastic	1200	0.005	0.4		
Aorta	Elastic	1200	0.005	0.4		
Thoracic vertebrae	Elastic	2500	0.354	0.3		
Thoracic intervertebral disc	Elastic-plastic	1000	0.005	0.4	0.0014	0.00265
Lumbar vertebrae	Elastic	2500	0.354	0.3		
Lumbar disc	Elastic-plastic	1000	0.005	0.4	0.0014	0.00265
Spleen	Viscous Foam	1100	E1=4.88E-04 N1=4.0 V2=0.015 N2=0.2, E2=.025 N2=0.2 PR=0.45			
Kidney	Viscous Foam	1100	E1=0.0012 N1=5.0 V2=0.015, N2=0.2, E2=0.015 N2=0.2 PR=0.45			
Diaphragm	Elastic	1000	0.0655	0.4		
Lower abdomen Flesh	Elastic	1200	8.0E-04	0.4		